Author:
Al Momany, Enaam

Title:
Expression, Distribution, and Trafficking of Pore-Forming and Auxiliary Subunits of Kainate Receptors

Expression, Distribution, and Trafficking of Pore-Forming and Auxiliary Subunits of Kainate Receptors

Enaam Mohammed Al Momany

A dissertation submitted to the University of Bristol in accordance with the requirements for award of the degree of Doctor of Philosophy by advanced study in the School of Physiology, Pharmacology and Neuroscience, Faculty of Biomedical Sciences

May 2019

Word count: 49,598

Abstract

Kainate receptors (KARs), a subgroup of ionotropic glutamate receptors (iGluRs), are modulators of neuronal excitability. When co-assembled with their auxiliary subunits Neto2 and Neto1, KARs display slow activation and deactivation. This allows temporal summation of the excitatory postsynaptic currents, which may be involved in epilepsy. While Neto2 and Neto1 regulate KARs' functions, their developmental expression profiles are unknown. KARs are also regulated by post-translational modifications (PTMs) that affect their surface expression and involvement in neuronal excitability/hyperexcitability. Palmitoylation of the GluK2 promotes KAR surface expression. However, it is unknown if changes to this PTM would lead to receptor internalisation.

Using *in situ* blotting, we identified developmental changes in Neto2 and Neto1 regional expression in the rat brain. We have also investigated epilepsy-related changes in iGluR expression using a lithium-low dose pilocarpine model (RISE).

Our results established different spatio-temporal changes for individual KAR proteins during development. In the hippocampus, Neto2 was mainly expressed in the hilus of the dentate gyrus, whereas Neto1 expression was prominent in the stratum lucidum of CA3. While in the cerebellum Neto1 and GluK5 immunolabellings were weak, Neto2 and GluK2/3 were clearly identified in the granular cell layer. Neto2 and Neto1 showed prominent expression in the inner cortical layers, which matched with other KAR subunits expression profiles. This co-expression suggests a regulatory role of Neto proteins and region-specific changes in subunit compositions and functional properties of KARs throughout development. Apart from a decrease in GluN2B NMDA receptor subunit, no detectable changes in other iGluR proteins were detected in the RISE model of epilepsy. We found that non-palmitoylation of the GluK2 increased its SUMOylation and reduced surface expression. This mimickes kainate-induced long-term depression (LTD), which reduces neuronal excitability. Taken together, we revealed aspects of KAR-Neto2 and Neto1 interplay and generated solid basis for the identification of the involvement of PTMs in downstream mechanisms of kainate-induced LTD.

Dedication

To my lovely parents, two brothers, and two sisters, a heartfelt thank you for all the love, warm feelings, visits, and prayers. Your faith in me makes every challenge worthwhile.

Acknowledgements

To my supervisors Professor Elek Molnar and Professor Jeremy Henley, thank you very much for welcoming me in your research groups and offering me a great opportunity of learning and progressing in science, I am very much grateful to you. And, thank you for all the constant and sincere support and guidance during this journey. Your tremendous encouragement, valuable input into my research, and support in developing my skills had great influence on my scientific character.

A very special thank you to all the extraordinary people in their generosity, kindness, support and friendship. Dr Kevin Wilkinson, thank you for the very detailed protocols, for always finding you around when I really needed guidance and support, and for teaching me molecular biology - you are unquestionably such a great and extraordinary teacher and scientist and I have been truly lucky. Dr Ashley Evans, thank you for all the extra lab meetings, ideas, thoughts, stimulating discussions, and for teaching me the imaging experiment - your input into my research is invaluable. Alexandra Fletcher-Jones, you have touched my heart with your kind nature, thank you so much for the very helpful tips and resources for image analysis - you saved my time and, undoubtedly, I am very fortunate to have worked with you. Dr Yasuko Nakamura, Dr Sonam Gurung, and Dr Vanilla Shi, thank you for all the advice, guidance, and help especially in dissection and cell culture - I am very much grateful to you. Dr Garry Whitehead and Dr Shahida Mallah, thank you for all your help, guidance and thoughtful insights during my journey - it is very much appreciated.

A sincere thank you to my advisory committee Professor Clear Warburton and Dr James Hodge. Your advice, suggestions, and support are very much appreciated.

Thank you to all the people in the lab for the enjoyable working environment, it will always be a very nice memory. And, I am especially thankful to my office mates, Dr Robert Thatcher, Dr Mark Irvine, and Dr Fang Guangyu - your kindness, support and advice will always be remembered. My sincere thanks to you Lujain Alsadder for your genuine and profound support and kindness and for your sweet friendship.

A special acknowledgment to my sponsor The Hashemite University of Jordan - I am overwhelmed by your generosity and support, thank you very much.

To my brother Abdullah, my deepest gratitude for your endless care, support, and love - I am really blessed to have you.

Author’s Declaration

I declare that the work in this dissertation was carried out in accordance with the requirements of the University's *Regulations and Code of Practice for Research Degree Programmes* and that it has not been submitted for any other academic award. Except where indicated by specific reference in the text, this work is my own work. Work done in collaboration with, or with the assistance of, others, is indicated as such. Any views expressed in the dissertation are those of the author.

SIGNED: ..... DATE: .....

Table of content

List of Figures

Chapter 1

Chapter 2

Chapter 3

Chapter 5

Appendix

List of Tables

Chapter 1

Chapter 2

Chapter 3

Chapter 4

Chapter 5

Appendix

Abbreviations

Acronym	Description
ABE	Acyl biotin exchange
AEDs	Antiepileptic drugs
AMPA	α-Amino-3-hydroxy-5-methyl-4-isoxazole propionate
ANOVA	Analysis of variance
AP	Alkaline phosphatase
AU	Arbitrary unit
BHK	Baby hamster kidney cells
BSA	Bovine serum albumin
CA	Cornu ammonis
Cb-g	Cerebellar granular cell layer
Cb-m	Cerebellar molecular layer
CCK1/CB1	Cholecystokinin/cannabinoid receptor 1
Cl^-	Chloride ion
CNS	Central nervous system
COPI	Coatomer protein complex I
CTD	C-terminal domain
CUB	Complement subcomponents C1s and C1r, embryonic sea urchin epidermal growth factor protein (Uegf), and bone morphogenetic proteins (Bmp 1)
CPu	Caudate putamen
Cx	Cerebral cortex
DAPI	4’,6-diamidino-2-phenylindole
DG	Dentate gyrus
DMEM	Dulbecco’s modified eagle’s medium
DMSO	Dimethyl sulfoxide
DNA	Deoxyribonucleic acid
DRG	Dorsal root ganglion
E. Coli	Escherichia coli
EDTA	Ethylenediamine tetra-acetic acid
E_{GABA}	GABAergic currents reversal potential
EPSC	Excitatory postsynaptic current
$EPSC_{AMPAR}$	AMPAR-mediated excitatory postsynaptic current
$EPSCs_{KAR}$	KAR-mediated excitatory postsynaptic currents
ER	Endoplasmic reticulum
GABA	γ-Aminobutyric acid
GFP	Green fluorescent protein
GRIP	Glutamate receptor interacting protein
H	Hilus
HBSS	Hank's balanced salt solution
HEK293T	Human embryonic kidney cells expressing a mutant version of the SV40 large T antigen
iGluR	Ionotropic glutamate receptor
KA	Kainic acid
KD	Knockdown

KCC2	Potassium-coupled chloride co-transporter 2
KRIP6	Kainate receptor interacting protein for GluK6
LB	Luria-Bertani
LBD	Ligand binding domain
LCMS	Liquid chromatogrphy-mass spectrometry
LDLa	Low-density lipoprotein class A
LTD	Long-term depression
mEC	Medial entorhinal cortex
MEM	Minimum essential medium
mRNA	Messenger ribonucleic acid
NBT	Nitro-blue tetrazolium chloride
NEM	N-Ethylmaleimide
Neto	Neuropilin and tolloid-like proteins
NKCC1	Na+-K+-2Cl- cotransporter 1
NMDA	N-methyl-D-aspartate
NTD	N-terminal domain
OE	Overexpression
PDZ	Postsynaptic density protein-95 (PSD-95), Drosophila disc large tumor suppressor (Dlg1), and zonula occludens-1 protein (zo-1)
PFA	Paraformaldehyde
PI	Protease inhibitor
PICK1	Protein interacting with C kinase-1
PKC	Protein kinase C
PLL	Poly-L-Lysine
PMA	Phorbol 12-myristate 13-acetate
PMSF	Phenylmethanesulfonyl fluoride
PSD	Postsynaptic density
PTMs	Post-translational modifications
RIPA	Radioimmunoprecipitation assay
RISE	Reduces Intensity Status Epilepticus
rMF	Recurrent mossy fibre
sAHP	Slow afterhyperpolarisation
SDS-PAGE	Sodium dodecyl sulfate polyacrylamide gel electrophoresis
SE	Status epilepticus
SL	Stratum lucidum
SLM	Stratum lacunosum-moleculare
SM	Stratum moleculare
SNAP-25	Synaptosomal-associated protein 25
SO	Stratum oriens
SR	Stratum radiatum
SRSs	Spontaneous recurrent seizures
SUMO	Small ubiquitin-like modifier
SynDIG1	Synapse differentiation-induced gene 1
T	Thalamus
TARPs	Transmembrane AMPAR regulatory proteins
TBS-T	Tris-buffered saline with 0.1% Tween 20
TLE	Temporal lobe epilepsy
TTX	Tetrodotoxin

Ubc9	Ubiquitin conjugating protein 9
WT	Wild type
YFP	Yellow fluorescent protein
zDHHC	Aspartate-Histidine-Histidine-Cysteine within a zinc finger-like domain

1 Introduction

1.1 Neurotransmission in health and disease

One of the great challenges to medical and biological sciences is understanding the central nervous system (CNS). Many brain diseases remain poorly understood and the development of drugs for their treatment has been challenging due to the complexity and relative inaccessibility of the brain. The most burdensome chronic brain disorders are preceded by potentially reversible chemical changes (Gustavsson et al., 2011).

Aberrant excitatory neurotransmission is a prominent pathological component in many neurological, psychiatric and neurodegenerative diseases and for this reason the majority of excitatory signalling proteins in the CNS are considered attractive targets for drug development (Swanson, 2009).

Glutamate, a neurotransmitter used by the overwhelming majority of excitatory synapses in the brain, acts on ionotropic (ion channel-coupled) and metabotropic (second messenger system-coupled) receptors (Lerma and Marques, 2013). Glutamate and its receptors participate in synaptic transmission, neuronal development, learning, memory and excitotoxicity (Bridges and Esslinger, 2005). Consistent with this, changes in glutamatergic neurotransmission have been implicated in a range of neurological and psychiatric disorders, including epilepsy, Alzheimer's disease, amyotrophic lateral sclerosis and stroke (Lerma et al., 2001).

1.2 Ionotropic glutamate receptors

Ionotropic glutamate receptors (iGluRs) (Figure 1.1) are ligand-gated cationic channels formed from the assembly of four subunits. They are subdivided into three main classes based on their sequence homology, electrophysiological properties, and the agonist that preferentially activates them (Lerma and Marques, 2013). These are α-amino-3-hydroxy-5-methyl-4-isoxazole propionate (AMPA), *N*-methyl-D-aspartate (NMDA), and kainic acid (KA) receptors (Lerma and Marques, 2013).

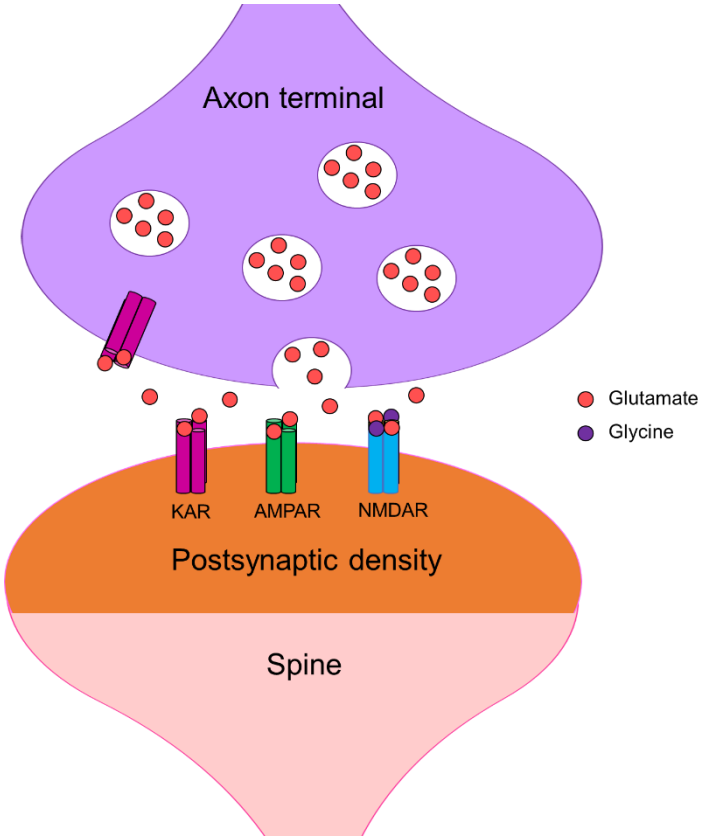

Figure 1.1 Ionotropic glutamate receptors at an excitatory synapse. Ionotropic glutamate receptors are a subclass of glutamate receptors. They are liganed-gated ion channels permeable to Na^+, K^+, and Ca^{2+} ions. They subcategorized into different subtypes (KA, AMPA, and NMDA receptors) that are formed as tetramers from different combinations of functional subunits. They are activated by the neurotransmitter glutamate to mediate the majority of the CNS excitatory synaptic transmission.

1.2.1 AMPA receptors (AMPARs)

AMPARs are distributed abundantly throughout the CNS with the tetramer receptor formed from the assembly of different combinations of the four subunits GluA1, GluA2, GluA3, and GluA4 (Beneyto and Meador-Woodruff, 2004). The four subunits have approximately 70% amino acid sequence homology (Collingridge et al., 2004). Each subunit contributes distinctly to the properties of the channel kinetics, ion selectivity and receptor trafficking leading to considerable functional diversity by heteromerisation (Greger et al., 2017). GluA2 is subjected to RNA editing very soon after birth and is almost fully edited by postnatal day 7 in rats (Greger et al., 2003; Longone et al., 1998). This renders the ion channel of the edited receptors (GluA2-containing receptor) to be calcium impermeable

(GluA2-CI). GluA2-lacking Ca^{2+}-permeable AMPARs are expressed at various levels in neurons and neurological conditions and this minority of AMPARs has an important role in synaptic plasticity (Park et al., 2018; Cull-Candy et al., 2006; Liu and Zukin, 2007; Luscher and Malenka, 2011; Traynelis et al., 2010).

AMPARs are responsible of most fast excitatory neurotransmission in the brain (Shi et al., 2009; Traynelis et al., 2010). This initiation of neuronal firing is important for information propagation. Considering their fast kinetics (on sub-millisecond time scale), they are responsible for the early component of the excitatory postsynaptic current. They also play a very important role in NMDA receptor-dependant synaptic plasticity through the induction of voltage-dependant Mg^{2+} blockage removal from NMDA receptor channel pore (Mayer et al., 1984; Nowak et al., 1984). The GluA subunits have PDZ [postsynaptic density protein-95 (PSD-95), Drosophila disc large tumor suppressor (Dlg1), and zonula occludens-1 protein (zo-1)] -binding domains in their C-termini. These sites promote their interaction with postsynaptic density (PSD) proteins to regulate AMPARs surface expression and synaptic trafficking (Song and Huganir, 2002; Malinow and Malenka, 2002; Barry and Ziff, 2002).

1.2.1.1 Transmembrane AMPAR regulatory proteins

Native iGluRs form macromolecular complexes with scaffolding proteins, enzymes, or trafficking chaperone (Tomita and Castillo, 2012). These transient interactors are important for several aspects. For example, a chaperone assists protein complex assembly, and scaffolding proteins retain channel complexes at synapses (Yan and Tomita, 2012). Some ligand-gated ion channel interacting proteins are classified as ‘auxiliary subunits’ based on four key criteria (Yan and Tomita, 2012):

a. They should not show any ion channel activity.

b. They interact directly and stably associated with their partner receptor.

c. They should regulate receptor channel properties and/or trafficking when co-expressed in heterologous cells.

d. They should be required for the proper receptor function *in vivo*.

Many auxiliary subunits have been identified to associate with AMPARs and regulate their trafficking, pharmacology, and channel gating like the transmembrane AMPAR regulatory proteins (TARPs) (Nicoll et al., 2006; Osten and Stern-Bach, 2006; Milstein and Nicoll, 2008; Ziff, 2007; Coombs and Cull-Candy, 2009; Sager et al., 2009). This highly increases the diversity of AMPARs in the brain (Jackson and Nicoll, 2011). TARPs structure (Figure 1.2) is composed from four transmembrane domains with both the N- and C-termini located in the cytoplasm (Kato et al., 2010). Between the first and second transmembrane domains there is a large extracellular domain (EX1), which is important for the receptor gating and pharmacological properties. The C-terminal domain (CTD) has a PDZ-binding motif (Kato et al., 2010). These auxiliary subunits regulate AMPARs functional properties with differential effects that depend on the TARP subtype (Cho et al., 2007, Milstein et al., 2007).

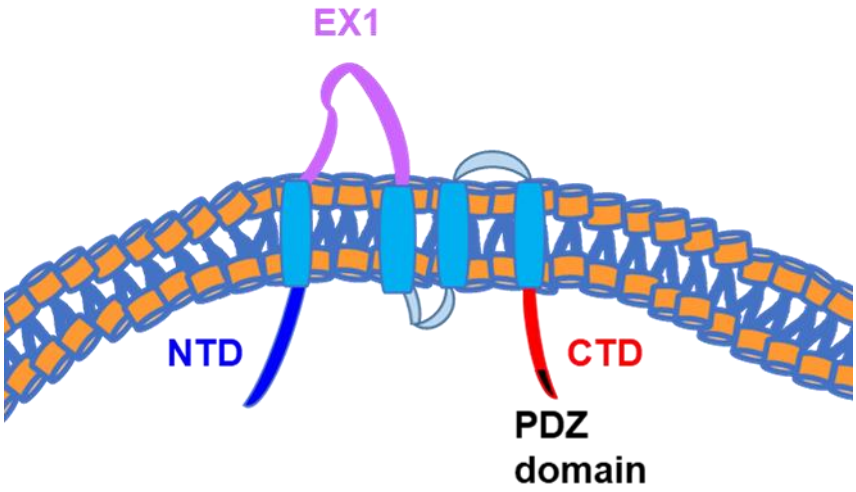

Figure 1.2. TARP subunit topology. The subunit is composed of four transmembrane domains with the N-terminal domain (NTD) and the C-terminal domain (CTD) located intracellularly. There is a large extracellular domain (EX1) between the first and second transmembrane domains. The C-terminal loop has a PDZ-binding motif (Kato et al., 2010).

The TARP family is divided into two subtypes (1 and 2) each with subsequent TARP isoforms (type 1: γ-2, γ-3, γ-4, and γ-8 TARP, type 2: γ-5 and -7 TARP) according to similarities of amino acid sequence and functional properties (Jackson

and Nicoll, 2011). Type 1 TARP was further sub classified to Type 1a (γ-2, γ-3) and type 1b (γ-4, γ-8). Type 1a slows AMPAR deactivation and desensitisation rate/extent and increases glutamate affinity to a lesser extent than type 1b. Both subtypes (1a and 1b) enhances the receptor trafficking to the plasma membrane through their PDZ-binding domain (Kato et al., 2010). PSD-95 interacts with the PDZ-binding motif of TARP (Chen et al., 2000; Dakoji et al., 2003). In cerebellar granule cells, γ-2 TARP (also called stargazin) traffics AMPARs to the plasma membrane (Chen et al., 2000) and then γ-2 interacts with PSD-95 through its PDZ-containing domain to localise the receptor to the postsynaptic density (Kato et al., 2010). Absence of PSD-95 in mice (knockout) led to decreased hippocampal AMPAR-mediated excitatory postsynaptic current ($EPSC_{AMPAR}$) (Beique et al., 2006). This suggests that PSD-95 stabilises synaptic AMPARs via its association with their auxiliary subunits TARPs (Martenson and Tomita, 2015). Importantly, the post-translational modification phosphorylation of TARP modulates the association of PSD-95 and the PDZ-binding domain of TARP (Martenson and Tomita, 2015). Consistent with this, a phospho-mimic mice mutant of γ-2 enhanced cerebellar $EPSC_{AMPAR}$, while a phospho-null mutant mice of γ-2 inhibited it (Tomita et al., 2005; Sumioka et al., 2010).

γ-7 of type 2 TARPs also slows AMPAR deactivation and desensitisation rate/extent and increases agonist efficacy but to a lesser extent compared to type 1a (Kato et al., 2010). However, γ-5 subunit shows unique features. It accelerates specifically GluA2 channel desensitisation rate/extent and increases GluA2 deactivation rate by decreasing the affinity to glutamate (Kato et al., 2007, 2010). Both subunits of type 2 TARPs have no effect on AMPAR trafficking to the cell surface (Kato et al., 2008).

TARPs and their stoichiometry contribute to changes in the AMPAR functional properties (Greger et al., 2017). The stoichiometry of TARPs is variable, and it appears to depend on their expression levels (Greger et al., 2017). From one up to four TARPs can assemble and interact independently with an AMPAR (Kim et al., 2010). In addition, the number of assembled TARPs (zero, two, or four) into a recombinant receptor was found to contribute to the distinct receptor functional properties (Shi et al., 2009).

A naturally occurring mutant was found in mice (stargazer mice), in which TARP-γ-2 (stargazin) was deficient, lead to absence of $EPSC_{APMAR}$ at cerebellar mossy fibre-granule cell synapse (Chen et al., 2000, Hashimoto et al., 1999, Letts et al., 1998). The amplitude and decay time of excitatory currents were reduced in heterozygous stargazer mice compared to wild type (WT) animals indicating stargazin regulates AMPARs in a dose-dependent manner (Kim et al., 2010) and this regulation varies according to the stoichiometry of the receptor/auxiliary subunit complex (Shi et al., 2009). Moreover, overexpressing stargazin in WT granule cells resulted in a slow decay of the excitatory currents and enhanced agonist effect (a characteristic feature of TARP effect) indicating that TARPs were not saturating their associated receptors in the cerebellum (Milstein et al., 2007). Furthermore, it was shown that the effect of AMPAR activation by an agonist was halved in case of the receptor associated with two molecules of TARPs compared to four (Shi et al., 2009), demonstrating a readout of TARP stoichiometry.

In hippocampal CA1 pyramidal neurons, AMPARs interact with four γ-8 molecules [expressed preferentially in the hippocampus (Rouach et al., 2005)]. This depends on the expression level of γ-8, a reduction in γ-8 subunit expression leads to a reduction in stoichiometry (Shi et al., 2009). Furthermore, kainate efficacy of AMPAR and the receptor deactivation and desensitisation kinetics in CA1 pyramidal neurons were affected by the expression levels of γ-8 subunit. In addition, they were in good agreement with the stoichiometry of AMPAR/TARP (Shi et al., 2009).

1.2.2 NMDA receptors (NMDARs)

NMDARs are tetramers, containing the obligatory GluN1 subunit in various combinations with GluN2A-D and GluN3A/B. Glutamate, glycine (co-agonist), and membrane depolarisation are required for NMDAR to be activated, leading to the opening of the Na^+, K^+ and Ca^{2+} permeable channel pore. At resting membrane potential, the ion channel of NMDAR is blocked by a Mg^{2+} ion (voltage-dependent Mg^{2+} blockage; Mayer et al., 1984; Nowak et al., 1984). This can be relieved when there is a strong enough membrane depolarisation (sustained AMPAR activation). Once this happens and glutamate and glycine bind to the NMDAR, the ion channel

will open permitting the conductance of Ca^{2+} as well as Na^{+} and K^{+} ions. Ca^{2+} conductance activates a cascade of intracellular signalling pathways that lead to persistent long-term changes in synaptic strength (Bliss and Collingridge, 1993; Huganir and Nicoll, 2013; Kessels and Malinow, 2009). These changes mediate synaptic plasticity that underlies learning and memory.

Like other iGluRs, NMDAR subunits are subjected to many variations through alternative splicing, thus, contributing to different functional and pharmacological properties of the various receptor subtypes (Molnar, 2008).

IGluRs			
	KARs	**AMPARs**	**NMDARs**
Agonist/ (co-agonist)	KA	AMPA	NMDA (Glycine)
Subunits	GluK1-5	GluA1-4	GluN1, GluN2A-D, GluN3A-B
Cationic channel selectivity and conductance	Na^+, K^+ Unedited GluK1/2: Ca^{2+}	Na^+, K^+ Unedited GluA2: Ca^{2+}	Na^+, K^+, Ca^{2+} at depolarised potentials
Function	Mediate synaptic transmission and modulate presynaptic release	Mediate most fast glutamatergic excitatory synaptic transmission	Mediate synaptic plasticity

Table 1.1. A comparison of the three subclasses of iGluRs; KARs, AMPARs, and NMDARs.

1.2.3 Kainate receptors (KARs)

KARs exhibit a complex diversity in subcellular localisation and signalling mechanisms that allow them to act as regulators of synaptic transmission and plasticity. They contribute to excitatory postsynaptic transmission at only a relatively restricted subset of synapses, whereas AMPA and NMDA receptors are responsible for most of the excitatory neurotransmission in the brain and induce synaptic plasticity (Straub et al., 2011a; Carta et al., 2014). In addition, KARs regulate excitatory and inhibitory neurotransmitters release and impact neuronal excitability.

KARs and AMPARs are closely related. Their tetrameric structure forms an ion channel that is mainly permeable to Na^+ and K^+. At resting membrane potential and upon glutamate binding, the receptor is activated and the ion channel opens. The driving force of ions movement favours an inward Na^+ current that will lead to membrane depolarisation.

1.2.3.1 KAR subunits

Various combinations of GluK1, GluK2, GluK3, GluK4, and GluK5 subunit proteins (formerly named as GluR5, GluR6, GluR7, KA1, and KA2, respectively), form the tetramer of the KAR (Jane et al., 2009; Contractor et al., 2011; Lerma and Marques, 2013). While GluK1, GluK2, and GluK3 [low affinity kainate binding subunits (50-100 nM)] can assemble into both homo- and heteromeric receptors, GluK4 and GluK5 [high affinity kainate binding subunits (5-15 nM)] can just make heteromers with GluK1-3 (Pinheiro and Mulle, 2006; Contractor et al., 2011; Copits and Swanson, 2012). The low-affinity subunits share 75-80% homology and the high-affinity subunits has 68% homology. The two subclasses of KAR subunits have 45% homology (Pinheiro and Mulle, 2006; Lodge, 2009). Each subunit is composed of a large extracellular N-terminal domain, followed by the first transmembrane domain (M1), a re-entrant channel pore-forming domain (M2), the third transmembrane domain (M3), an extracellular S2 domain, followed by M4 and the intracellular C-terminal domain (Figure1.3; Hollmann, 1994; Wo and Oswald, 1994). The ligand binding domain (LBD) is formed by two loops; the one before the first

transmembrane domain (S1) and the S2 extracellular domain between M3 and M4 transmembrane domains (Contractor et al., 2011). This topology of the KAR subunit is similar to AMPAR and NMDAR subunits, which also form tetramers (Pinheiro and Mulle, 2006; Contractor, 2011).

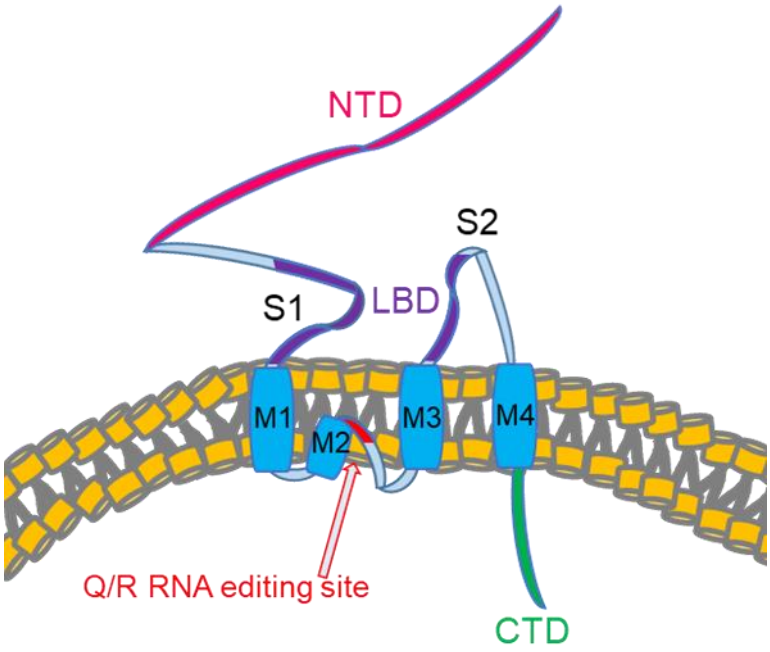

Figure 1.3. KAR subunit topology. The subunit is composed of two large extracellular domains [the N-terminal domain (NTD) and the ligand binding domain (LBD)], a transmembrane domain [three membrane-spanning helices (M1, M3, and M4) and a membrane re-entrant loop (M2)] which represents part of the ion channel pore and an intracellular C-terminal domain (CTD). The Q/R RNA editing site is located in the lining that form the ion channel pore of the assembled tetramer (Hollmann, 1994; Wo and Oswald, 1994; Pinheiro and Mulle, 2006; Contractor, 2011).

1.2.3.2 RNA editing and alternative splicing of KARs

KAR subunits are subjected to several modifications at the mRNA level (Figure 1.4). The mRNA of GluK1 and GluK2 is edited by RNA deaminase in the membrane re-entrant loop (Figure 1.2) where a glutamine (Q) residue is substituted with an arginine (R) residue forming calcium (Ca^{2+}) impermeable ion channel (Egebjerg and Heinemann 1993, Contractor et al., 2011). This Q/R editing is also responsible for the Ca^{2+} impermeability of the GluA2 subunit of the AMPAR (Burnashev et al., 1992). As indicated on Figure 1.4, GluK1 exhibits alternative splice variants in its N-terminal and C-terminal, GluK2 and 3 exhibit alternative

splice variants only in their C-termini (Sommer et al., 1992; Gregor et al., 1993; Barbon et al., 2001; Schiffer et al., 1997). These alternative splice modifications affect KARs' trafficking and interacting proteins (Schiffer et al., 1997; Jaskolski et al., 2004; Coussen et al., 2005).

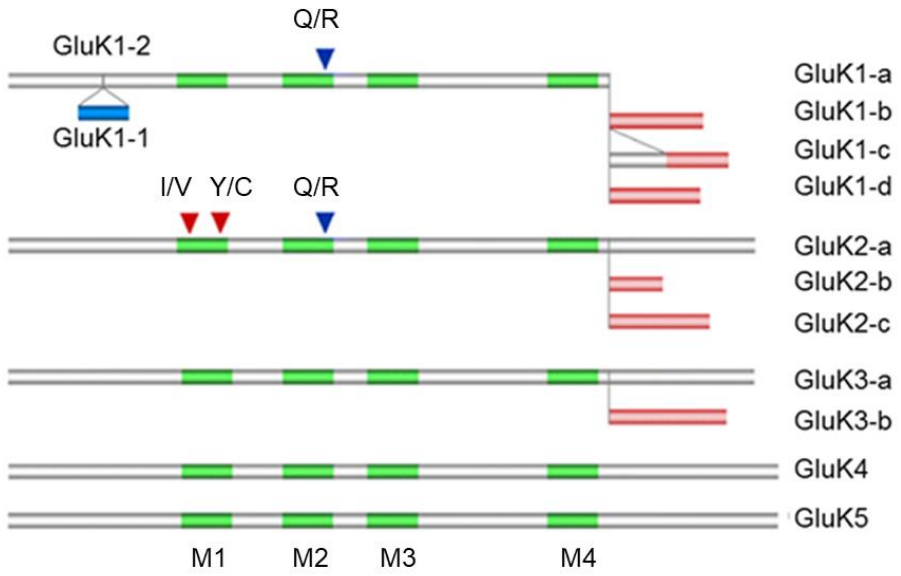

Figure 1.4. RNA editing and alternative splicing of KAR subunits. The mRNA of the KAR subunits undergoes many post-transcriptional modifications. GluK1 and GluK2 are subjected to mRNA editing [glutamine/arginine (Q/R), isoleucine/valine (I/V) and tyrosine/cysteine (Y/C)] which render the receptor's channel impermeable to calcium. In addition, more diversity in KAR subunits is generated through alternative splicing, which in most cases occurs at the cytoplasmic C-termini. The transmembrane domains are M1, M3, and M4. The re-entrant loop is M2. (Adapted from Pinheiro and Mulle, 2006).

1.2.3.3 KAR subunits trafficking

KARs trafficking to the plasma membrane is influenced by the subunit composition, which is further diversified according to the different alternative splicing isoforms (Pinheiro and Mulle, 2006). GluK1c is mainly retained in the endoplasmic reticulum (ER) as it has an ER retention motif (RXR) in its C-terminus (Ren et al., 2003b; Jaskolski et al., 2004). Similarly, GluK5 has an ER retention motif of five positively charged arginines (RRRRR) in its C-terminus and so is strongly prevented from trafficking to the plasma membrane and retained in the ER unless this polyarginine stretch is shielded by the co-assembly of GluK5 with one of the low-affinity subunits (GluK1-3) (Gallyas et al., 2003;

Hayes et al., 2003; Ren et al., 2003a). GluK2a and GluK3a isoforms have an ER exit motif (CQRRLKHK) that promote their trafficking to the plasma membrane as well as the surface expression of other subunits that have ER retention motifs (Jaskolski et al., 2004; Yan et al., 2004; Jaskolski et al., 2005). In addition to the role of the C-terminal domain of the different KAR subunit isoforms in plasma membrane trafficking, the N-terminal domain has also an important role (Mah et al., 2005; Valluru et al., 2005). It was established that non-functional receptors, which have mutated glutamate binding site, are retained in the ER and that an intact ligand binding domain is important for the forward trafficking and cell surface expression (Mah et al., 2005; Valluru et al., 2005).

1.2.3.4 KAR subunits post-translational modifications

Post-translational modifications have regulatory impact on many aspects of a receptor function like receptor subunit assembly, protein-protein interactions, trafficking, endocytosis, and synaptic targeting (Mao et al., 2011). Different post-translational modifications, in particular when they occur at proximal locations, appear to interact with each other (Mao et al., 2011). Modifications of specific AMPA, KA, and NMDA receptor subunits regulate the receptor endocytosis and surface expression (Lavezzari et al., 2004; Lavezzari et al., 2003; Ahmadian et al., 2004; Pickering et al., 1995; Copits and Swanson, 2013; Hayashi et al., 2005; Konopacki et al., 2011; Chamberlain et al., 2012; Martin et al., 2007; Naumenko and Ponimaskin, 2018). Such protein modifications include phosphorylation, palmitoylation and SUMOylation (Pahl et al., 2014).

Phosphorylation occurs to specific amino acids (serine, threonine, and tyrosine) and its level is regulated by many kinases and phosphatases. Palmitoylation, the fatty acylation, occurs at cysteine residues. SUMOylation occurs at lysine residues. The dynamic and reversible nature of these modifications make them sensitive to synaptic inputs changes allowing them to regulate the expression and function of iGluRs in basal and activity-dependent manners. Post-translational modification malfunction contributes to the pathology of many neuropsychiatric conditions such as anxiety, Parkinson’s disease, and schizophrenia (Mao et al., 2011).

KAR phosphorylation is highly involved in their internalisation from the cell surface and is also connected in an independent way (so far) to each of receptor SUMOylation and palmitoylation (Chamberlain et al., 2012; Pickering et al., 1995; Copits and Swanson, 2013). Under basal conditions, GluK2-containing KARs are expressed on the cell surface (Jaskolski et al., 2004). Upon kainate stimulation (Figure 1.5/I-IV), these receptor subtypes are phosphorylated by protein kinase C (PKC) at two cytosolic serine residues (S846 and S868) leading to increased GluK2 SUMOylation and receptor internalisation (Konopacki et al., 2011).

Moreover, GluK2 phosphorylation antagonises the interaction with 4.1N protein, thus, destabilising KAR surface expression. Conversely, GluK2 palmitoylation enhances this interaction (Figure 1.5/1-3) leading to stabilising KAR at the cell surface (Copits and Swanson, 2013). Interestingly, Pickering et al. (1995) observed a prominent increase in GluK2 phosphorylation when the receptor cannot be palmitoylated (mutated). Thus, these post-translational modifications act in concert to fine-tune neuronal transmission.

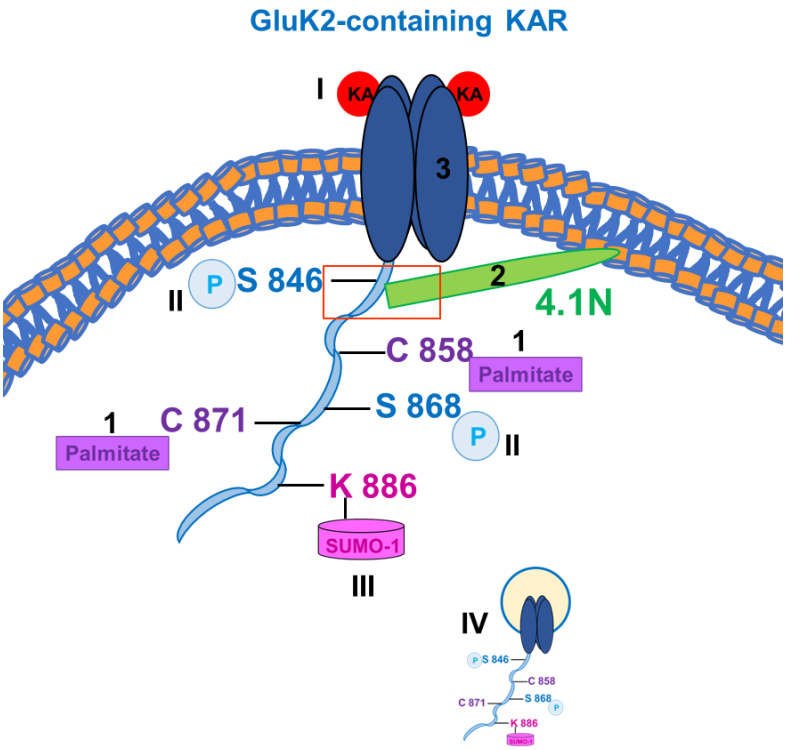

Figure 1.5. A schematic diagram of GluK2 post-translational modifications. GluK2 palmitoylation (1) promotes 4.1N binding (2) to the membrane proximal domain (red box) of GluK2 C-terminus and stabilises the receptor on the cell surface (3). However, upon kainate stimulation (I), GluK2

phosphorylation is enhanced (II) leading to increase its SUMOylation (III) followed by endocytosis (IV) (Chamberlain et al., 2012; Konopacki et al., 2011; Copits and Swanson, 2013.

1.2.3.5 Physiological roles of KARs and their unique properties

Many important functional aspects of KARs remain poorly understood and difficult to resolve due to limited availability of KARs' selective pharmacological (subunit-specific agonists and antagonists) and biochemical tools (antibodies for specific KAR subunits) (Jane et al., 2009; Copits and Swanson, 2012). For example, kainate is a mixed agonist that can also activate AMPARs (Herb et al., 1992; Lerma et al., 2001; Pinheiro and Mulle, 2006; Jane et al., 2009; Lerma and Marques, 2013). And, there are overlapping sensitivities between KARs and AMPARs to most competitive antagonists (Jane et al., 2009). However, with the development of relatively selective AMPAR antagonist, elimination of the synaptic AMPAR currents was possible (Paternain et al., 1995; Wilding and Huettner, 1996) and the contribution of KARs to postsynaptic depolarisation was detected through KAR-mediated excitatory postsynaptic currents ($EPSCs\text{-}_{KAR}$) at mossy fibre-CA3 synapses (Castillo et al., 1997; Vignes and Collingridge, 1997).

$EPSCs\text{-}_{KAR}$ have only been detected in a few central synapses. Therefore, KAR-mediated effects are relatively restricted to specific neurons and synapses compared to other iGluRs. For example, they have been detected in mossy fibre to CA3 pyramidal neurons, the synapses between Schaffer collaterals and CA1 interneurons, at thalamocortical connections, and in the basolateral amygdala (Pinherio and Mulle, 2006; Contractor et al., 2011; Lerma and Marques, 2013).

1.2.3.5.1 Presynaptic KARs

In addition to their contribution to postsynaptic depolarisation, KARs have other physiological roles in neuronal transmission that allow them to act as modulators of synaptic transmission. KARs have been found presynaptically to regulate both excitatory and inhibitory neurotransmitters release (Chittajallu et al., 1996; Pinheiro and Mulle, 2008; Contractor et al., 2011).

One of the examples of presynaptic KARs regulating excitatory neurotransmitters release is at mossy fibre-CA3 synapses, which contribute to the

complexity of KARs function at this synapse. Presynaptic KARs at these synapses are activated by the released glutamate following a single action potential and are release facilitators by enhancing Ca^{2+} signals (Schmitz et al., 2001; Contractor et al., 2001; Lauri et al., 2001; Pinheiro et al., 2007). However, kainate as an exogenous agonist regulates the neurotransmitter release according to the agonist concentration and synapse type (Huettner, 2003; Lerma, 2006; Pinheiro and Mulle, 2008). In general, KAR-mediated synaptic transmission is promoted by low-moderate kainate activation and reduced by a strong stimulation of kainate (Schmitz et al., 2001). On CA1 pyramidal cells, presynaptic GluK2-containing KARs are involved in GABA release inhibition upon kainate stimulation (Mulle et al., 2000) and GABA release facilitation at inhibitory synapses on CA1 interneurons (Mulle et al., 2000; Cossart et al., 2001).

The subunit composition of KARs differs between pre- and post-synaptic sites. GluK1-containing KARs are targeted presynapticaly (Chittajallu et al., 1996; Vignes et al., 1998; Clarke and Collingridge, 2002) and GluK2/3 subunits mediate the presynaptic KAR at mossy fibres-CA3 synapses (Contractor et al., 2001; Schmitz et al., 2003; Breustedt and Schmitz, 2004; Pinheiro et al., 2007). GluK2/5 KARs are targeted postsynapticaly to the dendrites of the CA3 pyramidal neurons in the hippocampus (Isaac et al., 2004; Mulle et al., 1998). This differential subunit distribution implies the presence of mechanisms that regulate KARs trafficking and targeting in a subunit-specific manner (Figure 1. 6; Nasu-Nishimura et al., 2010).

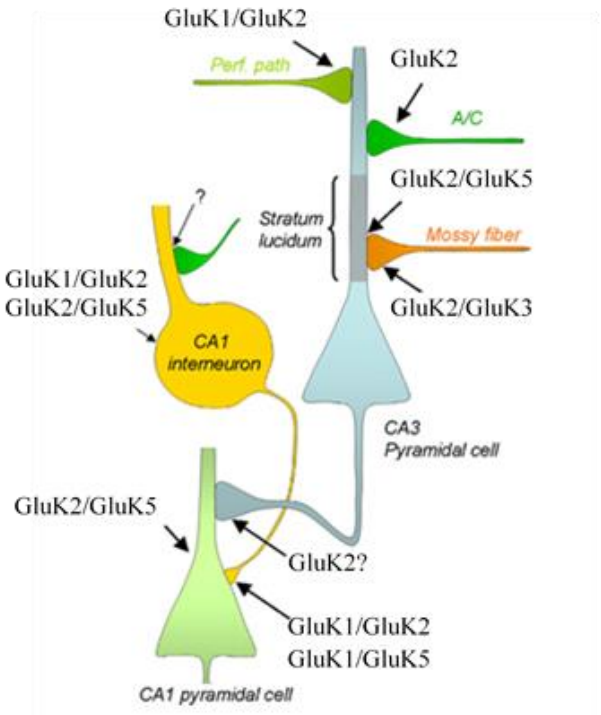

Figure 1.6. Expression and subcellular localization of KARs in hippocampal CA3 neurons network. The expression pattern of each subunit varies between different cell types. Notice the presence of postsynaptic KARs at synapses formed with mossy fibre inputs and their absence at distal synapses (on the same neuron) with associational/commissural (A/C) inputs. (Adapted from Pinheiro and Mulle, 2006).

1.2.3.5.2 Metabotropic signalling of KARs

In parallel to KARs ionotropic function, pre- and post-synaptic KARs signal through metabotropic mode of action where a second messenger is activated through a G–protein (Figure 1.7). This unconventional signalling pathway of an ion channel receptor functions in an unrelated manner to their ionotropic role.

Postsynaptically at mossy fibres-CA3 synapses, KAR activation leads to the slow afterhyperpolarisation (sAHP) inhibition and hence enhanced excitability (Ruiz et al., 2005; Chamberlain et al., 2013). In CA1 pyramidal cells, GluK2-containing KARs are activated by the synaptically-released glutamate and signal via metabotropic pathway involving a PKC-dependent mechanism to inhibit the sAHP current (Melyan et al., 2002). In dorsal root ganglion (DRG) neurons, which mainly express GluK1 and GluK5 KAR subunits and lack other iGluRs-mediated responses (Bettler et al., 1990; Bahn et al., 1994), high-frequency stimulation of KARs activates a G-protein signalling pathway that leads to PKC activation and the

Ca^{2+} release of intracellular Ca^{2+} stores (Rozas et al., 2003; Rivera et al., 2007). PKC phosphorylates serine residues in GluK1-2b subunit and triggers KAR internalisation. This feedback mechanism through KAR-metabotropic signalling works to limit neuronal overactivation by repetitive stimulation (Rivera et al., 2007).

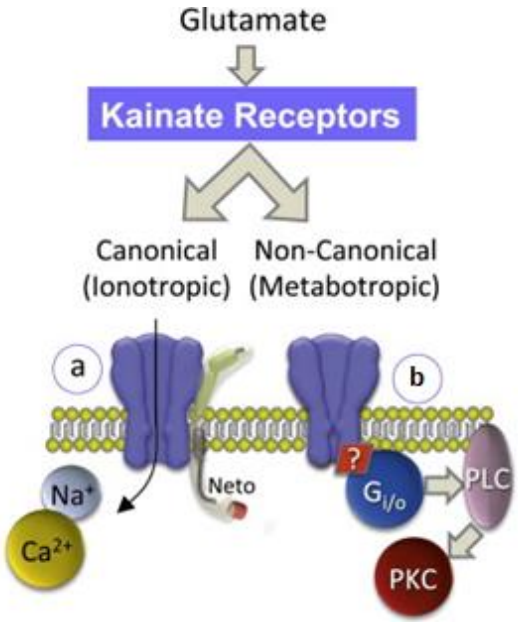

Figure 1.7. Two different pathways of KARs signalling. The ionotropic mechanism (a) is responsible for membrane depolarization and postsynaptic responses. These receptors incorporate auxiliary proteins, like Neto. The metabotropic signalling pathway of KARs activates G proteins (b) to stimulate phospholipase C and PKC in an independent way of ion flux. Neto proteins also regulate this function but the linker between the receptor and the G-protein is still unclear (Adapted from Lerma and Marques, 2013).

1.2.3.5.3 KARs' unique properties: slow kinetics

The EPSC-$_{KAR}$ identified a unique characteristic of KARs by exhibiting a lower amplitude and slow decay kinetics when compared to AMPARs-mediated currents at the same synapse (Figure 1.8). Originally, this distinct feature of EPSC-$_{KAR}$ was identified at mossy fibre-CA3 synapses (Castillo et al., 1997; Vignes and Collingridge, 1997). The EPSC-$_{KAR}$ recording identified one of several conserved principles of KARs signalling, which is their exceptionally

slow decay kinetics making the receptor gating temporal range extended (Copits et al., 2011; Copits and Swanson, 2012).

These unique properties of KARs kinetics were not matched with the fast kinetics of the overexpressed receptors in recombinant systems. The decay time constant of EPSC-$_{KAR}$ in most neurons is between 50-200 ms (Bannister et al., 2005; Castillo et al., 1997; Kidd and Isaac, 1999; Vignes and Collingridge, 1997). However, the values of deactivation (2-5 ms) and desensitization (5-10 ms) are much more reduced in the recombinant receptors, which have time constants similar to those of AMPARs (Dingledine et al., 1999; Erreger et al., 2004). These discrepancies between native and recombinant KARs formed in heterologous systems were solved by indicating that the receptor does not operate in isolation. The receptor interacts with auxiliary proteins (see below) to regulate its key properties as gating, pharmacology and subcellular localisation (Yan and Tomita, 2012; Tomita and Castillo, 2012).

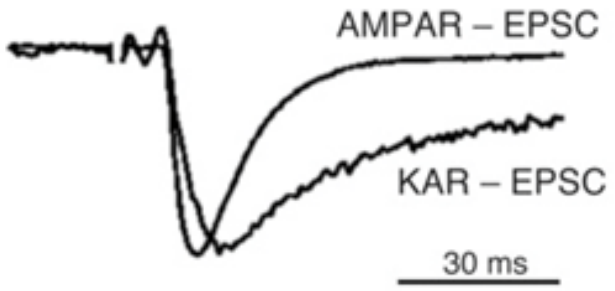

Figure 1.8. Distinct kinetics of KARs. The slow EPSCs-$_{KAR}$ (recorded in the presence of AMPAR antagonist) compared to the fast EPSCs-$_{AMPAR}$ at mossy fibre-CA3 synapses. (Adapted from Castillo et al., 1997).

1.2.3.6 KARs-protein interactions

KARs interact with several proteins that contribute to their targeting and function. They regulate the subcellular trafficking, synaptic localisation and channel gating of KARs. Many of these interactors are PDZ motifs and so are non-specific to KARs and interact with other iGluRs (Pinheiro and Mulle 2006; Contractor et al., 2011; Copits and Swanson 2012; Lerma and Marques 2013; Phal et al., 2014).

Such PDZ-containing proteins are the PSD-95, PICK1 (protein interacting with C kinase-1) and GRIP (glutamate receptor interacting protein), which were found to affect mainly KAR trafficking. For example, when PSD-95 binds the PDZ-binding domain in the C-terminus of KARs, it enhances KARs clustering and accelerates the recovery from desensitisation (Garcia et al., 1998; Bowie et al., 2003). In addition, other PDZ-domain proteins (PICK1 and GRIP) associate with the C-terminus of GluK1 and GluK2 and preserve KAR-mediated synaptic transmission at mossy fibre-CA3 contacts (Hirbec et al, 2003). The kainate receptor interacting protein for GluK6 (KRIP6) interacts with the C-terminus of GluK2a and modifies its functional properties (without affecting its surface expression) by decreasing the amplitude of the peak current and steady-state desensitisation, leading to decreased KAR-mediated transmission (Laezza et al., 2007; Contractor et al., 2011).

Another type of KAR-interacting proteins are the 4.1N proteins, which are spectrin-actin binding proteins (Copits and Swanson 2013). This interaction between the membrane-proximal domain in the C-termini of the KAR subunits and 4.1N is promoted by the post-translational modification palmitoylation of the KAR distal cysteine residues, preventing internalisation of the KAR (Figure 1.5). However, the post-translational modification phosphorylation antagonises this interaction, leading to receptor internalisation and reduced surface expression. The synaptosomal-associated protein 25 (SNAP-25) interacts with the KARs in an activity-dependent manner that increases PKC-dependent phosphorylation and leads to receptor internalisation (Selak et al., 2009). Furthermore, the coatomer protein complex I (COPI), which has a prominent role in the retrograde trafficking from the Golgi apparatus to the endoplasmic reticulum (ER), interacts with an ER retention motif (RRRRR) in the C-terminus of GluK5 preventing plasma membrane delivery (Vivithanaporn et al., 2006). However, when GluK5 forms heteromeric receptor with GluK2 its interaction with COPI is reduced to allow for plasma membrane expression. Recently, the C1q-like proteins (C1ql2 and C1ql3) released by mossy fibres in association with the presynaptic protein neurexin 3 isoform were found to interact with the amino terminal domain of KAR subunits and stabilise them postsynaptically at hippocampal mossy fibres-CA3 synapses (Matsuda et al.,

2016). In addition, C1ql2 and C1ql3 proteins provided by recurrent mossy fibres have recruited KARs in the dentate granule cells (DGCs) in a pilocarpine-based temporal lobe epilepsy (TLE) model (Matsuda et al., 2016).

1.2.3.7 Auxiliary proteins of KARs

Relatively new interacting proteins, neuropilin and tolloid like proteins (Neto2 and Neto1) were identified as KAR auxiliary subunits determining key properties of native receptors (Figure 1.9; Tomita and Castillo, 2012).

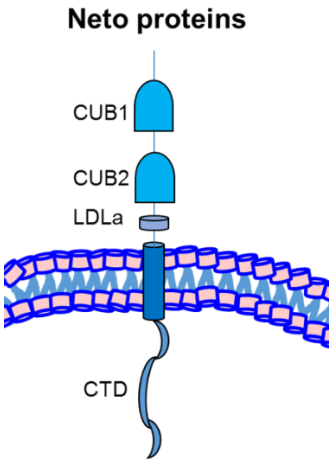

Figure 1.9. KAR auxiliary subunits (Neto2 and Neto1). Neto2 and 1 subunits are single-pass transmembrane proteins that have two extracellular CUB domains followed by a low-density lipoprotein class A (LDLa) domain, a transmembrane domain and an intracellular C-terminal domain (CTD) (Tomita and Castillo, 2012; Ng et al., 2009; Zhang et al., 2009; Michishita et al., 2003; Michishita et al., 2004).

The assembly process of Neto proteins with KARs affects almost all KAR signalling aspects, as channel gating properties, receptor pharmacology, and receptor trafficking in heterologous and neuronal systems (Copits and Swanson, 2012). Both receptor subtype and Neto isoform affect these aspects in receptor function (Copits et al., 2011; Straub et al., 2011a).

The next sections summarise the current evidence in support of regulating the above-mentioned key properties of KARs by their auxiliary subunits including Table 1.2, which also summarises the available evidence of Neto proteins-mediated regulation of KARs signalling.

1.2.3.8 Channel gating properties of KARs

Several studies observed that Neto2 protein slowed the desensitization and deactivation of glutamate-mediated currents from many homomeric and heteromeric subunit combinations (GluK1, GluK2, GluK1/5, GluK2/5) in heterologous systems and neurons (Figure 1.10A; Copits et al., 2011; Straub et al., 2011a; Straub et al., 2011b; Zhang et al., 2009). On the other hand, for Neto1, a bidirectional effect on receptor kinetics was obvious. Neto1 slowed the deactivation and desensitization of GluK2/GluK5 heteromeric receptors but, for GluK1 receptors speeded the entry into the desensitized state in recombinant systems (Figure 1.10 B) (Copits et al., 2011; Straub et al., 2011a). However, the rate of KARs recovery from desensitization is generally increased by both Neto2 and Neto1 (Copits et al., 2011; Straub et al., 2011a; Straub et al., 2011b; Zhang et al., 2009).

In vivo studies showed that KARs function was decreased in Neto1 knockout (Neto1 KO) mice as indicated by a severe deficit in EPSC-$_{KAR}$ and a faster decay kinetics at mossy fibre-CA3 synapses compared to wild-type mice (Figure 1.10C). However, the EPSC-$_{KAR}$ at mossy fibre-CA3 synapses from Neto2 knockout (Neto2 KO) mice was indistinguishable from wild-type mice (Straub et al., 2011a; Tang et al., 2011). Thus, Neto1 protein is required in the molecular mechanisms underlying the slow kinetics of mossy fibre EPSCs-$_{KAR,}$ which are thought to promote the initiation of action potential during recurrent bursts of input from the dentate granule cells (Copits and Swanson, 2012). In agreement with this, a study (Wyeth et al., 2014) reported that in wild-type and Neto2 KO mice, the spontaneous EPSC-$_{KAR}$ (isolated by applying the AMPAR antagonist, GYKI-53655) at mossy fibres-CA3 synapses was detected and exhibited slow kinetics (means no alterations in decay kinetics by Neto2 deletion). However, in Neto1 KO mice and Neto1/2 double KO mice, the spontaneous EPSCs-$_{KAR}$ were undetectable and the average decay time of spontaneous EPSCs (before GYKI-53655) was faster, which is consistent with the loss of the slow KAR contribution to a subset of the spontaneous EPSCs that was present in wild-type and Neto2 KO cells, given that the expression of Neto1 in the CA3 pyramidal cell layer predominates over Neto2 (Straub et al., 2011a). Considering the *in*

vivo results, it appears that Neto1 rather than Neto2 is required for normal KARs signalling at mossy fibre-CA3 synapses (Straub et al., 2011a).

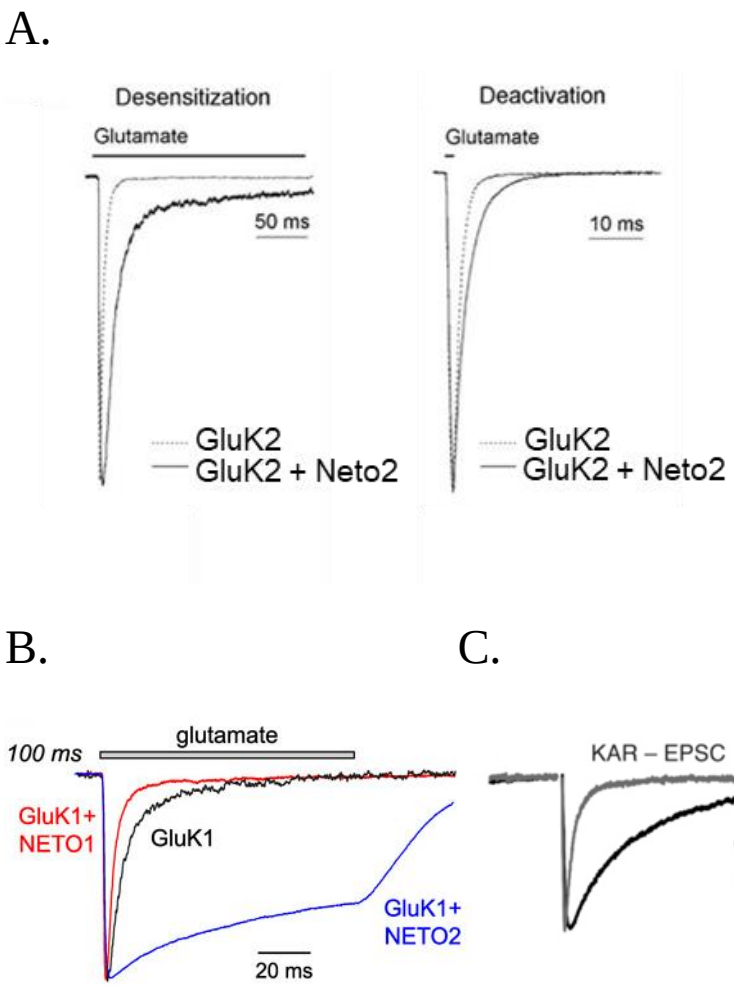

Figure 1.10. Neto proteins modulation of KAR kinetics. A, slowing of desensitization and deactivation by co-expression of GluK2 and Neto2 as identified by glutamate responses from cells transfected with GluK2 alone or GluK2 and Neto2. (Adapted from Zhang et al., 2009). **B**, GluK1 KAR desensitization was bi-directionally altered by Neto proteins. (Adapted from Copits et al., 2011). **C**, the accelerated decay kinetics of mossy fibre-CA3 EPSCs-$_{KAR}$ in Neto1 KO mice (Neto1 $^{-/-}$). (Adapted from Straub et al., 2011a). All amplitudes were normalised.

1.2.3.9 Pharmacological properties of KARs

The binding of [^{3}H]kainate in the hippocampus was determined in 3-genotypes; these were wild-type (WT), GluK2 KO, and Neto1 KO (Straub et al., 2011a). Compared with WT mice signal, the hippocampus of GluK2 KO mice had a reduced [^{3}H]kainate binding activity by almost 80% and Neto1 KO mice signal was 50%

less. This indicated the important role of Neto1 for kainate binding to its receptors as evidenced by the difference in K_D values for kainate (48.8 nM in wild-type and 202.6 nM in Neto1 KO calculated from kainate-binding curve) without any change in KAR expression. Additionally, kainate affinity for recombinant GluK2 receptors was enhanced by Neto1 co-expression (Straub et al., 2011a). Also, the efficacy of the partial agonist kainate relative to the full agonist glutamate was increased when Neto2 co-expressed with GluK2 in oocytes as evidenced by their kainate and glutamate-evoked currents compared to oocytes injected with only GluK2 (Zhang et al., 2009).

1.2.3.10 KAR trafficking, targeting, and localization

In a study (Wyeth et al., 2014) using postembedding immunoelectron microscopy to examine GluK2/3 expression at mossy fibre-CA3 synapses in wild-type and Neto1/2 double KO mice, fewer mossy fibre-CA3 synapses were labelled in Neto-null mice which showed the importance of Neto interactions for GluK2/3 postsynaptic targeting. However, contradictory results were obtained from different studies for the regulation of KARs localization by both Neto isoforms (Copits et al., 2011; Straub et al., 2011a; Zhang et al., 2009; Tang et al., 2011).

In Neto1 KO mice the expression of GluK2 and GluK5 was significantly reduced in hippocampal synapses (Tang et al., 2011). In contrast, the surface expression of the same subunits was not found to be significantly different between Neto1 KO and wild-type mice (Straub et al., 2011a). Moreover, in cultured hippocampal neurons the dendritic redistribution of GluK1 was not enhanced by the presence of Neto1 (Copits et al., 2011). On the other hand, the synaptic abundance of GluK2 and GluK5 was not different in the PSDs between Neto2 KO and wild-type mice (Tang et al., 2011). Additionally, GluK2 surface expression has not changed after Neto2 co-expression with GluK2 in oocytes (Zhang et al., 2009). However, surface expression of recombinant GluK1 was doubled by co-transfection with Neto2 in mammalian cells, indicating an enhanced trafficking of GluK1 by Neto2. Moreover, in cultured hippocampal neurons, co-expression of GluK1 with Neto2 not only promoted GluK1

localisation to the plasma membrane, but also redistributed these receptors to dendritic spines and sites of synaptic contact (Copits et al., 2011).

In summary, the comparison of research results obtained from various labs that used different experimental protocols to identify the roles of Neto proteins on several aspects of KAR function is challenging. It is worthy that the effects of Neto proteins on all predominant KARs subtypes in the CNS be investigated under the same experimental conditions. Nevertheless, we can still extract some general rules from all these studies. Moreover, we should take into consideration some of the issues not addressed in previous work regarding the composition of KAR protein complexes and their stoichiometry:

1. How many molecules of the Neto proteins could be included into a tetrameric ion channel?

2. Can both Neto proteins be incorporated into the same KAR ion channel?

3. Do Neto proteins compensate for each other in case one of them was absent?

Table 1.2. A summary of the literature regarding Neto protein-mediated regulation of KAR signalling.

Property/Neto isoform	Neto2	Neto1	Reference
Trafficking and distribution	No effect on GluK2 and GluK5	Regulate synaptic abundance of GluK2 and GluK5 in hippocampal PSD (Neto1 KO mice)	Tang et al., 2011
	Increase GluK1-2a and GluK1-2b surface localization in COS-7 cells Increase GluK1-2a surface and dendritic localization to spines in transfected rat hippocampal neurons Co-localise GluK1-2a with PSD-95 and bassoon	No increase in GluK1-2a surface and dendritic localisation in transfected rat hippocampal neurons No co-localisation with the PSD-95 and bassoon	Copits et al., 2011
	No effect on GluK2 surface expression in Xenopus laevis oocytes GluK2 increases Neto2 surface expression when co-expressed in oocytes		Zhang et al., 2009

	Absence of GluK2 (KO) from mice cerebella, reduces total and surface Neto2.		
	Regulate GluK2 localisation in PSD in the cerebellum (Neto2-null mice)		Tang et al., 2012
	Increase surface expression of GluK1, 2, and 3 in HEK293T cells	Increase surface expression of GluK1, 2, and 3 in HEK293T cells	Palacios-Filardo et al., 2016
	Does not regulate synaptic targeting of GluK2 in CA1 and CA3 pyramidal neurons	Does not regulate synaptic targeting of GluK2 in CA1 and CA3 pyramidal neurons	Sheng et al., 2017
	Regulates the expression of synaptic GluK2/3 and GluK5 in the medial prefrontal cortex, amygdala, and hippocampus (fear-related brain regions)		Mennesson et al., 2019
		No effect on hippocampal GluK2/3 & GluK5 surface expression, synaptic localisation and surface GluK2 in oocytes No effect on synaptic localisation (SL of CA3 and hippocampal PSD) of GluK2 and GluK5 Reduced from mouse hippocampal PSD when GluK2 is knocked out	Straub et al., 2011a

		Maintain normal PSD abundance (targeting or stability) of GluN2A-containing receptors at CA1 synapses No effect on PSD-95 and NMDAR subunits (GluN1, GluN2A, GluN2B) surface expression	Ng et al., 2009
	Enhance postsynaptic localisation of GluK2/3 on CA3 pyramidal cell spines		Wyeth et al., 2014 (dKO study)
Receptor desensitisation and deactivation	No effect on KAR decay kinetics at MF-CA3 synapses	Slow KAR decay kinetics	Tang et al., 2011
	Slow GluK1-2a and GluK1-2b desensitisation in HEK 293T cells	Increase GluK1-2a desensitisation in HEK293T cells	Copits et al., 2011
	Slow GluK2 desensitisation in tsA201 cells and co-transfected cerebellar granule cells (GluK2 K696R + Neto2) Slow GluK2 deactivation in tsA201 cells		
	Slow GluK1 and 3 desensitisation in HEK293T cells.	Increase GluK1 and 3 desensitisation in HEK293T cells.	Palacios-Filardo et al., 2016

	Reduce GluK2 desensitisation in HEK 293T cells	Reduce GluK2 desensitisation in HEK 293T cells	
		Slow GluK2/GluK5 desensitisation and deactivation in tsA201 cells Slow KARs decay kinetics in hippocampal CA3 region	Straub et al., 2011a
	Slow GluK1, GluK1/5 and GluK2/5 desensitisation and deactivation in tsA201 cells		Straub et al., 2011b
	Slow GluK1 & GluK2 desensitisation in HEK293 cells	Increase GluK1 desensitisation onset (agonist sites are saturated) and slow desensitisation onset when receptor unsaturated in HEK 293 cells	Fisher, 2015
Recovery from desensitisation	No effect on GluK1-2a recovery in HEK293T cells	Increase GluK1-2a recovery in HEK293T cells	Copits et al., 2011
	Increase GluK2 recovery in tsA201 cells		Zhang et al., 2009
	Increase GluK2 recovery but not GluK1 and 3 in HEK 293T cells	Increase GluK1, GluK2 and GluK3 recovery in HEK 293T cells	Palacios-Filardo et al., 2016
		Increase GluK2/GluK5 recovery in tsA201 cells	Straub et al., 2011a

	Increase Gluk1, GluK1/5 and GluK2/5 recovery in tsA201 cells		Straub et al., 2011b
	Increase GluK2 recovery but not GluK1 in HEK293 cells	Increase GluK1 and GluK2 recovery in HEK293 cells	Fisher, 2015
KAR currents	No effect on $EPSCs_{-KAR}$ at MF-CA3 synapses	Enhance $EPSCs_{-KAR}$ at MF-CA3 synapses of CA3	Tang et al. 2011
	Increase GluK1-2a and GluK1-2b current peak amplitude in HEK293T cells Detectable $EPSC\text{-}_{KAR}$ in transfected neurons with Gluk1-2a and Neto2 under conditions of elevated release probability		Copits et al., 2011
	Enhance GluK2 kainate and glutamate-evoked currents in oocytes when co-expressed Reduce kainate and glutamate-evoked currents in hippocampal neurons when Neto2 expression was suppressed Increase GluK2 steady state and peak currents in tsA201 cells		Zhang et al., 2009

	Enhance GluK2 (K696R) miniature EPSCs when both were co-transfected in cerebellar granule cells Slow the decay of spontaneous EPSCs when GluK1 was transfected in neurons		
	Increase steady state currents of GluK1, GluK1/5 and GluK2/5 in tsA201 cells		Straub et al., 2011b
	No effect on metabotropic KAR signalling	Regulates ionotropic and metabotropic KAR signalling in CA3 pyramidal cells (reduced when Neto1 is absent)	Wyeth et al., 2014
KAR pharmacology	Highly increase GluK1 glutamate affinity in HEK 293T cells Modestly increase GluK2 glutamate affinity in HEK293T cells	Highly increase GluK1 glutamate affinity in HEK 293T cells Modestly increase GluK2 glutamate affinity in HEK293T cells	Palacios-Filardo et al., 2016
		Increase GluK2 kainate affinity when Neto1 is overexpressed in HEK293T cells with GluK2 and in hippocampal membranes compared to Neto1 KO mice	Straub et al., 2011a

		Increase GluK2/5 glutamate affinity when expressed in tsA201 cells	
	Increase GluK1-glutamate sensitivity in HEK293 cells	Increase GluK1-glutamate sensitivity in HEK293 cells	Fisher, 2015
Regulation in development	Enhance KAR modulation of DRG neuron processes outgrowth (regulate neurite regrowth in adult sensory neurons following nerve injury)		Vernon and Swanson, 2017
	Promote axonal targeting of KAR subunits in mice hippocampal neurons	Promote axonal targeting of KAR subunits in mice hippocampal neurons Guide the development of rodent hippocampal CA3-CA1 circuitry Required for GluK1 tonic suppression of glutamate release early postnatally	Orav et al., 2017
	Regulate presynaptic KARs affinity to kainate at CCK/CB1 interneurons (reduced agonist sensitivity in Neto2 KO)	Facilitate presynaptic KARs activation at CCK1/CB1 interneurons leading to tonically supressing their release Increase kainate activation of interneuronal somatodendritic KARs leading to inhibitory currents in CA3 pyramidal cells	Wyeth et al., 2017

	No effect on the visual cortex pyramidal cells maturation	No effect on the visual cortex pyramidal cells maturation Promote dendrites elongation of visual cortex interneurons through regulating GluK1	Jack et al., 2018

1.2.3.11 The expression profile of KAR subunits during development

KAR subunits expression was identified previously at the mRNA level (Bahn et al., 1994; Wisden and Seeburg, 1993; Ritter et al., 2001; Ritter et al., 2002). Table 1.3. Summarises the available evidence of KAR subunits expression in the developing and adult brain.

The expression of the KAR subunit transcripts starts in the embryonic brain and peaks around birth (late embryonic and early postnatal) (Bahn et al., 1994). The peak levels of GluK1 are detected in the sensory cortex, thalamus, and in the interneurons of the stratum oriens of hippocampal CA1 region (all in the perinatal period of E19 to P5) and late postnatally (P12) in the Purkinje cells of the cerebellum and thereafter. Other hippocampal regions (CA3 and DG) have a very weak signal at any age.

The peak levels of GluK2 are found in the thalamus prenatally (E17 and E19) after which they decline; in the granular cerebellar cell layer at birth and continue thereafter; and in hippocampal CA3 and DG late postnatally (P12) till the adulthood (Bahn et al., 1994). Other brain regions (inner cortical layers and hippocampal CA1) show a weak labelling throughout development and until the adulthood. After a few days of birth, 50% and 80% of the GluK1 and GluK2 mRNA, respectively, undergo Q/R editing rendering the receptor Ca^{2+} impermeable (Bernanrd et al., 1999). This is in contrast with the GluA2 subunit of AMPAR, which is almost completely edited after birth (Burnashev and Rozov, 2000).

The expression level of GluK3 (Bahn et al., 1994) peaks prenatally (E17 and E19) in the thalamus and early postnatally (P5) in hippocampal DG. It shows a very high expression level throughout development (E17 to the adulthood) in the cortex (embryonic) and inner cortical layers (P0 and thereafter).

GluK4 transcript expression (Bahn et al., 1994) is the most restricted of all other KAR subunits. It is expressed mainly in hippocampal CA3 and DG regions. It peaks in CA3 at birth and continues toward the adulthood, while it is weakly detected in the DG.

The expression of GluK5 (Bahn et al., 1994) is strongly detected all over the brain, especially in the cortex, caudate putamen, cerebellar granular cells, and hippocampus, late prenatally (E17) and continues toward the adulthood.

1.2.3.12 Functional roles of KARs during CNS development

KARs have important roles in neuronal networks maturation and developing synaptic connectivity (Pinheiro and Mulle, 2006; Lerma and Marques, 2013; Carta et al., 2014; Lauri et al., 2005; Lauri et al., 2006). Tonic activation of presynaptic KARs at CA3 synapses by ambient glutamate early postnatally decreases glutamatergic inputs to CA3 and CA1 pyramidal neurons and facilitates the release of glutamate on CA3 interneurons (Lauri et al., 2005; Lauri et al., 2006). This leads to neuronal network bursting upon high-frequency stimulation and synchronisation in the immature hippocampus (Lerma and Marques, 2013; Carta et al., 2014).

Furthermore, KARs differentially regulate filopodial motility during cerebral development (Tashiro et al., 2003). Activation of KARs promotes filopodial motility in immature slices of the hippocampus while inhibiting it in mature slices. This activation is bidirectionally regulated according to the agonist dose. Strong KAR stimulation inhibits axonal growth while a weaker stimulation promotes filopodial motility (Tashiro et al., 2003). Transient activation of GluK2-containing KARs mediates synaptic stabilisation by a fast growth cone stalling (Ibarretxe, 2007). This could be of importance in immature neurons when short glutamate signals contribute to increase the expression of GluK2-containing receptors at the plasma membrane promoting new synapses stabilisation (Martin et al., 2008). In addition, in GluK2-deficient mice, the maturation of hippocampal mossy fibre-CA3 synapses is delayed (Lanore et al., 2012), indicating the important role of KARs in developing neuronal connectivity (Lerma and Marques, 2013).

Subunit	Main embryonic expression	Main postnatal expression	Main adult expression	Study
GluK1 GluK2 GluK3 GluK4 GluK5	Cx , T CPu, T, Cx, CA1,3, Cb Cx, T, Cpu CA3 Cx, CPu, T, Cb, CA1 & 3	Cx (II), T, Purkinje, CA1 DG, CA3, Cb-g Cx (VI), DG Cx (VI), DG, CA3 Cx (II, VI), DG, CA1 & 3, CPu, Cb-g	Purkinje CPu, Cb-g, DG, CA3 Cx (VI) CA3 Cx (II, VI), DG, CA1 & 3, CPu, Cb-g	- Rat, mRNA expression - E14, E17, E19, P0, P5, P12, Adult - Cx, CPu, HP, T, Cb - Bahn et al (1994)
GluK1 GluK2 GluK3 GluK4 GluK5			T, Purkinje Cb-g, DG Cx (VI), T, DG, CPu DG, CA3 Cx (II, VI), DG, CA1 & 3, CPu, Cb-g, T	- Rat, mRNA expression - Adult - Cx, CPu, HP, T, Cb - Wisden & Seeburg (1993)
	At birth main expression	Early postnatal	Late postnatal	- Rat, mRNA expression - Postnatal day 1 to 35 - HP (CA1-4, DG) - Ritter et al (2002)
GluK1 GluK2 GluK3 GluK4 GluK5	CA1 CA2 & 3 CA1 & 2, DG CA2, 3 & 4 CA1, 2 & 3	CA1 & 2, DG CA1, 2 & 3 CA3 & 4, DG CA2, 3 & 4 CA1, 2 & 3	CA2 & 3 CA1, 2, 3 & 4 DG, CA3 CA2, 3 & 4 CA2, 3 & 4, DG	
	First-trimester (GD 89)	Second-trimester (GD 116)		- Human fetal, mRNA - GD 89 & 116 - Cortex - Ritter et al (2001)
GluK1 GluK2 GluK3 GluK4 GluK5	 Cx	 Cx Cx		

Table 1.3. A summary of KAR subunits transcripts expression in developing and adult brains. Cx: cerebral cortex, CPu: caudate putamen, Cb-g: cerebellar granular cell layer, T: thalamus, HP: hippocampus CA: hippocampal cornu ammonis, DG: hippocampal dentate gyrus.

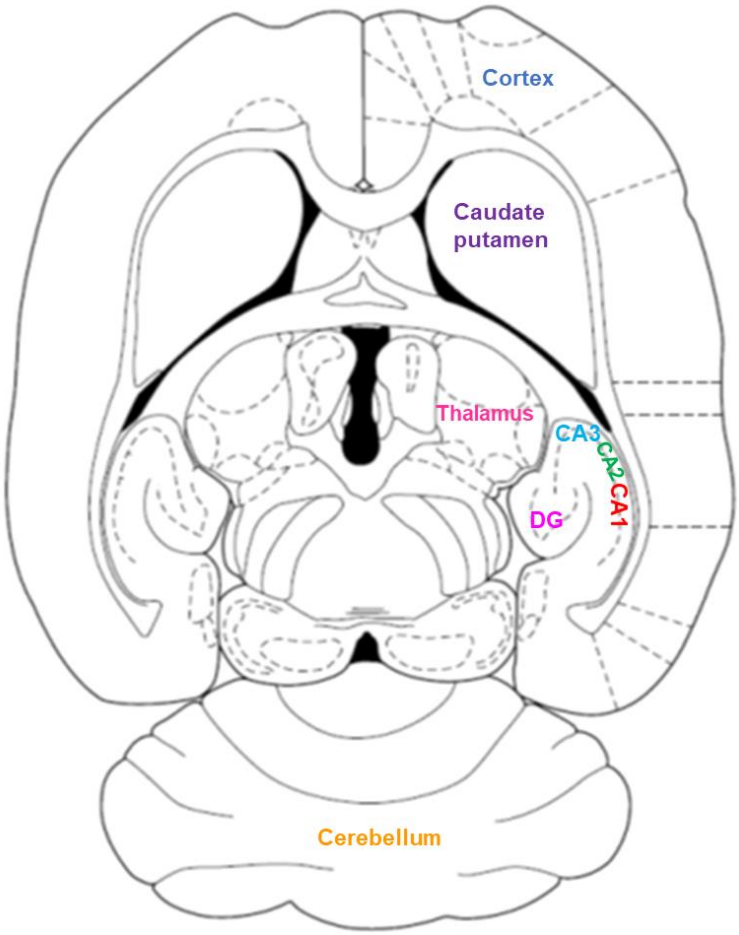

Figure 1.11. A schematic diagram of brain regions. The diagram illustrates the brain regions of Table 1.3. CA: hippocampal cornu ammonis, DG: hippocampal dentate gyrus.

1.2.3.13 KARs relevance in neurological disorders: Epilepsy

Epilepsy is a neurological disorder with spontaneous recurrent seizures and excessive, abnormal, and hypersynchronous neuronal activity (Crepel and Mulle, 2015). Approximately 50 million (~1%) people worldwide are affected by this disorder (Vizuete et al., 2018; Becker, 2018). The temporal lobe epilepsy (TLE), which affects the limbic system, is the most common form of partial epilepsy and resistance to anticonvulsive drugs in human (Vizuete et al., 2018; Crepel and Mulle, 2015). The term epileptogenesis summarizes the CNS mechanisms to acquire the capability to generate spontaneous recurrent seizures. The term addresses the cellular and structural mechanisms of turning a normal brain to an epileptic one after a transient insult. The generation of spontaneous recurrent seizures comes as

a result of equilibrium disruption between excitatory and inhibitory neuronal networks that leads to abnormal neuronal discharges (Casillas-Espinosa et al., 2012; Fukata and Fukata, 2017). Thus, disturbances in synaptic transmission play a role in the pathogenesis of seizures and epilepsy. This includes any component of synaptic transmission, like post- and pre-synaptic receptors and their interacting proteins (Casillas-Espinosa et al., 2012). Among receptors are the KARs, which are distributed throughout the brain pre- and postsynaptically modulating synaptic transmission and neuronal excitability (Contractor et al., 2011).

KARs modulation of the neuronal networks' activity is achieved by opposite direction in that, presynaptically, KARs facilitate glutamatergic transmission and others regulate GABAergic (γ-aminobutyric acid) transmission, whereas postsynaptically, glutamate excits both pyramidal cells and GABAergic interneurons and so the excitability is determined by the balance between the activation of distinct subtypes of KARs (Vincent and Mulle, 2009).

The role of KARs activation by glutamate in the induction and propagation of seizures in human and animal models of TLE epilepsy is not clear (Crepel and Mulle, 2015; Vincent and Mulle, 2009). The hippocampus in animal models of chronic epilepsy and human patients displays a phenomenon called reactive plasticity. This means major network remodelling (Coulter et al., 2002; Noebels et al., 2010; Ben-Ari et al., 2008) occurs in the hippocampus. Mossy fibres sprout forming *new* synaptic connections of recurrent excitatory circuits between dentate granule cells and this enhances epileptiform activity (Figures 1.12; Vincent and Mulle, 2009). The influence of mossy fibre inputs through these aberrant recurrent excitatory synapses onto DGCs is mostly via KARs (Vincent and Mulle, 2009, Peret et al., 2014).

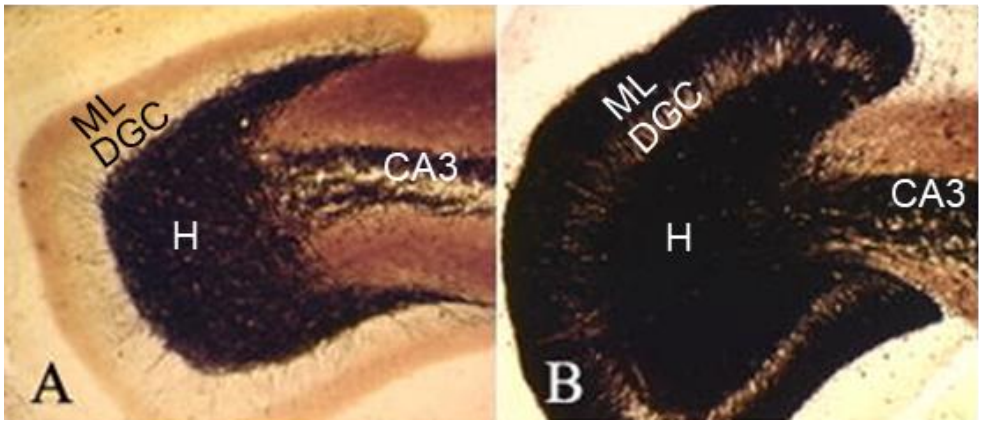

Figure 1.12. Hippocampal epileptic sprouting. These are DG hippocampal histological sections stained with Timm histochemistry. Mossy fibres (DGCs axons) projections are represented by the dark staining. **A,** normal rat DG showing heavy staining in the dentate hilus (H) and CA3 regions and absence staining in the dentate molecular layer (ML). **B,** the DG of an animal following status epilepticus shows obvious staining in the molecular layer which demonstrate mossy fibre sprouting into it. (Adapted from Cavazos and Cross, 2006).

Accordingly, a study investigated the role of these aberrant KARs in the generation of chronic and recurrent seizures in a pilocarpine model of chronic TLE using GluK2 KO mice and a GluK2/GluK5 receptor antagonist (UBP310; Peret et al., 2014). In this study, a strong reduction of both interictal and ictal activities was observed in the DG in GluK2 KO mice or with UBP310 use in wild-type mice, which demonstrated a role for GluK2-containing KARs at recurrent mossy fibre synapses in chronic seizures in TLE (see section 4.4.2.1 for further discussion of KARs role in epilepsy).

However, as the other iGluRs (AMPARs and NMDARs) contribute to the majority of the fast excitatory synaptic transmission in the brain, they also have been implicated in the process of epileptogensis. The imbalance between calcium permeable to impermeable AMPARs is related to epilepsy (Casillas-Espinosa et al. 2012). Furthermore, pharmacological targeting of AMPARs (e.g., the noncompetitve AMPAR antagonist perampanel) reduces seizure frequency in epileptic patients (Loscher and Schmidt, 2012; Rogawski and Hanada, 2013). NMDARs have been considered a target for developing new antiepileptic drugs as they have an important role in the regulation of excitatory neurotransmission in the brain by controlling synaptic plasticity (Casillas-Espinosa et al. 2012) (see sections

4.4.2.2 and 4.4.2.3 for further discussion of AMPARs and NMDARs role in epilepsy, respectively, and section 6.3 for the role of iGluRs).

By using animal models of epilepsy, we can improve our understanding of the above complex processes of synaptic transmission regulation in health and disease. Thus, facilitating the development of new therapeutic approaches for epilepsy as a significant percentage of all epileptic patients (15-35%) fail to achieve long-term remission with the currently available antiepileptic drugs (AEDs) (Shorvon and Goodridge, 2013). Moreover, research aiming to develop new, more efficacious AEDs, should use animal models simulating the chronic brain dysfunctions leading to epilepsy for the better understanding of its basic mechanisms (Loscher, 2002) and to enhance the model translational potential.

Animal models of TLE, that are used to study the process of epileptogenesis, include focal application of electrical stimulation (kindling) and chemical-inductive models (Sarkisian 2001). The most commonly studied chemical-inductive models of TLE are the kainate- and pilocarpine-induced models because they satisfy many of the criteria necessary for a good animal model including behaviours manifestations and pathological changes (Sarkisian 2001). In both models, status epilepticus (SE) is induced after administering the drug (kainate or pilocarpine) followed by a period of latency before the development of spontaneous recurrent seizures (SRSs, chronic epilepsy) (Sarkisian 2001). The hippocampus in these models displays major network remodelling (Coulter et al. 2002, Noebels et al. 2010) as the axons of the dentate granule cells, mossy fibres, sprout 2-3 weeks after SE forming new aberrant functional synaptic connections on the dendrites of granule cells in the inner molecular layer of the DG (Crepel and Mulle 2015, Karoly et al. 2015, Crepel 2013, Koyama and Ikegaya 2004, Ben-Ari 2001, Sarkisian 2001). This forms recurrent circuits of excitation between dentate granule cells, which enhance epileptiform activity generation (Crepel and Mulle 2015, Karoly et al. 2015, Crepel 2013, Koyama and Ikegaya 2004, Ben-Ari 2001, Sarkisian 2001).

1.3 Hippocampal neuronal circuit and connectivity

The surface of the temporal lobe forms ~ 17% of the human cerebral cortex volume (Kiernan, 2012). This includes regions involved in the auditory, olfactory, vestibular, and visual senses, and in the perception of spoken and written language. The temporal lobe contains many brain regions including the hippocampal formation (hippocampus and subiculum), and the entorhinal cortex. The subiculum is a transitional area between the hippocampus and entorhinal cortex. Damage to the temporal lobe can be caused by infection, trauma, ischaemia, and neoplasia. This can stimulate or inhibit the previously mentioned functions (Kiernan, 2012).

The hippocampus is a three-layered cortex comprises two distinct sub-regions: the dentate gyrus and the hippocampus proper (consisting of CA3, CA2, and CA1) (Witter, 2010). These regions form two interlocked "C" shape folds of the cortical mantel. The curved structure of the hippocampus, macroscopically, resembles the ram horns, in Latin it is called cornu ammonis (CA). The name hippocampus is derived from Latin for sea-horse as the structure's shape resembles that of a sea horse.

The hippocampal formation is easily differentiated from the entorhinal cortex by the later having six layers. The hippocampus formation deepest layer has basal dendrites of principal cells and a mixture of afferent and efferent fibres and local circuitry interneurons. Superficial to this layer is the cell layer which has principal cells and interneurons. The most superficial layer, situated on top, has the apical dendrites of the neurons and the large majority of axons that provide inputs. These layers in the dentate gyrus are, respectively, represented as: the hilus, granular cell layer, and molecular layer (stratum moleculare, SM). In the CA regions, the deepest layer and cell layer are called stratum oriens (SO) and stratum pyramidale (SP), respectively. The superficial layer is sub-divided into three (CA3) or two (CA1-2) sub-layers. The CA3 layers are the stratum lucidum (SL) where dentate gyrus mossy fibres inputs synapse, the stratum radiatum (SR) which have the apical dendrites of the stratum pyramidale neurons, and the stratum lacunosum-moleculare (SLM) which have the apical tufts of the apical dendrites. CA2 and CA1 lamination is similar to CA3 except there is no stratum lucidum. In the subiculum, layers are the stratum oriens (the deep layer) which is very thin and usually not specifically differentiated from the underlying white matter of the brain, the stratum

pyramidale, and the molecular layer (superficial layer). The hippocampal formation sub-regions are connected sequentially. The dentate granule cells provide a massive projection of axons called mossy fibres to CA3. Mossy fibres terminals are unique in their large size and their correlation with complex postsynaptic specialisations called thorny excrescences. On their way to CA3, mossy fibres contact large cells in the hilus called mossy cells. In addition, they form many collaterals that contact interneurons in the hilus. In turn, hilar mossy cells project axons to the dentate inner molecular layer to provide excitatory inputs to the proximal dendrites of the dentate granule cells. In contrast, hilar interneurons provide inhibitory inputs to the outer part of the molecular layer. Collaterals of CA3 axons contact dendrites of interneurons and spines of CA3 pyramidal cells which form a strong autoassociative network that characterise the CA3 connections. CA3 axons that project to CA1 are called Schaffer collaterals. They target CA1 interneurons and pyramidal cells in SR and SO. CA1 pyramidal cells project to the apical dendrites of the pyramidal neurons of the subiculum (the inner half of the molecular layer).

Neuronal cells in cortical regions, including the hippocampus, are broadly divided into two main types: principle or projection neurons (~80-90% of neuronal population) and interneurons. Principle cells are glutamatergic, excitatory neurons, whereas interneurons are GABAergic, inhibitory neurons. Hippocampal principle cells include CA pyramidal cells, DG granule cells, and mossy cells of the hilus. Each type of these cells form largely homogeneous populations. Pyramidal cells of CA areas are characterised by a pyramidal or ovoid soma in the stratum pyramidale, large-calibre apical dendrites in the stratum radiatum (form a dendritic tuft in stratum lacunosum-moleculare), and a number of small-calibre basal dendrites in the stratum oriens. DG granule cells are densely packed in the granule cell layer with small and round or ovoid cell bodies. They have bipolar morphology, spiny dendrites from the upper pole of the soma and an axon from the base. This axon, the so –called mossy fibre, provides the major output of the DG to the CA3 with its unique feature of large boutons that contact large complex spines in stratum lucidum of CA3 and mossy cells in the hilus. Hilar mossy cells have large triangular or ovoid soma with

large complex spines on proximal dendrites similar to CA3 proximal apical dendrites.

GABAergic interneurons have extensive local axonal arborisation to provide inhibitory innervation and control the activity of large sets of local neurons. Interneurons are heterogeneous in their morphology, physiological properties and neurochemical markers. They can be sub-divided into two main classes based on postsynaptic targets, perisomatic and dendritic inhibitory cells. Perisomatic inhibitory interneurons include basket cells and axo-axonic cells. They innervate soma, proximal dendrites, and axon initial segment of principle cells. Dendrite-inhibiting interneurons include many distinct types (bistratified, O-LM, and neurogliaform interneurons). They innervate various parts of their target cells dendritic tree. Different types of interneurons express a wide range of molecular markers. These include calcium-binding proteins (parvalbumin, calbindin, calretinin), neuropeptides (somatostatin, cholecystokinin, neuropeptide Y), and certain enzymes (nitric oxide synthase).

The entorhinal cortex is sub-divided into a medial (mEC) and a lateral (lEC) part. The six entorhinal cortex layers are: the molecular layer (layer I), the stellate cell layer (layer II), the superficial pyramidal cell layer (layer III), a cell-sparse lamina dissecans (layer IV), the deep pyramidal cell layer (layer V), and a polymorph cell layer (layer VI).

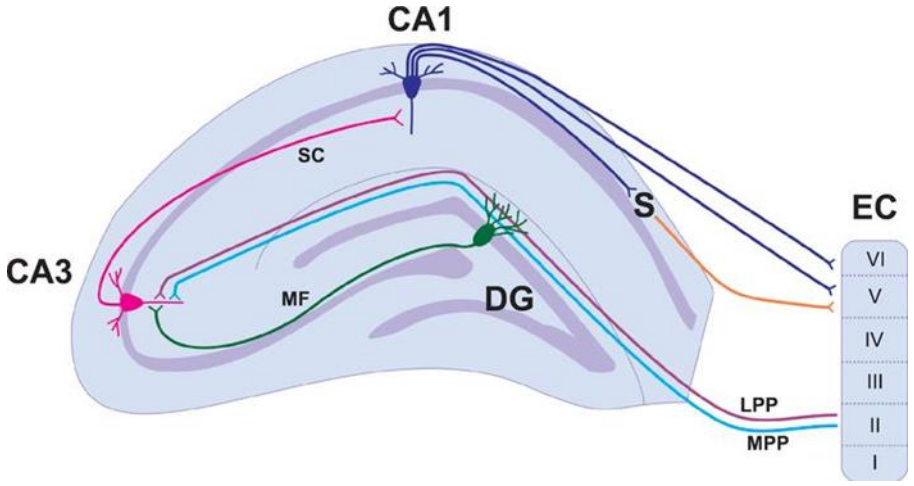

Figure 1.13. Schematic illustration of hippocampal neuronal connectivity. A schematic drawing illustrating the hippocampal network. The basic neuronal circuit of the hippocampus is commonly called the trisynaptic circuit: the entorhinal cortex (layers II and III) provides the main cortical input to the hippocampus, with its strongest projections by the perforant pathway to the dendrites of granule cells of the dentate gyrus

(DG) (Synapse 1). The DG targets the apical dendrites of the pyramidal cells in CA3 via mossy fibres (Synapse 2). CA3 pyramidale neurons contacts the apical dendrites of CA1 pyramidale cells via Schaffer collaterals (Synapse 3). Finally, CA1 pyramidal cells project back to the subiculum and entorhinal cortex (layers V and VI), completing the loop. Abbreviations: Cornu Ammonis (CA); Dentate Gyrus (DG); Entorhinal Cortex (EC); Lateral Perforant Path (LPP); Medial Perforant Path (LPP); Mossy Fibres (MF); Schaffer Collaterals (SC); Subiculum (S) (Adapted from Patten et al., 2015).

The main source of input to the hippocampal formation is the entorhinal cortex through the perforant pathway with projections aim at all sub-regions of the hippocampal formation. Layer II of the entorhinal cortex provides input to the dentate gyrus and CA3, while layer III aims at CA1 and the subiculum. Inputs from layer II of the lEC terminate in the outer half of DG SM and CA3 SLM, whereas Layer II projections from the mEC terminate deep to the lateral fibres. Layer III projections of the lEC target SLM of CA1 distal part which is closest to the subiculum and the SM of the close by subiculum proximal part. In contrast, mEC inputs target SLM in the proximal part of CA1 and SM of the subiculum distal part. The return projections from the hippocampal formation to the entorhinal cortex terminate in layers V and VI (Figure 1.13).

1.4 Project aims

The *modulatory* role of KARs in synaptic transmission offers interesting perspectives as fewer side effects might be presented from interfering with KARs than interfering with other iGluRs (Vincent and Mulle, 2009). In line with this appealing idea (interfering with modulators), the following two points should be taken into account for investigating and understanding the underlying mechanisms of aberrant synaptic transmission:

1. In theory, designing compounds to modulate the auxiliary subunit function could enable KARs selective targeting according, for example, to auxiliary subunit regional expression. Thus, minimizing adverse effects by receptor targeting in specific areas.

2. Leaving the synaptic transmission untouched by interfering specifically with the pathophysiologic mechanisms through auxiliary

subunits, protein-protein interactions, or post-translational modifications targeting, is a more suitable therapeutic goal than targeting the receptors themselves.

Because the expression pattern and synaptic and cellular signalling of KARs can be profoundly different between mature and immature networks (Rodriguez-Moreno and Sihra, 2011) and the fact that they have a critical role in the development and maturation of neuronal networks with the underlying exact mechanisms remained undefined (Lerma and Marques, 2013), it is worthy to investigate the developmental dynamics in Neto protein expression patterns (which have not been identified yet) in the brain. This will allow us to establish the interplay between pore-forming and their auxiliary subunits aiming to understand the molecular basis that determine the variation in KAR subunit composition, cellular localisation and KAR function. In addition, KARs are modulators of neuronal excitability with distinct property of slow decay kinetics, when co-assembled with Neto subunits. This unique Neto-dependent characteristic of KARs allows maintaining longer currents and may be involved in epilepsy pathogenesis. Furthermore to Neto proteins, the activity of KARs is influenced by many post-translational modifications that affect receptor surface expression and hence may enhance/diminish their role in neuronal excitability/hyperexcitability. Palmitoylation of the GluK2 subunits promotes the receptor surface expression. However, it is unknown if changes to this PTM (non-palmitoylation) would lead to receptor internalisation and hence may have functional implications in hyperexcitable conditions like epilepsy.

Therefore, our *specific* aims are concentrated on Neto proteins developmental expression profile, KAR (and other iGluR) subunits expression in a new epileptic model that mimic human TLE, and the post-translational modification palmitoylation of GluK2 subunit. And, these are:

1. To identify the regional expression profiles of Neto proteins during brain development

2. To identify activity-induced changes in the expression level and molecular composition of iGluRs during the chronic phase of epilepsy using a refined lithium-low dose pilocarpine model (Modebadze et al. 2016).

3. To identify the effects of GluK2 non-palmitoylation on GluK2 phosphorylation, SUMOylation and internalisation under basal and agonist stimulation conditions.

2 Materials and Methods

2.1 Materials

2.1.1 Chemicals and buffers

The chemicals used throughout this work were purchased from Sigma-Aldrich (Gillingham, UK) unless otherwise mentioned. Solvents were obtained from Fisher Scientific (Loughborough, UK). Non-fat powdered milk was from The Co-operative Food Convenience Store (Bristol, UK).

2.1.2 Heterologous cell line culture

2.1.2.1 Cell lines

Human Embryonic Kidney 293T (HEK293T) cells were from The European Collection of Authenticated Cell Cultures (ECACC). Baby Hamster Kidney-21 (BHK-21) cells were obtained from the American Type Culture Collection (ATCC) stocks. Aliquots of the cells (mixed with 1% dimethyl sulfoxide (DMSO) were frozen in liquid nitrogen and used as our stock.

2.1.2.2 Cell culture media

Dulbecco's Modified Eagle's Medium (DMEM, Sigma-Aldrich) was used to maintain HEK293T cells after adding 10% heat inactivated foetal bovine serum (FBS, Biosera, East Sussex, UK), 1% penicillin/streptomycin (Gibco, Invitrogen) and 1% Glutamine (Gibco, Invitrogen).

Alpha-minimum essential medium (MEM, Gibco, Invitrogen) was used to maintain BHK cells after adding 5% heat inactivated foetal bovine serum and 1% penicillin/streptomycin.

2.1.3 Histobloting

Nitro-blue tetrazolium chloride (NBT, 34035) was from Thermo Fisher scientific (Newport, UK). DNase I recombinant, RNase-free (04716728001) was from Roche

(Mannheim, Germany). Nitrocellulose membrane (0.45 µm) was obtained from Thermo Scientific.

2.1.4 Protein biochemistry

Protease inhibitor tablets (Roche) and phosphatase inhibitor tablets (A32957, Pierce) were used in lysis buffers. Acrylamide (30% v/v, Geneflow Ltd, Lichfield, UK) was used for preparing SDS-PAGE (sodium dodecyl sulfate polyacrylamide gel electrophoresis) gels. PVDF (polyvinylidene difluoride) immobilon membrane (Millipore Ltd, Watford, UK) was used for transfer. PageRuler pre-stained protein ladder (26616, ThermoFisher Scientific, Newport, UK) was used as the protein molecular weight marker. Immobilon Western Chemiluminescent HRP Substrate (WBKLS0500, Millipore, Watford, UK) was used for signal detection.

2.1.5 Bacterial reagents

Escherichia coli (E. coli):

- Strain: DH5α (Thermo Fisher)
- Genotype: *supE*44 Δ*lac u169* (φ80 *lacZΔ* M15) *hsdR17 recA1 end*A*1 gyrA96 thi*-1 *rel*A1

2.1.6 Bacterial growth

Luria-Bertani (LB) broth was obtained from the stores of the University of Bristol to grow E. coli during DNA cloning and amplification.

Agar was mixed with LB broth and ampicillin then poured in plates under sterile conditions to culture E. coli.

2.1.7 Antibiotic containing media and agar plates

Ampicillin stock (100 mg/mL, 50% ethanol) stored at -20°C was diluted to 100 µg/mL in LB broth or LB agar to have a positive selection during cloning and plasmid amplification.

2.1.8 Molecular biology

2.1.8.1 Stock plasmids

Stock plasmid	Description
Neto subunit proteins constructs for overexpression [all in pcDNA3.1(-)]	
Untagged Neto2	Rat full length Neto2
FLAG-GFP-Neto2	Rat full length Neto2 tagged with FLAG-GFP N-terminally after the signal peptide
Untagged Neto1	Rat full length Neto1
FLAG-GFP-Neto1	Rat full length Neto1 tagged with FLAG-GFP N-terminally after the signal peptide
shRNA plasmids: all are in a plasmid called pXLG3-GFP-100bp-stuffer and they were provided by Dr Kevin Wilkinson.	
sh-scrambled	Target sequence of scrambled: AATTCTCCGAACGTGTCAC
sh-Neto2	Target sequence of Neto2: AGTGTTGCTAATAACGGTA
sh-Neto1-a	Target sequence of Neto1-a: GCAAGTTTAATCATCCTCCAT
sh-Neto1-b	Target sequence of Neto1-b: CGAGAATGTGTCTACATCATA
YFP-Myc-GluK2 constructs: rat GluK2a with an N-terminal YFP and 6-Myc tags in pcDNA3.1	
WT, K886R, S846A + S868A, and S868D constructs	Published previously (Konopacki et al., 2011)
C858A + C871A mutant	Made by Rumnique Hullait.
Others	
For Sindbis viruses	The previous YFP-Myc-GluK2 inserts are in the vector pSinRep5(nsP2S) (Kim et al., 2004).
FLAG-Ubc9	FLAG-tagged human Ubc9 in the vector pCMV-3xFLAG (Invitrogen) (Kantamneni et al., 2011)
FLAG-SUMO1	Human SUMO1 in the vector pEYFP-C1 (Clontech), obtained from Frauke Melchior (University of Heidelberg, Germany) (Pichler et al., 2002)

Table 2.1. A summary of the stock plasmid constructs.

2.1.8.2 DNA purification kits

The DNA purification kit GeneJET™ Plasmid Midiprep (K0481) was from Thermo Scientific.

2.1.9 Electronic devices

The following table summarises the used electronic devices.

Electronic device	Company
Bench-top centrifuges	Eppendorf Ltd (Stevenage, UK)
Shaking bacterial incubators	RS Biotech Laboratory Equipment Ltd (Ayrshire, UK)
GBOX-Chemi-XRQ system	Syngene (Cambridge, UK)
Electroporation machine: Bio-Rad Gene Pulser II	Bio-Rad (Kidlington, UK)
Confocal microscope (University of Bristol Wolfson Bioimaging Facility): Leica SP5-II confocal laser scanning microscope attached to a Leica DMI 6000 inverted epifluorescence microscope with the laser lines: 405, 488, and 633 nm.	Leica Microsystems (Milton Keynes, UK)
Dissection microscope	Leica Microsystems Ltd (Milton Keynes, UK)

Table 2.2. A summary of the used electronic devices.

2.1.10 Imaging fixation and preparation

Paraformaldehyde (PFA) 16% (Electron Microscopy Sciences, 50-980-487, Hatfield, UK) was used as a stock for fixing hippocampal cells. The mounting medium Fluoromount-G with DAPI (e-Bioscience) was used to mount the cells at the glass slide.

2.1.11 Plasticware and glassware

The following table summarises the used plasticware and glassware.

Type of plasticware/glassware	Company
Plastic pipette tips (10 to 1000 µL)	Starlab Ltd (Milton Keynes, UK)
Stripettes (5-25 mL)	Sterilin (Newport, UK)
Gel loading tips	Fisher (Loughborough, UK)
Glass coverslips (25 mm)	VWR International Ltd (Lutterworth, UK)
Glass slides (frosted end)	VWR International Ltd (Lutterworth, UK)
Sterile cell culture plasticware (6 and 10 cm dishes, 6-well plates, 75 cm^2 and 175 cm^2 flasks)	Cellstar Ltd (Bishop Stortford, UK)
0.5 and 1.5 mL tubes	Eppendorf Ltd (Stevenage, UK)
15 and 50 mL tubes	Falcon (Leicestershire, UK)

Table 2.3. A summary of the used plasticware and glassware.

2.1.12 Antibodies

The tables below (2.4, 2.5, and 2.6) summarise the used primary and secondary antibodies for histoblot, immunoblot and immunocytochemistry. Anti-GluK1 and -GluK4 primary antibodies were not included in our studies (chapter 3 and 4) because the commercially available tools were poorly performing in biochemical and histological experiments (Molnar's lab unpublished data). Imaging of immunoblot was performed using Syngene chemiluminescence GBOX-Chemi-XRQ system (Cambridge, UK).

Antigenic target	Clonality	Host	Dilution	Company/Reference	Catalogue #
GluA1	Polyclonal	Rabbit	1:1000	Millipore	04-855
GluA2	Polyclonal	Rabbit	1:4000	Millipore	AB-1768-I
GluA1-4	Polyclonal	Rabbit	1:2000	Pickard et al., 2000	-
GluK2/3	Monoclonal	Rabbit	1:1000	Millipore	04-921
GluK5	Polyclonal	Rabbit	1:1000	Millipore	06-315
GluN1	Monoclonal	Rabbit	1:1000	Cell Signalling (London, UK)	D65B7
GluN2B	Polyclonal	Rabbit	1:1000	Millipore	06-600
Neto1	Polyclonal	Rabbit	1:1000	Straub et al., 2011a	-
Neto2	Polyclonal	Rabbit	1:1000	Zhang et al., 2009	-
Alkaline phosphatase (AP)-conjugated secondary antibody					
Rabbit IgG	Polyclonal	Goat	1:4000	Sigma	A3687

Table 2.4. A summary of primary and secondary antibodies used for histoblotting.

Antigenic target	Clonality	Host	Dilution	Company/Reference	Catalogue #
Phosphoserine/threonine	Monoclonal	Mouse	1:1000	BD Biosciences (Wokingham, UK)	612548
Phosphoserine	Monoclonal	Mouse	1:1000	Sigma-Aldrich	P5747
Phosphoserine PKC substrate	Polyclonal	Rabbit	1:1000	Cell Signaling	2261
FLAG	Monoclonal	Mouse	1:1000	Sigma-Aldrich	F3165
GFP	Monoclonal	Rat	1:2500	Chromotek	3H9
GluK2/3	Monoclonal	Rabbit	1:1000	Millipore	04-921
β-Actin	Monoclonal	Mouse	1:10000	Sigma	A5441
Neto1	Polyclonal	Rabbit	1:1000	Straub et al., 2011a	-
Neto2	Polyclonal	Rabbit	1:1000	Zhang et al., 2009	-
Horseradish peroxidase (HRP)-conjugated secondary antibodies					
Rabbit IgG	Polyclonal	Goat	1:10000	Jackson ImmunoResearch (Ely, UK)	111-35-144
Mouse IgG	Polyclonal	Goat	1:10000	Jackson ImmunoResearch	115-35-003
Rat IgG	Polyclonal	Goat	1:10000	Jackson ImmunoResearch	112-35-175

Table 2.5. A summary of primary and secondary antibodies used for immunoblotting.

Antigenic target	Clonality	Host	Dilution	Company	Catalogue #
GFP	Polyclonal	Chicken	1:1000	Abcam Cambridge, UK)	Ab13970
Alexa Fluor® 647- conjugated secondary antibody					
Chicken	Polyclonal	Donkey	1:400	Jackson ImmunoResearch	703-606-155
Cyanine Cy™2-conjugated secondary antibody					
Chicken	Polyclonal	Donkey	1:400	Jackson ImmunoResearch	703-225-155

Table 2.6. A summary of primary and secondary antibodies used for immunostaining.

2.2 Methods

2.2.1 Histoblot (Chapters 3 and 4)

The histoblot technique has the advantage of displaying proteins in their anatomical distribution with a reliable consistency for immunolabelling that allows the levels of protein expression to be compared quantitatively in various brain samples (Benke et al., 1995; Wenzel et al., 1997; Tonnes et al., 1999; Molnar, 2016; Aguado and Luján, 2019).

Brain samples sectioning: Unfixed frozen brain samples (obtained from our collaborators) were transferred from -80°C to -20°C 24 hours before sectioning. Cryostat sections (10 µm, from Bregma -5.6 mm to Bregma -6.1 mm) of horizontally positioned rat brains were layered onto uncoated glass slides and stored at -20°C until histoblotting. Some of the sections were mounted on gelatine-coated glass slides for Nissl staining. They were left for air dry for at least 24 hours before Nissl staining.

Protein transfer, processing and blotting: Each frozen brain section was directly transferred onto a pre-wetted (Transfer buffer: 48 mM Trise-base, 39 mM glycine, 2% SDS, 20% methanol, pH 10.5) nitrocellulose membrane (0.45 µm, Thermo Scientific, 88025) by applying a weight for 30 s without lateral movement. Then, membranes were transferred into blocking solution [5% w/v skimmed milk powder in TBS-T (Tris-buffered saline, 0.1% Tween 20)] for one hour at room temperature (20-22°C) without agitation. Next, the membranes were rinsed briefly (for one minute) with TBS-T and incubated with DNase I solution (5 units/mL) at 37°C for 20 min to remove DNA which could mask protein epitopes. After a series of washing steps [RIPEA (Radioimmunoprecipitation assay) for 20 min then TBS-T 2X 10 min at 20-22°C on shaker], the membranes were incubated with a strip buffer (0.1 M Tris-HCl, 2% SDS, and 0.1 M β-mercaptoethanol, pH 7.0) at 45 °C for 1 h to remove adhering tissue residues. Following incubation in blocking solution (1 h at room temperature 20-22°C), the appropriate dilution of affinity-purified primary antibodies (Table 2.4) was applied in blocking solution at 4°C overnight (14-16 h). Bound primary antibodies were visualised using an alkaline phosphatase (AP)-conjugated anti-rabbit secondary antibody (1:4000, Sigma) after 90 min incubation at room temperature (20-22°C). A substrate solution [0.033% Nitro Blue Tetrazolium (34035) and 0.0165% 5-bromo-4-chloro-3-indolyl

phosphate (B6149) in AP buffer (0.1 M Tris-HCl, 0.1 M NaCl and 5 mM $MgCl_2$, pH 9.5)] was used to detect AP activity.

Identification and quantification of immunopositive brain structures: Adjacent cryostat sections were stained with Nissl stain to facilitate the identification of different brain regions. A standard desktop scanner was used to obtain consistent digital greyscale images of histoblots that are treated identically for semi-quantitative comparisons. Matlab R2015a software (The MatWorks, Inc) was used to quantify grayscale images through measuring pixel densities in required brain regions. An adequate number of circles (with an appropriate diameter for the region of interest as 0.08 mm) for each immunolabeled area (e.g., stratum lucidum of CA3) were used to measure its pixel density. Adjacent cresyl violet-stained sections are used for the identification of areas of interest (Figure 2.1). The average pixel density of ten circles of the image background was calculated and subtracted from the average pixel density from the area of interest. The ″n″ refers to the number of brains/animals analysed. Figure 2.1 shows the selection process of different brain regions for quantification using a Nissl stained brain section for illustration purposes.

During the histoblotting work on the the RISE model (chapter 4), the undergraduate students Emma Hardy and Katie Skobelski provided some technical assistance.

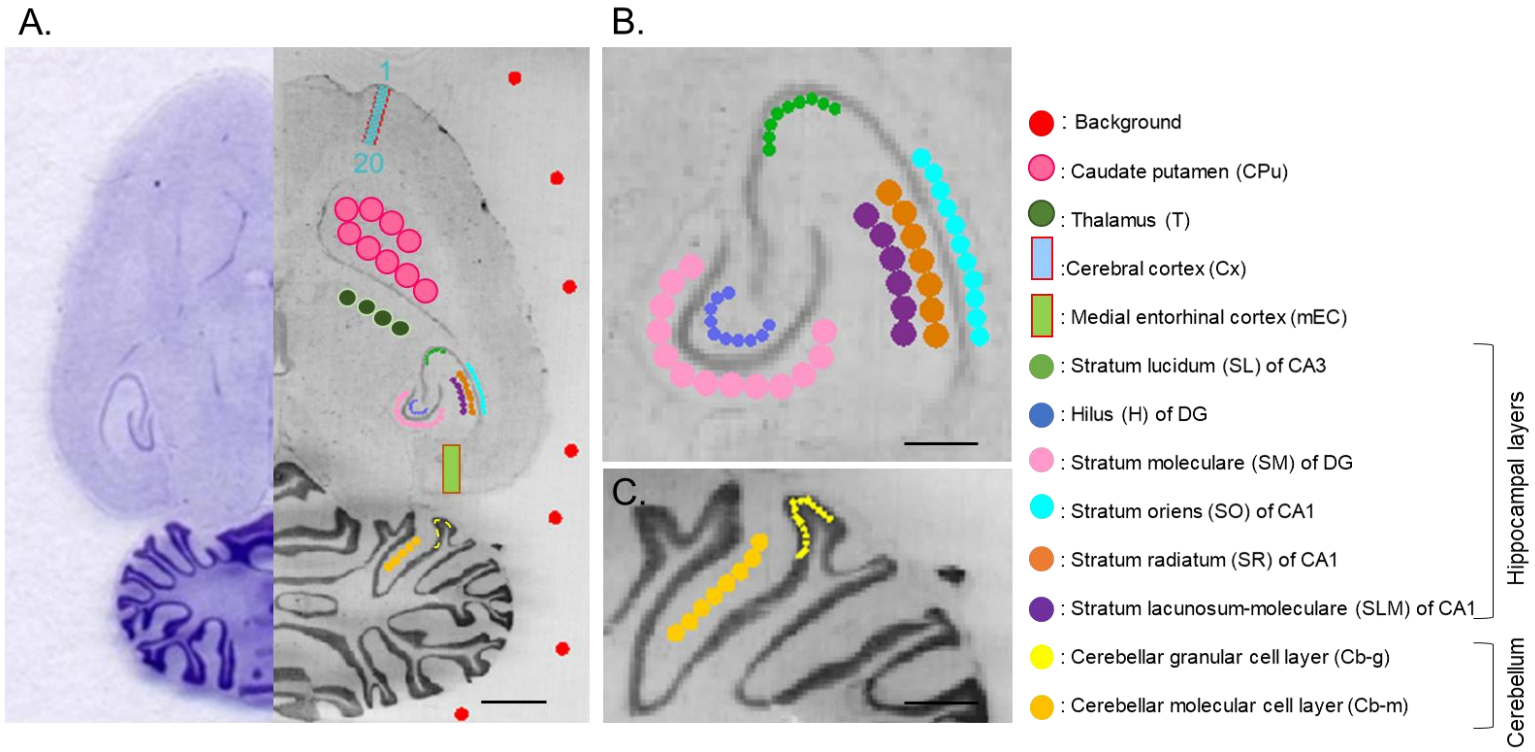

Figure 2.1. Brain regions selected for quantitative comparisons. The different regions are highlighted on Nissl-stained horizontal rat brain sections (**A**) and enlarged hippocampal (**B**) and cerebellar (**C**) regions according to the colour code. The Nissl staining highlights the cell body layers. For each region/sub-layer, a number of equal size circles was used to map the selected area and quantify its average pixel intensity except for the prefrontal and medial entorhinal cortex (mEC) where rectangles were used. Each rectangle was subdivided into 20 equal segments to map different cortical layers. The average pixel intensity of each circle/segment was measured by the Matlab R2015a software (The MatWorks, Inc) and then the pixel intensities of the six cortical layers were calculated using previously established procedures for the prefrontal cortex (Vilagi et. al., 2009) and mEC (Ray and Brecht, 2016). Scale bars: 2 mm (A), 1 mm (B, C).

2.2.2 Nissl staining (chapters 3 and 4)

For cresyl violet staining slides were immersed sequentially in each of the following for the indicated duration: 70% ethanol for 3-5 minutes, ddH_2O for 10 seconds, cresyl violet 0.1% for 30-45 minutes, 70% ethanol for 3-5 minutes and 100% ethanol for 5 minutes twice. Stain was checked, then slides were tapped-out onto a tissue paper to remove excess ethanol. Next, they were immersed in xylene twice for at least 15 minutes each time. After that, a drop of DPx mountant was placed on the stained section and a cover slip was placed gently over it using forceps. Air bubbles were removed by finger pressing down on the cover slip. Finally, slides were kept in the fume hood for 48 hours to dry.

2.2.3 Timm's silver sulphide staining (chapter 4)

Unfixed horizontal brain sections (10 µm) used for histoblotting were processed for autometallographic silver enhancement of zinc-enriched cells (Timm's staining; Jaarsma and Korf, 1990; Karoly et al., 2015). First, sections were allowed to dry at room temperature (20-22°C). Second, they were fixed using 0.1% sodium sulphide in 0.1 M phosphate buffer (pH adjusted to 7.3 with concentrated acetic acid) for 20 min in a fume cupboard. After that sections were washed with 96% ethanol twice (quick rise then for 6 min) followed by 50% ethanol for 10 min. Then, three washes with water for 5 min each. Next, sections were treated with freshly prepared Timm's classic physical developer (50% gum Arabic, 2 M citrate buffer pH 3.8, hydroquinone 5.67%, silver nitrate 17%) for 70-90 min with intermittent shaking in darkness. The following step was washing with 1% sodium acetate three times to stop the reaction. After the last wash, sections were placed on new glassware to prevent the subsequent gold solution from permanently staining the freshly silver-coated glassware. Following this, silver was replaced with 0.5% gold-toning solution, H[Au(Cl_4)], for 10 min. Again, sections were washed with 1% sodium acetate followed by 5% sodium thiosulphate for 5 min to remove gold ions. Finally, sections were washed briefly with water before mounting in DPx mountant. Sections were left to dry at the room temperature (20-22°C) and then scanned using a standard desktop scanner at a resolution of 1300 dpi. The differences in Timm's staining between the study groups

were assessed using one-way analysis of variance (ANOVA) at a confidence level of $p < 0.05$.

2.2.4 Cell culture (chapter 3 and 5)

Under sterile conditions, cell culture cabinets (Holten Safe LaminAir Thermo Fisher Scientific) were used for cell culturing.

2.2.4.1 Preparation of cell culture plates (chapters 3 and 5)

HEK293T cells: each cell culture plate (6-well plate or 6 cm dish) was coated with 100 µg/mL Poly-L-Lysine (PPL) for one hour. Then, plates were washed with sterile cell culture grade water (Hyclone, Fisher scientific) three times before adding 2-4 mL of complete DMEM (Plain DMEM supplemented with 1% L-glutamine, 1% Penicillin/Streptomycin, and 10% FBS).

2.2.4.2 HEK293T and BHK-21 cells thawing, passage and maintenance

Stored aliquots of HEK293T and BHK-21 cells in liquid nitrogen were taken out and placed in the cell culture water bath at 37°C to thaw. Next, cells were centrifuged at 1500 x g for 2 minutes after adding 10 mL of complete media. After that, they were suspended in 10ml of media before being transferred to a cell culture dish and placed in the cell culture incubator at 37°C and 5% CO_2.

When the cell confluency reached ~80%, cells were passaged by first washing them with Phosphate Buffer Saline (PBS) before treating them with 1-1.5 mL of 0.05% trypsin-EDTA of (Gibco) for 2-3 minutes at 37°C. Second, 9 mL of media were added using a pipette to dissociate cell aggregates. After that, 1 mL of this cell suspension was plated in a T75 flask that have 9 mL of pre-warmed (37°C) complete DMEM (HEK293T) or alpha-MEM (BHK-21). The remaining cell suspension was used to plate cells for transfection (HEK293T cells) or electroporation (BHK-21 cells).

2.2.5 Primary neuronal culture

2.2.5.1 Preparation of cell culture plates/glass coverslips (chapters 3 and 5)

6-well plates, 6 cm dishes or pre-treated glass coverslips (25 mm, VWR) were treated with 1 mg/mL PPL for overnight incubation. They were then washed with sterile cell culture grade water 3x before adding Neurobasal (Gibco, Invitrogen) plating media (supplemented with 5% Horse serum, 1% glutaMAX (Gibco, Invitrogen), 2% B27, and 1% penicillin/streptomycin).

Glass coverslips were pre-treated before PLL coating with 70% nitric acid overnight. They were then washed 3x in ddH_2O. Next, they were sterilised using 70% ethanol for 4 hours with gentle rotation. After that and under sterile conditions, coverslips were washed 3x with ddH_2O and kept in water until use. One coverslip was placed in each well of 6-well plate and coated with PPL before plating neurons.

2.2.5.2 Dissection

Wistar pregnant rat at embryonic day 17 (E17) was sacrificed according to the Home Office regulations (schedule 1). Then, the embryos were taken out and placed in HBSS (Hank's Balanced Salt Solution) prior to removing their heads. Brains were removed under the dissection microscope followed by the isolation of the hindbrains. The hemispheres were separated following the removal of meninges. Then, the hippocampus was dissected from the cortex and both were placed in two labelled 35 mm dishes filled with HBSS. Under sterile conditions, the collected hippocampi and cortex (after being chopped into smaller pieces of tissue using a sterile blade) were washed 3x in HBSS followed by adding 1 and 3 mL of trypsin-EDTA (Ethylenediamine tetra-acetic acid; final concentration 0.005%) to the dissected tissue in 9 and 30 mL of HBSS and incubated in water bath (37°C) for 9 and 15 minutes. Following this step, the tissue was washed again 3x with HBSS before a last wash with Neurobasal plating media. Next, 1 or 5 mL of plating media was used to dissociate the hippocampal and cortical cells using a one mL pipette. The cell suspension was diluted using 4 and 25 mL of plating media before cell density was established using trypan blue and a haemocytometer.

2.2.5.3 Maintaining neuronal culture

Primary cortical neurons were plated at 600,000 cells/well of a 6-well plate coated with PLL and filled with pre-warmed plating media. Hippocampal neurons were plated at 150,000 cells/glass coverslip (25 mm) coated with PLL and placed in a well of a 6-well plate filled with pre-warmed plating media. The media was changed to pre-warmed Neurobasal feeding media (plating media without Horse serum) 24 hours after plating the cells.

2.2.6 Biochemical methods (general)

2.2.6.1 Cell lysis

Cells (transfected HEK293T cells or virally infected cortical neurons counted using haemocytometer and plated at 600,000 cell/well) of a 30 mm well were lysed with 250 µL of either 2x Laemmli sample buffer (4% SDS, 20% glycerol, 0.004% bromphenol blue, 0.125 M Tris-Cl (pH 6.8), and 10% β-mercaptoethanol) or a cold lysis buffer as will be specified. Cell lysates were kept on ice for 30 minutes prior to centrifugation (21,000 x g, 4 °C, 30 min) to pellet cell debris. The supernatant was transferred into a new 1.5 mL pre-cooled tube and placed on ice for either mixing it with 2x Laemmli sample buffer or performing GFP-trap protocol to immunoprecipitate the protein of interest and then mixing the IP with 2x Laemmli sample buffer for SDS-PAGE (Sodium Dodecyl Sulfate Polyacrylamide Gel Electrophoresis).

2.2.6.2 SDS-PAGE

An 8%-10% SDS-PAGE running gel (375 mM Tris-HCl (pH 8.8), 8-10% acrylamide, 0.1% SDS, 0.1% APS, and 0.01% TEMED) was prepared to separate proteins. After gel polymerisation, the stacking gel was prepared (125 mM Tris-HCl (pH 6.8), 5% acrylamide, 0.1% SDS, 0.1% APS, and 0.01 TEMED) and layered on the top of the polymerised resolving gel. Then, a 10-15 well comb was placed into the stacking gel until it polymerised (~ 30 minutes). Next, a BioRad electrophoresis tank filled with running buffer (25 mM Tris base, 250 mM glycine, and 0.1% SDS) was used to run the samples after removing the comb and washing the wells with ddH_2O. Protein samples were

incubated at 95°C for 10 minutes after being mixed with 2x Laemmli sample buffer. The samples were allowed to cool to room temperature prior to being vortexed and centrifuged at 21,000 x g for 1 minute. After that, the samples and a pre-stained protein MW marker were loaded into the SDS-PAGE wells using gel loading tips. The samples were run starting at 90 V for ~ 15-20 minutes (until the ladder started to separate by reaching the resolving gel) and then at 120 V until the dye reached the bottom of the gel. The gel was removed and either used for electrophoretic transfer or was stained with Coomassie Brilliant Blue.

2.2.6.3 Immunoblotting

Wet transfer: Proteins were transferred (400 mA for 90-120 minutes) after electrophoresis from the SDS-PAGE gel onto a 0.45 µm PVDF membrane. The gel and membrane (pre-wetted with methanol first then transfer buffer) were faced onto each other between extra thick blotting paper (pre-wetted with transfer buffer). This was assembled in the transfer cassette and the membrane was put on the positive side (anode) so that proteins migrated from the gel into the membrane.

Immunoblotting: After the transfer process, the membrane was blocked in 5% non-fat milk powder in TBS-T (1x TBS + 0.1% Tween-20) for 1 hour with gentle shaking. Following this step, the membrane was incubated in the primary antibody prepared in 6% non-fat milk or BSA (Bovine Serum Albumin) in TBS-T overnight at 4°C or for 1 hour at room temperature. Next, the membrane was washed from the primary antibody 6x with TBS-T, each for 5 minutes on a shaker. Then, it was incubated in the HRP-conjugated secondary antibody (in 6% non-fat milk powder or BSA in TBS-T) for one hour with gentle shaking prior to three 5 min washing steps using TBS-T.

The transferred proteins were visualised using GBOX-Chemi-XRQ system after exposing the membrane to an HRP chemiluminescent substrate for 1-30 minutes at room temperature.

2.2.7 Transfecting HEK293T cells

HEK293T cells were plated in the PLL coated wells of a 6-well plate after being counted using a haemocytometer at 800,000 cells/well and left in the incubator for

two hours before being transfected. Forty minutes before transfection, the transfection mixture was prepared as follows:

For each transfection, 200 µL of plain DMEM was aliquoted into a 1.5 mL Eppendorf. Then, each target DNA (see table 2.7 for specific chapter details) was added to the appropriately labelled tube. Lipofectamine™ 2000 (Invitrogen) was added as 1.5x the total amount of DNA in each tube. The mixture was then briefly vortexed, centrifuged and left at room temperature (~22-24°C) for 30 minutes. Just before transfecting the cells, they were washed once in pre-warmed (37°C) plain media DMEM) and then 2 mL of pre-warmed (37°C) transfection media (complete DMEM without penicillin/streptomycin) were added to each well. After that, the transfection mixture was added dropwise to each well and mixed by gently rotating the dish before they were replaced into the incubator for 36-40 hours.

Table 2.7. A summary of target DNAs used to transfect HEK293T cells.

	Amount of target DNA for (co)transfecting HEK293T cells		
Transfecting HEK293T cells	**Target DNA-1**	**Target DNA-2**	**Target DNA-3**
Experiments done for chapter 3	0.5 µg Neto2		
	0.5 µg Neto2	1 µg sh-scrambled	
	0.5 µg Neto2	1 µg shNeto2	
	0.5 µg Neto2	1 µg shNeto1	
	0.5 µg Neto1		
	0.5 µg Neto1	1 µg sh-scrambled	
	0.5 µg Neto1	1 µg shNeto1	
	0.5 µg Neto1	1 µg shNeto2	
	0.5 µg GFP		
	0.5 µg GFP	1 µg sh-scrambled	
	0.5 µg GFP-Neto2	1 µg sh-scrambled	
	0.5 µg GFP-Neto2	1 µg shNeto2	
	0.5 µg GFP-Neto2	1 µg shNeto1	
	0.5 µg GFP-Neto1	1 µg sh-scrambled	
	0.5 µg GFP-Neto1	1 µg shNeto1	
	0.5 µg GFP-Neto1	1 µg shNeto2	
Experiments done for chapter 5	2 µg YFP	0.2 µg FLAG-SUMO1	0.1 µg FLAG-Ubc9

	2 µg WT YFP-Myc-GluK2	0.2 µg FLAG-SUMO1	0.1 µg FLAG-Ubc9
	2 µg C858A, C871A YFP-Myc-GluK2	0.2 µg FLAG-SUMO1	0.1 µg FLAG-Ubc9
	2 µg k886R YFP-Myc-GluK2	0.2 µg FLAG-SUMO1	0.1 µg FLAG-Ubc9
	2 µg S846A, S868A YFP-Myc-GluK2	0.2 µg FLAG-SUMO1	0.1 µg FLAG-Ubc9
	2 µg S868D YFP-Myc-GluK2	0.2 µg FLAG-SUMO1	0.1 µg FLAG-Ubc9
Experiments done for chapter 5 for mass spectrometry	2 µg WT YFP-Myc-GluK2		
	2 µg C858A, C871A YFP-Myc-GluK2		

HEK293T cells transfected with the Neto subunit protein constructs were lysed in 2x Laemmli sample buffer (2.2.6.1) and the samples processed as in sections 2.2.6.2 using 10% gel and transferred for 90 minutes (2.2.6.3). The membranes were immunolabelled for Neto2, Neto1, and GFP using the appropriate primary and HRP-conjugated secondary antibodies (Table 2.5).

2.2.8 GFP-trap protocol of transfected HEK293T cells (chapter 5)

GFP-trap protocol was used to immunoprecipitate GFP-fusion proteins (in this case YFP-tagged GluK2) from transfected HEK293T cell lysate. 36-40 hours after transfection, cells were checked under the fluorescent microscope for green color (YFP) to confirm the efficiency of the transfection. Then, medium was replaced with pre-warmed HBSS and the cells of each condition were treated with either a vehicle (water) or 100 µM kainate for 20 minutes. After kainate stimulation, cells were put on ice for 2-3 minutes before HBSS is aspirated. Cells were scraped after adding cold 400 µL/well lysis buffer (20 mM Tris-HCl (pH 7.4), 137 mM NaCl, 2 mM sodium pyrophosphate, 2 mM Ethylenediaminetetraacetic acid (EDTA), 1% Triton-X 100, 0.1% SDS, 25 mM β-glycerophosphate, 10% glycerol, 20 mM N-ethylmaleimide (NEM, freshly prepared), and 1x complete protease inhibitors) and put into 1.5 mL pre-labelled cold tubes. Then, five brief (~1 second) bursts of sonication (Misonix microson ultrasonic cell disruptor) at setting 5 were done. Cell lysate was then left on

ice for 20 minutes to allow for solubilisation. Next, lysate was centrifuges in a benchtop centrifuge at full speed (21,000 x g at 4°C for 20 minutes) to pellet cell debris.

During centrifugation, GFP-trap beads were aliquoted (7.5 µL/pulldown) and washed 3x with 500 µL wash buffer (lysis buffer without the protease inhibitors) at 1500 x g for 2 minutes each and left on ice immersed in buffer to avoid drying out. After the centrifugation, 20 µL (5%) of supernatant was taken as the total lysate sample to a pre-cooled fresh tube. The remaining supernatant was added to the washed GFP-trap beads (pulldown samples). These were rotated at 4°C for 1-2 hours. After pulling down the YFP-Myc-GluK2 from all conditions, the beads were pelleted by centrifugation at 1500 x g for 2 minutes at 4°C. The beads were washed 3x by re-suspension and centrifugation after which 40 and 20 µL of 2x Laemmli sample buffer was added to the beads and total lysate samples, respectively. All samples were heated to 95°C for 10 minutes and then left to cool for another 10 minutes. Just before loading the samples onto 8% gels, samples were briefly vortexed and centrifuged at full speed (21,000 x g) for one minute to pellet the beads.

GFP–trap protocol done for the ABE (acyl biotin exchange) assay and the mass spectrophotometry had 3 exceptions from the above protocol:

1. No kainate pretreatment
2. Lysis buffer for the ABE assay as in table 2.8 and for the mass spec is as above (2.2.8) with no NEM included.
3. Amount of GFP-trap beads/pulldown was 20 µL as the protein was not pooled from one well instead from 3-5 wells (ABE assay) and 3 wells (mass spec.).

2.2.8.1 Immunoblotting (chapter 5)

Samples were loaded onto an 8% acrylamide gel and starting to run on the stacking gel at 90 mV until they reached the resolving gel (marker proteins started to separate). Then, the voltage was changed to 120 mV for around 2 hours. Wet transfer was done at 400 mA for 90-120 minutes using PVDF membrane. Next, membranes were blocked in 6% BSA in TBS-T for at least one hour (1-2 hours) at room temperature (22-24°C) before being incubated with antibodies in the following order:

1. Mouse anti-phosphoserine (BD Biosciences 612548, 1:1000) in 6% BSA at 4°C overnight (~16 hours). Membranes were developed the next day with a very

sensitive HRP substrate (WBKLS0500, Millipore) after being washed from the primary antibody and incubated with anti-mouse HRP-conjugated secondary antibody (Sigma, 1:10000) for one hour at room temperature.

2. Since no signal was obtained with the anti-phosphoserine antibody, there was no need for stripping the membrane before incubating it with the anti-FLAG primary antibody. Mouse anti-FLAG (F3165 Sigma, 1:1000) in 6% milk powder was used to detect SUMOylated proteins (in pulldowns and total) overnight at 4°C. The next day membranes were washed (6x, 5 minutes each) and incubated with anti-mouse HRP-conjugated secondary antibody (Sigma) (1:10000) for one hour at room temperature before developing.
3. Membranes containing immunoprecipitated samples were stripped (Restore Plus Western Blot Stripping Buffer, Thermo Scientific) before re-probing with rat anti-GFP (3H9-100 Chromotek,1:2500 in 6% milk) for one hour at room temperature and then anti-rat HRP-conjugated secondary antibody (Sigma, 1:10000) for one hour at the room temperature (22-24°C).

2.2.9 Immunoprecipitation (IP) and acyl biotin exchange (ABE) assay (chapter 5)

The ABE assay was performed following recombinant GluK2 pull down step using the previous GFP-trap protocol (2.2.8) except for lysing the cells using the lysis buffer in table 2.8 added to it 50 mM NEM.

The first step (after the pulldown step) was to spin down GFP-trap beads at 1500 x g for one minute at 4°C to pellet the beads. The supernatant was removed, and the beads resuspended in 600 µL of lysis buffer + 10 mM NEM (N-Ethylmaleimide). For each sample, 1/3 (200 µL) was taken of the resuspended beads and added to a labelled pre-cooled tube to serve as negative control (no hydroxylamine treatment). The remaining 2/3 (400 µL) was used for hydroxylamine treatment. All tubes were topped up with lysis buffer + 10 mM NEM to a total volume of 500 µL/tube. Samples were left on ice for 10 minutes and then the beads were pelleted by centrifugation at 1500 x g for one minute at 4°C. Next, the samples were washed quickly once with stringent buffer (500 µL/tube) then 3x in lysis buffer pH 7.2. Following the last wash, freshly prepared hydroxylamine buffer (500 µL, pH 7.2) was added to each hydroxylamine-

treated beads with a final concentration of 1 M hydroxylamine. Lysis buffer (pH 7.2) was added to the corresponding negative control beads. Samples were left to rotate at room temperature (22-24°C) for one hour. Once hydroxylamine treatment was completed, the beads were washed once in lysis buffer (pH 6.2) and placed on ice after removing the supernatant. Next, maleimide-activated, sulfhydryl-reactive biotinylation reagent (BMCC-Biotin, Thermo Scientific, 21900) buffer (500 µL) was added to each sample at a final concentration of 4 µM. Samples were left to rotate at 4°C for one hour.

Following incubation with BMCC-Biotin, samples were washed once in lysis buffer (pH 6.2) and then 3x in lysis buffer (pH 7.2). After the final wash, all supernatant was removed and 2x Laemmli sample buffer (40-50 µL) was added to each sample and the protocol was completed as previously mentioned for the GFP-trap protocol except:

1. Streptavidin-HRP antibody (Pierce 21130, 1:5000) in 0.3% BSA in 1x TBS-T at 4°C overnight (~16 hours). Membranes were developed the next day with a very sensitive HRP substrate (WBKLS0500, Millipore) after being washed from the primary antibody.
2. Because no clear signal was detected for palmitoylated GluK2, there was no need for stripping the membrane before incubating it with rat anti-GFP primary antibody (chromotek 3H9-100,1:2500) and then anti-rat HRP-conjugated secondary antibody (Sigma, 1:10000), each for one hour at the room temperature.

Buffer/solution	Composition	[Working]
Lysis buffer (LB)	1% IGEPAL CA-630, 50 mM Tris-HCl pH 7.5, 150 mM NaCl, 10% glycerol, 1 mM PMSF, 1X protease inhibitor cocktail	
NEM solution	NEM powder in 100% ethanol	50 or 10 mM as indicated
Phenylmethanesulfonyl fluoride (PMSF)	Stock prepared in (Dimethyl sulfoxide) DMSO	1 mM
Protease inhibitor (PI) cocktail tablet		1x
Stringent buffer	10 mM NEM + 0.1% SDS in LB	
Hydroxylamine buffer	Stock solution in LB pH 7.2	1 M
Biotin-BMCC solution	Stock solution prepared in DMSO	1-5 µM in LB pH 6.2

Table 2.8. A summary of the buffers used in the IP-ABE assay.

2.2.10 Coomassie Brilliant Blue staining (chapter 5)

Coomassie brilliant blue (50% (v/v) methanol, 10% (v/v) acetic acid and 0.25% Coomassie Brilliant Blue in ddH_2O) was used to stain the immunoprecipitated (GFP-trap protocol in 2.2.8) proteins (WT and C858A, C871A YFP-Myc-GluK2) from transfected HEK293T cells (table 2.7) on an 8% gel from the SDS-PAGE (as in section 2.2.8.1). The gel was incubated in the stain for one hour with gentle shaking. After that, it was de-stained with a destaining solution (50% methanol, and 10% acetic acid in ddH_2O) 3 times to remove excess stain. Next, it was left in the destaining solution overnight before being sent to the University of Bristol Proteomics Facility [https://www.bristol.ac.uk/life-sciences/research/facilities/proteomics] for mass spectrophotometry.

2.2.11 Transfecting neurons for live labelling and imaging (chapter 5)

Under sterile conditions, hippocampal neurons were transfected at DIV 9-10 using lipofectamine 2000. YFP-Myc-GluK2 (WT and C858A, C871A, two coverslips each) DNA (1.5 µg/coverslip) was added to 100 µL of plain neurobasal media. In addition, 1.5x the DNA amount of lipofectamine (3 µL) was also added to another tube of 100 µL plain media. The tube contents were mixed and vortexed after 5 minutes of incubation and left for 20 minutes at the room temperature (22-24°C). The media of the hippocampal neurons on coverslips was removed and kept warm (37°C) for later on and pre-warmed (37°C) feeding media (without the antibiotic) was added to the cells. After 20 minutes, the transfection mixture was added gently to the cells which were then incubated (37°C, 5% CO_2) for 90 minutes for the transfection. Lastly, the transfection media was removed and replaced with the original feeding media. At DIV 14-15 cell were used for a live labelling experiment.

2.2.12 Live labelling for confocal imaging (chapter 5)

Hippocampal neurons on 25 mm coverslips were transfected with YFP-Myc-GluK2 (WT and C858A, C871A) at DIV 9-10 as previously described.

At DIV 14-15, media was replaced with pre-warmed HBSS treated with 2 µM TTX (Tetrodotoxin) and 40 µM GYKI53655 for 30 minutes to block neuronal activity

and AMPARs, respectively. Then half of the neurons of each condition was treated with 10 µM kainate for 20 minutes and the other corresponding half with vehicle (water). After kainate stimulation, neurons were incubated with chicken anti-GFP antibody (ab13970, 1:1000) in media for 20 minutes at 4°C. Next, neurons on cover slips were washed quickly in cold PBS (1x) 5x before being fixed with pre-warmed (37°C) 4% PFA for 20 minutes. Following fixation, neurons were washed 3x with PBS and then treated with glycine (0.2g/30 mL PBS, Severn Biotech) for one minute after which they were washed 3x in PBS. Then, 3% BSA was used for blocking for 10 minutes before the incubation with the Alexa 647-conjugated anti-chicken secondary antibody (1:400) in 3% BSA for one hour at room temperature in darkness.

Once finished, neurons were washed 3x with PBS and then permeabilised using 3% BSA and 0.1% Triton-X 100 (Fisher Scientific) for 10 minutes in darkness. After that, cover slips were incubated with chicken anti-GFP (1:1000) again to label the total transfected GluK2 for one hour in darkness. The next step was to wash off any unbound primary antibody with PBS (3x) before the addition of cy2-conjugated anti-chicken secondary antibody (1:400, green) in darkness for one hour. Cover slips were then washed 3x (each 5 minutes) before being mounted on prelabelled glass slides using Fluoromount-G with DAPI (eBioscience). Glass slides were kept in darkness to dry out for 24-48 hours before being imaged.

2.2.13 Neuronal imaging (chapter 5)

Confocal imaging [Leica SP5-AOBS confocal laser scanning microscope linked to a Leica DMI 6000 inverted epifluorescence microscope with the laser lines: 405 (blue for the nucleus), 488 (green for the total), 633 (far red for the surface)] was used. The transfected neurons were imaged by looking for the total labelling of GluK2 (green cells). A 63x oil immersion lens was used for image acquisition. Each image is composed from 5-6 stacks (0.4-0.5 µm stack interval) that were projected by maximum intensity. The untreated WT GluK2 condition was used to optimise the settings to avoid signal saturation, which remained constant throughout the same experiment. The immunofluorescence was quantified using ImageJ (FIJI).

2.2.14 Preparation of lentivirus using HEK293T cells (chapter 3)

HEK293T cells were passaged (2.2.4.2) one day before making the virus and plated at 6 million cells in 100 mm dish/virus. The next day, HEK293T cells were transfected as follows:

1. *Preparation of DNA-DMEM mixture*

For each virus to be made (sh-scrambled, shNeto2, shNeto1-a, and shNeto1-b), 10 µg XLG viral vector, 2.5 µg pMD2.G (expresses the VSV-G envelope protein), and 7.5 µg p8.91 (helper vector) were added to 2.5 mL plain DMEM.

2. *Preparation of the polyethylenimine (PEI)-DMEM mixture*

For each virus to be made, 24 µL of PEI (1 mg/mL) was added to each 1 mL of DMEM (here each virus needed 2.5 mL of plain DMEM) before inverting the tube several times for mixing. Then the mixture was sterile filtered and left for 2-3 minutes at room temperature.

3. *Preparation of the transfection mixture*

The PEI-DMEM mixture (2.5 mL/virus) was added to each DNA-DMEM mixture prepared earlier and mixed by inverting the tube several times. This final mixture was left for 30 minutes at room temperature.

4. *Transfecting HEK293T cells*

Cells were gently washed once with prewarmed (37°C) plain DMEM prior to adding each transfection mixture (5 mL) to each dish with cells. Cells were kept in the cell culture incubator for 4 hours after which the transfection mixture was replaced with 7 mL/dish of warm complete DMEM and placed back in the incubator.

After 40-48 hours, the virus-containing media was collected and centrifuged at 1500 x g for 10 minutes to remove any dead cells. Then, the virus was aliquoted and stored at –80°C.

2.2.15 Preparation of sindbis virus using BHK-21 cells (chapter 5)

Sindbis virus is an RNA virus that never goes through a DNA intermediate so, the first step in making the virus is that RNA encoding our construct should be made *in vitro*, along with RNA encoding the 'helper' vectors. Then, this RNA needs to be

electroporated into the BHK-21 cells to produce virus. The following are the steps for making the sindbis virus:

1. *Preparing the cells*

Two days before electroporating the BHK-21 cells, cells were plated at $1x10^6$ cells/T175 flask.

2. *Linearising templates*

25 µg (to account for loss of DNA during procedure) of the template plasmid (pSinRep5) DNA [GFP and YFP-Myc-GluK2 (WT, C858A +C871A, K886R, C858A +C871A + K886R, C858A +C871A + S846A + S868A)] was linearised overnight at 37°C by mixing the following: 25 µg of each DNA, 10 µL of 10x cutsmart buffer(Biolabs, B7204S), 2 µL Pac I (10000 unit/mL, Biolabs, R0547L), and up to 100 µL ddH_2O. The defective helper plasmid (pDH(26S)) was also linearised by mixing: 10 µg pDH (26S), 10 µL of H buffer, 5 µL of Xho I (10 u/µL, Biolabs, R0146S), and up to 100 µL ddH_2O. The next day, 4 µL of each digest was mixed with 1 µL of 6X DNA loading dye (Biolabs, B7024S) and run on 0.8% agarose gel (135 volte, 20 minutes) to confirm the completion of linearisation (one band). After that, the digest was put at -20°C for later treatment on the day of BHK-21 cells electroporation.

3. *Proteinase K digestion to remove trace nucleases*

To each digest, 5 µL of 10% SDS (L4522, RNase-free) and 1 µL of proteinase K solution (20 mg/mL, Ambion, 2546) were added and the mixture incubated at 50°C for 30 minutes. From here every next step was done using RNase-free 1.5 mL tubes.

4. *Phenol-Chloroform extraction (to remove proteinase K) and ethanol precipitation of DNA*

To each digest, 200 µL of DEPC (diethyl pyrocarbonate)-treated water (Ambion, AM9906) and 300 µL of phenol/chloroform were added, vortexed, and centrifuged at 21,000 x g for 1 minute. The upper aqueous layer was transferred into a fresh RNase-free tubes without taking the interface. After that, 300 µL of chloroform was added, vortexed, and centrifuged at 21,000 x g for 1 minute to remove phenol. Next, the upper aqueous layer phase was transferred into a fresh RNase-free tubes before adding 0.1X aqueous phase volume (30 µL) of 3 M sodium acetate (pH 5.2) and 2.5X aqueous phase volume (750 µL) of 100% ethanol. The mixture was vortexed for 30 seconds then centrifuged at

21,000 x g for 30 minutes. After centrifugation, the supernatant was discarded and 750 µL of 70 % ethanol added to the small white pellet (linearised DNA) before being centrifuged at 21,000 x g for 5 minutes. Again, supernatant was discarded using a P1000 pipette and any trace 70% ethanol was removed from the bottom of the tube using a P20 pipette prior to allowing the pellet to air dry while the tube kept open. Next, 10µL of DEPC-treated water was added to dissolve the pellet by placing the tube on a shaker at 4°C for at least 30 minutes. Then, the concentration of DNA was measured at 260/280 nm absorbance ratio using NanoDrop ND-1000 (LabTech) and diluted to 0.5 µg/µL and the tube was left on ice.

5. In vitro transcription of viral RNA

mMESSAGE mMACHINE SP6 Large Scale In Vitro Transcription kit (Ambion 1340, Invitrogen) and SUPERaseIn (Ambion 2694, Invitrogen) RNAse inhibitor were used for *in vitro* transcription of viral RNA.

For each electroporation reaction (including each gene of interest, one for the defective helper DNA, and one extra to account for any pipetting error), 0.55µL of DEPC-treated water, 2.5 µL of 2x ribonucleotide mix (2x NTP/CAP), 0.25 µL of 20 mM GTP, 0.5 µL of 10x transcription buffer, 0.1 µL of SUPERaseIn, 0.5 µL of 10 x SP6 enzyme mix, and 0.6 µL of linearised DNA (0.5 µg/µL) were mixed carefully and then incubated at 37°C for 2-4 hours. The preparation of BHK-21 cells was started 90 minutes before the end of this incubation period.

6. Preparation of BHK-21 cells

Cells (70-80% confluent) were washed with PBS (5 mL/flask) before 2-3 mL of trypsin-EDTA were added to each T1.75 flask. Cells were kept at room temperature for 1 minute prior to aspirating the Trypsin-EDTA. Then, cells were incubated at 37°C for 2 minutes. After that cells were collected in a 50 mL centrifuge tube by rinsing every two flasks with 10 mL growth medium and again another 10 mL for all flasks to collect any remaining cells. Next, collected cells were centrifuged at 1000 x g at 4°C for 4 minutes. Supernatant was then removed and 10 mL of 1x PBS were added to suspend the cells, after which another 10 mL PBS were added to the cell suspension and centrifuged at 1000 x g (4°C, 4 minutes). Supernatant was aspirated before adding 10 mL of PBS to triturate the cells, avoiding bubbles, at least 10 times. Next, cells were counted by mixing 100 µL of the cell suspension with 100 µL of trypan blue

solution (0.4% in saline, Sigma T8154) using a haemocytometer. After that, the suspension was centrifuged at 1000 x g (4°C, 4 minutes). During this final centrifuge step, 7 mL of growth medium (to make the virus) was added to each 100 mm dish and kept in the incubator at 37°C. The supernatant was aspirated, and PBS was added to reach 20 million cells/mL. The cell suspension was kept on ice for less than 20 minutes before electroporation.

7. Preparation of RNA for electroporation

Labelled RNase-free 1.5 mL tubes were put on ice before dispensing 5 µL of the Defective Helper RNA in every tube. Then, 5 µL of each gene RNA was added to the correctly labelled tube. The content was mixed thoroughly by triturating with P20 pipette and kept on ice. A Gene Pulser cuvette (Bio-Rad, 0.2 cm gap) for each virus was put on ice.

8. Electroporation

The Bio-Rad Gene Pulser II (electroporator) was set up (Voltage: 1.5 kV, capacitance: 25 µF, pulse controller: Off (resistance = ∞, infinity), low-use: on high range, high-use: ∞) prior to mixing 500 µL of the BHK-21 cell suspension with the RNA by pipetting up and down 3 times. Then, the content was transferred immediately into the ice-cooled Gene Pulser cuvette (Bio-Rad). The first pulse was applied as quickly as possible then (after flicking the cuvette), the second pulse was applied immediately (the time constant for the electroporation should be around 0.7-0.8 ms). The content was transferred back to the original labelled tube and stored on ice for 5-10 minutes. It is important to electroporate as quick as possible to avoid the attack of the RNA by RNases released from the cells once the RNA and the cells were mixed.

9. Plating cells

The tubes content was transferred to the 100 mm dishes and the tubes were rinsed with a little (0.5 mL) media to collect any more cells. The dishes were swirled to spread the cells evenly and incubated at 37°C with 5% CO_2.

10. Monitoring electroporation results

Dishes were observed 24 hours after electroporation under the fluorescent microscope with some of the positive observations included: some cytopathic effects evident (shrunk cells and lots of cell debris) and most of the cells fluoresce green.

11. Harvesting pseudovirion

The supernatant was collected after 48 hours from electroporation in a 15 mL centrifuge tube. The collected supernatant was centrifuged at 1500 x g (4°C for 10 minutes) to pellet any cell debris. The content was transferred into a fresh 15 mL tube and stored at 4°C for no more than 1 week. The virus was aliquoted (~100 µL) and stored at –80°C.

2.2.16 Infecting neurons with lenti (chapter 3) and sindbis (chapter 5) viruses

Cortical neurons (DIV 9-10, 600,000/35 mm well) were infected with 250 µL of lentiviruses (sh-scrambled, sh-Neto2, sh-Neto1). Then, at DIV 14-15, media was aspirated and 250 µL/well of 2x Laemmli sample buffer was used for lysis. Then, the procedure was completed as in sections 2.2.6.2 using 10% gel and 2.2.6.3 transferred for 90 minutes. The membranes were blotted for Neto2 and Neto1 using primary and HRP-conjugated secondary antibodies in Table 2.5.

Cortical Neurons (DIV 14, 600,000 cells/35 mm well) were infected with 20 (GFP) and 50 (all other viruses) µL sindbis viruses [GFP, WT YFP-Myc-tagged GluK2, C858A+ C871A YFP-Myc-GluK2, K886R YFP-Myc-GluK2, C858A+ C871A + K886R YFP-Myc-GluK2, and C858A+C871A + S846A+S868A YFP-Myc-GluK2) for 18 hours before being lysed in 250 µL/well of 2x Laemmli sample buffer. Then, the procedure was completed as in sections 2.2.6.2 using 8% gel and 2.2.6.3 transferred for 110 minutes. The membranes were blotted for GFP using the primary and HRP-conjugated secondary antibodies in Table 2.5.

2.2.17 GFP-trap from sindbis virus infected neurons (chapter 5)

GFP-trap protocol was used to immunoprecipitate GFP-fusion proteins (in this case YFP-tagged GluK2) from sindbis virus (GFP and WT YFP-Myc-GluK2) infected cortical neurons (DIV 16, 600,000 cells/35 mm well, for each condition protein pooled from 3 wells) lysate. 18-20 hours after the infection, cells were checked under the fluorescent microscope for green color (YFP) to confirm the efficiency of the infection. Then, medium was replaced with pre-warmed HBSS and the cells of each condition were treated with either a vehicle (water) or 1 µM PMA (Phorbol 12-

myristate 13-acetate) for 20 minutes. After PKC activation, cells were put on ice for 2-3 minutes before HBSS is aspirated. Cells were scraped after adding cold 125 µL/well lysis buffer (50 mM Tris-HCl (pH 7.4), 150 mM NaCl, 2 mM sodium pyrophosphate, 2 mM EDTA, 1% Triton-X 100, 0.1% SDS, 25 mM β-glycerophosphate, 10% glycerol, 1x phosphatase inhibitors, and 1x complete protease inhibitors) and put into 1.5 mL pre-labelled cold tubes. Cell lysate was then left on ice for 30 minutes to allow for solubilisation. Next, lysate was centrifuged in a benchtop centrifuge at full speed (21,000 x g at 4°C for 20 minutes) to pellet cell debris.

During the spin time, GFP-trap beads were aliquoted (8 µL/pulldown) and washed 3x with 500 µL wash buffer (lysis buffer without phosphatase and protease inhibitors) at 1500 x g for 2 minutes each and left on ice immersed in buffer to avoid drying out. After centrifugation, 20 µL (~5 %) of supernatant was taken as the total lysate sample to a pre-cooled fresh tube. The remaining supernatant was added to the washed GFP-trap beads (pulldown samples). These were kept and rotated at 4°C for 1-2 hours. After that, the beads were pelleted by centrifugation at 1500 x g for 2 minutes at 4°C. The beads were washed 3x after which 40 and 20 µL of 2x Laemmli sample buffer was added to the beads and total lysate samples, respectively. All samples were heated to 95°C for 10 minutes and then left to cool for another 10 minutes. Just before loading the samples into an 8% gel, samples were briefly vortexed and centrifuged at full speed (21,000 x g) for one minute to pellet the beads.

The SDS-PAGE was carried out as in 2.2.6.2 and the immunoblotting as in section 2.2.6.3 using BSA for blocking and antibody dilution. The BD Biosciences antibody (612548) (Table 2.5) was used to detect phosphorylated GluK2.

GFP–trap protocol done to validate the phosphoserine PKC substrate antibody (CS 2261) had the following exceptions from the above protocol:

1. WT and C858A, C868A + S846A, S868A YFP-Myc-GluK2 were immunoprecipitated.
2. Protein pooled from 4 wells/pulldown
3. No PMA pretreatment
4. Amount of GFP-trap beads/pulldown was 20 µL.

2.2.18 Molecular biology

2.2.18.1 Transformation and amplification of DNA

The plasmid DNA was amplified using DH5α E. coli. First, the bacteria (10 µL) was thawed on ice for 10 minutes before adding the plasmid DNA (1 µL) to be incubated with the bacteria for 10 minutes. After that, the cells were placed at 42ºC for 90 seconds (heat shock) before being placed again onto ice for 2 minutes. 100 µL of LB Broth was added to the bacteria before spreading this mixture into a prewarmed (37ºC) agar plate that has the appropriate antibiotic (Ampicillin) for overnight incubation at 37ºC. Next day, a bacterial colony was selected and added to 100 mL of LB Broth (for a Midiprep) containing the appropriate antibiotic (Ampicillin 100 µg/mL) to grow over ~18 hours at 37ºC while being shaking.

2.2.18.2 Purification of DNA

The Midiprep Kit was used to extract and purify the plasmid DNA from the E. coli culture. First, the bacterial cells were pelleted by centrifugation at 4000 x g (4ºC for 20 minutes). The next steps were followed according to Thermo Scientific protocol. Lastly, the concentration of the purified plasmid DNA was measured by the NanoDrop ND-1000 (260/280 nm absorbance ratio).

2.2.18.3 Ethanol precipitation

To concentrate the extracted plasmid DNA, an ethanol precipitation protocol of the Midiprep DNA was carried out. First, 0.1x and 2.5x the volume of DNA of 3 M sodium acetate (pH 5.6) and ethanol, respectively, were added to the DNA. This mixture was vortexed for 1 minute before being centrifuged at 21,000 x g for 30 minutes at 4ºC. The supernatant was removed, and the pelleted DNA was then washed with 70% ethanol prior to centrifugation again at 21,000 x g for 1 minute. The supernatant was removed, and any remaining ethanol was left to air dry for ~30 minutes (the tube lid left open). The pelleted DNA was dissolved in ddH_2O at the desired concentration.

3 Differential distribution of kainate receptor (KAR) pore-forming and auxiliary subunits in adult and developing rat brain

3.1 Background

Based on the available evidence (Tang et al., 2011; Straub el al., 2011a; Straub et al., 2011b; Copits et al., 2011; Zhang et al., 2009; Wyeth et al., 2014; Ng et al., 2009; Vernon and Swanson, 2017; Tang et. al., 2012; Fisher, 2015; Orav et al., 2017; Palacios-Filardo et al., 2016; Wyeth et al., 2017; Sheng et al., 2017; Jack et al., 2018; Mennesson et al., 2019), one of the fine-tuning mechanisms of KAR signalling is the regulation of KAR function by Neto proteins.

Neto2 and Neto1 (Figure 3.1) are single-pass transmembrane proteins that have two extracellular CUB domains, followed by a low-density lipoprotein class A (LDLa) domain, a transmembrane domain and an intracellular C-terminal domain (Copits and Swanson 2012). Neto proteins are not only important as auxiliary subunits of KARs, but also as a member of the CUB-domain containing protein family. It is a wide-spread domain that was first identified in the complement subcomponents **C**1s and C1r. Then, it was found in an embryonic sea urchin epidermal growth factor protein (**U**egf) and later in bone morphogenetic proteins (**B**mp 1). From these first identified proteins, the name **CUB** was proposed. Generally, CUB-domain containing proteins are involved in developmental processes as embryogenesis or organogenesis (Bork and Beckmann 1993). Neto proteins were the first of the CUB protein family to act as auxiliary subunits in mammals (Stohr et al. 2002). However, the developmental changes in Neto2 and Neto1 protein expression profiles have not been established.

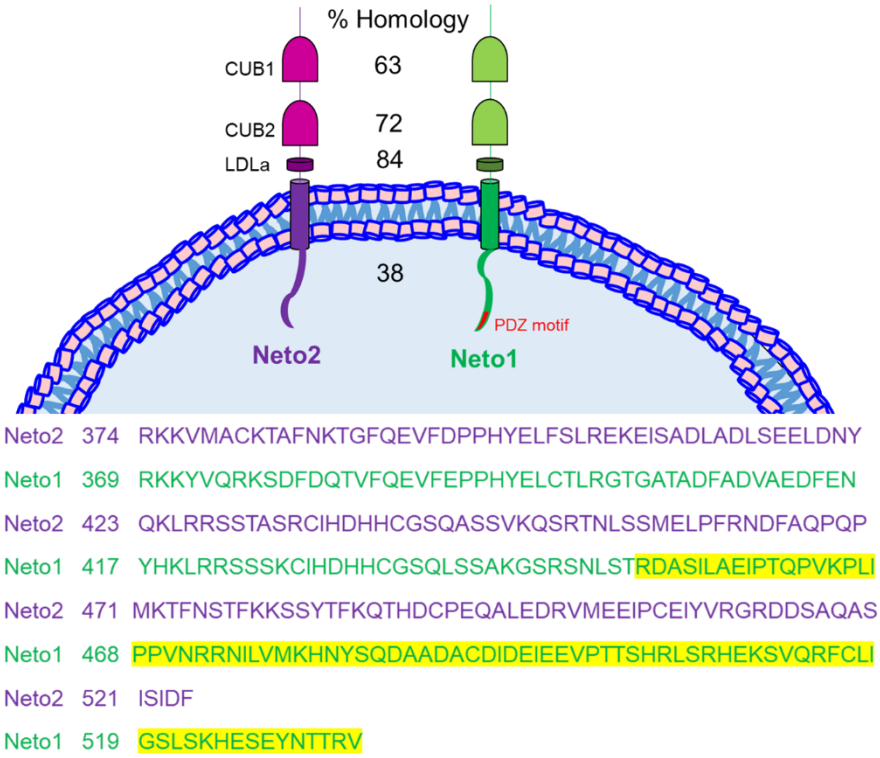

Figure 3.1. KAR auxiliary subunits (Neto2 and Neto1). As single-pass transmembrane proteins, both Neto subunits have two extracellular CUB domains. These domains are followed by a low-density lipoprotein class A (LDLa) domain, a transmembrane domain and an intracellular C-terminal domain. The intracellular sequence is the most variable part of both proteins. The highlighted Neto1 sequence is the part of the intracellular sequence that anti-Neto1 antibody was raised against (Straub et al., 2011a).

Neto (Neuropilin and tolloid-like proteins) nomenclature is based on their sequence homology (31% amino acid identity) to the CUB motifs of neuropilins (transmembrane receptors for the axon guidance molecules semaphorins) (McCawley and Matrisian, 2001; Tashiro et al., 1993; Shaw et al., 1986) and the *Drosophila* dorsal-ventral patterning protein tolloid (Stohr et al., 2002).

Both proteins share significant overall sequence identity (~56%) and amino acid similarity (~80%) and thus may also have functional similarities (Stohr et al., 2002; Michishita et al., 2004; Zhang et al., 2009; Straub et al., 2011a). The specific % identity of each domain of the two proteins is as follows: 63% CUB1, 72% CUB2, 84% LDLa, and 38% intracellular domains (Stohr et al., 2002; Michishita et al., 2004).

The most variable region between Neto proteins is their C-terminal domains (155 for Neto2 and 168 for Neto1 amino acids; Fisher and Mott, 2012). In addition, this region is not significantly similar to any other known proteins, suggesting that Neto proteins are a distinct subfamily (Stohr et al., 2002). Neto2 (525 amino acid residues) has a calculated molecular weight of ~56 kDa (after signal peptide cleavage) and an observed molecular weight of ~60 kDa (Zhang et al., 2009). Rat and human Neto2 share 97% of sequence identity (Zhang et al., 2009).

Neto1 (533 amino acid residues) has two potential N-linked glycosylation sites within its N-terminal domain (Stohr et al., 2002; Michishita et al., 2003) and many potential cytosolic phosphorylation sites (Michishita et al., 2003). In addition, it has a PDZ-binding domain at the end of its C-terminus (Ng et al., 2009; Tomita and Castillo, 2012). The calculated molecular weight is ~60 kDa. Three different mRNA isoforms were identified of human Neto1. Isoform 1 form a soluble protein that have one CUB domain and lack the LDLa domain (Stohr et al., 2002). Isoforms 2 and 3 translate into putative different signal peptides and otherwise similar structure of the Neto1 protein. Only the third isoform is expressed in the foetal and adult brain (Stohr et al., 2002; Michishita et al., 2003). Mouse and human Neto1 share 87% of the nucleotides and 95% of the amino acid identities (Stohr et al., 2002).

Because KARs have roles in brain development and Neto proteins, their auxiliary subunits, are from the CUB-domain containing protein family, which is also implicated in developmental processes, it is important to establish their expression profiles during CNS development. Because many aspects of KAR signalling are regulated by Neto proteins, it is tempting to think the potential of modulating KAR function by Netos throughout brain development. As studies of KARs assembly have suggested, the diverse possibilities of KAR subunits combinations are based on their overlapping expression profiles in various brain regions (Cui and Mayer, 1999; Gallyas et al., 2003).

Previous expression studies identifying the developmental profile of KAR pore-forming and auxiliary subunits in the brain were at the mRNA level. Thus, identifying the expression profiles of Neto proteins and correlating these to the expression of other KAR subunits helps the identification of their spatiotemporal correlations during brain development. In addition, it allows comparing whether Neto proteins expression during CNS development matches that of KAR subunits taking into consideration that Neto proteins are important modulators of KAR function.

This is the first study correlating the expression of KAR auxiliary proteins to their associated pore-forming proteins in the adult and developing rat brain (Dr IK-Hyun Cho unpublished data).

Here, we used the histoblot (*in situ* blotting) technique (Molnar, 2016) to map the regional expression profiles of pore-forming KAR and auxiliary Neto2 and Neto1 subunit proteins at different stages of rat brain development from embryonic day 14 to postnatal day 90 (E14, E17, P0, P14, P21, P28 and P90, n = 2-3) in unfixed horizontal brain sections (prepared previously by Dr IK-Hyun Cho). This is an easy, fast and direct technique that comes between immunohistochemistry and immunoblotting. By directly transferring proteins from unfixed brain tissue to immobilising membrane, the accessibility to proteins' epitopes is improved compared to immunohistochemistry where fixation could impair the antibody accessibility to its epitope. Thus, it is reliable for quantitative comparisons of the immunochemical labelling. In addition, it preserves the anatomical resolution of proteins (Benke et al., 1995; Wenzel et al., 1997; Tonnes et al., 1999; Aguado and Luján, 2019). However, in relation to co-expression in this study, regional does not mean cellular (Hepp et al., 2015).

All primary antibodies (Neto2, Neto1, GluK2/3, GluK5, GluA1-4) used here were validated previously in either Professors Susumu, Molnar, or Henley's laboratory.

3.2 Aim and objectives

Hypothesis: Regional and temporal patterns of Neto protein expression overlap with the distribution of pore-forming KAR subunits.

Aim: To identify regional distributions of KARs' auxiliary subunits in adult brain and during development.

Objectives:

1. To establish the regional expression profiles of Neto proteins during rat brain development.

2. To correlate the protein distribution of Neto2 and Neto1 to pore-forming KAR subunits.

3.3 Results

First of all, we started this work by validating the primary antibodies to Neto proteins, which were generated in Professor Susumu Tomita (Yale School of Medicine, United States) laboratory and generously provided by him.

3.3.1 Validation of Neto2 and Neto1 antibodies using transiently expressed auxiliary KAR subunit proteins in HEK293T cells

3.3.1.1 Validation of Neto2 antibody in HEK293T cells

The specificity of two different anti-Neto2 primary antibodies was evaluated by expressing rat Neto2 and Neto1 proteins in HEK293T cells (i) alone, or in combination with (ii) sh-scrambled (negative control), (iii) sh-Neto2 or (iv) sh-Neto1 constructs (Figure 3.2A). The anti-Neto2 labelled bands were normalised to the β-actin content of each sample for semi-quantitative comparisons of related samples.

The rabbit anti-Neto2 polyclonal antibody raised against the whole C-terminus of rat Neto2 amino acid sequence (the C-terminal 192 amino acids; Zhang et al. 2009) labelled a band at ~60 kDa, which corresponds to the predicted molecular weight of Neto2 (The UniProt Consortium, 2019, Zhang et al, 2009). This antibody produced no detectable

cross-reaction with Neto1 (Figure 3.2A). Furthermore, the immunolabelling was reduced in samples where Neto2 was co-expressed with sh-Neto2, but not with sh-Neto1 or sh-scrambled (negative control). These findings confirmed the Neto2 selectivity of the antibody.

A commercially supplied rabbit anti-Neto2 IgG (ab109288, Abcam, References: Vernon and Swanson, 2017; Hu et al., 2015) produced very similar labelling pattern (Figure 3.2B). The detected bands correspond to the predicted molecular weight of Neto2, and only very weak cross-reactivity was detected with Neto1. While co-expression with sh-Neto2 markedly reduced the intensity of the immunopositive band, no similar changes were detected when Neto2 was expressed in the presence of sh-scrambled or sh-Neto1 (Figure 3.2B).

The selectivity of the Neto2 antibody (Zhang et al. 2009) was further investigated using GFP-FLAG-tagged Neto proteins (GFP-Neto2, GFP-Neto1) without and with sh-scrambled, sh-Neto2 or sh-Neto1 co-expression (Figure 3.2C). The antibody identified a ~100 kDa band, which is consistent with the predicted molecular weight of the GFP-FLAG-Neto2 construct. The cross-reaction with GFP-Neto1 was weak and sh-Neto2 selectively reduced the intensity of the immunopositive band compared to sh-scrambled and sh-Neto1 (Figure 3.2C).

These tests confirmed that both anti-Neto2 antibodies are suitable for the identification of Neto2 proteins in HEK293T cells. Unless stated otherwise, we used the anti-Neto2 developed by Zhang et al. (2009) for our experiments.

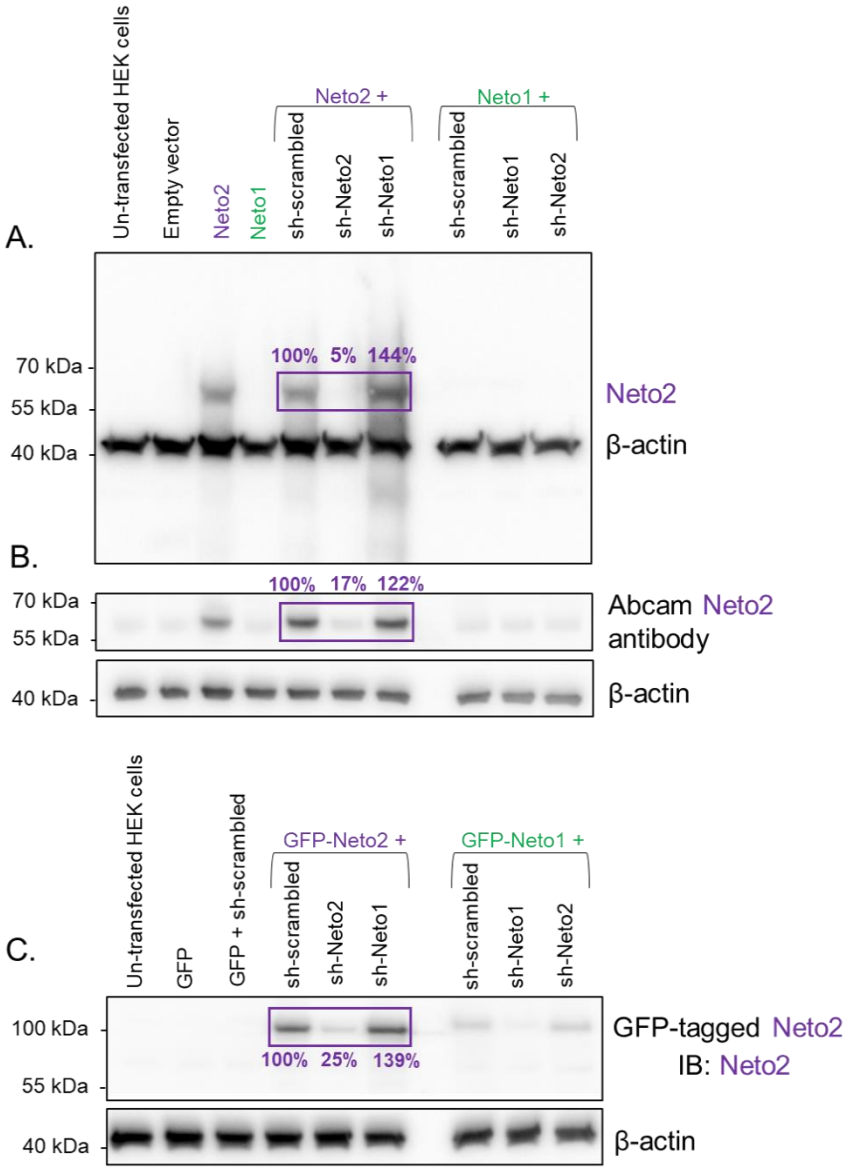

Figure 3.2. Validation of Neto2 primary antibodies using wild-type (WT) and green fluorescent protein (GFP)-tagged Neto2 and Neto1 individually expressed in HEK293T cells. The specificity of the homemade (Zhang et al. 2009, **A** and **C**) and Abcam supplied (**B**) Neto2 primary antibodies was evaluated using WT (**A** and **B**) and GFP-FLAG-tagged (**C**) Neto2 and Neto1 expressed in HEK293T cells in combination with three rat sh-RNAs: sh-scrambled (KD negative control), sh-Neto2 or sh-Neto1 as indicated. Both anti-Neto2 antibodies selectively labelled bands that correspond to the molecular weights of WT Neto2 (~60 kDa; **A** and **B**) and GFP-Neto2 (~100 kDa; **C**) proteins. No (**A**) or very week (**B**, **C**) labelling was obtained with WT Neto1 or GFP-Neto1-containing samples. Co-expression of WT or GFP-Neto2 with sh-Neto2 reduced the optical density of the immunopositive band to ~5-25% of the corresponding sh-scrambled negative control. Similar reduction in Neto2 immunoreactivities were not detected in the presence of sh-Neto1. Neto2 immunolabelling was normalized to β-actin before compared to its sh-scrambled control. WT Neto2, n = 2; GFP-Neto2, n = 1.

3.3.1.2 Validation of Neto1 antibody in HEK293T cells

The specificity of the rabbit anti-Neto1 polyclonal primary antibody raised against the second half of the C-terminal cytoplasmic domain (Straub et al. 2011a) was verified using immunoblots of rat Neto2 and Neto1 proteins expressed in HEK293T cells (i) alone, or in combination with (ii) sh-scrambled (negative control), (iii) sh-Neto2 or (iv) sh-Neto1 constructs (Figure 3.3) as described in 3.3.1.1.

The anti-Neto1 antibody identified a ~60 kDa band in all samples, including the un-transfected HEK293T cells, which is consistent with the predicted molecular weight of the human Neto1 isoform. In (rat) Neto1 transfected cells, the rat isoform of the protein was selectively identified at ~66 kDa (Figure 3.3A). The anti-Neto1 antibody produced no detectable cross-reaction with Neto2. Also, the intensity of the rat Neto1 band was reduced by co-expression with sh-Neto1 but not with sh-Neto2 or sh-scrambled (negative control).

The human Neto1 (~60 kDa) immunoreactivity somewhat increased (by ~25-52%) in rat Neto1 transfected HEK293T cells. Similar increase was not detected in Neto2 transfected cells (pink bars, Figure 3.3A).

To further characterise the anti-Neto1 antibody, the specificity tests were also performed using GFP-FLAG-Neto1 and GFP-FLAG-Neto2 expressed in HEK293T cells (i) alone, or in combination with (ii) sh-scrambled (negative control), (iii) sh-Neto1 or (iv) sh-Neto2 constructs (Figure 3.3B). In GFP-Neto1 transfected samples the anti-Neto1 antibody identified a ~100 kDa band, which is consistent with the predicted molecular weight of GFP-FLAG--Neto1 protein. There was only very weak reaction with GFP-Neto2 (Figure 3.3B). Like with the WT Neto1 (Figure 3.3A), GFP-Neto1 immunoreactivity was reduced in sh-Neto1 co-transfected samples compared to sh-scrambled or sh-Neto2 expressing cells. Again, the expression of endogenous human Neto1 appeared to be higher (~57% increase) in rat GFP-Neto1 transfected HEK293T cells (pink bars, Figure 3.3B). There was also a marked reduction (~53%) in human Neto1 expression of rat sh-Neto1 compared to sh-Neto2 and sh-scrambled.

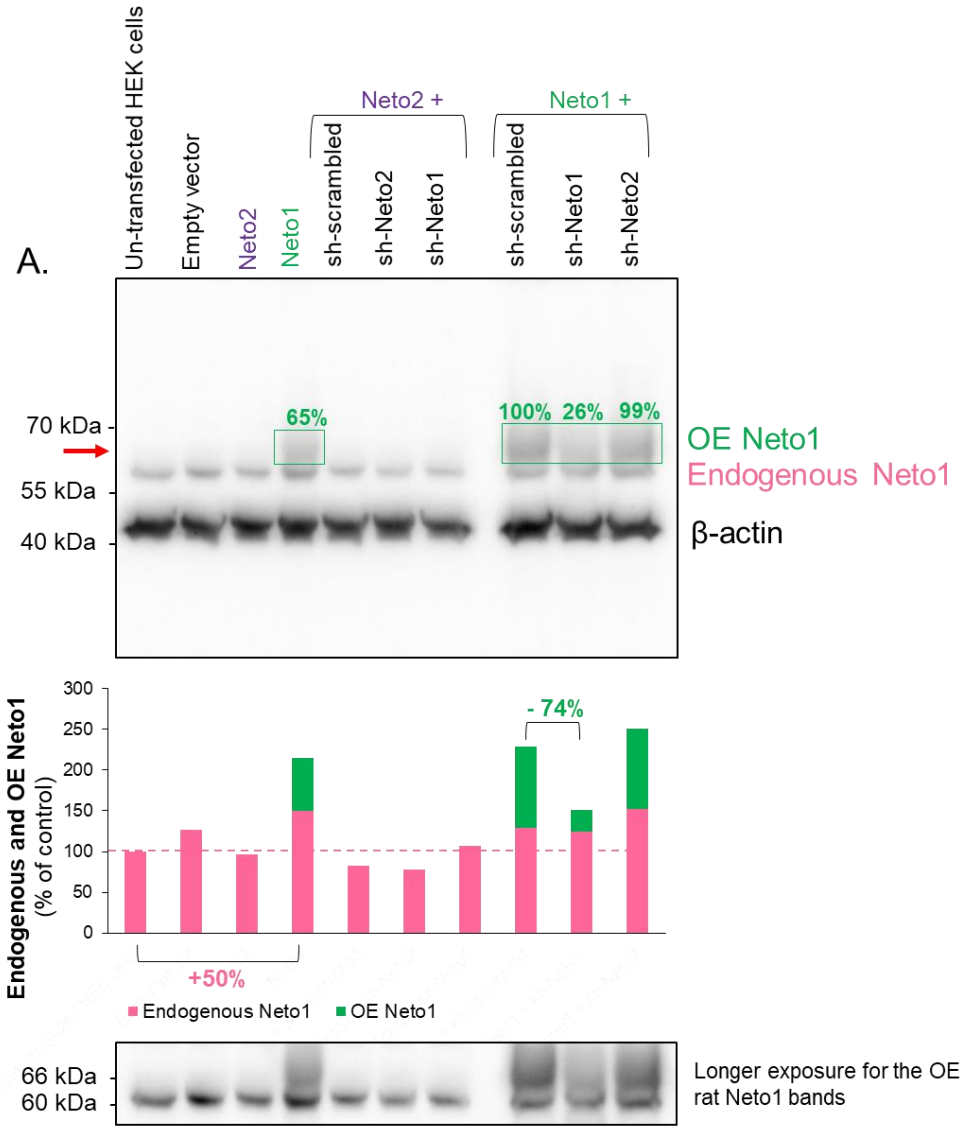
A.
Un-transfected HEK cells
Empty vector
Neto2
Neto1
Neto2 +
sh-scrambled
sh-Neto2
sh-Neto1
Neto1 +
sh-scrambled
sh-Neto1
sh-Neto2
70 kDa
55 kDa
40 kDa
65%
100%
26%
99%
OE Neto1
Endogenous Neto1
β-actin
Endogenous and OE Neto1
(% of control)
300
250
200
150
100
50
0
- 74%
+50%
Endogenous Neto1
OE Neto1
66 kDa
60 kDa
Longer exposure for the OE
rat Neto1 bands

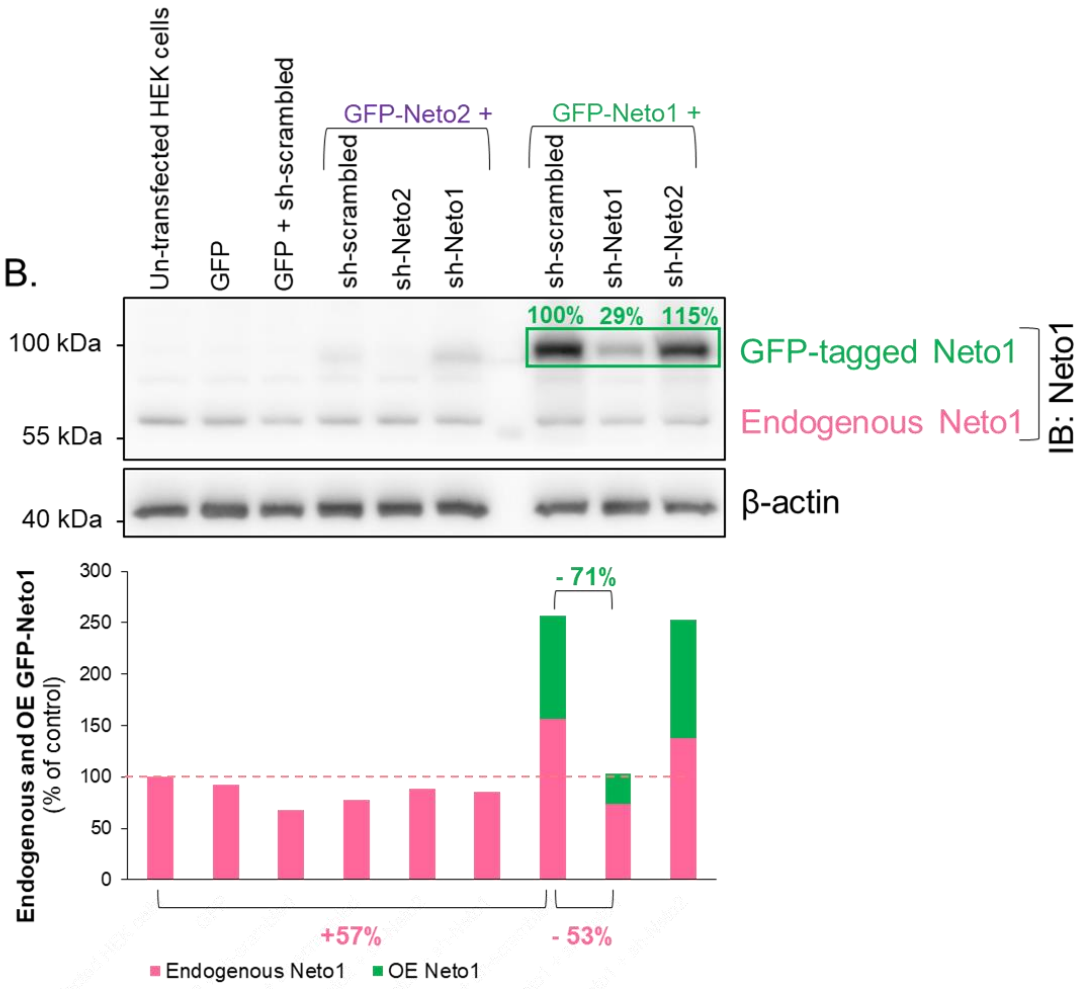

Figure 3.3. Validation of Neto1 primary antibody using wild type (WT) and green fluorescent protein (GFP)-tagged Neto2 and Neto1 individually expressed in HEK293T cells. The specificity of the rabbit anti-Neto1 IgG (Straub et al. 2011, **A** and **B)** was evaluated using WT (**A**) and GFP-FLAG-tagged (**B**) Neto2 and Neto1 expressed in HEK293T cells in combination with three rat sh-RNAs: sh-scrambled (KD negative control), sh-Neto2 or sh-Neto1 as describe in Figure 3.2. The Neto1 antibody identified immunopositive bands at ~60 kDa in all samples, including un-transfected HEK293T cells (**A** and **B**). Somewhat higher molecular weight bands (~66 kDa, **A**) were identified in WT Neto1-transfected samples (**A**). (OE Neto1, also see the blot of a longer exposure). The anti-Neto1 antibody selectively identified a band in samples prepared from GFP-Neto1 transfected HEK293T cells with the expected molecular weight (~100 kDa, **B**). Co-expression of WT or GFP-Neto1 with sh-Neto1 reduced the optical density of the immunopositive band to ~26-29% of the corresponding sh-scrambled negative control. Similar reduction in Neto1 immunoreactivities were not detected in the presence of sh-Neto2. The result (**B**) confirmed that at ~100 kDa (the green rectangle) the overexpressed GFP-tagged Neto1 was identified when co-expressed with either sh-scrambled or sh-Neto2 (100% and 115% of the KD control). However, it showed 71% reduction in its expression when knocked down (GFP-tagged Neto1 + sh-Neto1 compared to GFP-tagged Neto1 + sh-scrambled). Neto1 antibody picked up a very small percent (2% up to 13% compared to the GFP-tagged Neto1 + sh-scrambled) of the overexpressed GFP-tagged Neto2. This membrane blot was stripped and re-probed with the homemade Neto1

antibody after being visualised with anti-GFP antibody. All bands were normalised to their corresponding β-actin bands before being normalised to their control. The overexpressed rat Neto1 or GFP-tagged Neto1 bands were normalised to the Neto1 expression level in Neto1 (or GFP-tagged Neto1) + sh-scrambled condition. The bands representing endogenous Neto1 expression were normalised to the expression level of the un-transfected cells. Statistical testing could not be performed due to the small n number (WT Neto1, n = 2; GFP-Neto1, n = 1).

3.3.1.3 Validation of Neto2 and Neto1 knockdown constructs in HEK293T cells.

To evaluate the specificity of the knockdown constructs (sh-scrambled, sh-Neto2 and sh-Neto1), GFP-FLAG-tagged Neto2 (GFP-Neto2) and GFP-FLAG-Neto1 were co-expressed with each one of the KD constructs in HEK293T cells. The harvested cell membranes were analysed using a rat anti-GFP antibody (Chromotek 3H9) to assess the levels of GFP-FLAG-Neto2 and GFP-FLAG-Neto1 following co-expression with sh-scrambled, sh-Neto2 and sh-Neto1 (Figure 3.4). The GFP positive bands (just under 100 kDa) were not reduced/unaffected when co-expressed with the KD control construct or the other Neto protein KD construct (233% expression level of GFP-Neto2 when co-expressed with sh-Neto1 and 97% expression level of GFP-Neto1 when co-expressed with sh-Neto2, each was compared to its KD control). Furthermore, GFP expression was significantly reduced (75% - 82% compared to its KD control) when co-expressed with its KD construct (GFP-Neto2 + sh-Neto2 and GFP-Neto1 + sh-Neto1, respectively).

Neto2 expression seems to be highly cross-linked to Neto1 expression in HEK293T cells. Recombinant Neto2 expression was increased when the cells were co-transfected with the Neto1 KD construct (Figures 3.2 and 3.4). This Neto1-dependent increase in Neto2 expression in HEK293T may be due to the potential presence of endogenous Neto1 in HEK293T cells (see Figure 3.3). This may suggest that by using sh-Neto1 (reducing endogenous Neto1 expression), a compensatory increase in Neto2 expression was observed. Or, it could be that the KD construct of Neto1 was not specific and cross-reacted with Neto2 and showed off-target effects by increasing Neto2 expression (Figure 3.4).The stability of the protein (Neto2) may be increased in response to a reduction in its mRNA levels (non-specific sh-Neto1). Furthermore, if the sh-RNA will lead to translation inhibition without mRNA degradation, then when the protein level will go down a feedback mechanism will lead to increased gene transcription. This may lead to increased protein level.

Notably, HEK293T cells were chosen as the heterologous system to overexpress Neto proteins because previous evidence (mice tissue distribution of Neto1 and Neto2 mRNA and RT-PCR analysis of human Neto1) shows no expression in the kidney (Stoher et al., 2002; Michishita et al., 2003; Michishita et al., 2004). In addition, HEK293T cells have been widely used to successfully overexpress KARs. Moreover, in the field of studying Neto proteins as auxiliary subunits of KARs, HEK293T cells were largely used by many research groups for this purpose (mainly for electrophysiological studies and no one has used this system for expression studies (Table 1.2/Introduction). However, in my work to validate Neto proteins antibodies, it was surprising that HEK293T cells appear to express Neto1. These antibodies were successfully validated in Professor Susumu lab using E coli lysate expressing recombinant Neto proteins, Neto1 KO mice brain tissue, Neto2 transfected CHO cells, rat brain, and primary cerebellar mouse culture (Straub et al., 2011a; Zhang et al., 2009).

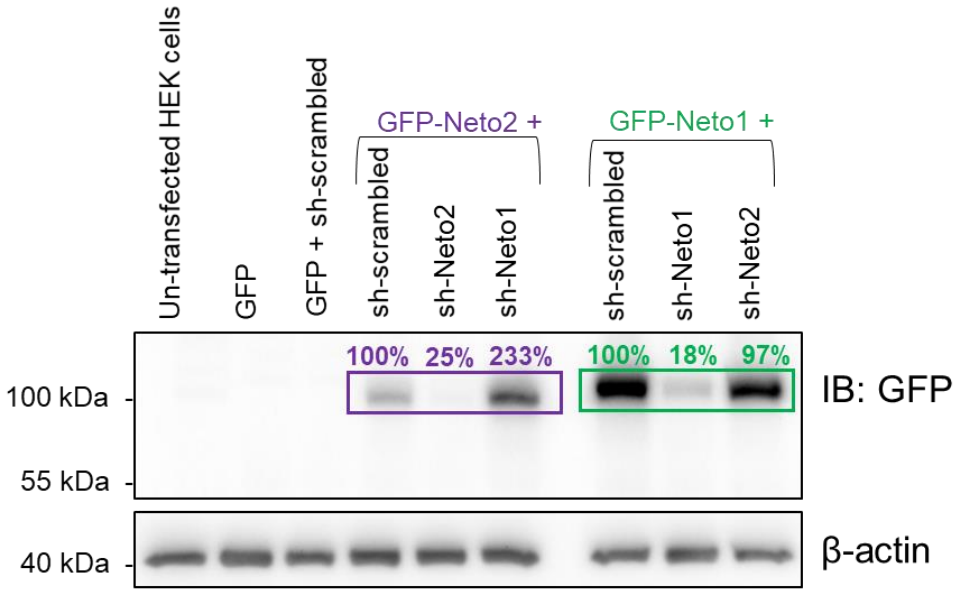

Figure 3.4. Validation of Neto2 and Neto1 sh-RNA constructs using GFP-Neto2 and GFP-Neto1 expressed in HEK293T cells. The specificity of the knockdown (KD) sh-RNAs of rat Neto2 and Neto1 was evaluated using rat GFP-FLAG-tagged Neto2 and Neto1 individually expressed in HEK 293T cells in combination with sh-scrambled (KD negative control), sh-Neto2 or sh-Neto1. Anti-GFP antibody labelling identified GFP-Neto2 and GFP-Neto1 as ~100kDa immunopositive bands. Compare to sh-scrambled samples (100%), co-expression of sh-Neto2 reduced GFP-Neto2 expression (25% of sh-scrambled) without a similar decrease in Neto1 levels (97% of sh-scrambled). In contrast, co-expression of sh-Neto1 reduced GFP-Neto1 expression (18% of sh-scrambled) without a similar decrease in Neto2 levels (233% of sh-scrambled). β-Actin labeling was used to normalize anti-GFP immunopositive bands before semi-quantitative comparisons (n = 2).

3.3.2 Validation of antibodies in primary cortical cultures using knockdown of endogenous Neto2 and Neto1

Vectors of lentiviruses [rat sh-Neto2 and two different rat sh-Neto1 (a and b)] were previously made by Dr Kevin Wilkinson and used here to knockdown endogenous neuronal Neto2 (n = 10) and Neto1 (n = 6). The sh-scrambled was also used as a KD control. The blots (A and C) and their quantification (B and D) in Figure 3.5 show the expression levels of neuronal Neto2 and Neto1 in different conditions compared to the knockdown control (sh-scrambled). Neto2 expression (Figure 3.5/A and B) was significantly reduced by ~98% when it was knocked down [4.2 ±0.8 vs 162.0 ±23.6, $p < 0.001$]. In addition, Neto2 was reduced significantly by ~63% when Neto1 was knocked down (sh-Neto1-b) [60.2 ±13.3 vs 162.9 ±23.6, $p < 0.001$]. However, compared to the sh-Neto2 condition this reduction was still significant [60.2 ±13.3 vs 4.2 ±0.8, $p = 0.045$]. Regarding Neto1 expression (Figure 3.5/C and D), sh-Neto1-b lentivirus significantly decreased Neto1 expression by ~76% compared to the KD control [31.1 ±7.1 vs 129.7 ±7.7, $p < 0.001$] and ~72% compared to sh-Neto2 [31.1 ±7.1 vs 112.2 ±7.1, $p < 0.001$]. In case of knocking down Neto2, Neto1 expression has not changed compared to the KD control [112.5 ±7.1 vs 129.7 ±7.7, $p = 0.25$]. The virus vector of the sh-Neto1-a construct was not used more than twice (n = 2) as it was shown to be not efficient in knocking down Neto1 (~55%). Each band was normalized to its β-actin band before being normalized to its control. One-way ANOVA was performed to statistically analyse the results at a statistically significant level of 0.05. Data expressed as mean ±SE.

There is a ~6 kDa difference between the the observed molecular weights of both Neto isoforms (Neto1> Neto2) in HEK293T cells and neurons, which could be due to N-glycosylation. A similar difference was also observed by others (Copits et al., 2011; Straub et al., 2011a).

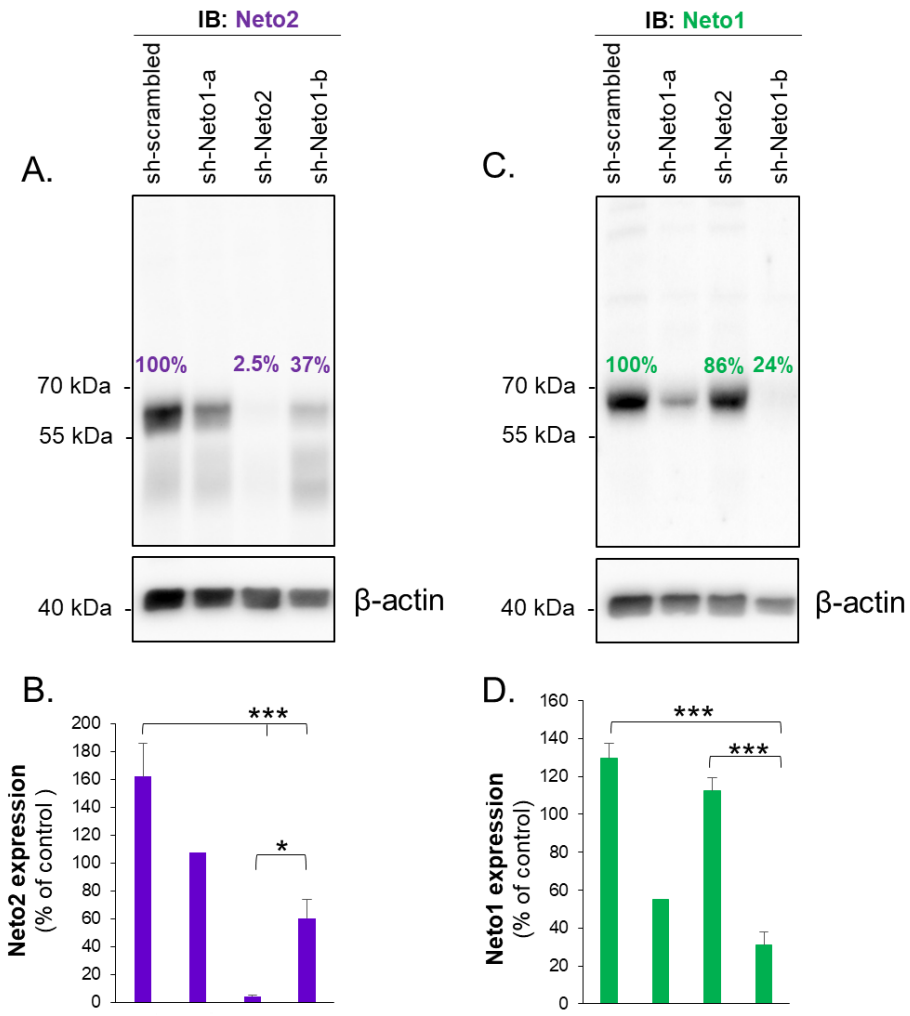

Figure 3.5. Validation of Neto2 and Neto1 antibodies in primary cultures of cortical neurons using sh-Neto1 and sh-Neto2 knockdown. Lentiviral rat sh-RNA vectors were used to knockdown the protein expression of Neto2 (sh-Neto2) and Neto1 (sh-Neto1-a and sh-Neto1-b) in rat cultured cortical neurons at 14-15 DIV (Neto2, **A** and **B,** n = 10) and (Neto1, **C** and **D,** n = 6). The less effective sh-Neto1-a was included only in two initial experiments (n = 2). The Neto2 immunoblot **(A)** and its quantification **(B)** show that sh-Neto2 lentivirus reduced endogenous Neto2 levels to 2.5% of sh-scrambled controls (***$p < 0.001$). Interestingly, when knocking down Neto1 using sh-Neto1-b, Neto2 was also reduced to 37% of sh-scrambled controls (***$p < 0.001$). The sh-Neto1-b lentivirus significantly (***$p < 0.001$) decreased Neto1 expression to 24% of sh-scrambled controls **(C** and **D)**. The sh-Neto2 produced no significant change in Neto1 levels ($p = 0.25$). This demonstrates the specificity of the antibodies and their ability to react selectively with endogenous Neto2 and Neto1 proteins in rat cortical neurons. In each sample, Neto2 and Neto1 immunoreactivities were normalized to the corresponding β-actin band for quantitative comparisons. One-way ANOVA was used to statistically analyse the results. Error bars indicate the standard error (SE) and p - value is significant at 0.05.

3.3.3 Differential distribution of KAR auxiliary subunits in adult and developing rat brain

3.3.3.1 Immunochemical mapping of the regional expression of Neto2 and Neto1 in unfixed adult rat brain

To correlate the regional expression profile of Neto2 and Neto1 proteins in the adult rat brain to pore-forming KAR subunits, we performed the histoblot technique using the previously validated Neto antibodies (section 3.3.1 and 3.3.2). Neto2 and Neto1 proteins are widely expressed in the adult rat brain (3 - 8 months, n = 3) as indicated by their histoblot immunoreactivities (Figure 3. 6). While the overall adult expression patterns of Neto2 and Neto1 proteins are overlapping in the cerebral cortex and caudate putamen (CP), their distribution differs in the hippocampus and cerebellum where Neto2 localises in the hippocampal dentate gyrus and cerebellar granule cells and Neto1 is prominently expressed in hippocampal CA3 region and weak in the cerebellum.

3.3.3.1.1 Adult Neto2 expression pattern

Neto2 labeling is prominent in the inner cortical layers, CP, hilus (polymorphic layer) of hippocampal DG (Figure 3.6) and the granular cell layer of the cerebellum. It has very weak expression in other hippocampal sub-regions (CA1 and CA3) (Table 3.1).

3.3.3.1.2 Adult Neto1 expression pattern

The strongest Neto1 immunostaining is found in the stratum lucidum (SL) (Figure 3.6) of the CA3 region of the hippocampus (HIP) followed by moderate levels of labeling in the deeper layers of the cerebral cortex and CP (Table 3.1). However, the cerebellar Neto1 immunopositivity is relatively weak (Table 3.1).

3.3.3.1.3 Correlation of Neto2 and Neto1 expression patterns to KAR pore-forming subunits GluK2/3 and GluK5

The histoblot labelling patterns of Neto2 and Neto1 proteins is similar to KAR pore-forming subunits GluK2/3 and GluK5 (Figure 3.6) in the cerebral cortex, CP and HIP

(just for Neto1). In the hippocampus, the immunolabelling of Neto1, GluK2/3 and GluK5 overlap in the SL layer of CA3 while Neto2 labels the dentate hilus (Figure 3.6). In contrast, the immunoreactivity obtained for GluA1-4 AMPAR subunits, which share a high degree of sequence homology with KAR pore-forming subunits, showed a clear difference compare to pore-forming and auxiliary KAR subunits. For example, the highest level of GluA1-4 was identified in the outer cortical layers, CA1, stratum molecular layer of hippocampal DG and the molecular cell layer of the cerebellum (Table 3.1).

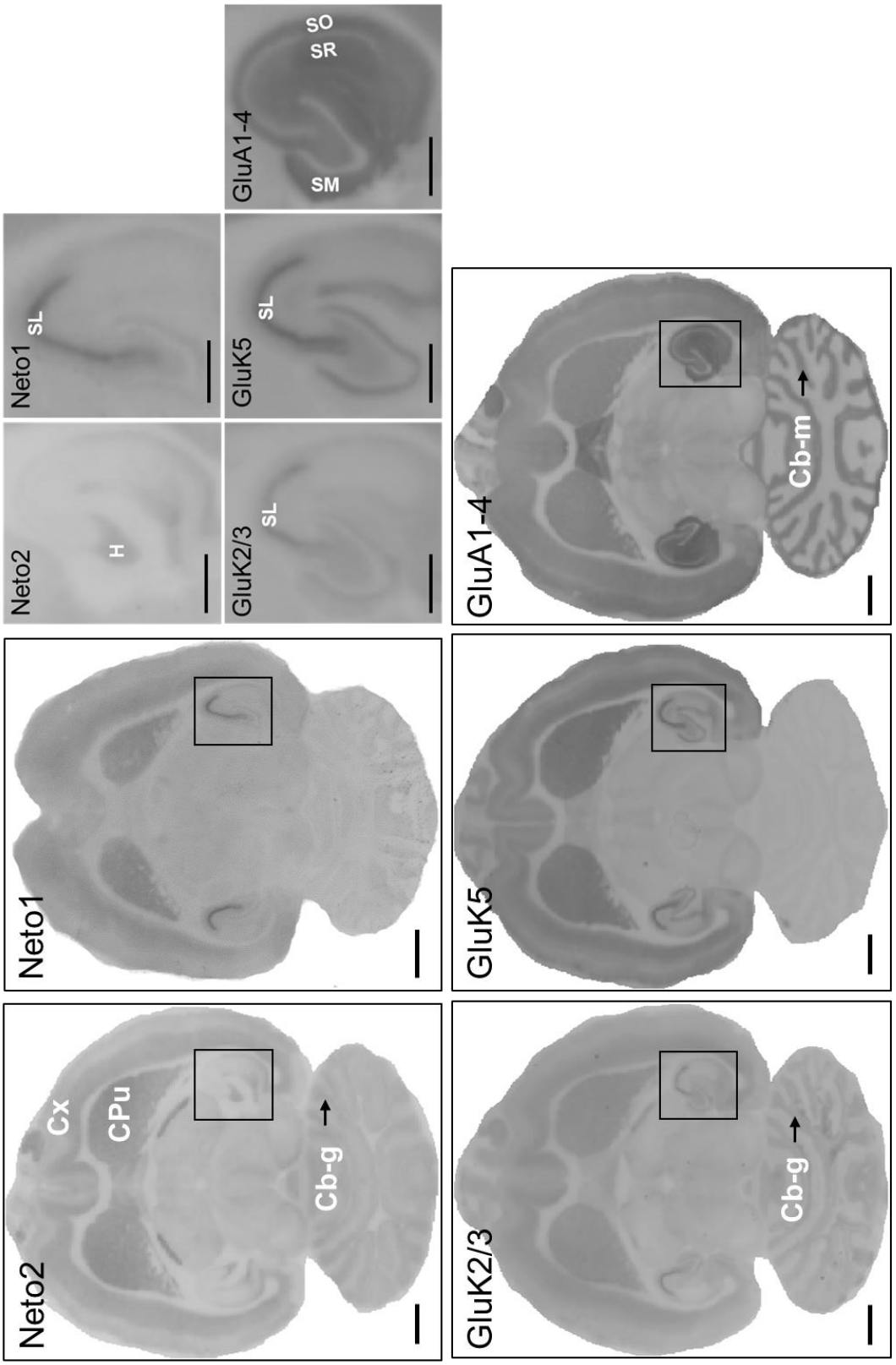
Neto2
Cx
CPu
Cb-g
Neto1
GluK2/3
Cb-g
GluK5
GluA1-4
Cb-m
Neto2
H
Neto1
SL
GluK2/3
SL
GluK5
SL
GluA1-4
SO
SR
SM

Figure 3.6. Differential distribution of auxiliary and pore-forming subunits of KARs in adult rat brain. Representative histoblots showing differential distribution of auxiliary Neto2 and Neto1 (n = 3) and pore-forming GluK2/3 and GluK5 (n = 6) subunits of KARs and the closely related AMPAR subunits GluA1-4 (n = 6) in adult (3 - 8 months) horizontal rat brain sections. All these iGluR proteins are widely distributed in the adult rat brain; in the cerebral cortex, caudate putamen, hippocampus and cerebellum. There is an overlap in Neto2 and GluK2/3 immunoreactivities in the cerebellum and deeper cortical layers. Neto1 labelling overlaps with GluK2/3 and GluK5 in the hippocampal CA3 sub-layer stratum lucidum. The regional distribution patterns of the auxiliary and pore-forming KAR subunits are different from the distribution of the related GluA1-4 AMPAR subunits. The hippocampal regions (squares) are enlarged and sub-layers labelled. Cx: cerebral cortex, CPu: caudate putamen, Cb-g: cerebellar granular cell layer, Cb-m: cerebellar molecular layer, H: hilus (DG), SM: stratum moleculare (DG), SL: stratum lucidum (CA3), SO: stratum oriens (CA1), SR: stratum radiatum (CA1). Scale bars: 2 mm.

Brain region	Neto2	Neto1	GluK2/3	GluK5	GluA1-4
Outer Cx	+	++	++	++	+++
Inner Cx	+++	+++	+++	+++	++
CA1	±	+	±	+	++++
CA3	±	++++	++++	++++	++
DG	+++[a]	++	++	++	+++[b]
CPu	+++	+++	+++	+++	++
Cb-g	+++	±	+++	±	±
Cb-m	++	+	++	±	++

Table 3.1. Semi-quantitative comparison of pore-forming and auxiliary subunit immunoreactivities in selected brain regions. Selected regions of adult rat brain horizontal section histoblots (Figure 3.6) were analysed: Cx: cerebral cortex, CA: hippocampal cornu ammonis, DG: hippocampal dentate gyrus, CPu: caudate putamen, Cb-g: cerebellar granular cell layer, Cb-m: cerebellar molecular layer. a: hilus (polymorphic layer), b: stratum molecular layer. Degree of immunoreactivity: ++++, very strong; +++, strong; ++, moderate; +, weak; ±, very weak.

3.3.3.1.4 Summary of the KAR subunit protein distribution patterns in adult rat brains:

The regional expression profiles of adult Neto2 and Neto1 correspond to GluK2/3 and GluK5 KAR subunit proteins:

1. All 4 subunits have high immunoreactivity in the caudate putamen and in the inner cortical layers compared to outer layers.
2. Neto1, GluK2/3 and GluK5 predominantly expressed in the CA3 region in the hippocampus.
3. Neto2 and Gluk2/3 share a similar distribution pattern in cerebellum where both are highly expressed in granular cell layer.
4. Neto1 and GluK5 weakly expressed in the cerebellum.
5. Neto2 and Neto1 expression is overlapping in cortex and caudate putamen and distinct in hippocampus and cerebellum.

3.3.3.2 Developmental changes in the expression of Neto2 and Neto1 proteins in the rat brain

Regional developmental changes in Neto2 and Neto1 expression patterns (Figure 3.7) were examined and quantified (Figure 3.8) in horizontal sections (n = 2-3) of the rat brain from embryonic day 14 to postnatal day 90 (E14, E17, P0, P14, P21, P28, P90).

While the developmental series provided important qualitative data regarding changes in the regional expression profiles of Neto2 and Neto1, statistical analysis could not be performed due to the small sample size (n = 2-3).

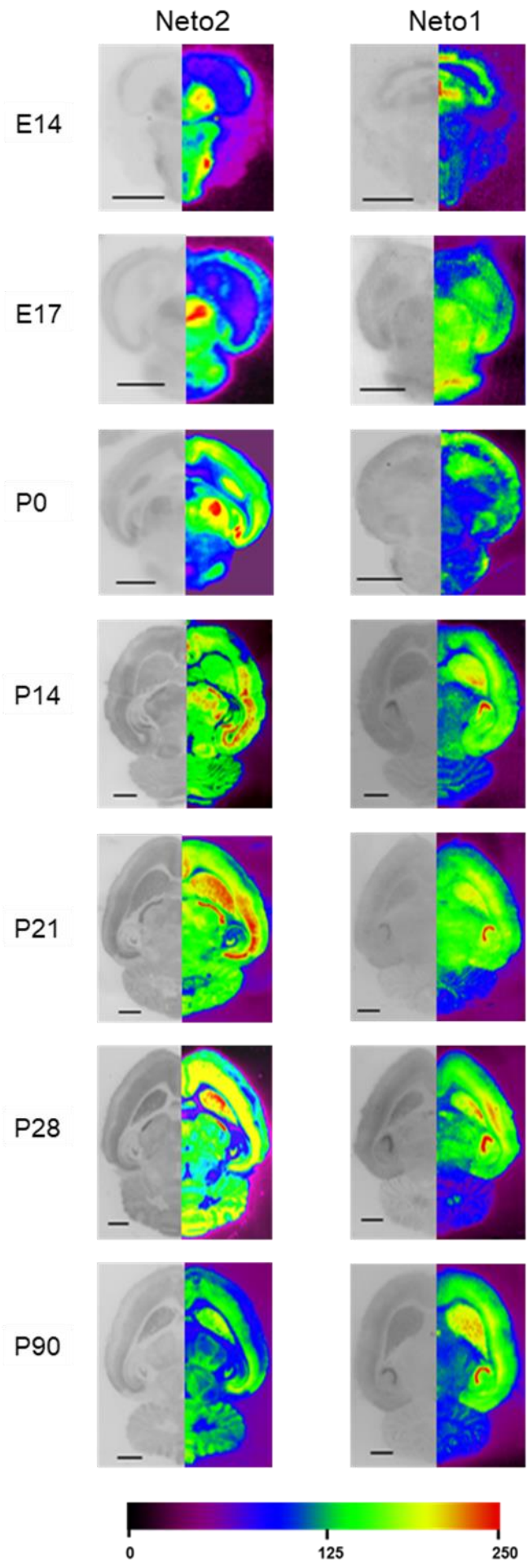
Neto2
Neto1
E14
E17
P0
P14
P21
P28
P90
0
125
250

Figure 3.7. Regional distribution of Neto2 and Neto1 in the developing brain. Grayscale histoblots (left) and their corresponding colour gradients (right) illustrate the regional distribution of Neto2 and Neto1 immunoreactivities at various stages of rat embryonic and postnatal development (E14, E17, P0, P14, P21, P28, P90) in horizontal brain sections (n = 2-3). In general, Neto2 immunostaining peaks during the first 2-3 weeks of life (P14 and P21), after which it starts to decline in all brain regions. In contrast, Neto1 immunolabelling increases with development in many regions of the rat brain (cerebral cortex, caudate putamen and hippocampus). Colour gradients images were generated by assigning the grayscale images to the RGB (red-green-blue) channels in Adobe Photoshop CS2. All images were treated identically. Scale bars: 2 mm.

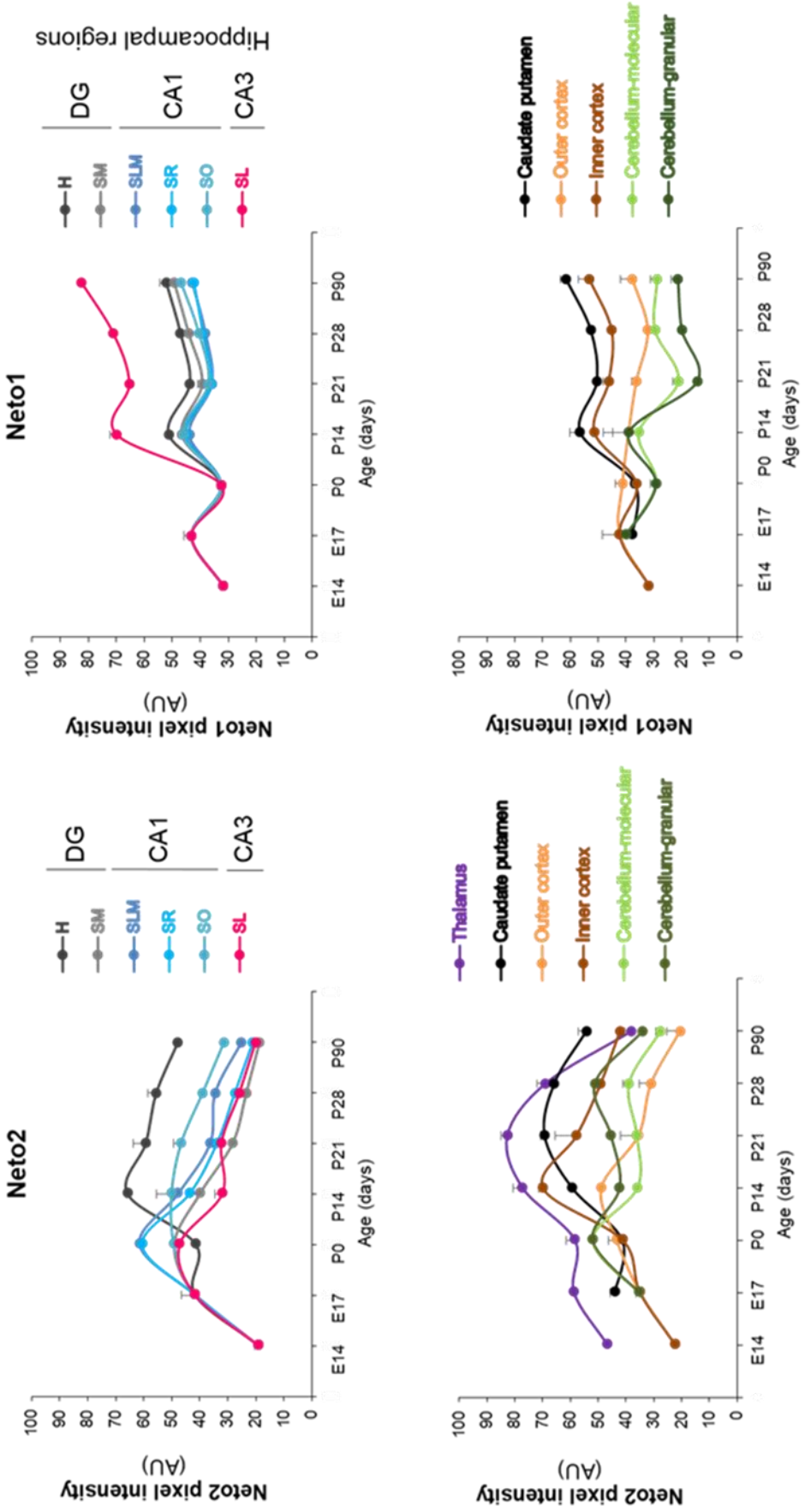
Neto1
Neto2
Hippocampal regions
DG
CA1
CA3
H
SM
SLM
SR
SO
SL
Thalamus
Caudate putamen
Outer cortex
Inner cortex
Cerebellum-molecular
Cerebellum-granular
Neto1 pixel intensity (AU)
Neto2 pixel intensity (AU)
Age (days)
E14
E17
P0
P14
P21
P28
P90
0
10
20
30
40
50
60
70
80
90
100

Figure 3.8. Developmental changes in Neto2 and Neto1 expression in the rat brain. Histoblot immunoreactivities (Figure 3.7) were quantified in various regions of the rat brain using optical densitometry and expressed in arbitrary units (AU). Neto2 and Neto1 immunoreactivities were determined at E14, E17, P0, P14, P21, P28, P90 in hippocampal sub-regions (DG, CA1, CA3) and their layers: hilus (H), stratum moleculare (SM), stratum lacunosum-moleculare (SLM), stratum radiatum (SR), stratum oriens (SO) and stratum lucidum (SL) (top panels). Neto2 immunoreactivity is predominant in the hilus of hippocampal DG after birth with a peak level around P14. In contrast, Neto1 immunostaining is prominent in the SL of hippocampal CA3 region after birth and continues to rise thereafter. Lower panels illustrate developmental changes in Neto2 and Neto1 levels in the cerebral cortex (O. Cx: outer cortex, I. Cx: inner cortex), caudate putamen (CPu), thalamus (T) and cerebellum (Cb-m: cerebellar moleculare layer, Cb-g: cerebellar granular layer). Neto2 expression peaks around P14-21 of rat brain development with a strong immunolabelling in the T, CPu, I.Cx and moderate in the Cb-g. Moderate Neto1 immunoreactivities were identified in the CPu and inner cortical layers throughout rat brain development and weak expression in the cerebellum. Data expressed as the mean of pixel intensities (AU). Error bars indicate the standard error (SE).

3.3.3.2.1 Neto2 expression during rat brain development

In general, Neto2 labelling was detected during embryonic development (E14, E17). It reached peak expression around P14-P21 followed by a decline to adult levels in most brain regions (Figure 3.7).

In the cerebral cortex, Neto2 immunoreactivity was detectable at E14 (Figure 3.8). Neto2 expression increased until P14, followed by a gradual decline until P90. The contrast between the inner cortical layers (layers V and VI) and the outer layers is noticeable from the second week after birth when the labelling intensity of the inner layers increased by ~30% compared to the outer layers. This difference continued to increase until it reached its maximum (~50%) at P90 compared to the outer layer.

The strongest labelling of Neto2 was detected in the thalamus followed by CPu with peak levels of expression at P21 for both regions (Figure 3.8). In the thalamus, Neto2 staining gradually declined toward P90 when it reached more than 50% reduction of its peak level (at P21). However, the reduction in the CPu staining after P21 was much less steep than in the thalamus around 20% decrease from P21 at P90.

In the cerebellum (Figure 3.8), Neto2 had a similar moderate pattern of labelling throughout development in both cerebellar layers with a predominant staining in the granular layer over the molecular one. It increased gradually in the first weeks of life until

reaching a peak level at P28 with a maximum increase difference between the two layers of around 25%. Then, it underwent a steep decline to P90 (Figure 3.8).

In the HIP (Figure 3.8), Neto2 immunopositivity was detectable at E17 and started to increase to moderate and high levels at P0 in all layers of the hippocampus except the dentate hilus which remained low. In contrast, after birth the reverse happened with a decrease of labelling in all layers other than the hilus toward P90 and an increase in the hilus staining to peak level at P14. Although the hilus staining started to decline after P14, it remained the predominant Neto2 labelling in the HIP and reached its maximum labelling difference from the other layers around 35-60% at P90 (Figure 3.8).

3.3.3.2.2 Neto1 expression during rat brain development

Throughout rat brain development (Figure 3.7), most Neto1 immunoreactivity was observed in the cerebral cortex, CPu and hippocampal CA3 region with relatively low levels in the cerebellar layers. The expression pattern that resembles the adult pattern is noticeable by the end of the first weeks of life (P14).

In the cerebral cortex (Figure 3.8), the first Neto1 labelling was weakly to moderately detected at E14, E17 and then at birth (P0). Clearer labelling was observed during the second postnatal week in the inner cortical layers (layers V and VI). Although the contrast of the inner layers to the outer layers is pronounced starting from the second week of life, the difference in labelling intensity was most prominent at P28 and P90.

In the CPu (Figure 3.8), Neto1 expression started with moderate levels prenatally then increased during the early postnatal period and continued to reach its maximum increase (40% of E17) by P90.

The staining pattern of Neto1 protein in the molecular and granular cell layers of the cerebellum was similar throughout development (Figure 3.8). Initially it was expressed moderately, followed by a decrease to low levels.

In the HIP (Figure 3.8), the staining pattern of Neto1 was detected at moderate levels prenatally. Differential labelling of hippocampal layers is clearly detectable within the first two weeks after birth. Neto1 immunoreactivity in SL was clearly

dominated as increased progressively and highly toward the adult period. However, moderate immunoreactivity was seen in the hilus (H) and stratum molecular (SM) layers of DG and weak to moderate labelling in the CA1 layers (SO, SR, SLM).

3.3.3.3 KAR pore-forming subunits (GluK1, GluK2/3 and GluK5) protein expression during development

The expression of different KAR subunit (GluK1, GluK2/3, and GluK5) proteins (Dr IK-Hyun Cho unpublished findings using the same developmental series brain sections, Figure 3.9) starts as early as E14 and increases in all labelled brain regions till adulthood, except GluK1 immunoreactivity, which peaks at P28 followed by a prominent reduction towards adulthood. During development (till P28), GluK1 expression increases in cortical layers, caudate putamen, thalamus, cerebellar molecular cell layer, and hippocampal regions (hilus of dentate gyrus, CA1 and CA3) followed by a decline toward adulthood.

GluK2/3 (Figure 3.9) is mainly expressed in an increasing manner (except the caudate putamen and dentate hilus where GluK2/3 protein expression peaks at P21) in the inner cortical layers, thalamus, cerebellar granular cell layer, and hippocampal CA3 stratum lucidum throughout brain development until adulthood.

GluK5 (Figure 3.9) is very weakly expressed during embryonic period and in the first week of life. It starts to increase postnatally at P14 until P28 when it reaches a plateau toward the adulthood in all regions with a predominant expression levels in the inner cortical layer, caudate putamen, and hippocampal CA3 stratum lucidum.

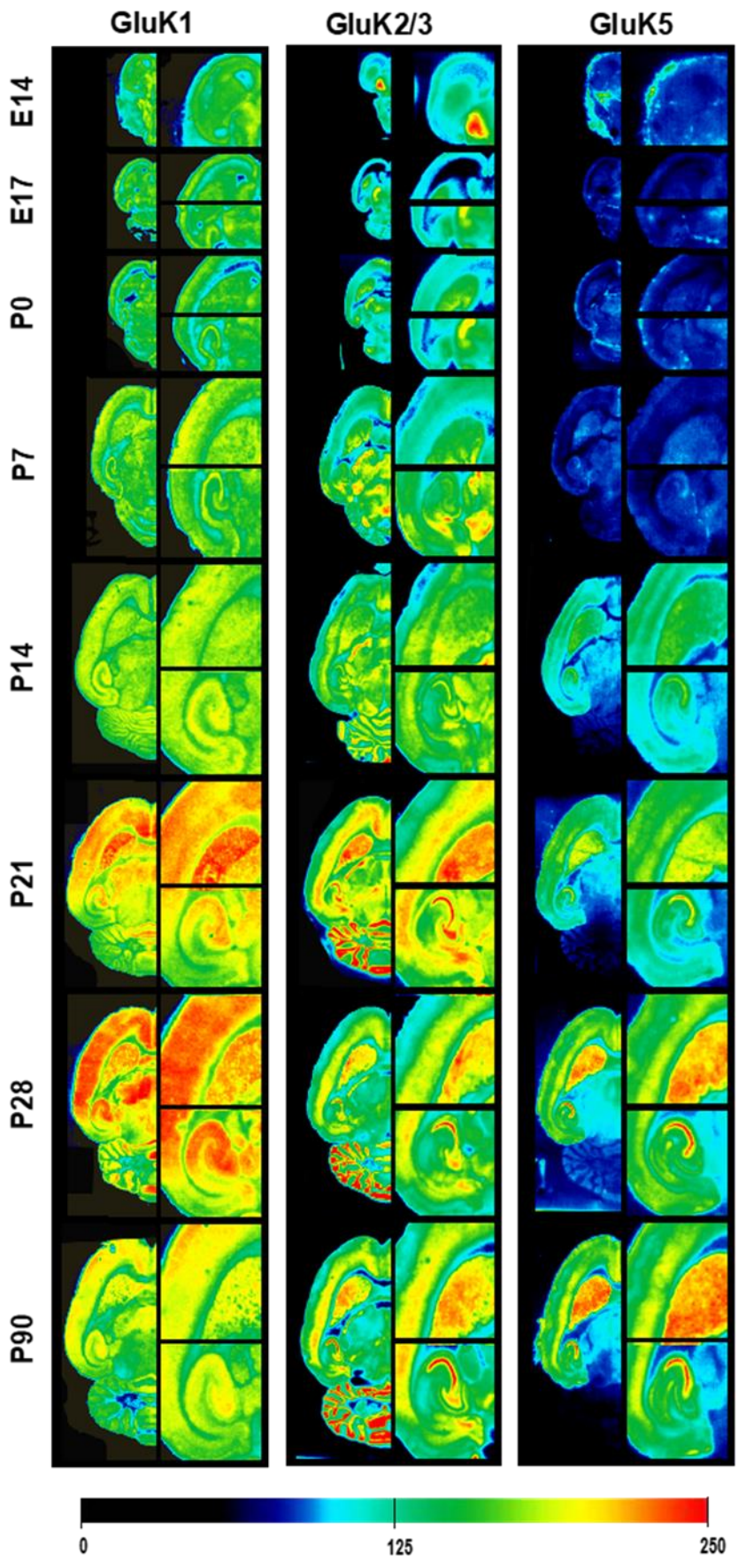
GluK1
GluK2/3
GluK5
E14
E17
P0
P7
P14
P21
P28
P90
0
125
250

Figure 3.9. Localisation of native KAR subunit proteins during brain development. Colour gradients of histoblots illustrate the regional distribution of GluK1 (using home-made antibody), GluK2/3, and GluK5 immunoreactivities at various stages of rat embryonic and postnatal development (E14, E17, P0, P14, P21, P28, P90) in horizontal brain sections (n = 3). In general, GluK1 immunostaining peaks during the first month of life (P28), after which it starts to decline in all brain regions. In contrast, GluK2/3 immunolabelling increases with development in many regions of the rat brain (cerebral cortex, caudate putamen and hippocampus). GluK5 immunolabelling appears late postnatally (P14) and reaches a plateau at P28. Colour gradients images were generated by assigning the grayscale images to the RGB (red-green-blue) channels in Adobe Photoshop CS2. Dr IK-Hyun Cho unpublished data.

3.3.3.4 Correlation of Neto2 and Neto1 expression patterns to KAR pore-forming subunits GluK1, GluK2/3 and GluK5

The correlation of the developmental expression pattern of pore-forming and auxiliary KAR subunits is as follows:

1. The developmental profiles of Neto2 and GluK1 are similar in the caudate putamen and thalamus in that their immunoreactivity peaks late postnatally and then decline toward adulthood.
2. The developmental profiles of Neto2 and GluK2/3 are similar in the dentate hilus as their immunolabelling peaks late postnatally.
3. The developmental changes in Neto1 and GluK2/3 expression levels are similar in the inner cortical layers, caudate putamen and hippocampal CA3 stratum lucidum since their immunoreactivity continues to increase throughout development and toward adulthood.

3.3.3.4.1 Concluding remarks

1. Neto2 and Neto1 protein expression overlaps in the deeper layers of the cerebral cortex and caudate putamen.
2. Neto2 and Neto1 proteins are differentially expressed in the cerebellar granular cell layer and dentate hilus (Neto2) and hippocampal CA3 stratum lucidum (Neto1).
3. Parallel developmental changes of pore-forming & auxiliary subunits of KARs as follows:

Neto isoform	KAR subunit	Brain region
Neto2	GluK1	CPu, T
	GluK2/3	Dentate hilus
Neto1	GluK2/3	I.Cx, CPu, Hippocampus

3.4 Discussion

3.4.1 Regional distribution of Neto2 and Neto1 proteins

In this study, we established the spatiotemporal expression profiles of Neto2 and Neto1 proteins and correlated them to pore-forming KAR subunits. This will help to understand the molecular basis that underlies the variation in KAR subunit composition, regional distribution and KAR function, as much previous research work showed that Neto2 and Neto1 proteins modulate key aspects of KAR signalling (Tomita and Castillo, 2012; Copits et al., 2011; Straub et al., 2011a; Zhang et al., 2009; Straub et al., 2011b; Tang et al., 2011; Wyeth et al., 2014; Copits and Swanson, 2012).

3.4.1.1 Regional distribution of Neto proteins in the adult rat brain

Our findings of the regional distribution pattern of Neto1 protein in the adult rat brain is consistent with the available evidence in the literature (Ng et al., 2009; Straub et al., 2011a; Tang et al., 2012). In *situ* hybridisation for Neto1 mRNA in adult mice brain sections showed a wide expression profile throughout the CNS with strong expression in CA3 hippocampal region, cerebral cortex and caudate putamen (Ng et al., 2009). Moreover, Neto1 protein localisation in mouse brain was strongly revealed by immunohistochemistry at the hippocampal stratum lucidum where mossy fibre and CA3 pyramidal cells form synapses and also agrees well with the strong [^{3}H]kainate binding pattern that detected the distribution of KARs in the same hippocampal layer (Straub et al., 2011a). However, Neto1 expression is very weak in the cerebellum compared to other brain regions, a finding that is supported by the results of others (Straub et al., 2011a). On the other hand, we found that Neto2 protein expression is complementary to Neto1 as the former is strongly expressed in hippocampal dentate hilus and the cerebellum, particularly in the granular cell layer, which was also

evidenced by its strong immunofluorescent staining of cerebellar sections (Tang et al., 2012).

3.4.1.1.1 Correlating Neto protein expression to KAR subunits in the adult rat brain

There is a clear overlap in the regional distribution of Neto1, GluK2/3 and GluK5 KAR subunits in the inner cortical layers, caudate putamen and hippocampal CA3 region. This suggests a regulatory role for Neto1 to KAR subtypes containing these subunits in these areas (Table 1.2). The same principal also applies to Neto2 and GluK2/3 in the inner cortical layers, cerebellum and dentate hilus (Table 1.2.). This regional expression match does not imply that the auxiliary and pore-forming subunits are co-expressed/co-assembled in the same subcellular compartment. Therefore, it is only a circumstantial evidence for their association at the protein level. It is worth noting that the expression pattern of the closest KAR relative of the ionotropic glutamate receptor family, AMPAR, does not show this expression overlap using the histoblot analysis of the same brain samples. Furthermore, previous studies demonstrated the association of Neto proteins with neuronal GluK2/3 and GluK5 KAR subunits but not with AMPAR subunits to modify KARs functional responses to glutamate (Straub et al., 2011a; Zhang et al., 2009; Tang et al., 2011).

3.4.1.2 Regional distribution of Neto proteins during development in the rat brain

The widespread distribution of Neto proteins in the developing brain, particularly after birth, and their sustained expression in the adult may suggest a consistent role in the maturation and adult function of neuronal networks. Appropriate receptor assembly and clustering is critical for the establishment and preservation of excitatory synapses because newly formed synapses are thought to be activity dependent (Molnar et al., 2002). This suggests that to maintain and mature the new synapse, synaptic transmission need to be preserved, probably by the help of developmentally regulated proteins. For example, Neto proteins may enhance the maturation of excitatory synapses through promoting functional responses and clustering of KARs.

Our results on the regional distribution of Neto1 protein in the developing rat brain using the histoblot technique confirmed the embryonic and postnatal mice brain mRNA expression pattern (Michishita et al., 2004) in the caudate putamen, cerebellum, and hippocampus. *In situ* hybridization experiments (Michishita et al., 2004) showed that Neto1 mRNA staining was weakly detected in the embryonic stage in the cortex, thalamus, cerebellum and hippocampus and was moderate in the caudate putamen. At P5 and P21, the staining was dense in the caudate putamen and CA3 region, weak in DG and CA1 hippocampal regions, and absent from the cerebellum which qualitatively and quantitatively comes in good agreement with our result of Neto1 protein immunoreactivity in these regions. However, some discrepancies were found between the results of the two experimental methods in other brain regions. Throughout postnatal day P5 to P21, Neto1 mRNA expression was observed in the entire cortex but concentrated in cerebral layers V, VI and the superficial part of layers II/III at which it reached a plateau at P14 then gradually decreased (Michishita et al., 2004). This could be explained by the maturation process of the excitatory glutamatergic synaptic transmission during early postnatal period which needs the increase in the number and/or strength of receptor synaptic contacts and so labelling was concentrated not only in deep layers but also in superficial layers. Also, thickening of the cortex during the third week of life might be responsible for dispersed staining and as a result the observed gradual decrease in expression after P14. These discrepancies between the protein and mRNA expression patterns might also be due to different sensitivities of the two methods and/or different species used (rat versus mouse).

In addition, our developmental expression pattern of Neto2 in the rat brain is consistent qualitatively with mice brain mRNA expression in cerebral cortex, caudate putamen, thalamus, cerebellum (moderate in the granular layer and absent from the molecular layer), and hippocampal CA1 and CA3 (Michishita et al., 2004). Quantitatively, the expression of Neto2 mRNA in these areas was weak to moderate which matches our quantitative result for the molecular cerebellar layer and hippocampal CA1 and CA3. Again, this quantitative discrepancy could be due to different sensitivities of the two methods and/or different species used (rat versus mouse). However, the only significant difference is in the hippocampus particularly Neto2 expression in the dentate hilus. We found Neto2 immunolabelling predominant

in the hilus and moderate in CA regions after birth while Michishita et al. group found no Neto2 mRNA signal in the same region and moderate labelling in the CA1 and CA3. This could be due to differences in the area of the hilus region between the brain sections used in the two studies (Scharfman and Myers, 2013). Michishita et al. used sagittal sections where the hilus has a very small area of the DG (CA3 encompasses most of the space between the supra- and infra-pyramidal blades) and so, the observed mRNA signal in that very narrow area might be due to Neto2 and not a trace from CA3. In comparison, our sections were in the horizontal plane where the hilus is a large area (Figure 3.10).

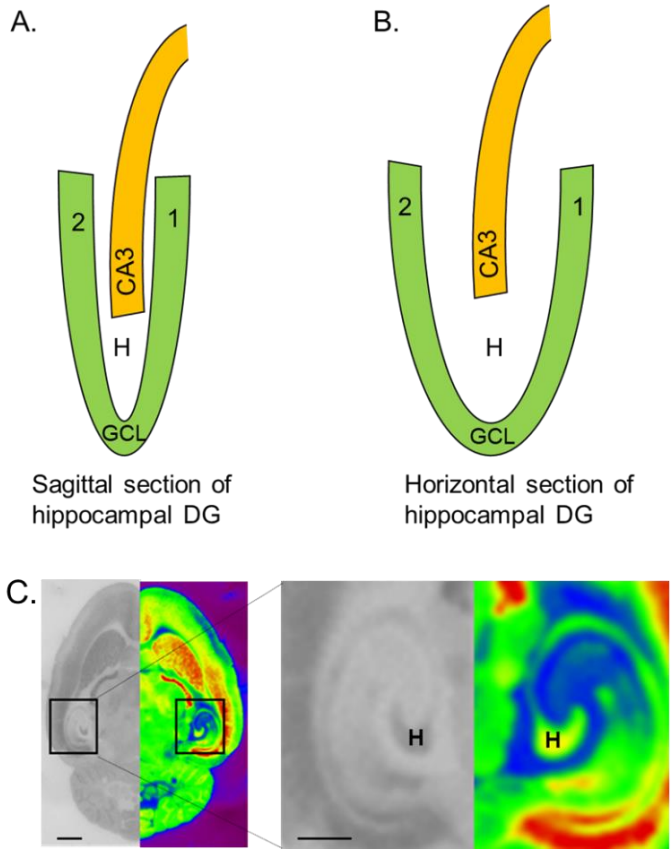

Figure 3.10. The dentate hilus area of sagittal and horizontal planes. A schematic representation of hippocampal DG from a sagittal brain section (**A**) and a horizontal plane (**B**). Neto2 protein expression in a horizontal section of the rat hippocampus at P21 (**C**). CA3: cornu ammonis 3, GCL: granular cell layer, H: hilus, 1: supra-pyramidal blade, 2: infra-pyramidal blade.

The mRNA expression indicates the early steps of a long cellular regulatory process to produce a protein (Payne, 2015) making the correlation between mRNA and protein expression not an easy task (Payne, 2015). Thus, differences in the expression levels

(qualitative and quantitative) between the mRNA and the protein could also be attributed to several other factors including:

1. Translation time lag from mRNA to significant protein accumulation
2. The differences between synthesis and decay rates of both mRNA (lifetime is in minutes) and protein (lifetime is in hours-days).

In addition, the clear differences between the strength of the signal labelling between the mRNA and its protein expression (the quantitative discrepancy) in some regions like Neto2 expression in the cerebral cortex for example could be explained by the non-straightforward relationship between mRNA and protein expressions.

3.4.1.2.1 Correlating the regional distribution of Neto proteins to KAR subunits in CNS development

After correlating the regional distribution of Neto proteins to KAR subunits during rat brain development, it is expected to observe some parallel expression profiles as very recent evidence (Orav et al., 2017; Jack et al., 2018, Vernon and Swanson, 2017; Wyeth et al., 2017) suggests an enhancement of KAR-mediated developmental processes by Neto proteins. However, this does not necessary mean that the Neto-modulatory roles of KARs are restricted to such a parallel pattern. As long as both types of proteins show a regional co-expression pattern, this may suggest their regulatory roles.

We found very similar pattern of the developmental expression of Neto2 and GluK1 in caudate putamen and thalamus where both subunits peak late postnatally (P21-28). Furthermore, there is a parallel developmental expression pattern of Neto2 and GluK2/3 in the dentate hilus where both peaks around P14-P21. In addition, Neto1 developmental profile is similar to GluK2/3 in most brain regions except the cerebellum. This may suggest a special role for Neto proteins in regulating these KAR subunits in a particular spatiotemporal manner.

For example, Neto1 promotes the maturation of interneuronal dendrites in organotypic culture of the visual cortex (Jack et al., 2018) probably by enhancing GluK1 surface expression (Wyeth et al., 2017). Neto1 and GluK1 subunits have functional PDZ-binding motifs (the last 4 amino acids of each) that have similar

homology to type 1-PDZ-binding motif. This regulates their interaction with PSD95 for synaptic targeting (Sheng et al., 2018).

In addition, the similarity between the adult pattern of Neto1, GluK2/3, and GluK5 subunits and their postnatal pattern may represent an important contribution of them in developmental plasticity. Neto1 augments kainate activation of KARs at mature somatodendritc interneurons, a neuronal population that express GluK1, GluK2, and GluK5, producing inhibitory currents in CA3 pyramidal neurons (Wyeth et al., 2017). In contrast, tonic suppression of inhibitory interneurons release results from Neto1 and Neto2 regulating the function of presynaptic KARs at a subset of mature inhibitory hippocampal interneurons by facilitating KARs activation and their agonist affinity (Wyeth et al., 2017). Moreover, early postnatally (P4-6), Neto1 is needed for GluK1-containing KARs presynaptic tonic suppression of glutamate release at immature CA3-CA1 synapses (Orav et al., 2017). Neto proteins are required for axonal targeting of most KARs subunits in immature hippocampal CA3-CA1 circuitry (Orav et al., 2017). Loss of Neto1 leads to loss of presynaptic KARs function and impairment in the synaptogenesis of this circuit. This indicates the importance of Neto proteins in the development of synaptic connectivity.

3.5 Conclusion

In conclusion, our findings imply Neto proteins and KAR subunits show distinct regional expression profiles during rat brain development toward the adulthood. In addition, the expression of both Neto protein isoforms is differentially regulated in adult brain and throughout development suggesting distinct roles. Furthermore, identifying their cellular and subcellular distribution could improve our understanding of neuronal circuit formation.

4 Expression patterns of pore-forming kainate, AMPA and NMDA receptor subunit proteins in a rat model of chronic epilepsy

4.1 Background

4.1.1 Normal vs epileptic hippocampal networks

The reactive plasticity, major network reorganisation in epilepsy mainly in the DG, has been observed in various types of epilepsies in both human and rodents (Represa et al., 1986; Represa et al., 1989; Sutula et al., 1989; Houser et al., 1990; Gabriel et al., 2004). Figure 4.1 illustrates part of the normal hippocampal neuronal network (A) and its pathological reorganisation in epileptic conditions (B). Information from the entorhinal cortex enters the hippocampus via the perforant pathway after being filtered by the dentate gyrus (Henze et al., 2002; Acsady et al., 2007). The dentate gyrus is composed of 3 main layers (Amaral et al., 2007).

First, the relatively cell-free molecular layer with the granule cells dendrites, which receive excitatory inputs from the entorhinal cortex through the perforant pathway.

Second, the densely packed granule cell layer, which also contains interneurons (e.g. basket cells). The main projection of the granule cells is hippocampal mossy fibres toward the stratum lucidum of CA3 (Figure 4.1A). Thus, providing excitatory inputs to the CA3 pyramidal cells from the entorhinal cortex. The CA3 pyramidal cells make excitatory connections with CA1 pyramidal cells. Furthermore, collaterals of mossy fibres make excitatory synaptic connections with a) inhibitory interneurons such as the pyramidal basket cells in the granular cell layer and b) excitatory interneurons such as the mossy cells in the dentate hilus.

Third, the dentate hilar cell layer. This area has the mossy cells and various other interneurons. The mossy cells project to dentate basket cells and provide excitatory input. In turn, basket cells provide dentate granule cells with an inhibitory feedback.

The dentate gyrus functions as a high-resistance gate, filtering information inputs from the entorhinal cortex to the hippocampus (Koyama, 2016). This function is compromised in epilepsy, making the hippocampal formation an epileptic focus in TLE (Heinemann et al., 1992; Lothman et al., 1992). In epilepsy, instead of acting as a safety gate, the dentate gyrus amplifies the entorhinal cortex input of the epileptic activity through recurrent circuits of excitation and the loss of inhibitory interneurons.

In patients and animal models of TLE, the axons of the dentate granule cells, mossy fibres, branch [recurrent mossy fibres (rMF)] in the dentate hilus to form excitatory synapses with the dendrites of the granule cells in the inner molecular layer (Figure 4.1B). This reorganisation does not occur under normal conditions (Nadler, 2003; Koyama and Ikegaya, 2004; Sloviter et al., 2012; Buckmaster et al., 2002; Cavazos et al., 2003). In addition, mossy cells are damaged in human epilepsy patients (Babb et al., 1984) and animal models of TLE (Nadler et al., 1980; Sloviter et al., 1987). And, it was suggested that the sprouting of mossy fibres is a result of mossy cell death (Epsztein et al., 2005; Cavazos and Sutula, 1990; Houser, 1990; Houser, 1999; Babb et al., 1991). This indicates that the sprouting might be a mechanism to account for the loss of the glutamatergic inputs (of mossy cells) to the granule cells and the inhibitory basket cells (Epsztein et al., 2005; Koyama, 2016).

Additionally, in patients and animal models of TLE (Houser, 1990; Lurton et al., 1998; Riban et al., 2002; Parent and Murphy, 2008; Scharfman et al., 2007), the granule cells of the dentate gyrus are dispersed compared to the densely packed organisation in normal conditions (Houser, 1990; Lurton et al., 1998) with abnormal ectopic granule cells in the hilus (Scharfman et al., 2007; Figure 4.1B). These ectopic cells are stimulated by excitatory inputs from normal granule cells and the pyramidal cells of hippocampal CA3. They also form excitatory contacts with the dendrites of the granule cells in the inner molecular layer and CA3 pyramidal cells leading to loops of excitation that trigger epileptogenesis.

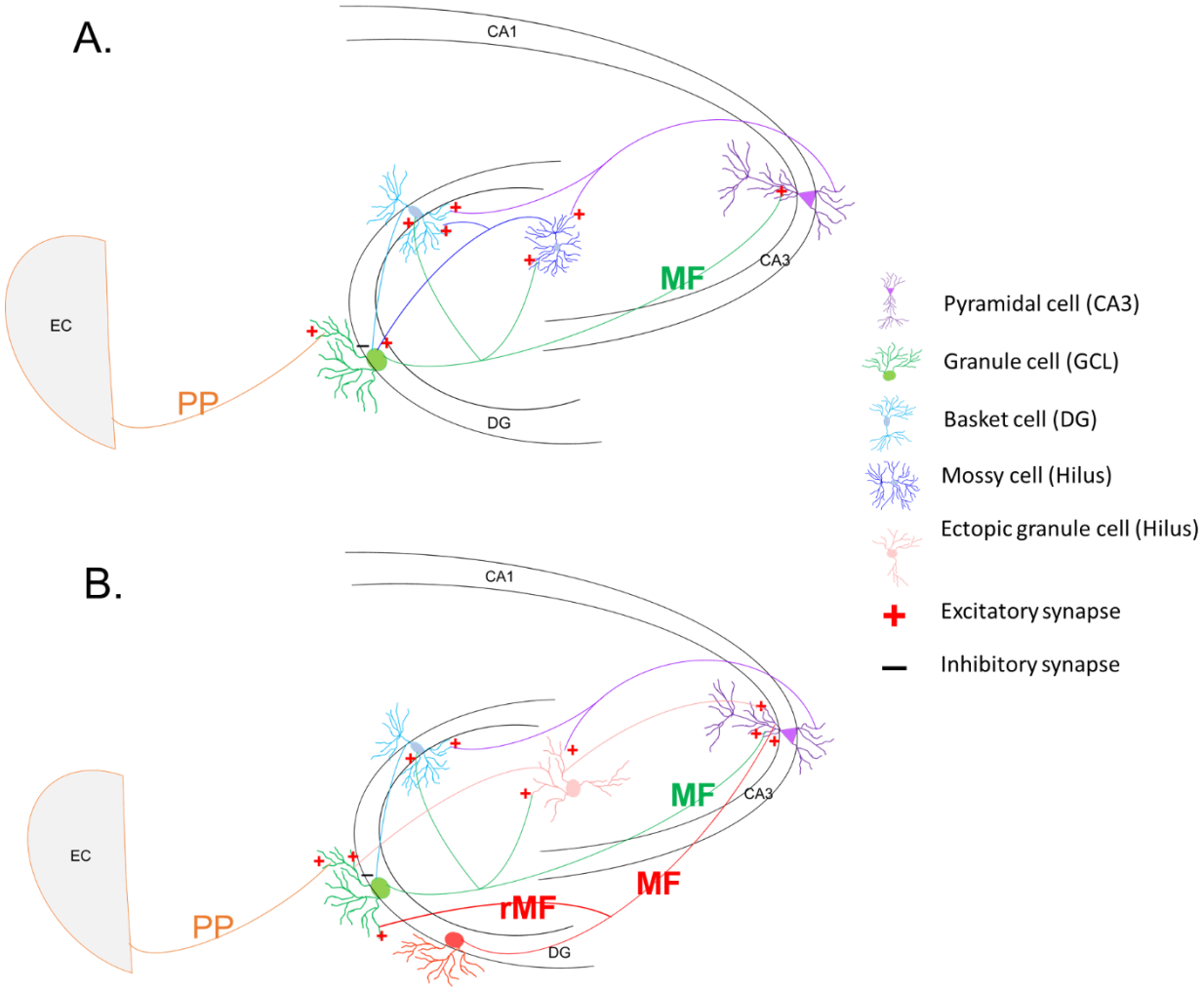

Figure 4.1. Schematic illustration of normal and pathological hippocampal neuronal circuits. A schematic drawing showing normal hippocampal network (**A**) and hippocampal reactive plasticity in epilepsy (**B**). The granule cells of DG normally send mossy fibre axons to CA3 region and form synaptic contacts with cells in the hilus of the DG, pyramidal cells of CA3 and various interneurons. In temporal lobe epilepsy, new collaterals [recurrent mossy fibres (rMF)] arise from the hilus, project to the molecular layer of DG, CA3 region, and contact with dendrites of other granule cells (granule cells are interconnected) forming a recurrent circuit that dentate granule cells excite each other which can be the focus of seizure activity (Koyama and Ikegaya; Epsztein et al., 2005; Koyama, 2016).

4.1.2 Pilocarpine-based models of epilepsy

The cholinergic agonist pilocarpine is widely used in animal models of TLE (Curia et al., 2008). Pilocarpine-treated animals are useful to study epileptogenesis and are also used as models of multiple drug resistance to antiepileptic drugs (Vizuete et al., 2018). Pilocarpine acts on muscarinic receptors to activate the cholinergic system which is believed to be the initiating factor for triggering seizures and SE (Curia et al., 2008; Vezzani, 2009). Knocking out muscarinic receptors in mice prevented seizure development in response to pilocarpine (Curia et al., 2008). Additionally, atropine, a muscarinic antagonist, blocked pilocarpine-induced SE (Curia et al., 2008). Furthermore to direct cholinergic system activation in the brain, pilocarpine-induced seizures are also derived from its primary proinflammatory actions involving the periphery (Vezzani, 2009). The peripheral proinflammatory mechanisms induced by pilocarpine lead to blood–brain barrier (BBB) leakage, prior to the onset of status epilepticus. This BBB leakage causes ionic imbalance as K^+ accumulate in the extracellular space, which is required for pilocarpine to produce its convulsant activity (Vezzani, 2009). Changes in BBB permeability seem to synergistically potentiate direct CNS action of the drug leading to seizures (Vezzani, 2009; Marchi et al., 2007). To minimize the contribution of systemic cholinergic activation in favour of CNS effects, pilocarpine systemic effects are antagonized by pretreatment with the peripherally-acting muscarinic antagonist methyl scopolamine (0.5–1 mg/kg, SC) (Marchi et al., 2007; Cavalheiro et al., 2006). Methyl scopolamine is a quaternary amine and therefore has no effect on the CNS because it cannot penetrate the BBB (Dowd, 2017). However, at the used doses of pilocarpine, it is possible that peripheral muscarinic blockade by methyl scopolamine is insufficient (Vizuete et al., 2018). This is because pilocarpine dose used to induce SE is well in excess of that capable of fully displacing antagonist's binding (Marchi et al., 2007). In addition, peripheral pilocarpine's effects on WBC were not significantly antagonized by methyl scopolamine although it was useful in diminishing a number of events like salivation, body tremors, and diarrhea (Marchi et al., 2007). Thus, some peripheral events may take place in spite of methyl scopolamine pretreatment that may not be capable of fully counteracting all systemic pilocarpine effects (Vizuete et al., 2018; Marchi et al., 2007).

The pilocarpine-based model of chronic epilepsy is considered one of the most appropriate animal models of human TLE (Curia et al., 2008). This is because many of the human features of the disease are reproduced in it. First, the limbic system is the main

location of seizure foci with the entorhinal cortex, hippocampus, and amygdala being the most damaged regions in TLE patients (Bartolomei et al., 2005). Second, the presence of an initial trigger (febrile seizure, perinatal hypoxia, head trauma, and infection in humans or status epilepticus in animals) before the development of TLE (Mathern et al., 2002). Third, the presence of a silent (normal behaviour and EEG activity) period after the initial precipitating injury. And fourth, reorganisation of hippocampal neuronal networks occurs like mossy fibres sprouting, abnormal proliferation of dentate granule cells into the dentate hilus, and neuronal loss in CA regions and dentate hilus (Wieser, 2004; Mathern et al., 1997). It worth noting that in the pilocarpine model of epilepsy, the neuronal damage is widely spread including the olfactory cortex, amygdala, thalamus, neocortex, hippocampus and substantia nigra (Turski et al., 1989). High-dose pilocarpine (300-400 mg/kg) produced a mortality rate of ~30-55 % in Wister rats (Turski et al., 1983; 1989; Cavalheiro et al., 1991; Liu et al., 1994; Esclapez et al., 1999; Leite et al., 1990). Adding lithium to the pilocarpine model increased the sensitivity to pilocarpine, hence, allowing the use of a lower dose (30 mg/kg) (Clifford et al., 1987; Fujikawa et al., 1999; Glien et al., 2001) with higher rate of status epilepticus in treated animals. However, the mortality rate remained high (24-45%) and was decreased (7%) by dividing the low-dose pilocarpine (Fujikawa et al., 1999; Glien et al., 2001) (Table 4.1). Notably, the behaviour, electrographical, and neuropathological changes were very similar between high-dose pilocarpine and lithium-low-dose pilocarpine models (Curia et al., 2008). Pilocarpine application (10 µM) to horizontal entorhinal cortex-hippocampus brain slices induced epileptic activity as ictal discharges that started in the entorhinal cortex, then propagated to the dentate gyrus, after which they moved to the hippocampus (Nagao et al., 1996).

SE duration (min)	Lithium pre-treatment (3 mEq/kg)	Pilocarpine (mg/kg)	Rat strain	Mortality rate (%)	Reference
90		320-360	Sprague-Dawley	17	Williams et al., 2002
120		320-360	Wistar	55	Esclapez et al., 1999
120		380	Sprague-Dawley	50	Biagini et al., 2006, 2008
>120		380	Sprague-Dawley	5	Poirier et al., 2000
>120		380	Wistar	30	Leite et al., 1990
90	Lithium	30 (single dose)	Wistar	45	Fujikawa et al., 1999 Glien et al., 2001
90	Lithium	30 (10 mg/30 min)	Wistar	7	Glien et al., 2001
120	Lithium	30 (10 mg/30 min)	Wistar	40	Glien et al., 2001
>120	Lithium	30 (single dose)	Sprague-Dawley	24	Glien et al., 2001
>120	Lithium	30 (single dose)	Wistar	100	Fujikawa et al., 1999

Table 4.1. A summary of high-dose or lithium-low-dose pilocarpine models of epilepsy mortality rates.

4.1.3 A refined model of the lithium-low-dose pilocarpine

As part of our collaboration with Professor Gavin Woodhall's research group at Aston University [https://www2.aston.ac.uk/lhs/staff/az-index/woodhagl], we have investigated the regional expression patterns of kainate, AMPA, and NMDA receptor subunit proteins in a new epileptic animal model (Modebadze et al., 2016, Table 4.2).

Our collaborators have developed a refined model of epilepsy to reduce animal usage and suffering aiming to adopt the 3Rs principle of the research ethics framework (Reduction, Refinement and Replacement of animals) and to improve the correlation of the rodent model to the human neurological condition.

Animal group	Age when killed	Number of animals	Time elapsed since SE	Total number
Control animals (untreated)	8 months	2	-	6
	9 months	2	-	
	12 months	2	-	
Non-epileptic animals (treated)	8 months	1	3 months	4
	11 months	3	10 months	
Epileptic animals (treated)	8 months	1	3 months	7
	9 months	4	8 months	
	10 months	1	9 months	
	11 months	1	10 months	

Table 4.2. A summary of the used RISE model animal groups. The age of the animals across the three study groups (untreated control, lithium-low-dose pilocarpine treated non-epileptic and treated epileptic animals) is comparable (8-12 months). The time elapsed since status epilepticus induction for the treated animals (non-epileptic and epileptic) is between 3 and 10 months [chronic phase of the Reduces Intensity Status Epilepticus (RISE) model; Modebadze et al., 2016].

The new refined chronic model of epilepsy is called the Reduces Intensity Status Epilepticus (RISE) model (Modebadze et al., 2016) which is based on the lithium-low-dose pilocarpine model (Glien et al., 2001). The refinement process (Modebadze et al., 2016) of the standard lithium-low-dose pilocarpine model was achieved by minimizing the highly stressful convulsive activity during acute status epilepticus through the use of a muscle relaxant (2.5 mg/kg xylazine intramuscularly) and a

cocktail of anticonvulsant/antiepileptic (MK-801, diazepam, and MPEP). The result was a very low mortality rate (1%), which means fewer animals are required (the Reduction R), as compared to the high mortality rate of the standard lithium-low-dose pilocarpine model (7-40%) (Glien et al., 2001). However, this refined model also led to spontaneous recurrent seizures (SRS) after a latent period, which meant high epileptogenic morbidity (Figure 4.2).

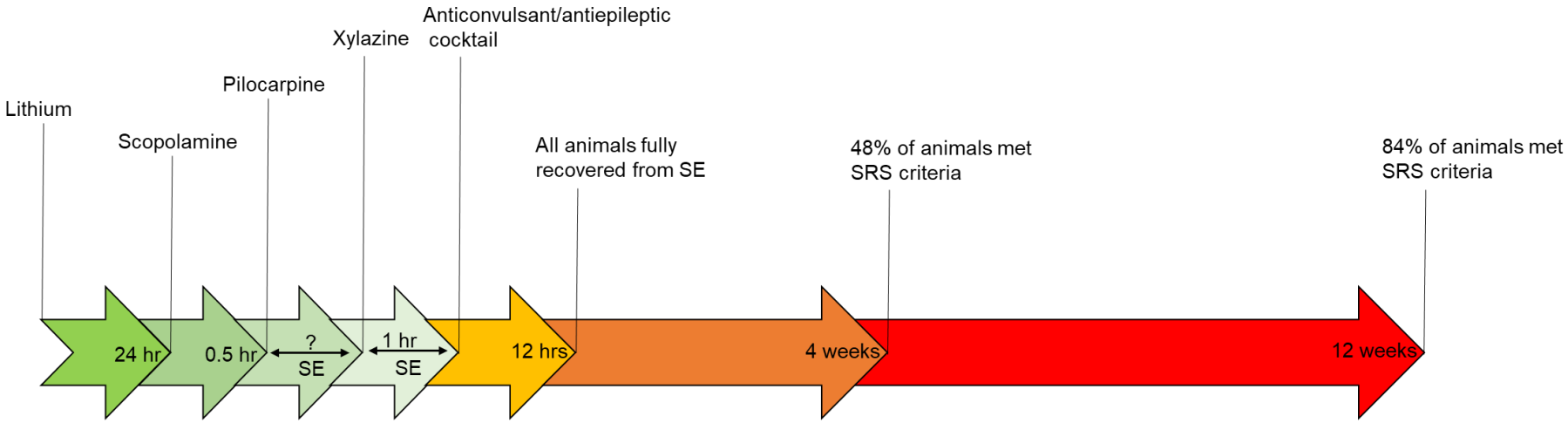

Figure 4.2. Timeline of the development of spontaneous recurrent seizures in the RISE model of TLE. 24 hours before pilocarpine treatment, rats (8-11 months) were treated with lithium. After that, pilocarpine (25 mg/kg subcutaneously) was administered (after pre-treatment with α-methyl scopolamine (1 mg/kg subcutaneously) to prevent pilocarpine peripheral effects). Animals were then closely monitored. And, when they showed bilateral forelimb clonus with rearing [seizure severity rate >3 on Racine's scale (Racine, 1972)], xylazine (a muscle relaxant to reduce seizure severity) was administered immediately. Animals were left in a non-convulsive status epilepticus (xylazine-modified SE) for one hour after which anticonvulsants and anti-epileptics (MK-801, diazepam, and MPEP) were administered to terminate the seizure activity. Most animals (84%) met spontaneous recurrent seizure (SRS) criteria within 12 weeks of status epilepticus (SE) induction in the RISE model of chronic epilepsy (Modebadze et al., 2016).

Indeed, RISE model reflects a close homology of the natural history of epileptogenesis: (i) it lacks the gross damage of the brain that was evidenced by examining the entorhinal cortex and hippocampus regions of the epileptic animals and measuring the functional state of the neuronal networks in CA3 region which showed spontaneous activity *in vitro* throughout the development of chronic epilepsy (i.e. CA3 remained functionally intact in the acute, latent, and SRS periods). In contrast, the more aggressive models such as the unrefined high-dose pilocarpine model resulted in significant neurodegeneration of numerous brain regions (Lemos and Cavalheiro, 1995). (ii) It had a progressive profile of network alterations within the temporal lobe relevant to TLE and indicated by: 1) ictal-like events in hippocampus in the first week following induction, 2) normal spontaneous activity during the latent period and again 3) abnormal activity in the form of ictal-like events in the medial entorhinal cortex and hippocampal CA3 region following the development of SRS.

4.2 Aim and objectives

Aim: To identify activity-induced changes in the expression level of kainate, AMPA, and NMDA receptor subunit proteins using a refined lithium-low dose pilocarpine model of chronic epilepsy (Modebadze et al. 2016).

Objectives:

1. To compare the regional expression levels of GluK2/3, GluK5, GluA1-4, GluA1, GluA2, GluN1, and GluN2B iGluR subunit proteins in lithium-low-dose pilocarpine treated rats (epileptic and non-epileptic) with untreated controls.
2. To assess iGluR subunits levels during the SRS phase in vulnerable brain regions (e.g. medial entorhinal cortex (mEC) and hippocampus).
3. To establish the presence of recurrent mossy fibre circuits in epileptic animals through the investigation of mossy fibre sprouting during the chronic phase of the RISE model.

4.3 Results

Using the refined rat model of chronic epilepsy, RISE (Modebadze et al. 2016), we used the histoblot technique to examine changes in the regional expression pattern of KAR (GluK2/3 and GluK5), AMPAR (GluA1-4, GluA1 and GluA2) and NMDAR (GluN1 and GluN2B) subunit proteins in vulnerable brain areas (mEC and hippocampus) that showed ictal activity in electrophysiological studies (Modebadze et al. 2016).

4.3.1 Comparison of KAR subunit distribution patterns and expression levels in control and epileptic brains

The distribution and expression levels of GluK2/3 (Figure 4.3 and Table 4.3) and GluK5 (Figure 4.3 and Table 4.4) were investigated in control and low dose lithium/pilocarpine-treated chronically epileptic and non-epileptic rats. The GluK2/3 and GluK5 immunolabelling patterns were very similar between the study groups in the mEC layers and hippocampal sub-regions (CA1, CA3, DG). No significant differences were identified in GluK2/3 or GluK5 expression levels in any of the brain regions studied in the three treatment groups.

The GluK5 v. GluK2/3 ratios were compared to detect possible shifts in the subunit composition between the three study groups (Figure 4.3). There were no detectable changes in any of the studied brain regions.

The immunolabelling of the studied KAR subunits in this model was prominent in the inner cortical layers, CPu, SL of hippocampal CA3, moderate in DG and granular cerebellar cell layer (GluK2/3), and weak in CA1 and the cerebellum (GluK5).

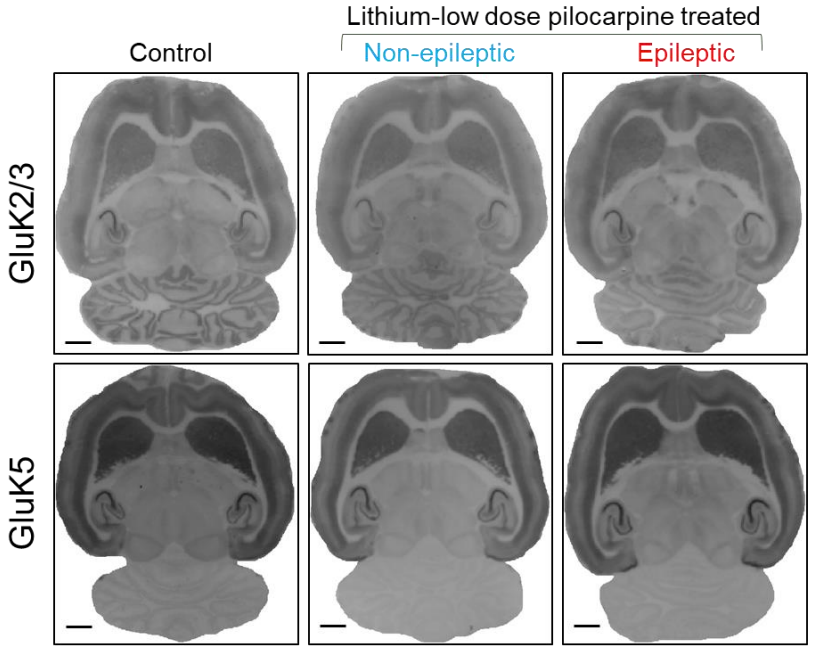
Lithium-low dose pilocarpine treated
Control
Non-epileptic
Epileptic
GluK2/3
GluK5

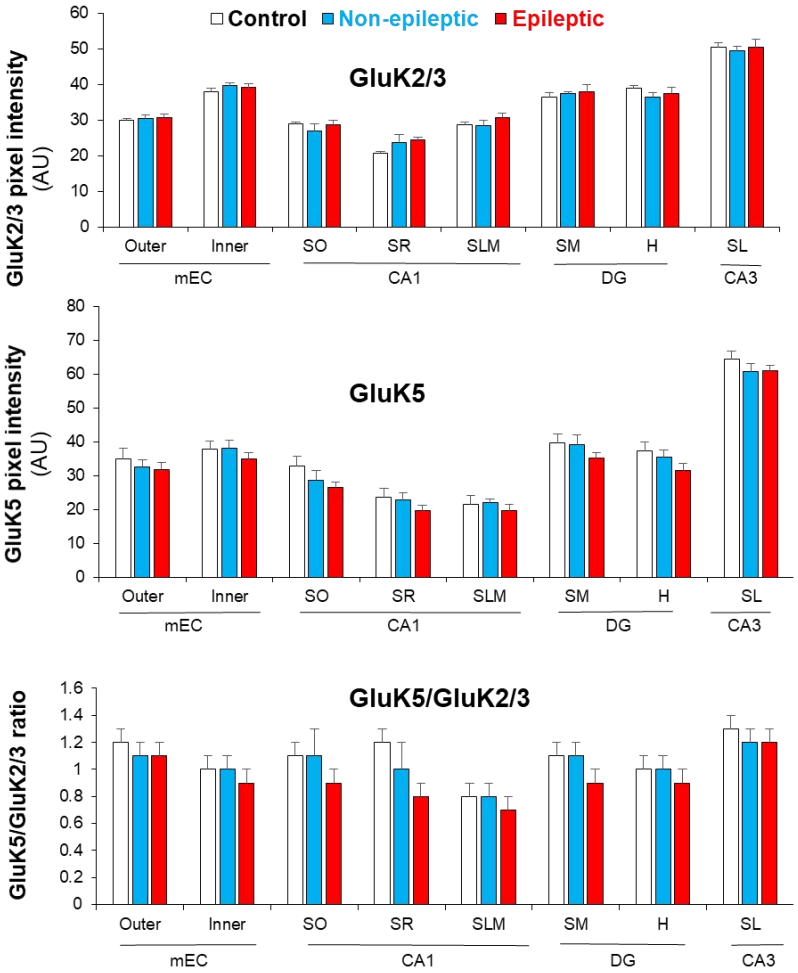
Control
Non-epileptic
Epileptic
GluK2/3
GluK2/3 pixel intensity (AU)
GluK5
GluK5 pixel intensity (AU)
GluK5/GluK2/3
GluK5/GluK2/3 ratio
Outer
Inner
SO
SR
SLM
SM
H
SL
mEC
CA1
DG
CA3

Figure 4.3. Comparison of GluK2/3 and GluK5 KAR subunit protein expression levels in control and spontaneously epileptic rats. Histoblots of horizontal adult (8-12 months) rat brain sections were obtained from sham treated (Control, n = 6) and lithium-low dose pilocarpine-treated (Modebadze et al., 2016) rats without (Non-epileptic, n = 4) and with spontaneous seizures (Epileptic, n = 7). Expression profiles of GluK2/3 and GluK5 KAR pore-forming subunits were studied in the following brain regions: medial entorhinal cortex (mEC) outer and inner layers and hippocampal sub-regions (DG, CA1, CA3) and their layers: hilus (H), stratum moleculare (SM), stratum lacunosum-moleculare (SLM), stratum radiatum (SR), stratum oriens (SO) and stratum lucidum (SL). The bar diagrams represent the pixel intensities of GluK2/3 and GluK5 in vulnerable brain regions (mEC and hippocampus) in the three study groups. The relative expression ratios of GluK5:GluK2/3 are included on the bottom panel. There are no statistically significant differences in GluK2/3 and GluK5 expression between the three groups of rats.Two-way analysis of variance (ANOVA) was used for the statistical analysis at a minimum confidence level of $p < 0.05$ with Sidak post hoc test for between conditions analysis to assess different animals' variations between their corresponding brain regions.Error bars indicate the standard error (SE). Scale bars 2 mm.

Sub-region/layer	**Group1 vs Group2**		**Group2 mean ±SE of GluK2/3**	***p* - value**
Outer mEC	Control	Control Non-epileptic Epileptic	29.8 ± 0.6 30.4 ± 1.0 30.6 ± 1.0	 0.98 0.94
	Non-epileptic	Epileptic		1.00
Inner mEC	Control	Control Non-epileptic Epileptic	37.9 ± 1.0 39.7 ± 0.8 39.1 ± 1.0	 0.77 0.87
	Non-epileptic	Epileptic		0.98
SO	Control	Control Non-epileptic Epileptic	28.8 ± 0.5 26.9 ± 1.9 28.6 ± 1.2	 0.72 1.00
	Non-epileptic	Epileptic		0.75
SR	Control	Control Non-epileptic Epileptic	20.6 ± 0.5 23.6 ± 2.2 24.4 ± 0.8	 0.38 0.10
	Non-epileptic	Epileptic		0.96

SLM	Control	Control Non-epileptic Epileptic	28.7 ± 0.8 28.3 ± 1.6 30.6 ± 1.4	 0.99 0.61
	Non-epileptic	Epileptic		0.58
SM	Control	Control Non-epileptic Epileptic	36.5 ± 1.1 37.3 ± 0.5 38.0 ± 1.9	 0.96 0.77
	Non-epileptic	Epileptic		0.98
H	Control	Control Non-epileptic Epileptic	38.9 ± 0.7 36.5 ± 1.1 37.4 ± 1.8	 0.55 0.76
	Non-epileptic	Epileptic		0.96
SL	Control	Control Non-epileptic Epileptic	50.3 ± 1.4 49.4 ± 1.3 50.5 ± 2.1	 0.96 0.99
	Non-epileptic	Epileptic		0.92

Table 4.3. Quantitative comparison of GluK2/3 immunoreactivities in different brain regions of control, low dose lithium/pilocarpine-treated non-epileptic and chronically epileptic rats. A summary of the mean pixel intensity (arbitrary numbers) of GluK2/3 immunolabelling in the medial entorhinal cortex and hippocampal layers in the three study groups alongside the *p* - value of each pairwise comparison. No statistically significant ($p > 0.05$) differences were identified.

Sub-region/layer	**Group1 vs Group2**		**Group2 mean ±SE of GluK5**	***p* - value**
Outer mEC	Control	Control Non-epileptic Epileptic	34.9 ± 3.3 32.5 ± 2.1 31.7 ± 2.1	 0.98 0.94
	Non-epileptic	Epileptic		1.00
Inner mEC	Control	Control Non-epileptic Epileptic	37.7 ± 2.6 38.2 ± 2.2 34.9 ± 2.0	 0.77 0.87
	Non-epileptic	Epileptic		0.98

SO	Control	Control Non-epileptic Epileptic	32.9 ± 2.8 28.7 ± 2.9 26.4 ± 1.8	 0.72 1.00
	Non-epileptic	Epileptic		0.75
SR	Control	Control Non-epileptic Epileptic	23.7 ± 2.5 22.7 ± 2.3 19.7 ± 1.6	 0.38 0.10
	Non-epileptic	Epileptic		0.96
SLM	Control	Control Non-epileptic Epileptic	21.5 ± 2.6 21.9 ± 1.3 19.7 ± 1.7	 0.99 0.61
	Non-epileptic	Epileptic		0.58
SM	Control	Control Non-epileptic Epileptic	39.6 ± 2.7 39.2 ± 2.8 35.1 ± 1.8	 0.96 0.77
	Non-epileptic	Epileptic		0.98
H	Control	Control Non-epileptic Epileptic	37.3 ± 2.6 35.5 ± 2.1 31.6 ± 2.0	 0.55 0.76
	Non-epileptic	Epileptic		0.96
SL	Control	Control Non-epileptic Epileptic	64.3 ± 2.4 60.7 ± 2.5 60.9 ± 1.7	 0.96 0.99
	Non-epileptic	Epileptic		0.92

Table 4.4. Quantitative comparison of GluK5 immunoreactivities in different brain regions of control, low dose lithium/pilocarpine-treated non-epileptic and chronically epileptic rats. A summary of the mean pixel intensities of GluK5 immunolabelling in the medial entorhinal cortex and hippocampal layers in the three study groups alongside the *p* - value of each pairwise comparison. No statistically significant ($p > 0.05$) differences were identified.

4.3.2 Comparison of GluA1-4, GluA1 and GluA2 AMPAR subunit distribution patterns and expression levels in control and epileptic brains

The regional immunolabelling of AMPAR subunits is shown by the representative histoblots in Figure 4.4. The detectable histoblot differences in the immunoreactivities of the four AMPAR subunits (GluA1-4), expressed as mean pixel intensity (AU), was very similar and not statistically significant between the three study groups in the chronic phase of epilepsy (Figure 4.4 and Table 4.5). The GluA1-4 immunostaining of the mEC and hippocampal regions was predominant in CA1 and SM layer of DG

and moderate in cortex, CPu, cerebellar molecular layer, dentate hilus, and CA3. When examining individual AMPAR subunits, GluA1 (Figure 4.4 and Table 4.6) and GluA2 (Figure 4.4 and Table 4.7), there was no change in the labelling between the three study groups. These two subunits had a different expression pattern for their hippocampal distribution in horizontal brain sections. GluA1 labelled all hippocampal layers moderately, while GluA2 has similar hippocampal staining to GluA1-4 except a moderate labelling of dentate SM layer.

For AMPAR subunits ratios (Figure 4.4), we found no detectable change in the two individual subunits (GluA1 and GluA2) labelling relative to the total labelling of all subunits (GluA1-4), and in GluA2 staining to GluA1.

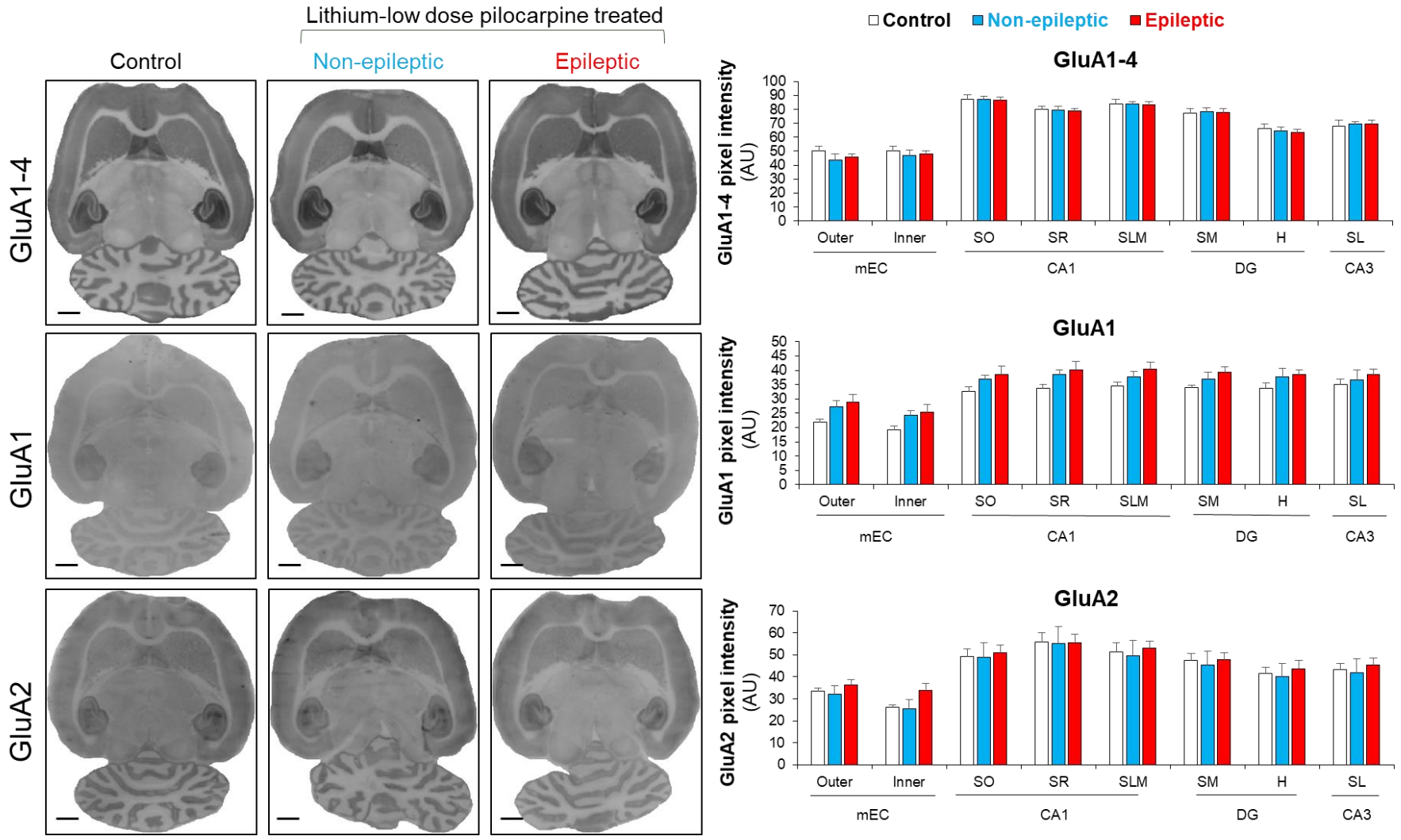
Lithium-low dose pilocarpine treated
Control
Non-epileptic
Epileptic
GluA1-4
GluA1
GluA2
Control
Non-epileptic
Epileptic
GluA1-4
GluA1-4 pixel intensity (AU)
GluA1
GluA1 pixel intensity (AU)
GluA2
GluA2 pixel intensity (AU)
Outer
Inner
SO
SR
SLM
SM
H
SL
mEC
CA1
DG
CA3

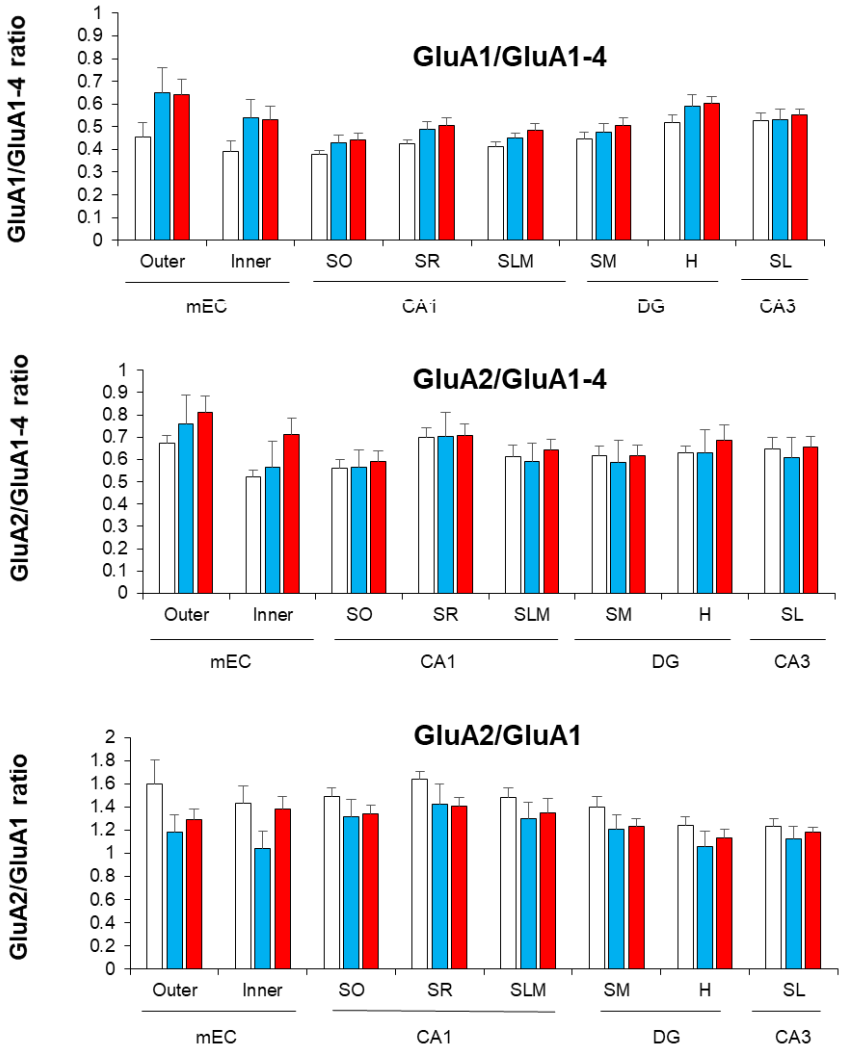

Figure 4.4. Comparison of GluA1-4, GluA1 and GluA2 AMPAR subunit protein expression levels in control and spontaneously epileptic rats. Histoblots of horizontal adult (8-12 months) rat brain sections were obtained from sham treated (Control, n = 6) and lithium-low dose pilocarpine-treated (Modebadze et al., 2016) rats without (Non-epileptic, n = 4) and with spontaneous seizures (Epileptic, n = 7). Expression profiles of GluA1-4, GluA1 and GluA2 AMPAR pore-forming subunits were analysed in the following brain regions: medial entorhinal cortex (mEC) outer and inner layers and hippocampal sub-regions (DG, CA1, CA3) and their layers: hilus (H), stratum moleculare (SM), stratum lacunosum-moleculare (SLM), stratum radiatum (SR), stratum oriens (SO) and stratum lucidum (SL). The bar diagrams represent the pixel intensities of GluA1-4, GluA1 and GluA2 in vulnerable brain regions (mEC and hippocampus) in the three study groups. The relative expression ratios of GluA1/GluA1-4, GluA2/GluA1-4 and GluA2/GluA1 are also included as indicated. There are no statistically significant differences in GluA1-4, GluA1 or GluA2 expression levels between the three groups of rats. Two-way ANOVA was used for the statistical analysis at a minimum confidence level of $p < 0.05$ with Sidak post hoc test for between conditions analysis to assess different animals' variations between their corresponding brain regions. Error bars indicate the standard error (SE). Scale bars 2 mm.

Sub-region/layer	Group1 vs	Group2	Group2 mean ±SE of GluA1-4	*p* - value
Outer mEC	Control	Control	50.3 ± 3.4	
		Non-epileptic	43.9 ± 4.0	0.47
		Epileptic	45.9 ± 2.1	0.64
	Non-epileptic	Epileptic		0.96
Inner mEC	Control	Control	50.5 ± 3.3	
		Non-epileptic	46.8 ± 3.8	0.79
		Epileptic	48.2 ± 2.1	0.91
	Non-epileptic	Epileptic		0.98
SO	Control	Control	87.3 ± 3.1	
		Non-epileptic	87.0 ± 2.2	1.00
		Epileptic	86.7 ± 2.0	0.99
	Non-epileptic	Epileptic		1.00
SR	Control	Control	79.8 ± 2.7	
		Non-epileptic	79.3 ± 2.9	0.99
		Epileptic	79.0 ± 1.6	0.99
	Non-epileptic	Epileptic		1.00
SLM	Control	Control	83.8 ± 3.2	
		Non-epileptic	83.9 ± 1.8	1.00
		Epileptic	83.5 ± 2.2	0.99
	Non-epileptic	Epileptic		0.99
SM	Control	Control	77.0 ± 3.6	
		Non-epileptic	78.3 ± 2.9	0.99
		Epileptic	77.9 ± 2.5	0.99
	Non-epileptic	Epileptic		1.00
H	Control	Control	66.2 ± 3.3	
		Non-epileptic	64.6 ± 2.6	0.97
		Epileptic	63.7 ± 2.1	0.87
	Non-epileptic	Epileptic		0.99
SL	Control	Control	67.9 ± 4.2	
		Non-epileptic	69.5 ± 1.9	0.98
		Epileptic	69.6 ± 2.5	0.97
	Non-epileptic	Epileptic		1.00

Table 4.5. Quantitative comparison of GluA1-4 immunoreactivities in different brain regions of control, low dose lithium/pilocarpine-treated non-epileptic and chronically epileptic rats. A summary of the mean pixel intensity and its standard error of GluA1-4 immunolabelling in the medial entorhinal cortex and hippocampal layers in the three study groups alongside the *p* - value of each pairwise comparison. None of the pairwise comparisons has reached the statistically significant level ($p > 0.05$).

Sub-region/layer	Group1 vs Group2		Group2 mean ±SE of GluA1	*p* - value
Outer mEC	Control	Control	21.9 ± 1.9	
		Non-epileptic	27.2 ± 2.1	0.67
		Epileptic	28.9 ± 2.5	0.38
	Non-epileptic	Epileptic		0.42
Inner mEC	Control	Control	19.1 ± 2.0	
		Non-epileptic	24.3 ± 1.9	0.89
		Epileptic	25.3 ± 2.7	0.08
	Non-epileptic	Epileptic		0.40
SO	Control	Control	32.7 ± 1.0	
		Non-epileptic	36.9 ± 2.2	0.57
		Epileptic	38.4 ± 2.7	0.21
	Non-epileptic	Epileptic		0.96
SR	Control	Control	33.8 ± 1.2	
		Non-epileptic	38.4 ± 1.4	0.49
		Epileptic	40.0 ± 2.7	0.15
	Non-epileptic	Epileptic		0.95
SLM	Control	Control	34.4 ± 1.6	
		Non-epileptic	37.7 ± 1.3	0.76
		Epileptic	40.4 ± 2.9	0.22
	Non-epileptic	Epileptic		0.85
SM	Control	Control	33.9 ± 1.2	
		Non-epileptic	37.0 ± 1.5	0.80
		Epileptic	39.3 ± 2.9	0.28
	Non-epileptic	Epileptic		0.88
H	Control	Control	33.6 ± 1.4	
		Non-epileptic	37.6 ± 1.7	0.58
		Epileptic	38.4 ± 2.5	0.32
	Non-epileptic	Epileptic		0.99
SL	Control	Control	34.9 ± 0.7	
		Non-epileptic	36.7 ± 2.3	0.89
		Epileptic	38.4 ± 1.8	0.38
	Non-epileptic	Epileptic		0.87

Table 4.6. Quantitative comparison of GluA1 immunoreactivities in different brain regions of control, low dose lithium/pilocarpine-treated non-epileptic and chronically epileptic rats. A summary of the mean pixel intensity and its standard error of GluA1 immunolabelling in the medial entorhinal cortex and hippocampal layers in the three study groups alongside the *p* - value of each pairwise comparison. None of the pairwise comparisons has reached the statistically significant level ($p > 0.05$).

Sub-region/layer	Group1 vs Group2		Group2 mean ±SE of GluA2	*p* - value
Outer mEC	Control	Control	33.3 ± 1.4)	
		Non-epileptic	32.1 ± 3.8	0.98
		Epileptic	36.4 ± 2.4	0.75
	Non-epileptic	Epileptic		0.61
Inner mEC	Control	Control	26.0 ± 1.1	
		Non-epileptic	25.5 ± 4.0	0.98
		Epileptic	33.9 ± 3.0	0.26
	Non-epileptic	Epileptic		0.21
SO	Control	Control	49.0 ± 3.6	
		Non-epileptic	48.8 ± 6.6	1.00
		Epileptic	50.9 ± 3.6	0.98
	Non-epileptic	Epileptic		0.98
SR	Control	Control	55.7 ± 4.4	
		Non-epileptic	55.0 ± 7.8	1.00
		Epileptic	55.6 ± 3.8	1.00
	Non-epileptic	Epileptic		1.00
SLM	Control	Control	51.3 ± 4.3	
		Non-epileptic	49.4 ± 7.0	0.99
		Epileptic	52.9 ± 3.1	0.99
	Non-epileptic	Epileptic		0.94
SM	Control	Control	47.3 ± 3.1	
		Non-epileptic	45.3 ± 6.2	0.98
		Epileptic	47.8 ± 3.2	1.00
	Non-epileptic	Epileptic		0.96
H	Control	Control	41.5 ± 2.5	
		Non-epileptic	40.1 ± 6.0	0.99
		Epileptic	43.4 ± 3.8	0.97
	Non-epileptic	Epileptic		0.92
SL	Control	Control	43.3 ± 2.8	
		Non-epileptic	41.9 ± 6.1	0.99
		Epileptic	45.4 ± 3.0	0.96
	Non-epileptic	Epileptic		0.89

Table 4.7. Quantitative comparison of GluA2 immunoreactivities in different brain regions of control, low dose lithium/pilocarpine-treated non-epileptic and chronically epileptic rats. A summary of the mean pixel intensity and its standard error of GluA2 immunolabelling in the medial entorhinal cortex and hippocampal layers in the three study groups alongside the *p* - value of each pairwise comparison. None of the pairwise comparisons revealed statistically significant differences.

4.3.3 Comparison of GluN1 and GluN2B NMDAR subunit distribution patterns and expression levels in control and epileptic brains.

GluN1 and GluN2B NMDAR subunit immunoreactivities were analysed in different brain regions on histoblots (Figure 4.5). GluN1 labelling (Figure 4.5 and Table 4.8) was comparable between control and treated brains in all selected brain regions (mEC, CA1, CA3 and DG). GluN1 immunoreactivity was high in SO and SR layers of CA1 and dentate SM, moderate in CPu, CA3 and mEC layers and weak in cerebellum. In addition, GluN2B staining (Figure 4.5 and Table 4.9) showed no change in immunolabelling between the different groups in almost all selected brain regions except a significant change (14.1%) in the SL, where epileptic animals had a lower immunoreactivity compared to the control [57.7 ± 0.4 vs 67.2 ± 2.3, p = 0.03]. Also, the reduced immunolabelling of the epileptic animals in SO and SM was statistically significant compared to the non-epileptic group [68.7 ± 1.3 vs 78.3 ± 4.0, p = 0.03 and 79.6 ± 1.6 vs 90.3 ± 4.3, p = 0.04, respectively]. The regional immunoreactivity of GluN2B was like GluN1.

To identify if there was a shift in the subunit composition of the NMDAR, the relative comparison of GluN2B to GluN1 labelling (Figure 4.5) was performed and was not different between control and treated animals in all regions.

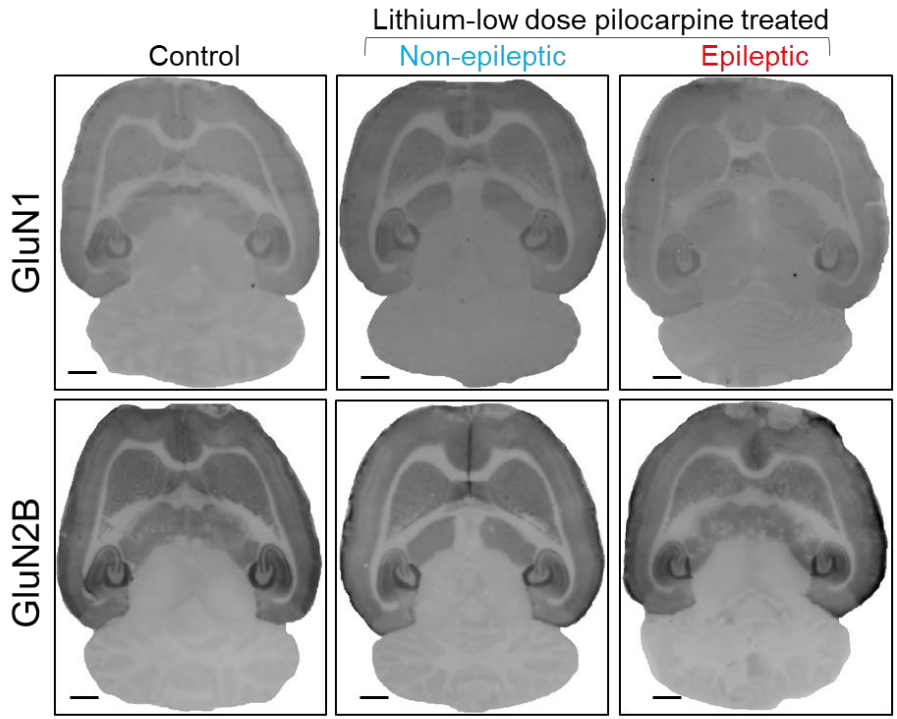
Lithium-low dose pilocarpine treated
Control
Non-epileptic
Epileptic
GluN1
GluN2B

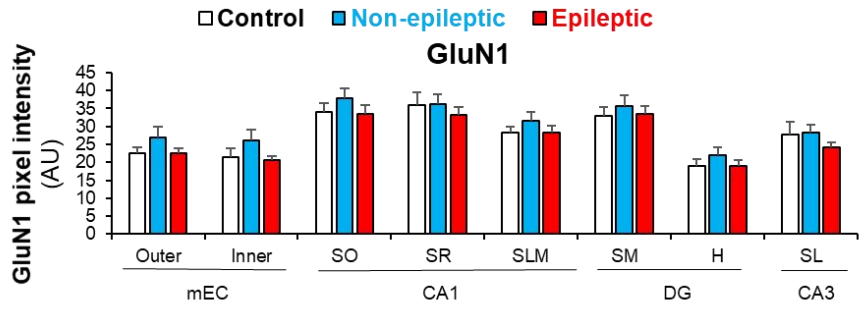
Control
Non-epileptic
Epileptic
GluN1
GluN1 pixel intensity (AU)
Outer
Inner
SO
SR
SLM
SM
H
SL
mEC
CA1
DG
CA3

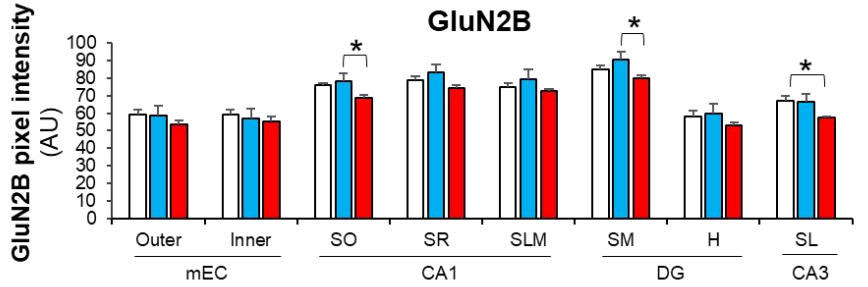
GluN2B
GluN2B pixel intensity (AU)
*
*
*
Outer
Inner
SO
SR
SLM
SM
H
SL
mEC
CA1
DG
CA3

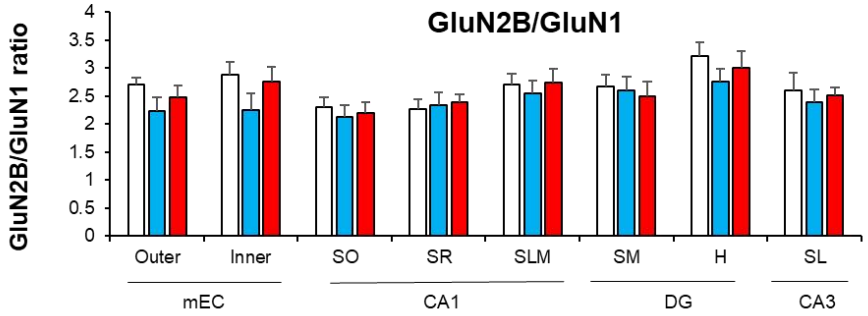
GluN2B/GluN1
GluN2B/GluN1 ratio
Outer
Inner
SO
SR
SLM
SM
H
SL
mEC
CA1
DG
CA3

Figure 4.5. Comparison of GluN1 and GluN2B NMDAR subunit protein expression levels in control and spontaneously epileptic rats. Histoblots of horizontal adult (8-12 months) rat brain sections were obtained from sham treated (Control, n = 6) and lithium-low dose pilocarpine-treated (Modebadze et al., 2016) rats without (Non-epileptic, n = 4) and with spontaneous seizures (Epileptic, n = 7). Expression profiles of GluN1 and GluN2B NMDAR pore-forming subunits were analysed in the following brain regions: medial entorhinal cortex (mEC) outer and inner layers and hippocampal sub-regions (DG, CA1, CA3) and their layers: hilus (H), stratum moleculare (SM), stratum lacunosum-moleculare (SLM), stratum radiatum (SR), stratum oriens (SO) and stratum lucidum (SL). The bar diagrams represent the pixel intensities of GluN1 and GluN2B in vulnerable brain regions (mEC and hippocampus) in the three study groups. The relative expression ratios of GluN2B/GluN1 are included on the bottom panel. No statistically significant differences were detected in the intensity of GluN1 labelling or GluN2B/GluN1 ratio between the three groups of rats. However, the immunostaining of GluN2B was significantly reduced in the epileptic animals compared to the treated but non-epileptic group in SO and SM (p = 0.03 and p = 0.04, respectively) and relative to the untreated animals in the SL hippocampal sublayer (p = 0.03). Two-way ANOVA was used for the statistical analysis at a minimum confidence level of $p < 0.05$ with Sidak post hoc test for between conditions analysis to assess different animals' variations between their corresponding brain regions. Error bars indicate the standard error (SE). Scale bars 2 mm.

Sub-region/layer	Group1 vs	Group2	Group2 mean ±SE of GluN1	p - value
Outer mEC	Control	Control	22.4 ± 1.7	
		Non-epileptic	26.9 ± 2.9	0.39
		Epileptic	22.5 ± 1.4	1.00
	Non-epileptic	Epileptic		0.36
Inner mEC	Control	Control	21.4 ± 2.4	
		Non-epileptic	26.2 ± 2.9	0.35
		Epileptic	20.5 ± 1.0	0.98
	Non-epileptic	Epileptic		0.18
SO	Control	Control	33.9 ± 2.6	
		Non-epileptic	37.8 ± 2.8	0.74
		Epileptic	33.5 ± 2.4	0.99
	Non-epileptic	Epileptic		0.64
SR	Control	Control	36.0 ± 3.3	
		Non-epileptic	36.1 ± 2.8	1.00
		Epileptic	33.1 ± 2.2	0.84
	Non-epileptic	Epileptic		0.86
SLM	Control	Control	28.2 ± 1.6	
		Non-epileptic	31.5 ± 2.3	0.68
		Epileptic	28.3 ± 2.0	1.00
	Non-epileptic	Epileptic		0.65

SM	Control	Control Non-epileptic Epileptic	32.9 ± 2.3 35.5 ± 3.2 33.6 ± 2.2	 0.88 0.99
	Non-epileptic	Epileptic		0.93
H	Control	Control Non-epileptic Epileptic	18.8 ± 1.9 21.9 ± 2.2 19.0 ± 1.5	 0.66 1.00
	Non-epileptic	Epileptic		0.66
SL	Control	Control Non-epileptic Epileptic	27.7 ± 3.6 28.3 ± 2.0 24.1 ± 1.3	 0.99 0.63
	Non-epileptic	Epileptic		0.57

Table 4.8. Quantitative comparison of GluN1 immunoreactivities in different brain regions of control, low dose lithium/pilocarpine-treated non-epileptic and chronically epileptic rats. Potential changes in GluN1 immunolabelling were investigated in the medial entorhinal cortex and hippocampal layers in the three study groups. None of the pairwise comparisons revealed statistically significant differences.

Sub-region/layer	**Group1 vs**	**Group2**	**Group2 mean ±SE of GluN2B**	***p* - value**
Outer mEC	Control	Control Non-epileptic Epileptic	58.9 ± 2.8 58.5 ± 5.7 53.4 ± 2.1	 1.00 0.56
	Non-epileptic	Epileptic		0.69
Inner mEC	Control	Control Non-epileptic Epileptic	59.1 ± 3.0 56.7 ± 5.9 55.2 ± 2.7	 0.96 0.82
	Non-epileptic	Epileptic		0.99
SO	Control	Control Non-epileptic Epileptic	75.7 ± 1.5 78.3 ± 4.0 68.7 ± 1.3	 0.81 0.09
	Non-epileptic	Epileptic		0.03*
SR	Control	Control Non-epileptic Epileptic	78.4 ± 2.2 82.9 ± 4.7 74.4 ± 1.6	 0.63 0.61
	Non-epileptic	Epileptic		0.14
SLM	Control	Control Non-epileptic Epileptic	74.5 ± 2.2 79.2 ± 5.7 72.3 ± 1.3	 0.67 0.92
	Non-epileptic	Epileptic		0.36

SM	Control	Control Non-epileptic Epileptic	85.0 ± 2.0 90.3 ± 4.3 79.6 ± 1.6	 0.45 0.34
	Non-epileptic	Epileptic		0.04*
H	Control	Control Non-epileptic Epileptic	58.0 ± 1.9 59.6 ± 5.4 53.0 ± 1.6	 0.98 0.62
	Non-epileptic	Epileptic		0.49
SL	Control	Control Non-epileptic Epileptic	67.2 ± 2.3 66.4 ± 4.3 57.7 ± 0.4	 0.99 0.03*
	Non-epileptic	Epileptic		0.08

Table 4.9. Quantitative comparison of GluN2B immunoreactivities in different brain regions of control, low dose lithium/pilocarpine-treated non-epileptic and chronically epileptic rats. GluN2B immunolabelling intensities were compared in the medial entorhinal cortex and hippocampal layers in the three study groups. There is a statistically significant reduction in GluN2B immunoreactivity in the epileptic animals compared to the non-epileptic control group in hippocampal sublayers SO (CA1) and SM (DG) (*p* - values = 0.03 and 0.04, respectively). In addition, the SL sublayer of hippocampal CA3 region has reduced GluN2B immunostaining in the epileptic group compared to untreated animals (*p* = 0.03). However, the immunoreactivites in the other hippocampal layers (SR, SLM, H) and mEC layers had not changed between the study groups.

4.3.4 Detection of mossy fibres sprouting using Timm's silver sulphide staining

The morphological evidence of mossy fibres sprouting is the simple and well-accepted method of Timm's silver sulphide staining of zinc rich neurons like mossy fibre terminals (Karoly et al., 2015; Koyama and Ikegaya, 2004; Ben-Ari, 2001). This histochemical technique was performed aiming to detect mossy fibre sprouting in the rat hippocampus of the RISE model.

The representative images of Timm's stained brain sections (Figure 4.6A) show Timm's positive hippocampal sub-regions (enlarged panels). Their quantification (Figure 4.6B) represented as the mean product of Timm's positive area (CA3 and DG) by its pixel intensity [area (cm^2) x pixel intensity (AU)] was not statistically significant between control (n = 4), low dose lithium-pilocarpine-treated non-epileptic (n = 3) and epileptic animals (n = 4). One-way ANOVA was used for the statistical analysis. Data represented as mean ± SEM.

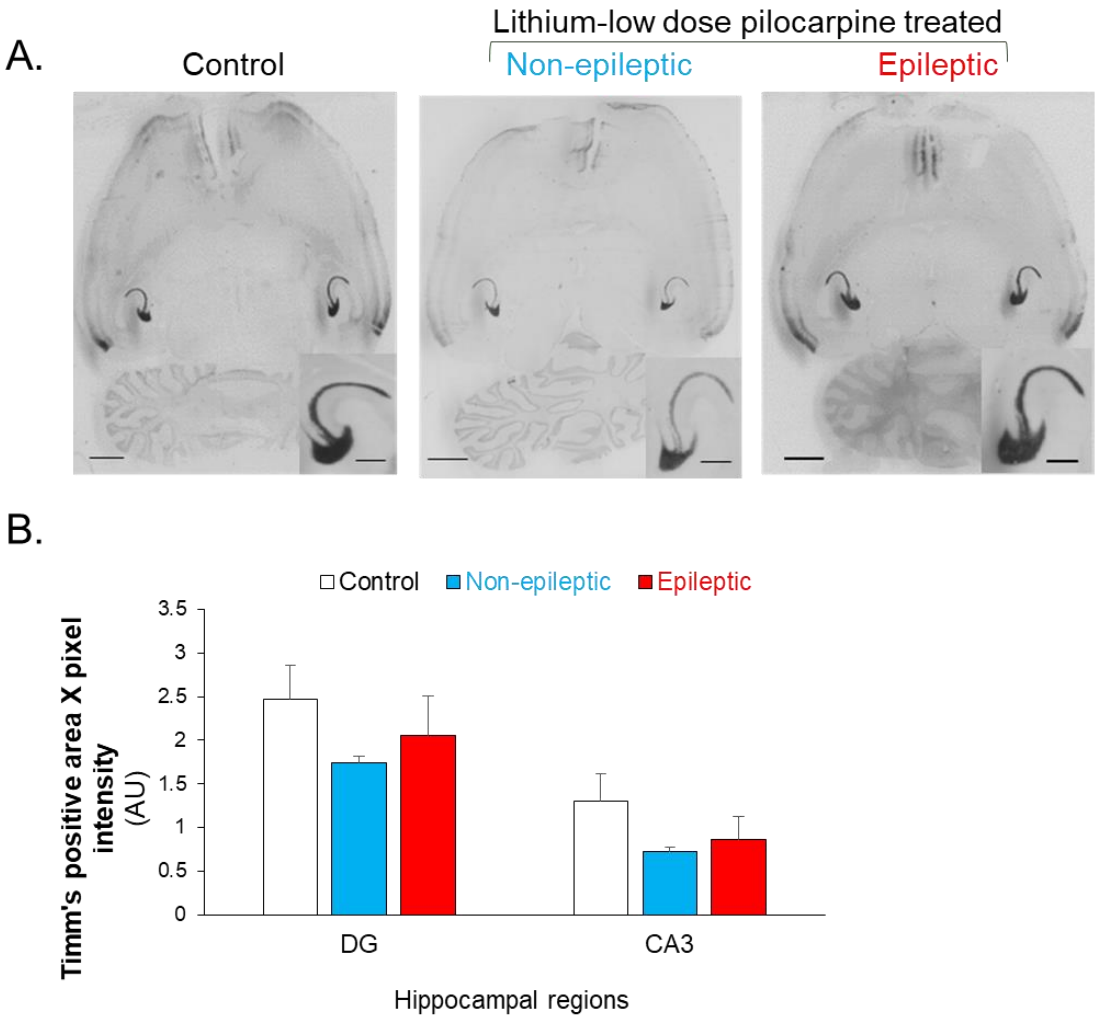

Figure 4.6. Mossy fibre inputs as shown by Timm's staining. Timm's silver sulphide staining (**A**) of horizontal adult (9-12 months) rat brain sections were obtained from sham treated (Control, n = 4) and lithium-low dose pilocarpine-treated (Modebadze et al., 2016) rats without (Non-epileptic, n = 3) and with spontaneous seizures (Epileptic, n = 4). The quantification (**B**) of Timm's positive hippocampal regions (DG and CA3) is presented as positive area x pixel intensity (arbitrary unit). There are no statistically significant differences in Timm's labelling between the three groups of rats using one-way ANOVA. Error bars represent the standard error (SE). Scale bars: 2 mm (main panel) and 0.5 mm (insert).

4.3.5 Concluding remarks

Our results from the chronic epileptic phase have showed the following:

1. There was no detectable region- and receptor type-specific changes in most iGluR subunits expression between the three study groups.
2. GluN2B expression is reduced in CA3 SL in epileptic animals compared to untreated rats.
3. GluN2B expression is reduced in CA1 SO and dentate SM in epileptic animals compared to treated non-epileptic ones.
4. There is no indication of mossy fibre sprouting in the RISE model of epilepsy.

4.4 Discussion

This study examined possible activity-induced changes in the expression levels of different iGluR subunits (GluK2/3, GluK5, GluA1-4, GluA1, GluA2, GluN1, and GluN2B) in different regions of the rat brain. The results indicate no detectable differences between the three study groups during the chronic phase of epilepsy except for a reduction in hippocampal GluN2B immunoreactivity in epileptic animals compared to non-epileptic rats (treated and untreated). In addition, there was no statistically significant difference in the Timm's staining between untreated, treated non-epileptic, and treated epileptic animals in hippocampal CA3 and DG.

4.4.1 Potential explanations of the results

There are some potential explanations of these results. First, the RISE model has the advantage of lacking significant neurodegeneration compared to other pilocarpine treatment-based models (Modebadze et al., 2016). It is an animal model of epilepsy induction of moderate severity (Modebadze et al. 2016) that caused less harm and cell death. Potentially, SRSs were generated through subtle and local network changes that would not be adequately detectable using the low-resolution method of *in situ* blotting. Although the used technique provides the anatomical resolution of brain regions, is reliable for quantitative comparisons, allows lesser usage of animals compared to immunoblotting (which requires greater number of animals to blot for each dissected

brain region), and is relatively cheap, it can just identify the total regional protein expression pattern and so subtle changes in the balance between calcium permeable and impermeable subunits and surface to total protein expression could not be detected. Moreover, the lack of standardized approach to the pilocarpine model (different dosage, pretreatment procedures, animal strain, duration of SE and drugs employed to terminate it) contributes to the variable iGluR results obtained from various research groups (Curia et al., 2008) (see below).

Second, this could not be explained without taking into account the widely connected network. For example, rearrangement of auxiliary subunits and interacting proteins or GABAergic transmission or both could be involved in the process. Third, activity-induced changes might be represented in channel gating properties not receptor expression. Forth, taking into consideration the general agreement by most researchers that mossy fibre sprouting is a prerequisite for SRSs (Karoly et al., 2015), Timm's staining that indicates sprouting of mossy fibres is seen in the IML of the DG (Karoly et al., 2015) which is a thin layer that could not be recognised in our unperfused brain sections. On the other hand, there might be no detectable mossy fibre sprouting in the gentle RISE model because it has no widespread neuronal damage like death of mossy cells (which is thought to result in sprouting) in the dentate hilus (Koyama and Ikegaya, 2004).

4.4.2 Role of iGluRs in epilepsy

In this study, we have expected to detect some changes in iGluR subunits expression either in the mEC and hippocampal CA3 regions or/and the dentate molecular layer (where mossy fibre sprouting is expected to occur) based on the following available evidence of their involvement in the process of epileptogenesis.

4.4.2.1 Role of KARs in epilepsy

In normal situations, the firing property of the dentate granule cells, which mainly operate via AMPARs demonstrating fast $EPSC_{AMPAR}$ (Epsztein et al., 2005), is sparse (Jung and Mcnaughton, 1993). This is because of the narrow time window for afferent inputs integration as the excitatory synaptic events have fast kinetics (Schmidt-Hieber et al., 2007). However, in epileptic conditions, the granule cells express KARs in

addition to AMPARs, which change the sparse firing to become sustained and rhythmic as the slow kinetics of $EPSC_{-KAR}$ lead to wide time window for input integration and prolonged depolarisation (Crepel, 2013).

The absence of GluK2 (GluK2 KO mice) protects against epileptic seizures evoked by kainate in the kainate model of TLE (Mulle et al., 1998; Fisahn, 2005; Fisahn et al., 2004). This suggests a main role for GluK2-containing KARs in seizure generation and a possible therapeutic effect of GluK2 antagonists by reducing the activity of the excitatory feedback network of mossy fibre sprouting as these aberrant synapses operate via KARs (Vincent and Mulle, 2009; Epsztein et al., 2005). However, in another study using GluK2 KO mice, low kainate doses resulted in only high threshold to EEG seizures but not behaviour seizure signs, while higher doses of kainate triggered seizures (Fritsch et al., 2014). This suggests the presence of other mechanisms/proteins that contribute to seizure generation by kainate (Fritsch et al., 2014). On the other hand, lack of GluK1 (GluK1 KO mice) increases epileptiform activity in the kainate model of TLE (Fisahn et al., 2004) and the GluK1 agonist, ATPA, inhibits seizure propagation (Khalilov et al., 2002). This suggests a protective role for GluK1-containing KARs by enhancing the inhibitory drive (Fisahn et al., 2004; Khalilov et al., 2002) as GluK1 subunit is the major KAR subunit in the GABAergic interneurons (Bureau et al., 1999). Interneuronal GluK1-containing receptors facilitate the release of GABA leading to downregulating synaptic transmission (Wu et al., 2007). However, in the pilocarpine model of TLE, antagonising GluK1 protects from epileptiform activity in hippocampal slices (Smolders et al., 2002). Furthermore, the selective GluK1 agonist, ATPA, triggered seizures in mice (Kaminski et al., 2004). Taken together, this indicates that different mechanisms of epileptogenesis are involved in the various animal models.

Mutations generated at the GluK2 Q/R editing site to prevent this post-transcriptional modification in mice render the animal more susceptible to kainate-induced seizures (Vissel et al., 2001). Additionally, following seizures, the Q/R editing of the GluK2 mRNA is upregulated in human and rat (Grigorenko et al., 1998; Bernard et al., 1999) suggesting a possibility to reduce susceptibility to seizures (Grigorenko et al., 1998; Bernard et al., 1999; Kortenbruck et al., 2001). Consistent with this, the developmental upregulation of GluK2 Q/R editing maybe the reason for spontaneous childhood seizure syndrome remission (Sillanpaa et al., 1998).

4.4.2.2 Role of AMPARs in epilepsy

AMPARs have a key role in epilepsy (Rogawski, 2013). In various animal models of seizures, AMPAR antagonists reduced the severity of seizures (Durmuller et al., 1994; Namba et al., 1994) or inhibited their development (Turski et al., 1992; Barton et al., 2003). NBQX is a selective AMPAR antagonist that has anticonvulsant activity in many animal models of seizure (Chapman et al., 1991; Taylor and Vartanian, 1992; Yamaguchi et al., 1993; Namba et al., 1994). Status epilepticus was terminated, and neuronal degeneration was reduced in many status epilepticus models after the use of various AMPAR antagonists (Rajasekaran et al., 2012; Fritsch et al., 2010; Langer et al., 2011; Pitkanen et al., 2007).

In addition, AMPAR inhibition prevented interictal-like activity from slices of TLE patients (Graebenitz et al., 2011) with evidence of increased AMPAR density in slices of epileptic patients (Graebenitz et al., 2011; Hosford et al., 1991). Moreover, perampanel is a non-competitive AMPAR antagonist that demonstrated clinical efficacy in epileptic patients (French et al., 2012; French et al., 2013; Krauss et al., 2012). In epileptic patients, GluA1 AMPAR subunit expression was increased in the hippocampus indicating high levels of GluA1-containing receptors, which demonstrate high channel conductance compared to GluA2-containing receptors (Ca^{2+}-impermeable) (Ying et al., 1998; Swanson et al., 1997).

A small number of AMPARs have the unedited Ca^{2+}-permeable GluA2 subunit expressed at the embryonic stage. However, > 99% of GluA2 subunits become edited and Ca^{2+}-impermeable soon after birth (Burnashev-Rozov, 2000). It has been reported that GluA2 expression level was reduced and Ca^{2+} -permeable AMPARs were increased in various brain regions (hippocampus, inferior colliculus, piriform cortex) in many animal models of epilepsy (kainate, audiogenic kindling, amygdala-kindling) (Sommer et al., 2001; Li et al., 2003; Prince et al., 2000). GluA2 levels were also reduced during rat brain development of hypoxic-induced seizures with an increase in Ca^{2+}- permeable AMPAR ratio (Sanchez et al., 2001). Furthermore, the expression levels of GluA2-lacking Ca^{2+}-permeable receptors were increased in hypoxic neonatal seizures (Talos et al., 2006a).

4.4.2.3 Role of NMDARs in epilepsy

Several studies indicated the involvement of NMDARs in epilepsy (Endele et al., 2010; Ding et al., 2010; Mathern et al., 1998). In addition, several NMDAR antagonists have been developed and showed antiepileptic effects (Sachdeo et al., 1992; Palmer et al., 1991).

The mRNA of the obligatory subunit of the NMDAR, GluN1, is highly expressed throughout the brain pre- and postnatally (Monyer et al., 1994; Watanabe, 1997). Early postnatally, NMDARs are composed mainly from GluN1 and GluN2B subunits. During development GluN2A subunit starts to be incorporated in the NMDAR toward the third to fourth week of rodent postnatal development (Monyer et al., 1994; Watanabe, 1997). Reaching the adulthood, NMDAR is composed now from GluN1/GluN2B/GluN2A in the neocortex and hippocampus (Hawkins et al., 1999; Chazot and Stephenson, 1997). The GluN2B subunit has slow deactivation kinetics compared to the fast deactivation kinetics of GluN2A leading to longer $EPSC_{-NMDAR}$ duration in younger animals (more GluN2B) (Cull-Candy et al., 2001). Furthermore, $EPSC_{-NMDAR}$ became larger and longer with a prominently enhanced LTP and learning scores in adult mice overexpressing the GluN2B subunit compared to normal animals (Tang et al., 1999). Taking this into consideration, it is unclear from our study if the detected reduction of GluN2B immunoreactivity indicates a protective mechanism from sustained activation by NMDAR or if this reduction could mean an impairment in new synapses formation. This is because GluN2B subunit is prominently expressed in early life as it has an important role in the maturation process of neuronal circuits. And, its deletion caused deficits in neuronal circuits assembly during development (Kutsuwada et al., 1996; Kelsch et al., 2012; Kelsch et al., 2014).

In animal models of epilepsy, GluN1 mRNA level was reduced in the dentate gyrus and CA1 and CA3 pyramidal cells of a pilocarpine and kainate (CA1 and CA3) models in rats (Lason et al., 1997a; Mathern et al., 1998). GluN2B mRNA level was increased in the dentate gyrus in the latent epileptic phase and reduced in the subiculum in the chronic phase of the pilocarpine model (Ghasemi and Schachter, 2011). GluN2A mRNA level was decreased in dentate gyrus cells in a kindling model in rats (Pratt et al., 1993) and unchanged in CA3 pyramidal cells (Kraus et al., 1994).

In human chronic TLE, NMDAR inhibition reduces dentate granule cells hyperexcitability where mossy fibres sprouting occurs but not in non-sprouted mossy fibres (Franck et al., 1995; Isokawa and Levesque, 1991; Masukawa et al., 1991). Additionally, patients of TLE had increased levels of GluN2A and GluN2B mRNA in dentate granule cells (Mathern et al., 1996). In patients with non-hippocampal sclerosis TLE, the hippocampus had increased levels of GluN1 and GluN2B mRNA in CA3 pyramidal cells (Ghasemi and Schachter, 2011). However, hippocampal sclerosis patients had decreased mRNA levels of GluN2A in CA3 pyramidal cells.

4.4.3 Detection of mossy fibre sprouting

Zinc is present in the synaptic vesicles of the dentate granule cells axons and axon terminals (Paolethi et al., 2009; Seress et al., 2001). Timm's staining is a histochemical technique used to label their zinc content (Danscher and Zimmer, 1978; Henze et al., 2000). This indicates that Timm's staining is not considered a marker of just mossy fibres terminals (Karoly et al., 2011). In epilepsy, mossy fibres terminate in the dentate hilus, stratum lucidum of hippocampal CA3, and the inner molecular layer of the dentate gyrus (Karoly et al., 2011). In a TLE model in rat, mossy fibres sprouting appeared after the development of spontaneous recurrent seizures (Nissinen et al., 2001) suggesting that it contributes to the chronicity of the disorder and seizure intensification (Koyama, 2016; Karoly et al., 2011). In the pilocarpine-induced chronic model of epilepsy, mossy fibres sprouting was identified in the inner molecular and granular cell layers of the dentate gyrus (Epsztein et al., 2005). However, in our study, there was no detected difference in Timm's staining between the three studied conditions suggesting no mossy fibre sprouting in the RISE model that lack the generalised neuronal damage observed in other comparable models. This could be explained by the fact that the brain sections used in our study were not perfused for fixation but fixed by immersion after sectioning. This could limit the exposure of the tissue to the fixative. This means that the inner molecular layer of the DG, where mossy fibres sprouting happens (Karoly et al., 2015), could not be identified clearly. In addition, in a 10 µm thick section the superimposition of the mossy fibres varicosities is large. Sections must be thin enough to avoid superimposition of various tissue components (typically 5 µm thick) (Schoen and Mitchell, 2013).

In our Timm's stained sections, the optical density of the well-stained synaptic area of the mossy fibres was already high in the control animals. Little, but significant increase in the numbers of mossy fibres varicosities might be missed due to the superimposition problem and only dramatic changes could be detected.On the other hand, mossy cell loss in the DG correlates with mossy fibre sprouting in epileptic pateints and pilocarpine-treated rats (Buckmaster, 2012). Thus, it is probable in the RISE model, which lacks neuronal damage compared to other related models, not to have mossy fibre sprouting. Or, to have mild level of sprouting as a result of forming recurrent aberrant synapses onto only a subset of granule cell dendrites in the inner molecular layer. Therefore, the used staining technique, in addition to the used tissue (method of fixation and thickness), was insensitive to detect any sprouting.

4.5 Conclusion

In conclusion, further investigations are needed to examine other potentially involved receptors and subunits (glutamatergic vs GABAergic), post-translational modifications, unedited (Ca^{2+}-permeable)/edited (Ca^{2+}-impermeable) subunits, surface protein to total ratio, and channel properties.

5 Interplay between palmitoylation and SUMOylation of GluK2 in regulating KAR internalisation

5.1 Background

5.1.1 GluK2 palmitoylation and phosphorylation

Palmitoylation is the reversible process of modifying a protein by covalently attaching palmitic acid, a 16-carbon saturated fatty acyl chain, to a cysteine residue by a thioester bond (Pickering et al., 1995; Hayashi et al., 2005; Aicart-Ramos et al., 2011; Globa and Bamji, 2017; Shipston, 2011). This modification is in dynamic regulation by the activity of two families of enzymes, palmitoyl acyltransferases (transmembrane proteins) and thioesterases, responsible for palmitoylation and depalmitoylation, respectively (Aicart-Ramos et al., 2011; Globa and Bamji, 2017; Shipston, 2011). Palmitoylation occurs at the cytosol, endoplasmic reticulum, Golgi compartment, and the cell membrane (Hancock et al., 1989; Berger and Schmidt, 1985; Olson and Spizz, 1986; Dolci and Palade, 1985; El-Husseini et al., 2002). Apparently, there is no required precise amino acid consensus for palmitoylation, but usually basic and hydrophobic amino acids surround the modified cysteine residues (Bijlmakers and Marsh, 2003; El-Husseini and Bredt, 2002; Gauthier-Campbell et al., 2004).

The palmitoylation of proteins increases their hydrophobicity, which promote their interaction with the membrane lipid bilayers. Hence, targeting proteins to cell membranes is the primary function of this post-translational modification (El-Husseini and Bredt, 2002). In addition, it has many other important roles including the regulation of neuronal development (Hess et al., 1993; Pepinsky, 1998; Chamoun, 2001), neurotransmitter release from synaptic vesicles (Hess et al., 1992; Washbourne, 2001), signal transduction of ion channels and neurotransmitter receptors (Dunphy and Linder, 1998; Bizzozero, 1997), the receptor-clustering function of synaptic scaffolding proteins, and the structural conformation of proteins (Topinka and Bredt, 1998; Gray, 1998; DeSouza et al., 2002).

Dysregulation in protein palmitoylation has been observed in many neurological disorders including Alzheimer’s, Huntington’s, schizophrenia, and mental retardation (Cho and Park, 2016; Sanders and Hayden, 2015). In addition, many palmitoyl acyltransferases have been implicated in these neurological diseases (Fromer et al., 2014; Bhattacharyya et al., 2013; Mizumaru et al., 2009; Korycka et al., 2012;

Hornemann, 2015). More than 40% of synaptic proteins are identified as substrates for palmitoylation (Sanders et al., 2015) with many neurotransmitter receptors were known to be palmitoylated including serotonin, dopamine, $GABA_A$, NMDA, AMPA and kainate receptors (Naumenko and Ponimaskin, 2018).

The kainate receptor subunit GluK2 is a substrate for protein palmitoylation at two distal cytosolic cysteine residues (C858 and C871) that are conserved in all KAR subunits except GluK1 (Pickering et al., 1995; Copits and Swanson, 2013). They are considered the major sites of GluK2 palmitoylation and are surrounded by many positively charged amino acid residues (Pickering et al., 1995; Copits and Swanson, 2013). Their palmitoylation was confirmed by overexpressing GluK2 in heterologous systems, where metabolic labelling assays using [^{3}H]-palmitate were used (Pickering et al., 1995; Copits and Swanson, 2013).

GluK2 has also two serine residues in the intracellular C-terminal domain (S846 and S868) that are substrates for PKC-dependent phosphorylation (Nasu-Nishimura et al., 2010). These are the predominant C-terminal phosphorylation sites as the GluK2 double non-phosphorylatable mutant (S846A, S868A) showed an 87% reduction in PKC-mediated phosphorylation (Nasu-Nishimura et al., 2010). The first serine (S846) is located proximal to the plasma membrane and the other one (S868) exists distally close to the second cysteine residue (two amino acids away from the second palmitoylated cysteine residue; C871) (Figure 1.5).

Recently, the protein 4.1 family, which function as cytoskeletal adaptor proteins (Bennett, 1989), has been found to interact with kainate and AMPA receptors to coordinate their surface expression and stabilisation. 4.1N isoform associates with a region within the membrane-proximal domain of both receptors to promote their forward trafficking (Copits and Swanson, 2013). KARs association with 4.1N maintains an extrasynaptic pool of receptors on dendritic shafts (Copits and Swanson, 2013). This ready-to-use pool could contribute to synaptic plasticity once needed in a way similar to AMPARs (Heine et al., 2008; Petrini et al., 2009). Notably, the 4.1N isoform association with kainate and AMPA receptors is regulated by palmitoylation and phosphorylation (Figure 1.5) of the receptors' subunits in an opposing direction (Copits and Swanson, 2013) (see the discussion section 5.4.1).

5.1.2 GluK2 SUMOylation and phosphorylation

SUMOylation is the dynamic reversible process of the covalent protein modification at a lysine residue by the Small Ubiquitin-like Modifier protein (SUMO) (Martin et al., 2007; Coelho-Silva et al., 2017). The best-defined SUMO isoforms to date are SUMO1, 2, and 3 (Coelho-Silva et al., 2017). SUMO proteins have diverse cellular functions like regulating nuclear transport, transcription, DNA repair, protein-protein interaction, subcellular localisation, and protein conformational structure (Johnson, 2004; Geiss-Friedlander and Melchior, 2007; Dohmen, 2004; Wilkinson and Henley, 2010). SUMO isoforms are conjugated to their substrates via three sequential enzymatic reactions of an E1 activating enzyme, an E2 conjugating enzyme (ubiquitin-conjugating 9 or Ubc9), and an E3 protein ligation enzyme (Wilkinson and Henley, 2010). Ubc9 is capable of conjugating SUMO to its substrate in an E3 ligase-dependent and –independent way (Coelho-Silva et al., 2017). Alterations in the SUMOylation process of proteins has been implicated in some neurological disorders like Alzheimer, Parkinson, and epilepsy (Anderson et al., 2017). The kainate receptor subunit GluK2 has a distal lysine residue (K886) that is subjected to SUMO1 modification in an activity-dependent manner. GluK2 SUMOylation at this cytosolic residue occurs rapidly at the surface upon kainate binding promoting receptor endocytosis and $EPSC_{-KAR}$ reduction (Martin et al., 2007).

Phosphorylation of GluK2 C-terminus regulates the trafficking of KARs. The PKC-mediated phosphorylation of S846 or S868 prevents GluK2 surface expression (Nasu-Nishimura et al., 2010; Copits and Swanson, 2013) by enhancing its endoplasmic reticulum retention and so, retarding its forward trafficking in neurons (Nasu-Nishimura et al., 2010). Notably, phosphorylation of only S846 promotes constitutive surface GluK2 endocytosis (Nasu-Nishimura et al., 2010) and it was found to have a major impact on the reduction of neuronal GluK2 surface expression compared with the modest effect of S868 phosphorylation (Copits and Swanson, 2013).

Phosphorylation and SUMOylation of KARs and their interplay have been studied by many research groups (Konopacki et al., 2011; Martin et al., 2007; Chamberlain et al., 2012). Phosphorylation of S846 does not enhance GluK2 SUMOylation at K886 (Konopacki et al., 2011) whereas S868 phosphorylation facilitates it (Martin et al., 2007; Konopacki et al., 2011; Chamberlain et al., 2012). Interestingly, PKC-mediated

phosphorylation of GluK2 at S868 has shown to have two opposing effects on KAR localisation depending on the presence or absence of SUMOylation (Chamberlain et al., 2012). The equilibrium between the two determines the net result (Chamberlain et al., 2012). Phosphorylation of S868 can increase GluK2 SUMOylation which lead to endocytosis (Figure 1.5) and reduced surface expression or, in the absence of SUMOylation, it can increase the receptor recycling back to the neuronal plasma membrane (Chamberlain et al., 2012).

5.1.3 GluK2 palmitoylation, phosphorylation and SUMOylation interplay

As discussed, the interplay between palmitoylation and phosphorylation and phosphorylation and SUMOylation of the GluK2 subunit have been studied individually. However, any possible crosstalk between palmitoylation and SUMOylation has not been investigated. And here is a clarification on why such a possibility could be happening. SUMOylation of GluK2 is required for kainate-induced endocytosis but the exact mechanism on how the activation of GluK2-containing KAR increases receptor SUMOylation is not fully characterised (Martin et al., 2007). Since the removal of palmitate from GluK2 promotes its PKC-mediated phosphorylation (Pickering et al., 1995) and considering that agonist-induced endocytosis of GluK2 depends on PKC activity (Martin and Henley, 2004; Nasu-Nishimura et al., 2010), it worth studying if GluK2 non-palmitoylation is required for SUMO1-dependent KAR endocytosis and whether phosphorylation regulates this process. In other words, is GluK2 depalmitoylation a prerequisite for subsequent downstream PKC-dependent phosphorylation, SUMO1 conjugation and GluK2 internalisation?

5.2 Aim and objectives

Hypothesis: GluK2 depalmitoylation is an upstream post-translational modification of phosphorylation and subsequent SUMOylation for LTD (Figure 5.1).

Aim: To identify the effects of GluK2 non-palmitoylation on GluK2 phosphorylation, SUMOylation and internalisation under basal and agonist stimulation conditions.

Objectives:

1. To determine the recombinant GluK2 SUMOylation levels in WT and mutants (non-palmitoylated, phosphor-null, phosphor-mimetic) under basal and kainate-stimulated conditions in HEK293T cells.
2. To identify the effect of the WT GluK2 and non-palmitoylated mutant on neuronal surface expression under basal and kainate-stimulated conditions.

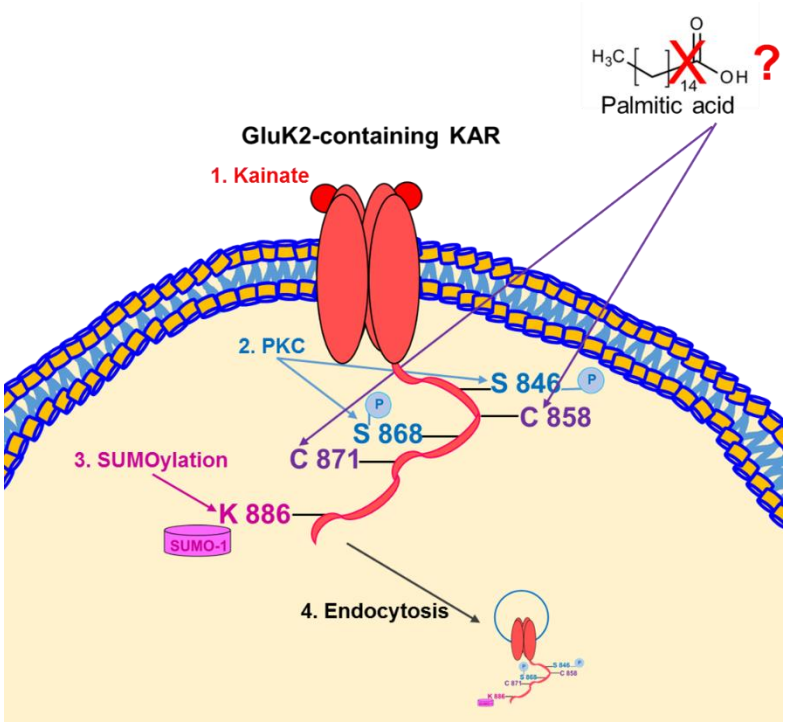

Figure 5.1. A schematic model of the effect of GluK2 depalmitoylation on a series of downstream post-translational modifications and receptor internalisation. The C-terminus of the KAR subunit GluK2 has many sites for post-translational modifications (PTMs). It has two cysteine residues (C858 and C871) that considered substrates for palmitoylation. A series (**1-4**) of events relating other PTMs (phosphorylation and SUMOylation) to KAR internalization (Konopacki et al 2011, Chamberlain et al 2012) are shown. Very close to the palmitoylation sites, there are two serine residues (S846 and S868), which are substrates for PKC phosphorylation upon agonist stimulation (**1** and **2**). This will lead to SUMO1 conjugation of the lysine residue (K886) at the end of the C-terminus (**3**) and receptor endocytosis (**4**). However, based on evidence of increased PKC phosphorylation of non-palmitoylated GluK2 (Pickering et al., 1995), it is not clear if depalmitoylation of the cysteine residues leads to downstream phosphorylation, SUMOylation and then KAR internalisation upon kainate stimulation.

5.3 Results

5.3.1 Effects of targeted mutation of phosphorylation and palmitoylation sites on ct-GluK2 on SUMOylation

To define the roles of possible cross-talk between post-translational modifications of GluK2 we investigated a series of point mutants (Table 5.1) with key residues substituted to prevent or mimic specific modifications. We first transfected HEK293T cells with FLAG-SUMO1 and FLAG-Ubc9 alongside YFP (negative control) or one of several YFP-Myc-tagged GluK2 DNA constructs [WT, C858A, C871A (non-palmitoylated), K886R (non-SUMOylated), S846A, S868A (phospho-null), and S868D (phospho-mimetic)]. After 36–48 hours, the effect of 20 minutes of 100 µM Kainate on GluK2 phosphorylation and SUMOylation in the different conditions was assessed using pull-down assays (GFP-trap protocol).

YFP-Myc-GluK2 point mutants	
Non-palmitoylated	C858A, C871A
Non-SUMOylated	K886R
Phospho-null	S846A, S868A
Phospho-mimetic	S868D

Table 5.1. A summary of GluK2 point mutants. The table summarises the point mutants of YFP-Myc-tagged GluK2 used to study their effects on GluK2 SUMOylation. The double cysteines (C858 and C871) were mutated to alanine to prevent GluK2 C-terminal palmitoylation. The distal lysine residue (K886) was converted to an arginine to prevent SUMOylation. A proximal (S846) and distal (S868) serine residues were changed to alanine to block their PKC-mediated phosphorylation. The distal serine (S868) was mutated to aspartate to mimic the phosphorylation status.

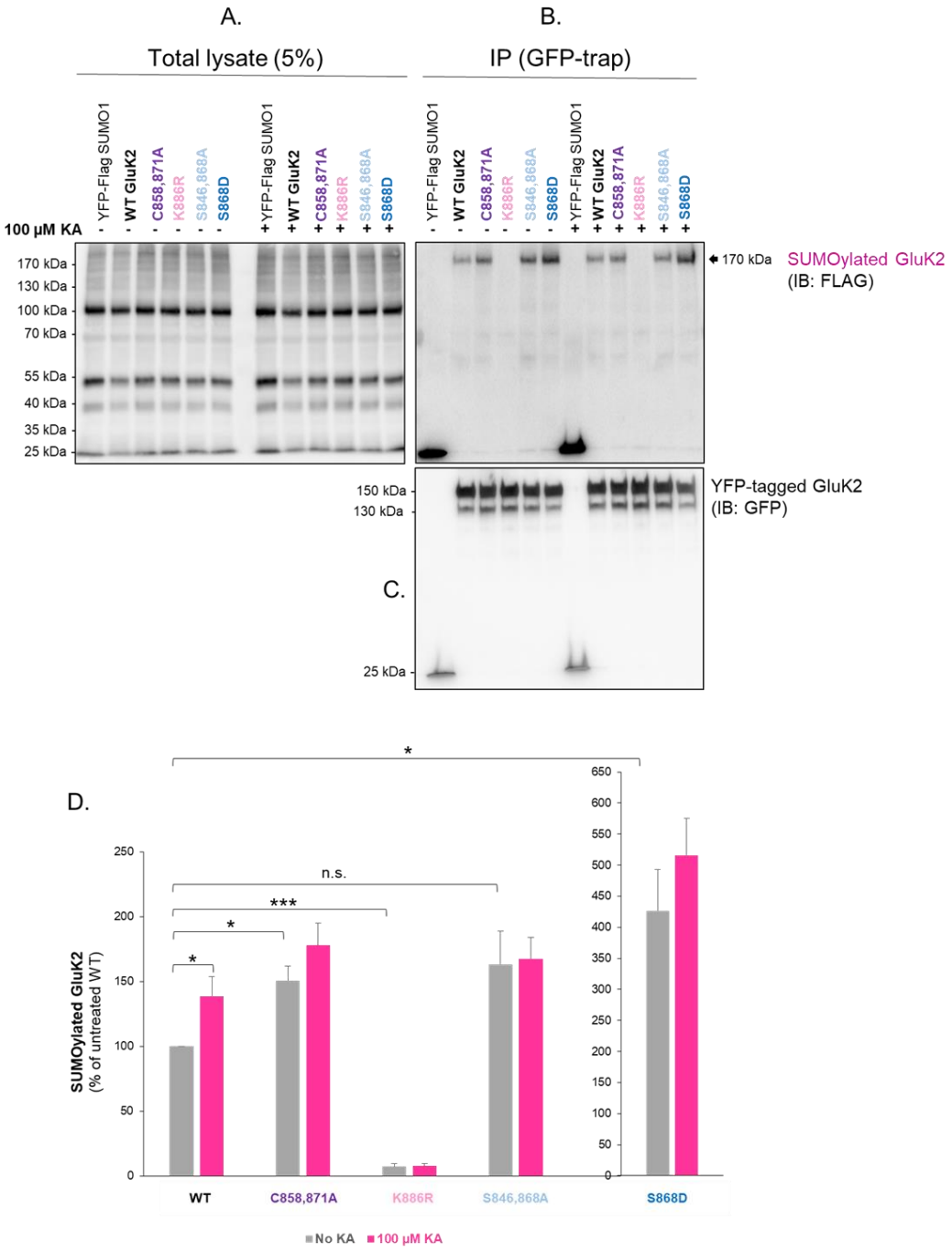

Figure 5.2. Non-palmitoylation of GluK2 mimics agonist-induced SUMOylation. HEK293T cells were transfected with yellow fluorescent protein (YFP) DNA (negative control) and five different constructs of YFP-Myc-tagged GluK2: 1) WT, 2) C858A, C871A (non-palmitoylated), 3) K886R (non-SUMOylated), 4) S846A, S868A (phospho-null) and, 5) S868D (phospho-mimetic) along with FLAG-tagged SUMO1 and FLAG-tagged Ubc9. Kainate (100 µM) for 20 minutes was used to stimulate the expressed KAR. **A**, represents the crude SUMOylated proteins (recognised by an anti-FLAG antibody) in the total cell lysate (5 % of all cell lysate). GluK2 was immunoprecipitated (IP) using GFP-trap protocol **(B)** and the levels of SUMOylated GluK2 were detected in the different conditions using anti-FLAG antibody. The immunolabelling of the SUMOylated GluK2 was first normalised to the GFP expression **(C)** before being normalised to the untreated WT

expression for comparison. The quantification **(D)** of the IP samples (n = 6) shows the non-palmitoylated GluK2 was SUMOylated more than the WT under basal conditions ($p = 0.0025$). However, under agonist stimulation the level of SUMOylated GluK2 was not different between the WT and the double cysteine mutant ($p = 0.11$). The non-SUMOylated GluK2 had very low levels of SUMOylation ($p < 0.0001$ compared to WT). The phospho-null mutant was SUMOylated almost like the WT ($p = 0.09$) under basal and stimulatory conditions. In contrast, the phospho-mimetic GluK2 SUMOylation was noticeably higher than the WT ($p = 0.008$ for basal conditions and < 0.0001 upon KA stimulation). The only statistically significant result between basal and KA stimulatory conditions was for the WT ($p = 0.03$) when its SUMOylation had increased with kainate treatment. All bands were normalised to the GluK2 expression level (GFP) and then represented as a percent of the untreated WT. To compare the different mutants (untreated and treated) with the WT (untreated and treated), Student *t*-test with four comparisons correction was applied (*p*-value significant at 0.05/4= 0.0125, *: *p*-value < 0.0125, **: *p*-value < 0.001, ***: *p*-value < 0.0001). To compare each treated condition with its untreated counterpart, Student *t*-test was applied (*p* - value significant at 0.05). Error bars represent the standard error (SE).

The blots in Figure 5.2 show the results of: *1*) the crude total cell lysate (5% of the total) of the SUMOylated proteins in the cell (membrane probed with anti-FLAG) (Figure 5.2 A); *2*) the SUMOylated fraction of the immunoprecipitated GluK2 that runs at 170 kDa (membrane probed with anti-FLAG) with no corresponding band for the negative control (YFP alone) (Figure 5.2B), and *3*) the expression level of the transfected YFP-Myc-tagged GluK2 at 150 kDa with no corresponding band for the negative control (YFP alone) (membrane probed with anti-GFP) (Figure 5.2C).

It worth noting that the expected molecular weight of the SUMOylated YFP-Myc-GluK2 is ~ 150 kDa [the predicted molecular weights for the following proteins/peptides in kDa are: 11.55 for SUMO1 (The UniProt Consortium, 2019), 28.13 for YFP (The UniProt Consortium, 2019), 7.2 (1.20 x 6) for six tags of Myc (c-Myc tag peptide (EQKLISEEDL) [online] Available at: http:// www.mblintl.com/products/3300-205 [Accessed February 2019]), and 102.47 for GluK2 (The UniProt Consortium, 2019). However, the difference between the expected and the observed molecular weights might be due to a possible series of SUMO conjugation or to other unknown protein interactors or the fact that SUMOylated proteins run higher than predicted.

The quantification (Figure 5.2D) of the immunoprecipitated GluK2 bands shown in B (SUMOylated GluK2) revealed a significant increase of the WT GluK2 SUMOylation level upon kainate stimulation (100.0 vs 138.8 ± 14.8, $p = 0.03$). This was also mimicked in the non-palmitoylated mutant (C858A, C871A) compared to the untreated WT (100.0

vs 150.8 ± 11.0, $p = 0.002$). However, in the double cysteine mutant kainate treatment has not affected the level of SUMOylation compared to the treated WT (138.8 ± 14.8 vs 177.8 ± 17.4, $p = 0.11$).

As expected (Konopacki et al., 2011), the non-SUMOylated mutant (K886R) has a very profound reduction in SUMOylation compared to the WT (untreated: 100.0 vs 7.1 ± 2.2, $p < 0.0001$ and treated: 138.8 ± 14.8 vs 7.6 ± 2.0, $p < 0.0001$).

The phospho-null GluK2 showed a similar SUMOylation level to the WT (untreated: 100.0 vs 163.2 ± 25.7, $p = 0.09$ and treated: 138.8 ± 14.8 vs 167.5 ± 16.5, $p = 0.26$). Lastly, the phospho-mimetic GluK2 (S868D) was highly SUMOylated compared to the WT (untreated: 100.0 vs 426.4 ± 66.6, $p = 0.008$ and treated: 138.8 ± 14.8 vs 516.0 ±59.7, $p < 0.0001$).

It is worth noting that the detection of GluK2 phosphorylation in the immunoprecipitate was tried first using an anti-phosphoserine (BD Biosciences 612548) before detecting SUMOylated levels aiming to connect the three post-translational modifications but all attempts showed no bands at all and membranes were then reprobed with anti-FLAG to identify GluK2 SUMOylation.

5.3.2 The surface expression of non-palmitoylatable GluK2 in neuronal cultures

We next used confocal imaging approaches to explore the distribution of non-palmitoylatable GluK2 in neurons. Cultured hippocampal neurons (DIV 9-10) were transfected with DNA constructs of YFP-Myc-tagged GluK2 (WT or C858A, C871A). At DIV 14-15, neurons were treated with 2 µM tetrodotoxin (TTX, to inhibit the activity-dependent release of glutamate) and 40 µM GYKI53655 (to block AMPARs) for 30 min and then with either vehicle (water) or 10 µM kainate (Martin and Henley, 2004; Martin et al., 2008; Konopacki et al, 2011) for 20 min before being live labelled for surface YFP expression followed later with staining of the total YFP expression.

Figure 5.3 shows representative confocal images of the transfected neurons. Red shows surface and green shows total YFP-tagged GluK2 localisation. The blue staining (DAPI) in the overlay image shows the nucleus. The magnification panel is a close up of one of the dendrites. Note the relatively strong red immunofluorescence

of the untreated WT compared to all other conditions which signifies that the WT GluK2 is expressed on the cell surface more than the non-palmitoylated receptor. This is also illustrated by the relatively prominent yellow colour (overlap between red and green) in the overlay image compared to the dim yellow in the other conditions.

The quantification of the images immunofluorescence (Figure 5.4) revealed a statistically significant reduction in the dendritic immunoreactivity of the total, surface and surface/total ratio of the WT GluK2 upon kainate stimulation (Total: 1.00 ± 0.14 vs 0.67 ± 0.01, $p = 0.04$, Surface: 1.00 ± 0.14 vs 0.61 ± 0.01, $p = 0.02$, Surface/total: 1.00 ± 0.005 vs 0.89 ± 0.017, $p < 0.001$) (Table 5.2).

Importantly, the dendritic surface/total immunofluorescence of the non-palmitoylated GluK2 mutant was significantly reduced compared to the WT under basal conditions (0.91 ± 0.007 vs 1.00 ± 0.005, $p = 0.001$) mimicking GluK2 (WT) upon kainate stimulation (0.89 ± 0.017 vs 1.00 ± 0.005, $p < 0.001$). Moreover, in direct contrast to GluK2 (WT), the proportion of surface expressed GluK2 (C858A, C871A) was not altered in kainate-stimulated conditions (0.91 ± 0.007 vs 0.91 ± 0.018, $p = 0.87$) (Table 5.2).

Interestingly, there were no significant changes in the soma. Specifically, total, surface and surface/total ratio reduction in the soma immunofluorescence within the WT basal and stimulated conditions and between the WT and the double cysteine mutant (data summarised in Table 5.3).

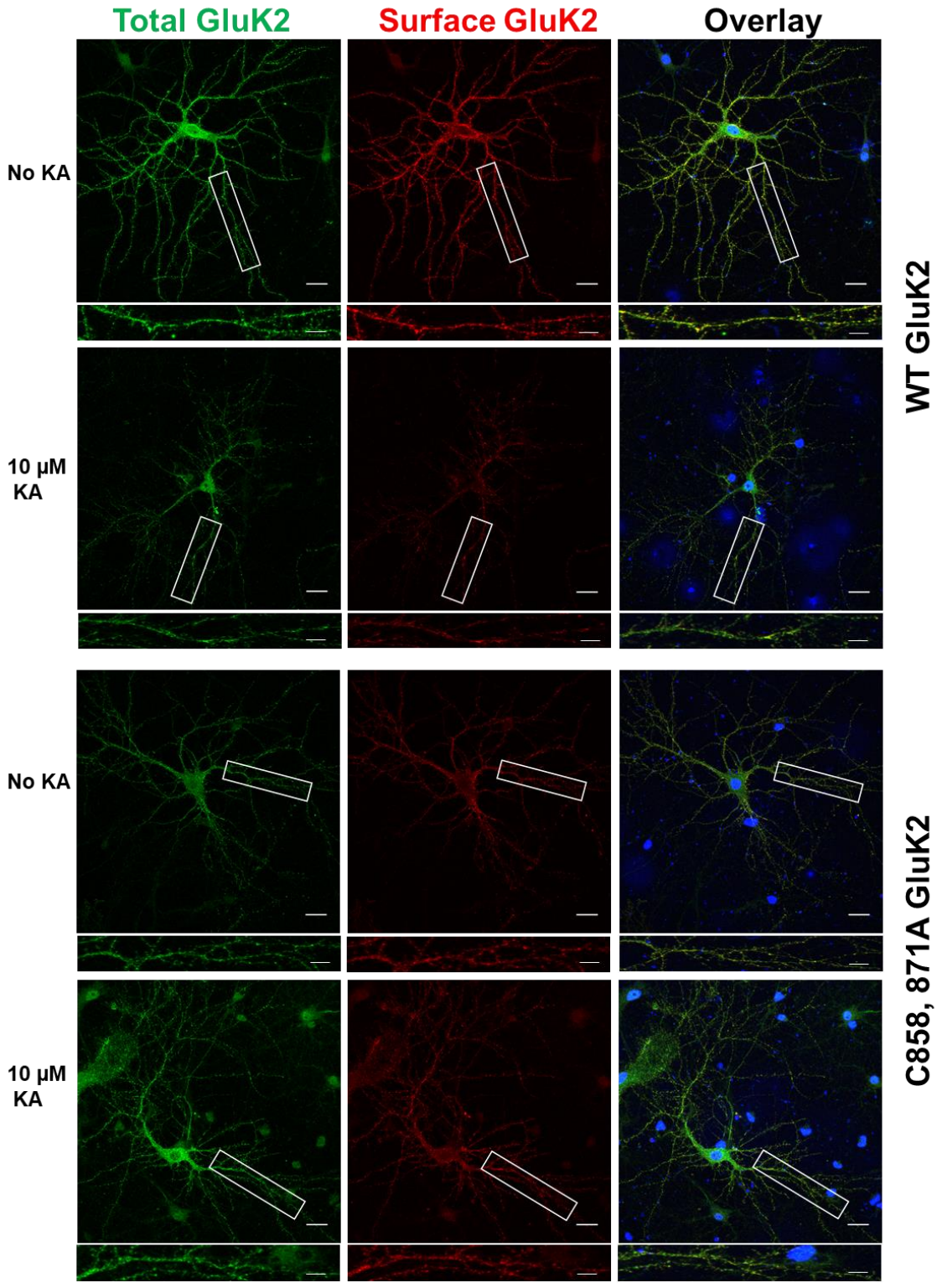

Figure 5.3. The effect of GluK2 non-palmitoylation on its surface expression using confocal imaging. Representative images of hippocampal neurons that were transfected with YFP-Myc-tagged GluK2 (WT or C858A, C871A) at DIV 9. At DIV 14 neurons were pre-treated with 2 µM tetrodotoxin (TTX) and 40 µM GYKI53655 for 30 min before being treated with 10 µM kainate (as indicated) for 20 min. Live labelling (using anti-GFP antibody followed by Alexa 647) was used to label the overexpressed surface GluK2 receptors (red). The total receptors were immunostained

by anti-GFP followed by Cy2 (green) after the red staining of the surface receptors as described in the methods. 5-15 cells per condition per experiment (a total of 3 independent experiments) were analysed using ImageJ Fiji software. Compared to the untreated WT, the surface expressed GluK2 (red channel) was noticeably decreased with agonist stimulation and in the non-palmitoylated condition.

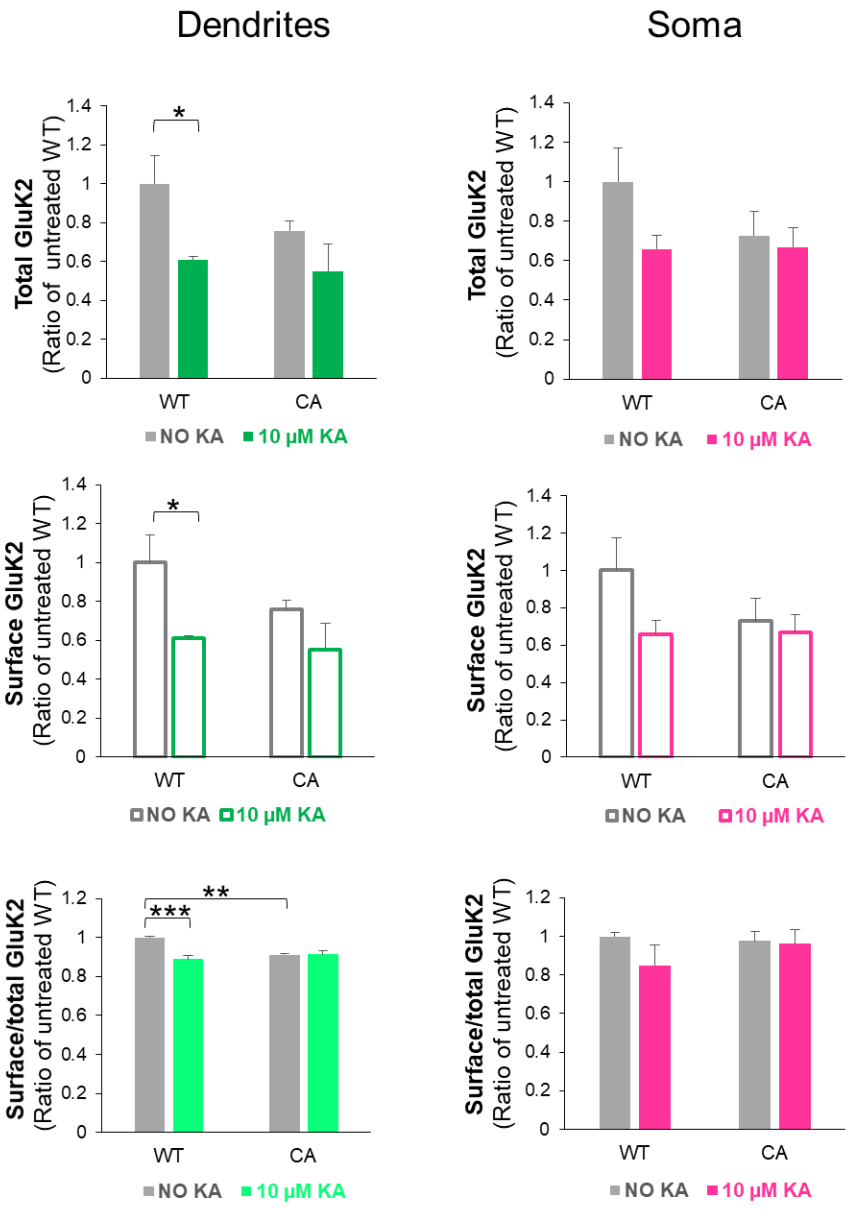

Figure 5.4. Quantification of the fluorescence imaging data. Immunofluorescence data were quantified from 5-15 cells/condition/experiment from 3 independent experiments. The results are presented as total, surface and surface/total ratio of GluK2 expression expressed as a ratio of the untreated WT in both the dendrites and soma. In the dendrites, there was a statistically significant ($p = 0.001$) reduction in the surface/total ratio of the non-palmitoylated GluK2 expression compared to the untreated control. This reduction mimics the treated WT surface/total expression ratio reduction ($p < 0.001$) compared to the untreated condition. However, there was no difference in the expression

of GluK2 between the different conditions in the soma as the somatic quantification result has more variability compared to the dendrites. Data presented as a percent of the untreated WT. Two-way ANOVA was used to analyse the results with Bonferroni (within a condition) and Sidak (between conditions) post hoc tests. *p* - Value significant at < 0.05. Error bars indicate the standard error. Scale bars: 20 µm (main panel) and 5 µm (magnification panel).

Total			
	WT	**C858A, C871A**	***p* - value**
No kainate	1.00 ± 0.14	0.82 ± 0.06	0.24
Kainate	0.67 ± 0.01	0.59 ± 0.13	0.63
***p* - value**	0.04 *	0.15	
Surface			
	WT	**C858A, C871A**	***p* - value**
No kainate	1.00 ± 0.14	0.75 ± 0.04	0.11
Kainate	0.61 ± 0.01	0.55 ± 0.14	0.69
***p* - value**	0.02 *	0.19	
Surface/total			
	WT	**C858A, C871A**	***p* - value**
No kainate	1.00 ± 0.005	0.91 ± 0.007	0.001 **
Kainate	0.89 ± 0.017	0.91 ± 0.018	0.25
***p* - value**	< 0.001 ***	0.87	

Table 5.2. The dendritic expression of the recombinant GluK2. A summary table of the neuronal dendritic total, surface and surface/total ratio of GluK2 immunofluorescence. Comparing the WT GluK2 to C858A, C871A GluK2 ± 10 µM kainate treatment, the total, surface, surface/total GluK2 is significantly reduced after kainate stimulation. In addition, the non-palmitoylated GluK2 surface/total basal expression is significantly reduced compared to its counterpart WT. Data are expressed as a ratio of the untreated WT ± SE. *p* - Value significant at < 0.05.

Total			
	WT	**C858A, C871A**	***p* - value**
No kainate	1.00 ± 0.17	0.74 ± 0.10	0.14
Kainate	0.78 ± 0.02	0.68 ± 0.04	0.58
***p* - value**	0.20	0.73	
Surface			
	WT	**C858A, C871A**	***p* - value**
No kainate	1.00 ± 0.17	0.72 ± 0.12	0.16

Kainate	0.65 ± 0.07	0.66 ± 0.09	0.96
***p* - value**	0.092	0.76	
Surface/total			
	WT	**C858A, C871A**	***p* - value**
No kainate	1.00 ± 0.02	0.97 ± 0.04	0.81
Kainate	0.84 ± 0.10	0.96 ± 0.07	0.33
***p* - value**	0.096	0.89	

Table 5.3. The somatic expression of the recombinant GluK2. A summary table of the neuronal soma total, surface and surface/total ratio of GluK2 immunofluorescence. Comparing the WT GluK2 to C858A, C871A GluK2, no statistically significant result was found. Data are expressed as a ratio of the untreated WT ± SE. *p* - Value significant at < 0.05.

5.3.3 Detection of GluK2 palmitoylated state

5.3.3.1 The Acyl-Biotin Exchange (ABE) assay

In an attempt to directly examine the palmitoylation state of GluK2, we used immunoprecipitation and then the acyl-biotin exchange assay (Brigidi and Bamji, 2013), summarised in Figure 5.5. These assays allow the immunoprecipitation of the protein of interest, then the specific detection of the palmitoylated form. As indicated by the representative blots of the several ABE attempts on the immunoprecipitated YFP-Myc-GluK2 (WT and double cysteine mutant) from HEK293T cells (Figure 5.6), the palmitoylated state of GluK2 was not robustly detected (very weak band for the hydroxylamine-treated WT around 150 kDa and no corresponding bands in the other conditions, red rectangle in Figure 5.6A). During the several experimental attempts (n = 3), the hydroxylamine was changed to a fresh product and the protein content was increased in the subsequent experiments (from protein pooled from 3 wells up to 5 wells) as the level of palmitoylated GluK2 might be low for detection. The weak signal (overexposed band of Figure 5.6A magnification) was only obtained in the third attempt when the protein content was increased the most of all attempts. In addition, there were strong bands detected between 55 and 70 kDa (A) in the hydroxylamine-treated WT condition of the GluK2-transfected HEK cell lysate. The membrane was stripped and then re-probed with anti-GFP [to confirm that transfected GluK2 (WT or mutant) was expressed] and again with anti-GluK2/3 antibodies (to test if the bands between 55 and 70 kDa are due to GluK2 being degraded from the hydroxylamine treatment) (Figure 5.6B

and C, respectively). The result shows a strong expression level of the GluK2 WT and C858A, C871A mutant in all conditions around 150 kDa. Note the red circle (Figure 5.6C), which indicates no evidence of GluK2 degradation products in the hydroxylamine-treated WT. This indicates that the detectable bands are not related to GluK2 degradation.

It worth noting that the NEM and biotin-BMCC were tested for being working using total HEK293T cells lysate that is either treated or untreated with NEM and without the hydroxylamine. The result showed a strong smear of crude palmitoylated HEK293T cells proteins without NEM treatment (available free thiols were not blocked) and almost nothing when the lysate was treated with NEM (free thiols were blocked and so did not react with biotin-BMCC).

There are more measures can be done to further optimise the protocol. Such measures can be increasing the biotin concentration [although the used concentration (4 µM) was already on the higher side of the recommended range (1-5 µM)] to increase the sensitivity of detecting the palmitoylated form which could be very low amount. In addition, the protein content could be increased more (use larger cell culture dishes and/or increase the DNA amount) as the very weak signal in the hydroxylamine-treated WT GluK2 sample can result from non-sufficient protein content to account for hydroxylamine-mediated protein degradation.

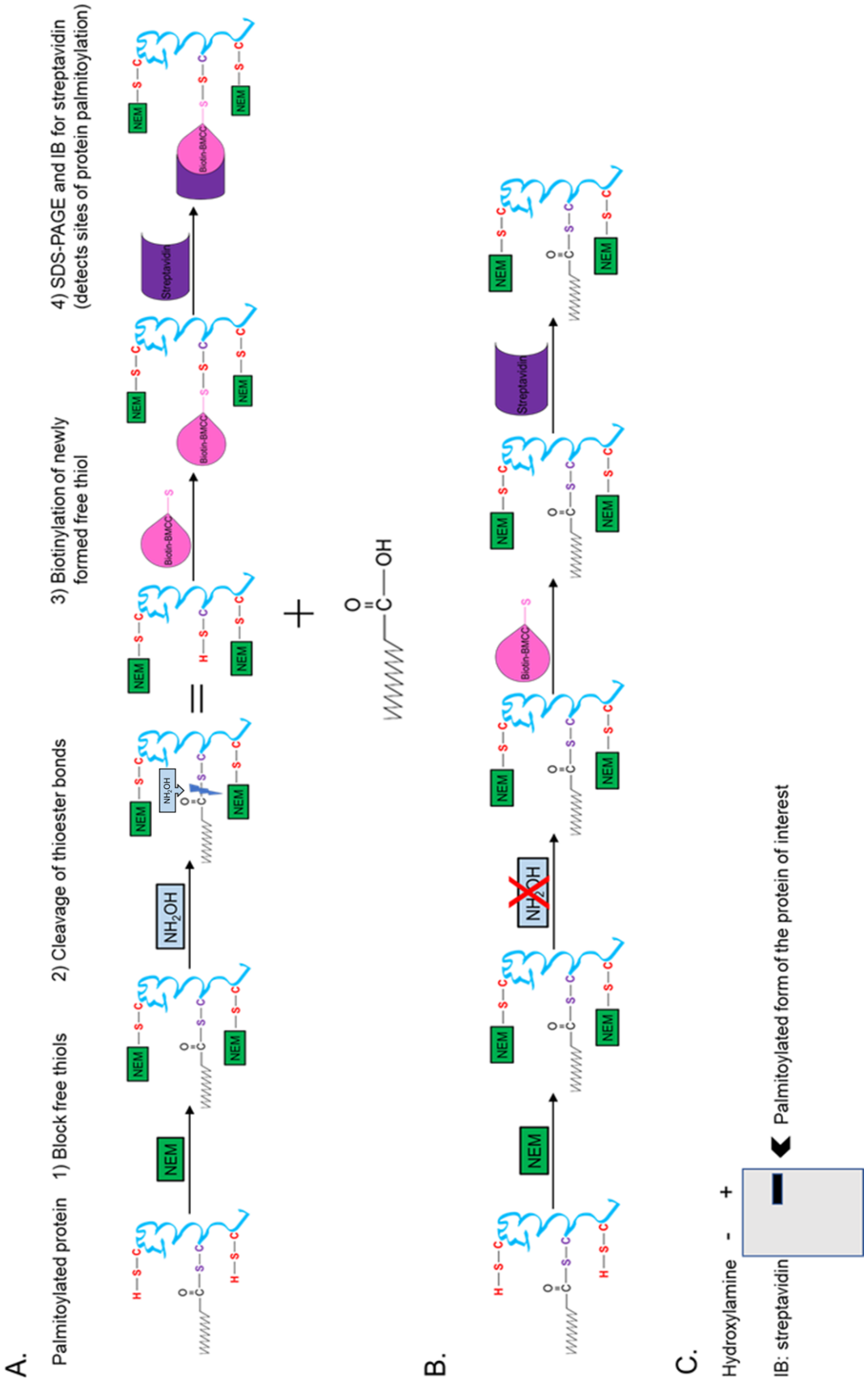
A.
Palmitoylated protein
1) Block free thiols
2) Cleavage of thioester bonds
3) Biotinylation of newly formed free thiol
4) SDS-PAGE and IB for streptavidin (detects sites of protein palmitoylation)
NEM
NH2OH
Biotin-BMCC
Streptavidin
B.
C.
Hydroxylamine - +
IB: streptavidin
Palmitoylated form of the protein of interest

Figure 5.5. A schematic diagram of the acyl-biotin exchange (ABE) assay. The ABE assay is a multistep protocol that has been used to detect palmitoylated proteins **(A)**. The first step aims to block the free thiols using N-ethylmaleimide (NEM) in the protein lysate prior to immunoprecipitation with either GluK2 antibody followed with protein A-sepharose beads (for endogenous GluK2 from hippocampal neurons) or GFP-beads (for recombinant protein from HEK293T cells). The second step uses hydroxylamine (NH_2OH) to cleave the thioester bond of the palmitoylated cysteine residue to release palmitic acid leaving a free thiol group at the site of palmitoylation. Thirdly, a sulfhydryl-reactive biotinylation reagent (Biotin-BMCC) is used to biotinylate the newly formed free thiol. Finally, using SDS-PAGE the protein is immunoblotted with streptavidin antibody. A parallel sample **(B)** is treated identically except the hydroxylamine treatment step is omitted so no free thiol group should be available to bind biotin. **C**, represents an example of the expected immunoblot result after probing for streptavidin.

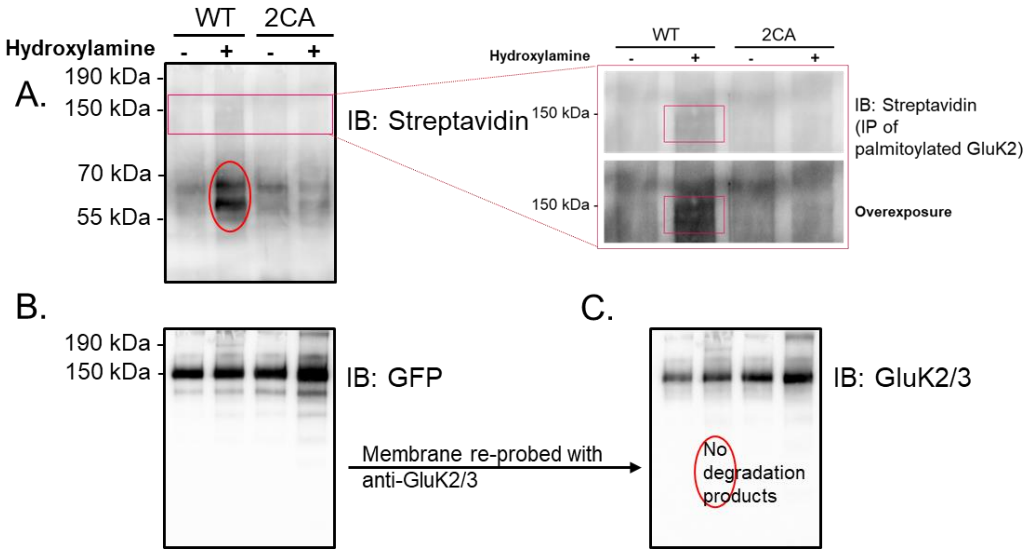

Figure 5.6. Using the acyl-biotin exchange (ABE) assay to detect GluK2 palmitoylated state. Both WT and C858A, C871A of YFP-Myc-tagged GluK2 were immunoprecipitated (GFP-trap protocol) from cell lysate of transfected HEK293T cells and then the ABE assay was performed. The blots represent the result of the last attempt of the assay (n = 3) when protein was pooled from 5 wells instead of 3 wells in the previous experiments. The first blot **(A)** shows very weak band at the expected molecular weight (~150 kDa) of YFP-Myc-GluK2 in the WT condition when treated with hydroxylamine to detect the palmitoylated state of the protein (see the close-up panel with the overexposed blot). Notably, GluK2 was overexpressed in all conditions **(B)** when the blot was re-probed for GFP. To investigate the bands (between 55 and 70 kDa) of the hydroxylamine-treated WT on blot A for being possible degradation products of GluK2 (the hydroxylamine increases protein degradation), the membrane was re-probed for GluK2. The result **(C)** shows no degradation products of GluK2 at the corresponding molecular weights of the bands shown in A.

5.3.3.2 The liquid chromatogrphy-mass spectrometry (LCMS) analysis of GluK2 palmitoylation

Since the result of the ABE assay to detect palmitoylated GluK2 was not robust and to enhance the sensitivity of detecting the palmitoylated form, we next attempted to identify palmitoylated GluK2 by mass spectrometry. After consultation with and advice from Dr Kate Heesom, (Director of the Bristol Proteomics Facility), we immunoprecipitated recombinant YFP-Myc- tagged GluK2 (WT and C858A, C871A) as shown by the coomassie brilliant blue stain of the IP gel (Figure 5.7A). The gel was then processed and analysed using LCMS for possible palmitoyl (cysteine residues, + 238.2 Da) peptide modifications. As expected, the results from the mass-spec indicated GluK2 was the top hit in each sample (See Appendix 8.2). In addition, the analysis showed the identified peptide fragments (highlighted in green) of the GluK2 protein sequence (Figure 5.7B and C for the WT and the double cysteine mutant bands, respectively) and their detectable modifications as indicated by the letter (C: carbamidomethyl, O: oxidation) above each fragment.

No palmitoylated peptides were identified in WT or mutant bands. The first cysteine residue (C858) of the GluK2 C-terminus (located within the tryptic peptide FS**C**SAMVEELR) was identified as being carbamidomethylated in the WT sample and converted to alanine in the mutant (see the red arrow heads). This modification occurs as a result of the incubation with iodoacetamide which is part of the standard sample processing. The other potential site (C871) is within a tryptic fragment which is too small to be detected (peptide **C**QR) and so to focus on this site we would need to digest the protein bands using an alternative endopeptidase enzyme to the standard trypsin.

We cannot rule out the possibility that palmitoylated forms also exits, but perhaps do not fragment as well in the mass-spec and remain undetected. Another consideration is the stability of the palmitoylation modification. It is possible that it could be displaced by the carbamidomethylation reaction. It is worthy to repeat the analysis without including the iodoacetamide incubation to assess this possibility.

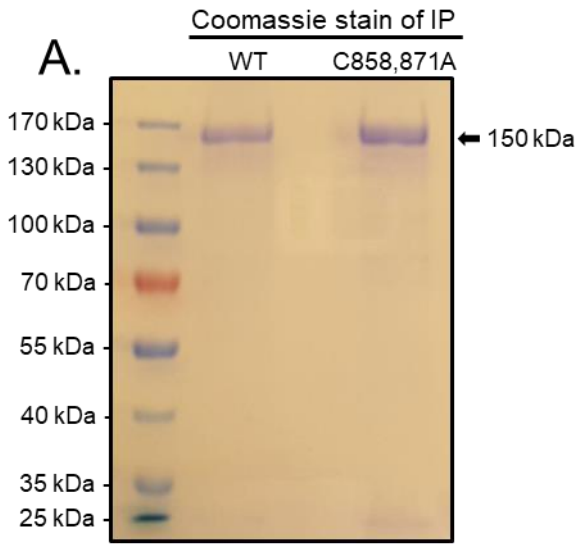
A.
Coomassie stain of IP
WT
C858,871A
170 kDa
130 kDa
100 kDa
70 kDa
55 kDa
40 kDa
35 kDa
25 kDa
150 kDa

B. WT GluK2


1
101
201
301
401
501
601
701
801
901
1001
1101
1201
1239
Sequence
Modification List

C. GluK2 C858A, C871A

Figure 5.7. Using LCMS analysis to detect GluK2 palmitoylated state. The coomassie brilliant blue stained gel **(A)** shows the immunoprecipitated (GFP-trap protocol) bands of both WT and C858A, C871A of YFP-Myc-tagged GluK2 from cell lysate of transfected HEK293T cells. These bands were cut and sent for LCMS to detect palmitoylation as a possible peptide modification. The GluK2 protein was found to be the top hit in each band (see appendix 8.2). **B** and **C** show the sequence coverage maps for the two bands (WT and C858A, C871A). These show where the identified peptides (highlighted with green) of the LCMS map on to the GluK2 protein sequence. The letters (C and O) above each identified peptide fragment indicate the identified peptide modifications (C: carbamidomethyl which result from the routine sample processing with iodoacetamide, O: oxidation) of the amino acid residue beneath it. The red arrow heads indicate the two expected palmitoylated cysteine residues (C858 and C871) in the WT GluK2 C-terminus **(B)** and their corresponding two alanine (C858A and C871A) in the mutant sequence **(C)**. The analysis result indicates that the first cysteine residue (C858) was identified as being carbamidomethylated while the other cysteine residue (C871) of the WT C-terminus was within a tryptic fragment that was too small to be detected.

5.3.4 Preparing and testing tools for future work

5.3.4.1 Overexpressing GluK2 in neurons

To extend and further augment the findings from HEK293T cells on GluK2 SUMOylation to neurons, the various GluK2 constructs were used to prepare sindbis virus vectors. Six different sindbis viruses were made to overexpress GFP and five different YFP-Myc-tagged GluK2 (1. WT, 2. C858A, C871A, 3. K886R, 4. C858A, C871A + K886R, and 5. C858A, C871A + S846A, S868A) in neurons. The initial results (Figure 5.8) indicate that these viruses effectively overexpress these proteins after 18 hours in cortical neurons. Two separate batches of viruses were prepared (shown on separate blots). Importantly, each YFP-Myc-GluK2 construct from each batch expresses at comparable levels so direct comparisons can be made. But, further expression validation of all the different sindbis viruses should be done to ensure comparable expression levels between all conditions.

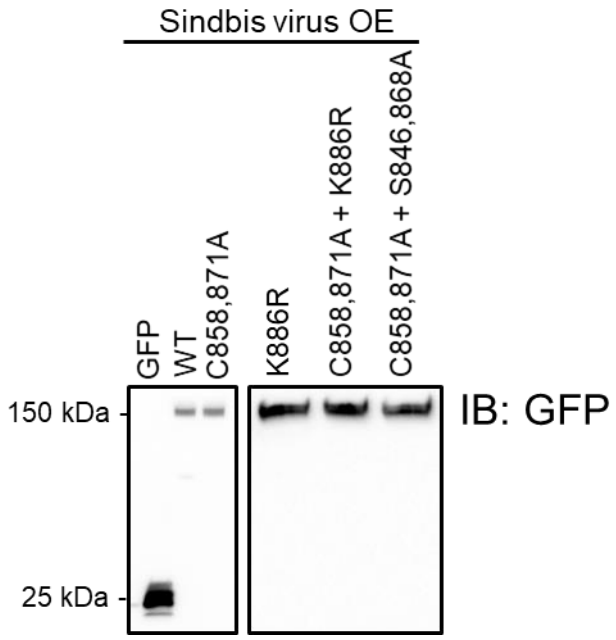

Figure 5.8. Using sindbis virus to overexpress YFP-Myc-GluK2. Sindbis virus was used for neuronal overexpression of GFP and several YFP-Myc-tagged GluK2 [WT, C858A, C871A GluK2 (non-palmitoylated), K886R GluK2 (non-SUMOylated), C858A, C871A + K886R GluK2 (non-palmitoylated and non-SUMOylated) and C858A, C871A + S846A, S868A GluK2 (non-palmitoylated and non-phosphorylated)]. The blots were probed for GFP and they show the expression level of these proteins at the expected molecular weights when sindbis virus (20 µL for GFP and 50 µL for the other viruses) was used for 18 hours at DIV14 cortical neurons.

5.3.4.2 Detecting PKC-phosphorylated GluK2 and testing a phosphoserine PKC substrate antibody

As previous trials of detecting PKC-mediated phosphorylation of GluK2 before detecting its SUMOylation levels were unsuccessful, we tried to facilitate this process by using the PKC activator phorbol 12-myristate 13-acetate (PMA) aiming to bring phosphorylated levels to detectable ranges. Cortical neurons at DIV 16 were treated with sindbis viruses for 20 hours to overexpress either WT YFP-Myc-GluK2 or GFP (negative control) (n = 3). Half of them were then treated with 1 µM PMA for 20 minutes before being lysed with a lysis buffer containing phosphatase inhibitors cocktail. Protein of interest was immunoprecipitated using GFP-trap protocol and membranes were probed for total and immunoprecipitated proteins using two anti-phosphoserine antibodies (BD Biosciences 612548 and Sigma-Aldrich P5747) before re-probing the immunoprecipitated proteins for GFP expression. The result (Figure

5.9) indicates that despite the successful overexpression of GluK2, phosphorylated levels (using BD Biosciences antibody) were not robustly detectable even in the presence of PMA. During the several attempts of this experiments, fresh PMA was used, and protein was pooled from 2-4 wells working towards detecting phosphorylated GluK2. No bands were obtained using Sigma-Aldrich anti-phosphoserine antibody (P5747).

In an attempt to study the level of PKC-mediated phosphorylation of S868 when GluK2 is non-palmitoylated, a specific anti-phosphoserine antibody was evaluated. The phosphoserine PKC substrate antibody [Cell Signaling (CS) 2261] is active toward a specific motif [(R/K)X(S*)(Hyd)(R/K)] that is similar to the S868 in the GluK2 C-terminus [(R)(M)(S*)(L)(K)]. The site-specific antibody was tested by using sindbis virus and immunoprecipitating the neuronal overexpressed GluK2 (WT and the available phosphor-null mutant: S846A, S868A + C858A, C871A). The result (Figure 5.10) indicated that the GluK2 was successfully overexpressed in both conditions (WT and the phosphor-null mutant). Unfortunately, however, the anti-phosphoserine antibody did not identify the expected band of the phosphorylated WT GluK2 around 150 kDa.

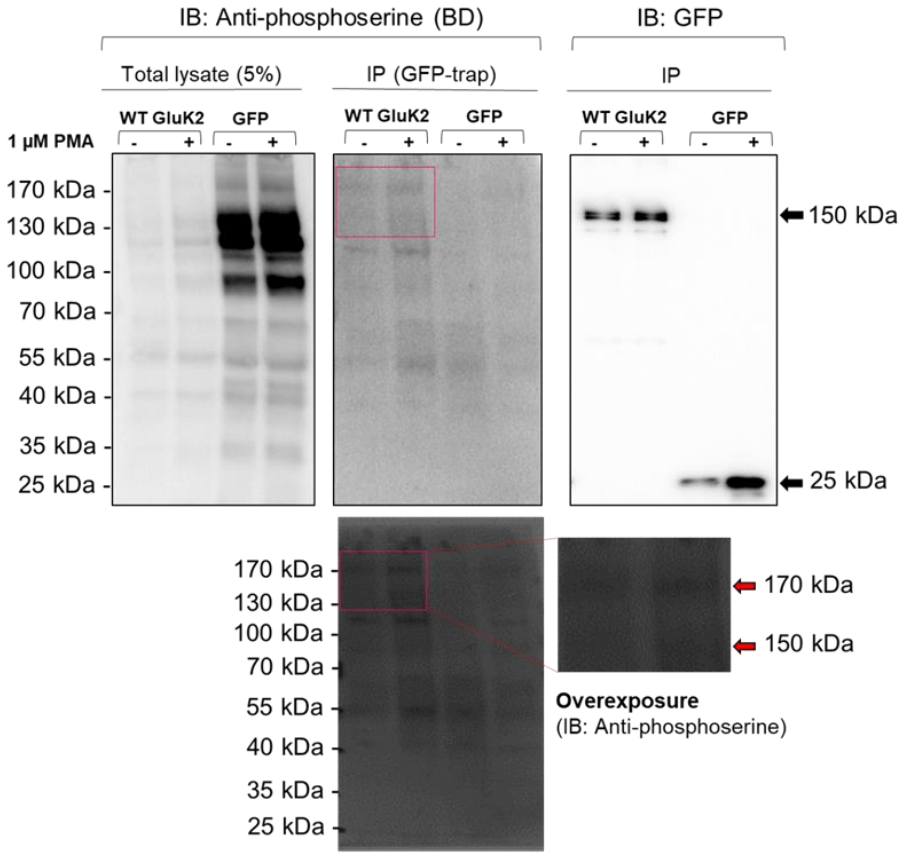

Figure 5.9. Detection of PKC-dependent phosphorylated GluK2 in neurons. YFP-Myc-tagged GluK2 (WT) and GFP were overexpressed in cortical neurons at DIV 16 using sindbis virus (n = 3). PKC-mediated protein phosphorylation was promoted by treating the cells with 1 µM PMA for 20 minutes. The proteins were immunoprecipitated (via the GFP-trap) in the presence of phosphatase inhibitors and the resulting membrane blots (total lysate and immunoprecipitated proteins) was probed for a phosphoserine/threonine residue using the previously validated (Konopacki et al., 2011) BD Biosciences antibody (612548). There were no robust bands at the expected molecular weight (~ 150 kDa) for phosphoserine. Membrane of immunoprecipitation was re-probed for GluK2 and GFP expression using anti-GFP antibody and both proteins were found to be overexpressed at the expected molecular weight.

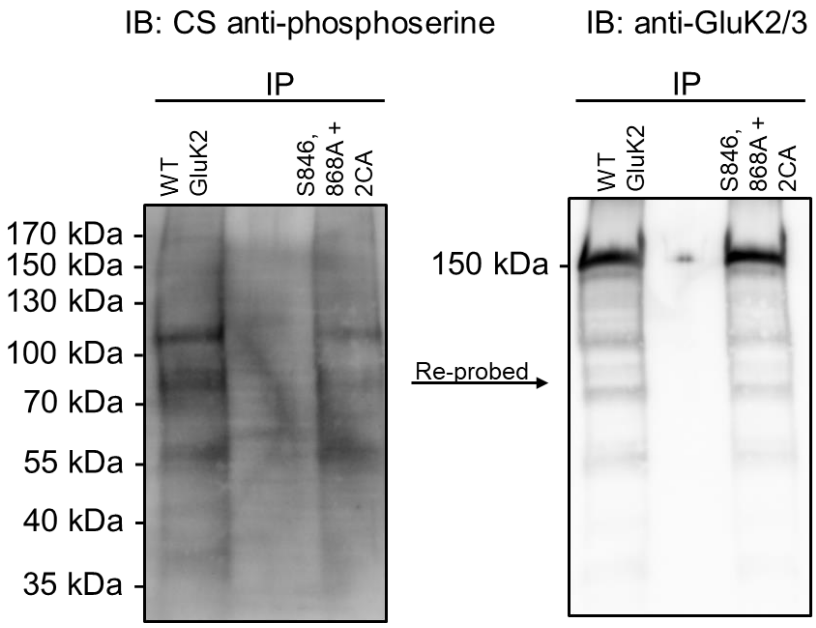

Figure 5.10. Using sindbis virus to validate the phosphoserine PKC substrate antibody. YFP-Myc-tagged GluK2 (WT and C858A, C868A + S846A, S868A) were overexpressed in cortical neurons at DIV 14 using sindbis virus. The proteins were immunoprecipitated (via the GFP-trap) and the resulting membrane blot was probed for a phosphoserine residue that is phosphorylated by PKC at serine residues surrounded by Arg or Lys at the -2 and +2 positions and a hydrophobic residue at the +1 position [motif: (R/K)X(S*)(Hyd)(R/K)] using Cell Signaling antibody 2261. This motif is equivalent to the S868 residue [(R)(M)(S*)(L)(K)] in the C-terminus of GluK2. There are no bands at the expected molecular weight (~ 150 kDa) for phosphoserine in the WT condition. Membrane was re-probed for GluK2 expression using anti-GFP antibody and both WT and the mutant proteins were found to be overexpressed.

5.3.5 Concluding remarks

1. GluK2 SUMOylation is enhanced when GluK2 cannot be palmitoylated, which is similar to the kainate effect on the WT.
2. Basal SUMOylation level of GluK2 remained unchanged in the phosphor-null mutant, but highly increased in the phosphor-mimetic condition compared to the WT.
3. Dendritic GluK2 surface expression is reduced in the non-palmitoylated receptor compared to the WT and is similar to kainate effect on the WT GluK2.

5.4 Discussion

The diversity of KARs trafficking, synaptic targeting and subcellular localisation is regulated by three determining factors (Copits and Swanson, 2013):

1. the intrinsic trafficking attributes of each subunit,
2. the interaction with a diverse pool of interacting proteins and
3. the interplay between different post-translational modifications.

In addition, the fine balance of several subcellular processes (protein's biosynthesis, forward trafficking, internalisation, recycling, and degradation) determines the cell surface expression of proteins (Shipston, 2011).

Here, we found that there is a cross-talk between two post-translational modifications of GluK2 that was not identified previously. The palmitoylation state of GluK2 C-terminus has shown to be important to its SUMOylation state and neuronal cell surface expression. However, we were unable to identify the effect of GluK2 palmitoylation state on GluK2 phosphorylated levels but my findings regarding the effects of the phospho mutants on GluK2 SUMOylation confirmed previous observations (Konopacki et al., 2011; Chamberlain et al., 2011). PKC-dependent phosphorylation of GluK2 C-terminus facilitates but is not required for its SUMOylation.

5.4.1 Palmitoylation- and phosphorylation-dependent enhancement of GluK2 SUMOylation

The non-palmitoylation state of GluK2, represented by the double cysteine mutant (C858A, C871A), has shown to have high SUMOylation levels in heterologous systems similar to the effect of agonist stimulation on the WT GluK2. This suggests that depalmitoylating GluK2 might increase the receptor SUMOylation. But, whether phosphorylation of GluK2 contributes as an intermediate process between depalmitoylation and SUMOylation is still unknown. The GluK2 SUMOylation level when it loses its main PKC-phosphorylated C-terminal sites (S846 and S868) is similar to the WT under basal conditions. This suggests that GluK2 SUMOylation can occur in an independent manner of PKC-mediated phosphorylation. However, GluK2 SUMOylation is highly promoted and increased in the phosphor-mimetic condition.

Although HEK293T cells have all the required SUMO machinery (Zhao et al., 2004), we were unable to detect GluK2 SUMOylation without co-transfecting HEK293T cells with Ubc9 (data not shown; empty blots). It seems that the endogenous SUMO machinery in HEK293T cells is insufficient or fails to SUMOylate recombinant proteins in a way similar to other heterologous systems (Langereis et al., 2007). Ubc9, the SUMO conjugating enzyme, was used here to promote recombinant GluK2 SUMOylation in HEK293T cells. Thus, there is a possibility that this might have contributed to our positive findings. However, this possibility is unfavourable considering that after co-transfecting HEK293T cells with 0.1 µg Ubc9 significant changes in SUMOylation levels could still be identified. In addition, 0.1 µg of Ubc9 was reached after several starting attempts of using higher amounts (1, 0.7, and 0.5 µg) of transfected Ubc9 that saturated the system and differences in protein SUMOylation levels between the different conditions could not be identified. Moreover, recombinant Ubc9 was used previously (Konopacki et al., 2011) to facilitate SUMOylation of recombinant GluK2 in heterologous systems.

Palmitoylation can decrease or increase phosphorylation depending on the protein substrate. Palmitoylation of the GluK2 (Pickering et al., 1995) and GluA1 (Lin et al., 2009) subunits inhibits the PKC-mediated phosphorylation of these proteins leading to inhibiting or promoting receptor internalisation, respectively. However, the palmitoylation of the NMDAR subunits GluN2A and GluN2B at the cysteine clusters in the membrane-proximal region increases the subunits tyrosine phosphorylation

which inhibits the receptor internalisation and stabilises its cell surface expression (Hayashi et al., 2009).

The interplay between palmitoylation and phosphorylation differentially regulates the surface expression of both AMPA and kainate receptors through their interactions with the neuronal scaffolding 4.1N protein (Copits and Swanson, 2013). 4.1N protein interacts with the GluA1-containing AMPARs to regulate their synaptic localisation into the cell surface (Shen et al., 2000; Coleman et al., 2003; Lin et al., 2009) by the possible coupling of the receptor to actin cytoskeleton (Shen et al., 2000). On the one hand, GluA1 palmitoylation reduces 4.1N association with the AMPAR resulting in a less stable and more susceptible receptor to agonist-induced endocytosis (Lin et al., 2009; Hayashi et al., 2005). On the other hand, proximal PKC-mediated phosphorylation of GluA1 enhances 4.1N interaction and hence promote AMPAR plasma membrane expression.

AMPAR subunits can be palmitoylated at two sites, both surrounded by basic and hydrophobic residues, to regulate receptor trafficking and localisation (Aicart-Ramos et al., 2011; Hayashi et al., 2005). The first cysteine residue is located three amino acid residues away from the Q/R editing site in the second transmembrane domain where its palmitoylation inhibits the receptor trafficking to the plasma membrane from the Golgi apparatus. The second cysteine residue is present in the C-terminus in a close proximity to the cell membrane and to the 4.1N protein binding location. This location may suggest the enhancement of attaching a palmitate via a cell membrane-bound palmitoyl acyltransferase and also promoting the binding of the adjacent basic residues to the acidic heads of the membrane phospholipids (El-Husseini and Bredt, 2002) stabilising cell membrane interaction. However, its palmitoylation/de-palmitoylation decreases/enhances the interaction with 4.1N protein leading to endocytosis/surface stabilisation in an agonist-induced manner (Shen et al., 2000; Hayashi et al., 2005; Coleman et al., 2003). This finding may suggest that the 4.1N protein interaction seems to be the key to receptor cell surface stabilisation and when interrupted by the nearby palmitoylation, likely due to steric hindrance, leads to receptor cell surface destabilisation.

In addition, the control of receptors trafficking and localisation is complicated by the fact that many of the iGluRs interacting proteins are substrates for palmitoylation (Hayashi et al., 2005) with the alternative splices of these proteins differentially regulating their palmitoylation (El-Husseini and Bredt, 2002). For example, the PSD-95

protein, in particular the PDS-96α isoform from the alternative splicing (Chetkovich, 2002) can be palmitoylated leading to forming a complex with stargazin via its C-terminal PDZ-binding domain. This association enhances AMPAR synaptic targeting and clustering by stargazin (El-Husseini et al., 2000a; El-Husseini et al., 2002; Tomita et al., 2003; Tomita et al., 2004; Vandenberghe et al., 2005). The synaptic clustering of AMPARs, regulated by palmitoylation, may suggest that palmitoylation may adjust synaptic strength and contribute to synaptic plasticity (El-Husseini and Bredt, 2002). Furthermore, changes in synaptic activity affect PSD-95 palmitoylation turnover as prolonged synaptic activity increases the rate of PSD-95 depalmitoylation which lead to receptor endocytosis representing a homeostatic feedback mechanism (El-Husseini and Bredt, 2002).

The membrane-proximal domain of GluK2 C-terminus also interacts with 4.1N protein to coordinate KAR synaptic targeting and endocytosis (Copits and Swanson, 2013). When KARs are associated with 4.1N, their forward trafficking to the neuronal cell surface is enhanced and their surface expression is stabilised by reducing their constitutive internalisation. In addition, 4.1N association preferentially localises KARs to the extrasynaptic sites on the dendritic shafts (Copits and Swanson, 2013). Similar to AMPARs, the interaction between the 4.1N and GluK2 KAR subunit is mediated by both palmitoylation and phosphorylation. However, in this case, palmitoylation occurs distally to the membrane-proximal domain enhancing 4.1N association and hence KAR surface expression while PKC phosphorylation antagonises it and induces endocytosis (Copits and Swanson, 2013). It is mainly the proximal PKC-mediated phosphorylation at S846 that was shown to prominently reduce the neuronal cell surface expression of GluK2 through 4.1N dissociation (Copits and Swanson, 2013). Thus, it is tempting to speculate that the proximity of the post-translational modification to the 4.1N binding site has an important role in regulating the receptor association with 4.1N protein but other factors like interacting proteins and other 4.1 protein isoforms can also play a role in regulating receptor surface stabilisation. A proposed explanation of this reciprocal relationship between palmitoylation and phosphorylation suggests palmitoylation of a positively charged region of cytosolic GluK2 interferes with the PKC activity by bringing the C-terminal tail close to the plasma membrane masking the serine residues for phosphorylation (Copits and Swanson, 2013). The same idea of adding a negatively charged phosphate

group might be responsible for concealing the cysteine residues from palmitoyl acyltransferases. In agreement with this, metabolic labelling (using [^{32}P]-ATP) of PKC-mediated phosphorylation of recombinant GluK2 was shown to be significantly increased in the non-palmitoylated mutant (C858A, C871A) compared to the wild-type GluK2 (Pickering et al., 1995).

Taking into account the interplay between palmitoylation and phosphorylation in regulating 4.1N protein interaction, and the interplay between each one of these individual post-translational modifications with SUMOylation (including our initial finding of a cross-talk between palmitoylation and SUMOylation), a link between 4.1N protein interaction and SUMOylation is plausible. The process of losing 4.1N interaction upon GluK2 phosphorylation and the subsequent increased SUMOylation-dependent endocytosis might act in concert to coordinate KARs expression and localisation and regulating neuronal excitability (Copits and Swanson, 2013).

Considering the previous evidence of the reciprocal relationship between palmitoylation and phosphorylation and the positive link between phosphorylation and SUMOylation, we aimed to investigate a cascade of downstream post-translational modifications with PKC-mediated phosphorylation being the common process that has been studied previously in relation to the other up- and down- stream events. However, despite the fact that we tried three different anti-phosphoserine antibodies to detect the phosphorylated levels of GluK2 both in HEK293T cells and neurons, we could not identify any GluK2 phosphorylated signal under basal conditions or following 20 minutes of kainate stimulation (transfected HEK293T cells) and 20 minutes of PMA (sindbis virus infected neurons). In addition, one of the used antibodies was validated and used previously for the same purpose with acceptable results (Konopacki et al., 2011). In this elegant study, the detectable phosphorylated levels of virally expressed GluK2 in neurons were observed at low levels under basal conditions and were significantly increased after 5 minutes of kainate stimulation. However, in this same study the detectable increase in GluK2 SUMOylation was observed after 20 minutes of kainate or PMA stimulation and this increase was not cumulative by both drugs suggesting a common pathway of action. This is very interesting as it might be resembling the "*SUMO enigma*[1]" (Hay, 2005; Martin et al., 2007) and may suggest that once PKC phosphorylates its substrate, it

[1] SUMO enigma: SUMOylation-mediated effects persist after the removal of SUMO.

initiates a signalling pathway to increase SUMOylation and this effect continues after phosphorylation rapid turnover by phosphatases. This also could explain why we could not detect phosphorylated GluK2 after 20 minutes of kainate or PMA stimulation as this duration might be too long for this very dynamic process. And, we were able to reproduce the SUMOylation changes after 20 minutes of kainate stimulation similar to Konopacki et al. findings.

In addition to the diversity of the SUMOylation machinery to control the temporal and spatial specificity of SUMOylation, the post-translational modifications as phosphorylation of targeted proteins contribute to the process (Wilkinson and Henley, 2010; Bossis and Melchior, 2006; Konopacki et al., 2011). One suggested mechanism that clarifies how phosphorylation mediates SUMOylation is that Ubc9, which has a cognate basic patch, is recruited to the close by SUMOylation motif by the phosphate group negative charge (Hietakangas et al., 2006; Mohideen et al., 2009). And although phosphorylation facilitates SUMOylation, it is not the only mechanism through which SUMOylation can occur (Konopacki et al., 2011). This was evident by detecting some SUMOylation in the GluK2 WT and phospho-null mutants (S846A and 868A) (Konopacki et al., 2011).

5.4.2 Palmitoylation-dependent reduced GluK2 cell surface expression in dendrites

In this study, we found that the non-palmitoylated GluK2 has lower dendritic surface expression compared to the normal situation under basal conditions. This may suggest that palmitoylated forms are mainly expressed at the cell surface as palmitate attachment enhances cell membrane and 4.1N protein interactions. Hence, the reduced surface expression when the receptor cannot be palmitoylated. Moreover, the effect of GluK2 non-palmitoylation on dendritic surface expression is similar to the effect of kainate on the WT, an observation that may suggest a possible involvement of this post-translational modification in activity-dependent regulation of receptor surface expression especially in the light of our new finding linking palmitoylation to SUMOylation which is also activity-dependent. Notably in the WT condition, not only the surface but also the total GluK2 expression is reduced upon kainate stimulation

which suggest that the main reduction of the surface expressed receptors is due to degradation.

Neuronal activity dynamics regulate the addition and removal of palmitate from various neuronal proteins (Kang et al., 2008) leading to differential subcellular localisation and protein-protein interactions (Noritake et al., 2009). The pamitoyl acyltransferase protein family includes 23 members containing the conserved catalytic motif "Aspartate-Histidine-Histidine-Cysteine" within a zinc finger-like domain (zDHHC) (Globa and Bamji, 2017). Synaptic activity regulates protein palmitoylation by modulating the trafficking of the palmitoyl acyltransferase enzymes and their subcellular localisation, their interactions with other proteins, and their post-translational modifications (Globa and Bamji, 2017). As an example, synaptic activity leads to the internalisation of zDHHC5, one of the 23 isoforms, from dendritic spines to shafts to palmitate the soluble protein δ-catenin which is abundant in dendritic shafts (Brigidi et al., 2014; Brigidi et al., 2015). Then, the palmitoylated δ-catenin is recruited to postsynaptic spines to stabilise AMPARs, thus contributing to synaptic connections strengthening. Moreover, the palmitoyl acyltransferase zDHHC2 is recruited to postsynaptic density after prolonged TTX treatment (activity-dependent movement from shafts to spines after activity blockade) to palmitate PSD-95. Hence, increasing AMPARs clustering at synapses (Noritake et al., 2009). Likewise, the palmitoylation of the AMPAR auxiliary subunit synapse differentiation-induced gene 1 (SynDIG1), which enhances AMPARs localisation at synapses (Kalashnikova et al., 2010), is enhanced by TTX-mediated block of synaptic activity (Kaur et al., 2016). This recruits SynDIG1 to postsynaptic spines and increases its stability and clustering at spines (Kaur et al., 2016) which may result as well in increasing postsynaptic AMPARs adding to homeostatic plasticity (Globa and Bamji, 2017).

Some of the palmitoyl acyltransferases are expressed throughout the brain but others show a distinct specific expression pattern like zDHHC2 and zDHHC7, which are highly expressed in the CA1 hippocampal pyramidal neurons (Zhang et al., 2014) and they localise to the dendrites (Woolfrey et al., 2015) and somatic Golgi (Thomas et al., 2012), respectively. Taking this into consideration and that the properties of hippocampal cultured neurons are similar to CA1 pyramidal cells (Martin and Henley, 2004), could zDHHC2 and zDHHC7 have a prominent role in the dynamic process of GluK2 palmitoylation to regulate its subcellular localisation in response to synaptic stimulation?

Importantly, although the specific zDHHC isoforms responsible for palmitoylating GluK2 have not been identied yet, Copits and Swanson (2013) have demonstrated a prominent increase in GluK2 palmitoylation in a [^{3}H]-palmitate metabolic labelling assay upon treating cells with zDHHC2, 3 and 7. Here, we found that the surface expression of the dendritic non-palmitoylated GluK2 was reduced similar to that of WT GluK2 in response to 20 minutes of kainate stimulation. This may suggest that changes in palmitoylation dynamics may be responsible for the agonist-induced internalisation of KARs. However, the somatic surface expression reduction in the non-palmitoylated form and upon 20 minutes of kainate stimulation was not significant. Rapid change in the palmitoylation status of a protein is likely mediated upon synaptic activity to regulate local subcellular protein localisation (Brigidi et al., 2014; Brigidi et al., 2015; Woolfrey et al., 2015; Thomas et al., 2012; El-Husseini et al., 2002). Apparently, the palmitoylation/depalmitoylation machinery responsible for the rapid processes would be in close proximity to their target proteins (Globa and Bamji, 2017). Thus, our significant findings of reduced dendritic surface GluK2 upon kainate stimulation may indicate a rapid response of internalising specific transmembrane palmitoyl acyltransferase like zDHHC2 leading to preventing the dynamic palmitoylation of cell membrane GluK2 or interacting proteins like PSD-95 and making them more susceptible to depalmitoylation. However, a slower change in protein palmitoylation happens for long-term static cellular events like targeting substrates to the cell membrane (Kang et al., 2004) using machinery in somatic Golgi (Kang et al., 2004; Ponimaskin et al., 2008; Lievens et al., 2016; Greaves et al., 2010). This may explain why the somatic surface expression of GluK2 was not significantly altered by kainate as enzymes mainly localised in somatic Golgi (like zDHHC3 and zDHHC7) might not be affected by the synaptic activity and that trafficking from the somatic Golgi to the cell membrane occurs within 20 minutes.

Activity-induced changes in the palmitoylation state of many receptors (Dopamine, β_2-adrenergic, transferrin) have been identified previously (Ng et al., 1994; O'Dowd et al., 1989; Alvarez et al., 1990). However, this was not the same for KARs, in particular GluK2 overexpressed by baculovirus in *Spodoptera frugiperda* (Sf9) insect cells (Pickering et al., 1995). The activity-induced palmitate turnover (identified during the last 5 and 30 minutes of the 4-hours [^{3}H]-palmitate metabolic labelling assay in the presence of 100 µM kainate) was similar to the non-stimulated

cells. An interesting question arises from the used model in this study; can Sf9 cells efficiently palmitate/depalmitate recombinant proteins? In this study two cell types were used to overexpress GluK2 (Sf9 infected with baculovirus or transfected HEK293 cells). As indicated from Pickering et al. (1995) findings, uninfected Sf9 cells with baculovirus have very low levels of palmitoylated proteins compared to un-transfected HEK293 cells total lysate in a metabolic labelling assay. Based on this observation, to which degree the palmitoylation/depalmitoylation machinery in Sf9 cells is adequate for a palmitate turnover in response to agonist stimulation? Another important consideration regarding Pickering et al. finding of absent activity-induced changes in GluK2 palmitoylation state is whether the specificity of the palmitoylation turnover machinery exists for both cysteine residues or one or for none of them. The process of the palmitoylation modification in Sf9 cells could resemble that of SUMOylation in Sf9 cells as these cells have SUMOylation machinery that fail to alter recombinant proteins expressed by baculoviruses infection (Langereis et al., 2007).

It is worthy to note that the statistically significant result obtained for the proportion of the surface expressed GluK2 (lower in the non-palmitoylated form compared to the WT) in our study is a result of three independent experiments. This is not powerful enough to assure that the “normal distribution of data” assumption in the applied parametric statistical test (Two-way ANOVA) has been met. Thus, the significant statistical result cannot be considered robust. In addition, a counterpart non-parametric test (to account for the possible non normality of data) is useless to perform in the case of an “n” less than 6 as it will never reach the 5% statistical significance.

So far, there is a large diversity of proteins that can be palmitoylated by a large family of palmitoyl acyltransferases. The specific characteristics of these enzymes are not fully defined and the specific enzymes that are responsible for palmitoylating and depalmitoylating the GluK2 subunit are still unknown. Identifying them and their contribution to activity-induced changes in the palmitoyltion dynamics of GluK2 and probably other related interacting proteins are key determinants to understand the molecular mechanisms that regulate these processes and identify potential targets for therapeutic interventions.

5.4.3 Optimising the ABE assay

The ABE assay (Brigidi and Bamji, 2013; Shipston, 2011) was used to detect the thioester bond as an indication of protein *S*-linked acylation (fatty acid bound to cysteine's thiol group via a thioester bound). Thus, it detects all S-acylations in proteins (Sobocinske et al., 2018). *S*-acylation is usually referred to *S*-palmitoylation because palmitate is the most common fatty acid in *S*-acylated proteins (palmitoleate, stearate, and oleate) (Tabaczar et al., 2017). In the ABE protocol, NEM is used to irreversibly block all reactive cysteines (and leaving palmitoylated cysteines), thus avoiding any false positive labelling. The Hydroxylamine (at neutral pH) cleaves the thioester bond between the cysteine and palmitoyl, and the newly formed free cysteine thiol will be reactive to a sulfhydryl-reactive biotinylation reagent (Biotin-BMCC). Thus, *S*-palmitoylation of proteins is specifically marked with biotin for identification.

Other less frequent types of palmitoylation like *N*-linked (palmitate attached to the glycine, cysteine, or lysine amine group) or *O*-linked (palmitate attached to the serine or threonine hydroxyl group) palmitoylation are distinguishable by the ABE assay because they are insensitive to the hydroxylamine cleavage (Sobocinska et al., 2018; Shipston, 2011).

Here, the very weak signal in the hydroxylamine-treated WT GluK2 may indicate the palmitoylated form especially that it was absent from the untreated WT and the non-palmitoylated samples. This may also indicate that the palmitoylated form of GluK2 is very little as this weak potential signal was identified only after pooling the amount of protein from 5 wells of a 6-well dish (instead of 3 wells). In addition, the turnover of palmitoylated GluK2 might be very rapid in which the thioester bond is lost early (before the hydroxylamine step) during the lengthy ABE assay contributing to the low levels. The non-specific bands observed in the immunoprecipitate could be due to other forms of *S*-acylation for proteins that are more abundant than GluK2 as the detection in this method depends on the sensitivity of the thioester bond in general and not specifically to *S*-palmitoylation. However, these bands were detected in all conditions (strongly in the hydroxylamine-treated WT sample and to a lesser extent in the other conditions). This could be a result of the used biotin-BMCC concentration which might be high enough to cause non-specific binding.

Other research groups were able clearly and specifically to detect the palmitoylated form of recombinant GluK2 in heterologous cells (Pickering et al., 1995; Copits and Swanson, 2013). Both have detected palmitoylated GluK2 by using [^{3}H]-palmitate in a metabolic labelling assay. This is a very sensitive assay which allow better detection of low amounts and of just palmitoylated proteins compared to the ABE method.

5.5 Conclusions and future work

In conclusion, this is the first finding of linking GluK2 palmitoylation state to its SUMOylation levels. The significance of this observation, if confirmed, augmented and further extended by the future work, will shed a light on new molecular mechanisms to regulate KARs trafficking and expression in response to neuronal activity. This means modulating new pathways to control neuronal excitability to prevent and treat hyperexcitable conditions.

To extend these findings, the following steps are recommended for future studies:

1. Overexpressing the complete set of mutated GluK2 proteins (in particular the C858A, C871A + K886R and C858A, 871A + S846A, S868A) to study the interplay between all three post-translational modifications (palmitoylation, phosphorylation and SUMOylation).
2. Using sindbis virus overexpression system, GluK2 phosphorylation then SUMOylation, and surface expression should be identified under basal and agonist-stimulated conditions in neurons (via GFP-trap and cell surface biotinylaition assays).
3. Antibody feeding assay should be applied to monitor GluK2 internalisation in response to agonist stimulation of the various mutated GluK2 proteins.
4. Identifying the palmitoylated form of GluK2 as discussed for the ABE and mass-spec methods.

6 General discussion

We started this research project with three main aims. (i) To identify the regional expression profile of Neto subunit proteins during rat brain development and correlate changes to pore-forming KAR subunits. (ii) To establish TLE-related changes in iGluR subunits using a novel rat model. (iii) To establish the effect of GluK2 non-palmitoylation on KAR SUMOylation and surface expression. Our findings have highlighted some aspects of the interplay between KARs and their auxiliary subunits. In addition, they shed light on a new potential downstream mechanism (depalmitoylation of GluK2) for kainate-induced long-term depression.

6.1 Putative effects of Neto proteins on KARs

Neto proteins have a characteristic developmental expression profile. The expression patterns of the two Neto isoforms show distinct distributions with marked spatial- and temporal stage-specific differences in their expression. In addition, they also have an overlapping protein distribution profile. However, the precise stoichiometry of Neto2 and Neto1 proteins associated with KARs has not been identified making their overlapping expression a possibility for the assembly of both Neto proteins with the same KAR in the same brain region. Furthermore, in a study of the modulatory effects of Neto proteins on KAR function, the ratio of KAR:Neto transfected DNA plasmids had an increased effect when the ratio changed from 1:2 to 1:4 (Fisher and Mott, 2012) suggesting the possibility of different effects according to different stoichiometry. This has also proved to be true for the close related AMPAR/TARP complexes (Introduction, section 1.2.1.1.).

One of the explanations of KAR currents continue after agonist removal (rebound currents) is that the agonist is released from the low-affinity sites first but is still bound to the high-affinity sites leading to an activated and non-desensitised receptor (Mott et al., 2010). These low- and high-affinity sites can be the result of either different subunits combinations or association with Neto proteins (Mott et al., 2010). This means that Neto proteins may contribute to different activation and deactivation profiles through increased agonist sensitivity and affinity. This is further supported by the functional properties of homomeric GluK1 and GluK2 KARs that are similar when Neto proteins are absent and demonstrate a low glutamate sensitivity and rapid and complete desensitisation with a slow recovery (Sommer et al., 1992; Heckmann et al.,

1996; Paternain et al., 1998; Fisher and Fisher, 2014). This may be important in case of low ambient glutamate concentration (as for extrasynaptic receptors), where the association with Neto proteins increases KAR's agonist affinity and slows their desensitisation rate (Perrais et al., 2009).

Furthermore, in the initial work done to examine the distribution of KARs based on high-affinity kainate binding sites distribution and identifying their K_D for kainate (Miller et al., 1990; Coyle, 1983; Hampson et al., 1987; Bettler et al., 1992; Herb et al., 1992), there was a big discrepancy between the observed K_D (in general < 10 nM in the postnatal and adult time points) and the expected K_D (based on the predicted KAR subtype in each examined brain region depending on the mRNA distribution of subunits, usually > 50 nM as low-affinity subunits are incorporated). For example, in hippocampal CA3 region the expected K_D for kainate would be between 50 and 100 nM based on the expressed subunits mRNA in this region (GluK2, GluK5). However, the observed K_D was 7.8 nM at P14 and 5.8 nM in the adult brain (Miller et al., 1990). These observations could be explained by the modulating effects of Neto proteins, which were not discovered at that time, on KARs.

The metabotropic signalling pathway of low-affinity subunits KAR, independently of their ionotropic function, is suggested to enhance the developmental outgrowth of neurite (Valbuena and Lerma, 2016). In the early developmental stages, KARs are mainly formed from low-affinity subunits [this is also supported by Dr. Ik-Hyun Cho's findings (Figure 3.9) of low- and high-affinity KAR subunit protein expression during development] and as the expression of high-affinity subunits (GluK4 and GluK5) increases with development KARs become heterotetramer of low- and high-affinity subunits (Fernandes et al., 2009). This renders the receptor to have strong ionotropic function (high channel conductance and delayed desensitisation onset) relative to early developmental stages when the receptors have low sensitivity to glutamate and channel conductance, fast desensitisation, and slow desensitisation recovery (Fisher and Mott, 2011; Paternain et al., 1998; Barberis et al., 2008). Thus, no further neurite outgrowth (Joseph et al., 2011; Ibarretxe et al., 2007; Tashiro et al., 2003) compared to early developmental stages as KARs signalling cascade switches from metabotropic to ionotropic (Marques et al., 2013). This may suggest that when Neto proteins interact with KARs (i.e. changing the receptor activation kinetics); they can control KARs signalling pathway (metabotropic vs ionotropic).

The differential variation in Neto and KAR subunits distribution in the different brain regions during rat brain development might reflect the various maturation profiles. Periods of increased plasticity could be due to transient increase in the expression of iGluR subunits (Arai et al., 1997), similar to the one that was observed for Neto2 at P14 and GluK1 at P28 (see section 3.3.3.2.1/Figure 3.8 and section 3.3.3.3/Figure 3.9, respectively). The change in the subunit protein expression (qualitative or quantitative) during development may reflect a change in the receptor complex subunit composition leading to different functional properties (Ritter et al., 2002), similar to the decline in Neto2 expression following birth in hippocampal CA regions and a parallel increase of Neto1 in the same region at the same time (see Figure 3.8). In addition, this may also suggest different functional properties arising from the various possible stoichiometry although the applied experimental method (histoblot technique) does not provide direct information about stoichiometry, assembly, or subunit composition of KARs. The decline seen in the expression of Neto2 and GluK1 during development may result from either gene downregulation or the death of their expressing cells due to KAR excitotoxic effects (Bahn et al., 1994). A similar circumstance of excitotoxic cell death was observed when GluK2 subunit was overexpressed in hippocampal CA3 neurons (Bergold et al., 1993).

KARs are expressed in hippocampal pyramidal cells and interneurons. However, activation of the network-wide KARs results in the prominent feature of increasing inhibitory drive onto hippocampal principle cells by the local interneuronal circuits (Christensen et al., 2004; Cossart et al., 1998; Cossart et al., 2001; Fisahn et al., 2004; Frerking et al., 1999; Jiang et al., 2001; Maingret et al., 2005; Mulle et al., 2000; Semyanov and Kullmann, 2001; Wondolowski and Frerking, 2009). The majority of hippocampal interneurons consists of different groups of GABAergic interneurons that regulate inhibitory transmission. All of these express GluK1, GluK2, GluK5, Neto1, and Neto2 (Wyeth et al., 2017). Because KARs are modulators of synaptic transmission, they are considered attractive therapeutic targets to control neuronal excitability without disrupting the ongoing synaptic transmission (Contractor et al., 2011; Jane et al., 2009). Thus, interneuronal KARs are suggested to be important targets (neuronal circuit's control key) in excitation/inhibition imbalance disorders (Christensen et al., 2004; Frerking and Nicoll, 2000; Khalilov et al., 2002).

6.2 The role of Neto2 in inhibitory neurotransmission

The main inhibitory neurotransmitter in the mature CNS is γ-amino-butyric acid (GABA). However, during the early postnatal period GABAergic neurotransmission is excitatory (Khazipov et al., 1997; Mueller et al., 1984; Reichling et al., 1994; Wang et al., 1994; Leinekugel et al., 1995; Yuste and Katz, 1991; Chen et al., 1996; Owens et al., 1996; Luhmann and Prince, 1991; Obrietan and van den Pol, 1995). GABAergic excitation (depolarization) versus GABAergic inhibition (hyperpolarization) is controlled by the electrochemical gradient of chloride ions (Cl^-) which are the main conductors of $GABA_A$ receptors. The chloride electrochemical gradient determines GABAergic currents reversal potential (E_{GABA}[2]). During development, there is a shift in E_{GABA} to a hyperpolarised potential leading to the GABAergic transmission switch. This change in E_{GABA} happens because of the developmental intracellular Cl^- concentration ($[Cl^-]_i$) reduction (Chen et al., 1996; Cherubini et al., 1990; Owens et al., 1996; Luhmann and Prince, 1991). Notably, this coincides with an increase in the mRNA expression of the neuronal potassium-coupled chloride co-transporter 2 (KCC2) (Lu et al., 1999; Rivera et al., 1999; Vu et al., 2000), which increases Cl^- extrusion and reduces $[Cl^-]_i$ (Jarolimek et al., 1999; Rivera et al., 1999; Kakazu et al., 1999).

The developmental shifts in chloride homeostasis (from high to low $[Cl^-]_i$) is regulated by the upregulation in KCC2 expression (Watanabe and Fukuda, 2015; Ludwig et al., 2003). Generally, the maturation schedule for neurogenesis shows a sequential pattern in which earlier brain structures develop mature chloride haemostasis in advance of later structures (Watanabe and Fukuda, 2015). The earliest strong upregulation of KCC2 expression occurs at P15 in the rat neocortex, pyramidal cells of hippocampal CA regions, and the DG granular cell layers and continues toward adulthood (Watanabe and Fukuda, 2015). This timing parallels the same duration when Neto2 subunit protein expression peaks in the developing brain (my finding/Figure 3.8). It was demonstrated that Neto2 associates with KCC2 (Ivakine et al., 2013) to maintain its normal activity, thus maintain synaptic inhibition. Loss of Neto2 causes reduction in the abundance of KCC2, its phosphorylated levels and its Cl^- extrusion efficacy, and subsequently depolarise E_{GABA} in neurons (Ivakine et al., 2013; Mahadevan et al., 2015). In addition, absence of Neto2 has led to a reduction in the latency of seizure induction, an increase in seizure severity,

[2] $E_{GABA:}$ the membrane potential that GABAergic currents change their direction at.

a reduction in hippocampal CA1 GABAergic transmission (spontaneous inhibitory postsynaptic currents), and a depolarised hippocampal CA1 E_{GABA} in mice (Mahadevan et al., 2015). All of this may indicate the possibility of reduced GABA release from presynaptic terminals due to loss of presynaptic interneuron GluK1 regulation by Neto2 (Mahadevan et al., 2015, Copits et al., 2011).

Moreover, KCC2 is localised at excitatory synapses where it is regulated by proteins of excitatory synaptic transmission (Pressey et al., 2017). GluK2 individually and in synergy with Neto2 increases KCC2 surface expression and PKC-dependent phosphorylation of GluK2 at S844 and S868 also enhances this effect further (Pressey et al., 2017). Thus, mechanism of synaptic inhibition and excitation acts in concert.

Decreased KCC2 levels and function leading to impaired synaptic inhibition is implicated in many neurological conditions as chronic pain, spasticity, and epileptic seizures (Coull et al., 2003; Huberfeld et al., 2007; Boulenguez et al., 2010; Puskarjov et al., 2012; Gagnon et al., 2013). However, it is noteworthy to highlight the role of NKCC1 (Na^+-K^+-$2Cl^-$ cotransporter 1), which generally show an opposite expression pattern to KCC2 (highly expressed in the embryonic and first few days after birth) in maintaining a high $[Cl^-]_i$ in the immature CNS. The differential expression of KCC2 and NKCC1 regulates the chloride haemostasis ontogeny. During rat P6-12, $[Cl^-]_i$ is high and GABA is excitatory while at P21-23 there is low $[Cl^-]_i$ and GABA is inhibitory (Li and Xu, 2008). Notably, recurrent epileptic seizures increase NKCC1 activity and internalises KCC2, thus, increasing chloride concentration intracellularly (Ben-Ari et al., 2007). Furthermore, many observations indicate that epileptic seizures inhibit the shift in GABAergic transmission from excitation to inhibition (Khalilov et al., 2003; Khazipov et al., 2004; Cohen et al., 2002). In the pilocarpine-induced temporal lobe epilepsy, the rat hippocampal protein expression of NKCC1 was increased (Eftekhari et al., 2014) promoting a depolarising GABAergic neuronal transmission.

Furthermore, KCC2 has an important role, apart from its chloride conductance activity, in promoting the maturation of cortical neuros, dendritic spines, and excitatory synapses (Li et al., 2007). In addition, the developmental upregulation of KCC2 parallels spinogenesis (Rivera et al., 1999; Yuste and Bonhoeffer, 2004). This regulation of neuronal maturation processes by KCC2 is done through its interaction with the cytoskeleton-associated protein 4.1N (Li et al., 2007). Thus, there is a good

correlation between KCC2 and 4.1N expressions and the excitatory synapses maturation (Ludwig et al., 2003; Walensky et al., 1999). Moreover, there is a role for 4.1N in the plasma membrane stabilisation of KCC2 (Medina et al., 2014) as disrupting their interaction leads to KCC2 lateral diffusion from excitatory synapses (Chamma et al., 2013). Taken together, proteins of excitatory and inhibitory neurotransmission are closely interconnected to keep the balance between excitation and inhibition in physiological conditions.

6.3 iGluRs in hyperexcitable conditions

Induction of seizures appears to involve a structural network of many brain regions including the hippocampus (Spencer and Spencer, 1994; Bragin et al., 2000; Bartolomei et al., 2008; Fabo et al., 2008). In addition, the site of seizure onset in patients (Lieb et al., 1976; Spencer et al., 1990; Spencer and Spencer, 1994; Spencer, 1998, 2002) and rodent models (Bertram, 1997; Bertram et al., 2001; Levesque et al., 2012) of TLE varies from one seizure to another. Moreover, epileptic activity can be driven from afferent inputs and also generated intrinsically (Fujita et al., 2014) by neuronal circuits of recurrent activities that are utilised for pathological synchronisation and seizure propagation (Vismer et al., 2015). Hence, the bidirectional communication (reciprocal) between the entorhinal cortex and hippocampus amplifies neuronal signals and propagates seizures (Vismer et al., 2015). The entorhinal cortex is a gate for neuronal inputs to the structures in the temporal lobe (Vismer et al., 2015) and it is a key brain region for TLE development (Beed et al., 2009). In particular, the medial entorhinal cortex, is one of the first brain areas to show severe neuronal death following epilepsy development (Beed et al., 2009). Cell loss and region atrophy of the entorhinal cortex enhances the propagation of seizures discharges. And so, the balance between neuronal excitation and inhibition maybe shifted by neuronal cell loss, inflammation, and changes in gene expression (Vismer et al., 2015).

The presence of GluA2 subunit, which is nearly all Q/R edited in the mature brain (Michaelis, 1998; Molnar and Isaac, 2002), protects from Ca^{2+} toxicity and hyperexcitation of neurons (Borbely et al., 2015). In addition, its downregulation enhances Ca^{2+} influx (increases GluA1/GluA2 ratio), thus, could contribute to neurodegeneration (Pellegrini-Giampietro et al., 1997). In kainate- and pilocarpine-induced epileptic seizures, GluA2 expression was down regulated in hippocampal CA3

region (Friedman et al., 1994; Friedman and Veliskova, 1998; Lason et al., 1997b; Rajasekaran et al., 2012) leading to enhancement of AMPAR Ca^{2+} permeability (Rajasekaran et al., 2012).

Similarly, interfering with GluK2 Q/R editing process (more Ca^{2+}-permeable receptors) demonstrated long-term potentiation at contacts of the entorhinal cortex-dentate gyrus and lowered the threshold to seizures (Vissel et al., 2001). GluK2 (mostly Q/R edited) is responsible for the KAR current of medial entorhinal cortex pyramidal neurons generated after kainate stimulation in the presence of AMPAR antagonist (GYKI 53655) (Beed et al., 2009). This indicates the importance of up/down regulation of the edited/unedited GluK2-containing KARs, which represent 80% and 20%, respectively, in the adult brain (Seeburg et al., 1998; Seeburg and Hartner, 2003; Sprengel et al., 1998), in regulating hyperexcitability (Beed et al., 2009).

Mechanisms of neuroprotection or neuronal cell loss and degradation could be developed and initiated following brain hyperexcitability (Vilagi et al., 2009). AMPARs undergo internalisation as a neuroprotection mechanism following strong activation and the release of high amount of glutamate during seizures (Vilagi et al., 2009). Synaptic adaptation and reorganisation as processes of neuroprotection were also showed by a reduction in somatosensory cortex general excitability and AMPAR and NMDAR subunits rearrangements following repeated seizures induced by 4-aminopyridine (Vilagi et al., 2009). However, in the hippocampus, acute seizures induced by repeated doses of 4-aminopyridine led to an increase in GluA1 and a reduction in GluA2 expressions in CA1 and dentate gyrus regions alongside an increase in neuronal Ca^{2+} influx in these two hippocampal regions (Borbely et al., 2009). This suggests a shift toward the formation of GluA2-lacking Ca^{2+}-permeable AMPARs after acute seizures (Borbely et al., 2009). In addition, the use of GYKI 52466 AMPAR antagonist demonstrated reduced sensitivity (less effective compared to control animals) as this drug shows more potency toward GluA2-containing AMPARs compared with GluA1 homomeric receptors (Johansen et al., 1995; Bleakman et al., 1996). Furthermore, GluA2 expression was reduced in the entorhinal cortex following 4-aminopyridine-induced seizures (Borbely et al., 2015), which again suggests a favourable increase in forming Ca^{2+}-permeable receptors and hyper-excitability.

Developmental processes like synaptogenesis and neuronal networks maturation are dependent on neuronal activity, which is characterised by excitatory neurotransmission outweighing inhibitory neurotransmission in the immature brain. This state of hyperexcitability has a distinct expression profile of neurotransmitter receptor subunits. In addition, this profile is recapitulated in other hyperexcitability states like epilepsy (Rakhade and Jensen, 2009; Sanchez and Jensen, 2001). From the proteins that have been shown to have similar expression profile in the immature brain and epileptic conditions are AMPARs, NMDARs, NKCC1 and KCC2. The expression ratios of GluA1/GluA2, GluN2B/GluN2A, and NKCC1/KCC2 are increased to facilitate developmental processes and the hyperexcitation state (Brooks-Kayal and Pritchett, 1993; Kumar et al., 2002, Monyer et al., 1994; Talos et al., 2006a; Talos et al., 2006b; Wong et al., 2002; Dunning et al., 1999). Thus, the subunit composition of iGluRs affects the neuronal network synaptic efficacy and seizure susceptibility (Jane et al., 2009).

6.4 Auxiliary subunits as potential therapeutic targets in epilepsy

As an example of a brain region-specific pharmacological targeting through neurotransmitter auxiliary subunits that have distinct expression profile is AMPAR-TARP-γ-$_8$ complex (Maher et al., 2016; Kato et al., 2016). The auxiliary subunit of AMPAR TARP-γ-$_8$, which is particularly expressed in the hippocampus to coordinate AMPARs pharmacology, gating, and trafficking (Straub and Tomita, 2012; Tomita et al., 2003), regulates hippocampal AMPAR effects of kainate-induced neurotoxicity (Tomita et al., 2007). Two unique amino acid residues in γ-$_8$ contribute to the selectivity of two AMPAR antagonists [JNJ-55511118 (Maher et al., 2016) and LY3130481 (Kato et al., 2016)] to receptors associated with γ-$_8$ but no other subtypes of TARPs. These compounds demonstrated antiepileptic activity in rodents (Maher et al., 2016; Kato et al., 2016).

Another example of the functional regulatory effects of iGluR auxiliary subunits on their associated receptors is demonstrated in that a gene mutation in the AMPAR auxiliary subunit stargazing (TARP-γ-$_2$), leads to a reduction in AMPARs in inhibitory neurons (Menuz and Nicoll, 2008) and the generation of seizures similar to human absence epilepsy (Rogawski, 2013). Thus, disinhibition of neuronal networks could be caused by reducing the function/expression of iGluRs in inhibitory interneurons through the specific targeting of the receptors' auxiliary subunits.

6.5 Palmitoylation as a potential therapeutic approach for hyperexcitable conditions

Our finding of the crosstalk between GluK2 palmitoylation and SUMOylation and its resemblance of the activity-dependent effect is tempting to speculate that by interfering with this series of post-translational modifications, one could control the function of GluK2 in conditions of hyperexcitability like epilepsy. This could be achieved by fine-tuning excitation/inhibition balance since enhancement of GluK2-containing KARs SUMOylation leads to their reduced surface expression, which may contribute to reducing neuronal excitability in epilepsy (Martin et al., 2007).

The surface delivery of iGluRs is important for their normal synaptic functioning as well as impacting their pathological roles (Sohn and Park, 2019). For example, GluA1 palmitoylation-deficient mice (C811S) (Itoh et al., 2018) demonstrated an increase in seizure susceptibility, an increase in GluA1 phosphorylation (S831), and an upregulation of GluA1 expression. This indicates that AMPAR palmitoylation, which is a key modification to regulate AMPAR trafficking to and from postsynaptic sites, is implicated in hyperexcitable conditions and the excitation/inhibition imbalance and suggest that GluA1 depalmitoylation leads to hyperexcitability and epileptic seizures (Itoh et al., 2018). Furthermore, the efficacy of the clinically used anticonvulsants was reduced in the GluA1 palmitoylation-deficient animals following induction of seizures (Itoh et al., 2018). These findings are consistent with the previously described (see section 5.4.1) relationship between GluA1 C811 palmitoylation residue and 4.1N protein. This is the second cysteine (C811) residue that is located in the plasma membrane proximal domain of GluA1 C-terminus. It regulates activity-dependent endocytosis and its palmitoylation inhibits GluA1 association with 4.1N protein (Hayashi et al., 2005). These findings also confirm the reciprocal relationship between palmitoylation and phosphorylation as GluA1 phosphorylation (S831) increased in the GluA1 palmitoylation-deficient mice (C811S) (Itoh et al., 2018).

In addition, the post-translational modification phosphorylation of two serine residues (S831 and S845) in GluA1 was enhanced in neonatal seizures and seizures in immature rats (Rakhade et al., 2012) leading to enhanced AMPAR activity. However, blocking this phosphorylation (transgenic mice at GluA1 S831 and S845 to

S831A and S845A) led to preventing seizures in later life suggesting a role of GluA1-AMPARs phosphorylation in the neuronal hyper-excitable state in later life (Hanada, 2014).

In another recent study, palmitoyl transferase (zDHHC8) expression was increased in the brains of TLE patients and chronic animal models of epilepsy (kainate and pilocarpine; Yang et al., 2018). In addition, absence of zDHHC8 delayed and reduced spontaneous recurrent seizures in *in vivo* kainate and pilocarpine models, decreased epileptiform-like discharges in an *in vitro* model of seizures, and decreased GluA1 expression (Yang et al., 2018). The zDHHC8 overexpression resulted in increased spontaneous recurrent seizures, ictal-like discharges, and GluA1 expression. In the zDHHC8 knocked down mice, GluA1 expression was reduced at the cell surface and increased intracellularly which suggest zDHHC8 regulates the trafficking of GluA1 to the postsynaptic membrane resulting in hyperexcitation and seizure generation (Yang et al., 2018).

AMPAR palmitoylation is one of the mechanisms that dynamically regulate the receptor trafficking to the plasma membrane for its synaptic functioning (Sohn and Park, 2019). Therefore, unmasking how iGluRs trafficking is regulated by specific palmitoylating and depalmitoylating enzymes in physiological and pathological conditions may help in the pharmacological targeting of specific pathways related to neurological disorders.

There are still many uncertainties, when it comes to protein palmitoylation, which need to be resolved in future studies:

1. Whether palmitoyl transferases are specific for an amino acid sequence, the position of cysteine residues (spacing between cysteines and nearby amino acid residues), a specific subcellular substrate location, or acylation like myristoylation or prenylation near the cysteine residue to be palmitoylated (how palmitoyl transferases recognise their substrate).
2. The exact subcellular localisation of the enzyme machinery (palmitoyl transferases and thioesterases) responsible for the dynamic modification of protein palmitoylation and, their relationships in terms of their temporal activity.

3. The variable effects of attaching one or two palmitates, or one plus another lipid (dual lipidation or multiple palmitate/lipids) to a substrate on its membrane stability.
4. The possibility of a preferential selection by the palmitoylation machinery for efficient versus inefficient palmitoylation (close proximity to the transmembrane domain, other lipid modification, or hydrophobic residues).
5. The presence of potential multiple mechanisms for regulating zDHHC activity like having potential sites for post-translational modification (phosphorylation, palmitoylation) and/or protein interaction domains.

7 References

Acsady L., Kali S. Models, structure, function: the transformation of cortical signals in the dentate gyrus. Prog Brain Res. 2007; 163:577– 599.

Aguado C., Luján R. The Histoblot Technique: A Reliable Approach to Analyze Expression Profile of Proteins and to Predict Their Molecular Association. In: Odagaki Y., Borroto-Escuela D. (eds) Co-Immunoprecipitation Methods for Brain Tissue. Neuromethods. 2019, vol 144. Humana Press, New York, NY.

Ahmadian G., Ju W., Liu L., Wyszynski M., Lee S. H., Dunah A. W., Taghibiglou C., Wang Y., Lu J., Wong T. P., Sheng M., Wang Y. T. Tyrosine phosphorylation of GluR2 is required for insulin-stimulated AMPA receptor endocytosis and LTD. EMBO J. 2004; 23:1040–1050.

Aicart-Ramos C., Valero R. A., Rodriguez-Crespo I. Protein palmitoylation and subcellular trafficking. Bba - Biomembranes. 2011; 1808(12):2981–2994.

Alvarez E., Gironès N., Davis R. J. Inhibition of the receptor-mediated endocytosis of diferric transferrin is associated with the covalent modification of the transferrin receptor with palmitic acid. J Biol Chem. 1990 Sep 25; 265(27):16644–16655.

Amaral D. G., Scharfman H. E., Lavenex P. The dentate gyrus: fundamental neuroanatomical organization (dentate gyrus for dummies). Prog. Brain Res. 2007; 163(3–22):788–790.

Anderson D. B., Zanella C. A., Henley J. M., Cimarosti H. Sumoylation: Implications for Neurodegenerative Diseases. In: Wilson V. (eds) SUMO Regulation of Cellular Processes. Advances in Experimental Medicine and Biology. 2017; 963: 261-281

Arai Y., Mizuguchi M., Takashima S. Developmental changes of glutamate receptors in the rat cerebral cortex and hippocampus. Anat Embryol (Berl). 1997; 195(1):65-70.

Babb T. L., Brown W. J., Pretorius J., Davenport C., Lieb J. P., Crandall P. H. Temporal lobe volumetric cell densities in temporal lobe epilepsy. Epilepsia. 1984; 25:729–740.

Babb T. L., Kupfer W. R., Pretorius J. K., Crandall P. H., Levesque M. F. Synaptic reorganization by mossy fibers in human epileptic fascia dentata. Neuroscience. 1991; 42:351-363.

Bahn S., Volk B., Wisden W. Kainate receptor gene expression in the developing rat brain. J Neurosci. 1994; 14(9):5525-5547.

Bannister N. J., Benke T. A., Mellor J., Scott H., Gurdal E., Crabtree J. W., Isaac J. T. Developmental changes in AMPA and kainate receptor-mediated quantal transmission at thalamocortical synapses in the barrel cortex. J Neurosci. 2005; 25:5259–5271.

Barberis A., Sachidhanandam S., Mulle C. GluR6/KA2 kainate receptors mediate slow-deactivating currents. J Neurosci. 2008; 28:6402–6406.

Barbon A., Vallini I., Barlati S. Genomic organization of the human grik2 gene and evidence for multiple splicing variants. Gene. 2001; 274(1):187–197.

Barry M. F. and Ziff E. B. Receptor trafficking and the plasticity of excitatory synapses. Curr. Opin. Neurobiol. 2002; 12:279–286.

Bartolomei F., Chauvel P., Wendling F. Epileptogenicity of brain structures in human temporal lobe epilepsy: a quantified study from intracerebral EEG. Brain. 2008; 131:1818–1830.

Bartolomei F., Khalil M., Wendling F., Sontheimer A., Regis J., Ranjeva J. P. Entorhinal cortex involvement in human mesial temporal lobe epilepsy: an electrophysiologic and volumetric study. Epilepsia. 2005; 46:677–687.

Barton M. E., Peters S. C., Shannon H. E. Comparison of the effect of glutamate receptor modulators in the 6 Hz and maximal electroshock seizure models. Epilepsy Res. 2003; 56(1):17–26.

Becker A. J. Review: animal models of acquired epilepsy: insights into mechanisms of human epileptogenesis. Neuropathol. Appl. Neurobiol. 2018; 44:112-129.

Beed P. S., Salmen B., Schmitz D., de la Prida L. M. Gluk2-mediated excitability within the superficial layers of the entorhinal cortex. Plos One. 2009; 4(5):e5576.

Béïque J. C., Lin D. T., Kang M. G., Aizawa H., Takamiya K., Huganir R. L. Synapse-specific regulation of AMPA receptor function by PSD-95. Proc Natl Acad Sci U S A. 2006; 103(51):19535-19540.

Ben-Ari Y. Cell death and synaptic reorganizations produced by seizures. Epilepsia. 2001; 42(3):5-7.

Ben-Ari Y., Crepel V., Represa A. Seizures beget seizures in temporal lobe epilepsies: the boomerang effects of newly formed aberrant kainatergic synapses. Epilepsy Curr. 2008; 8(3):68-72.

Ben-Ari Y., Gaiarsa J. L., Tyzio R., Khazipov R. GABA: a pioneer transmitter that excites immature neurons and generates primitive oscillations. Physiol Rev. 2007; 87(4):1215-1284.

Beneyto M. and Meador-Woodruff J. H. Expression of transcripts encoding AMPA receptor subunits and associated postsynaptic proteins in the macaque brain. J. Comp. Neurol. 2004; 468:530–554.

Benke D., Wenzel A., Scheuer L., Fritschy J. M., Mohler H. Immunobiochemical characterization of the NMDA–receptor subunit NR1 in the developing and adult rat brain. J Recept Signal Transduct Res. 1995; 15:393–411.

Bennett V. The spectrin-actin junction of erythrocyte membrane skeletons. Biochim. Biophys. Acta. 1989; 988, 107–121

Berger M. and Schmidt M. F. Protein fatty acyltransferase is located in the rough endoplasmic reticulum. FEBS Lett.1985; 187, 289–294.

Bergold P. J., Casaccia-Bonnefil P., Xiu-Liu Z., Federoff H. J. Tran- synaptic neuronal loss induced in hippocampal slice cultures by a herpes simplex virus vector expressing the GluR6 subunit of the kainate receptor. Proc Nat1 Acad Sci USA. 1993; 90:6165-6169.

Bernard A., Ferhat L., Dessi F., Charton G., Represa A., Ben-Ari Y., Khrestchatisky M. Q/R editing of the rat GluR5 and GluR6 kainate receptors in vivo and in vitro: evidence for independent developmental, pathological and cellular regulation. Eur J Neurosci. 1999; 11(2):604-616.

Bertram E. H. Functional anatomy of spontaneous seizures in a rat model of limbic epilepsy. Epilepsia. 1997; 38:95–105.

Bertram E. H., Mangan P. S., Zhang D., Scott C. A., Williamson J. M. The midline thalamus: alterations and a potential role in limbic epilepsy. Epilepsia. 2001; 42:967–978.

Bettler B., Boulter J., Hermans-Borgmeyer I., O'Shea-Greenfield A., Deneris E. S., Moll C., Borgmeyer U., Hollmann M., Heinemann S. Cloning of a novel glutamate receptor subunit, GluR5: expression in the nervous system during development. Neuron. 1990; 5(5):583-595.

Bettler B., Egebjerg J., Sharma G., Pecht G., Hermans-Borgmeyer I., Moll C., Stevens C. F., Heinemann S. Cloning of a putative glutamate receptor: a low affinity kainate-binding subunit. Neuron. 1992; 8:257-265.

Bhattacharyya R., Barren C., Kovacs D.M. Palmitoylation of amyloid precursor protein regulates amyloidogenic processing in lipid rafts J Neurosci. 2013; 33:11169-11183

Biagini G., Baldelli E., Longo D., Contri M. B., Guerrini U., Sironi L., Gelosa P., Zini I., Ragsdale D. S., Avoli M. Proepileptic influence of a focal vascular lesion affecting entorhinal cortex-CA3 connections after status epilepticus. Journal of Neuropathology and Experimental Neurology. 2008; 67(7):687–701.

Biagini G., Baldelli E., Longo D., Pradelli L., Zini I., Rogawski MA., Avoli M. Endogenous neurosteroids modulate epileptogenesis in a model of temporal lobe epilepsy. Experimental Neurology. 2006; 201(2):519–524.

Bijlmakers M. J. and Marsh M. The on-off story of protein palmitoylation. Trends Cell Biol. 2003; 13:32-42.

Bizzozero O. A. The mechanism and functional roles of protein palmitoylation in the nervous system. Neuropediatrics. 1997; 28:23–26.

Bleakman D., Ballyk B. A., Schoepp D. D., Palmer A. J., Bath C. P., Sharpe E. F., Woolley M. L., Bufton H. R., Kamboj R. K., Tarnawa I., Lodge D. Activity of 2,3-benzodiazepines at native rat and recombinant human glutamate receptors in vitro: stereospecificity and selectivity profiles. Neuropharmacology. 1996; 35:1689-1702.

Bliss T.V. and Collingridge G.L. A synaptic model of memory: long-term potentiation in the hippocampus. Nature. 1993; 361:31-39.

Borbély S., Czégé D., Molnár E., Dobó E., Mihály A., Világi I. Repeated application of 4-aminopyridine provoke an increase in entorhinal cortex excitability and rearrange AMPA and kainate receptors. Neurotoxicity Research: Neurodegeneration, Neuroregeneration, Neurotrophic Action, and Neuroprotection. 2015; 27(4):441–452.

Borbély S., Dobó E., Czégé D., Molnár E., Bakos M., Szucs B., Vincze A., Világi I., Mihály A. Modification of ionotropic glutamate receptor-mediated processes in the rat hippocampus following repeated, brief seizures. Neuroscience. 2009; 159(1):358–68.

Bork P., Beckmann G. The CUB-domain- A widespread module in developmentally-regulated proteins. Journal of Molecular Biology. 1993; 231(2):539-545.

Bossis G., Melchior F. SUMO: Regulating the regulator. Cell Div. 2006; 1:13.

Boulenguez P., Liabeuf S., Bos R., Bras H., Jean-Xavier C., Brocard C., et al. Down-regulation of the potassium-chloride cotransporter KCC2 contributes to spasticity after spinal cord injury. Nat. Med. 2010; 16:302–307.

Bowie D., Garcia E. P., Marshall J., Traynelis S. F., Lange G. D. Allosteric regulation and spatial distribution of kainate receptors bound to ancillary proteins. J. Physiol. 2003; 547:373–385.

Bragin A., Wilson CL., Engel J. Chronic epileptogenesis requires development of a network of pathologically interconnected neuron clusters: a hypothesis. Epilepsia. 2000; 41(6):S144–S152.

Breustedt J. and Schmitz D. Assessing the role of GLUK5 and GLUK6 at hippocampal mossy fiber synapses. J Neurosci. 2004; 24(45):10093-10098.

Bridges R. J. and Esslinger C. S. The excitatory amino acid transporters: pharmacological insights on substrate and inhibitor specificity of the EAAT subtypes. Pharmacology & Therapeutics. 2005; 107:271-285.

Brigidi G. S. and Bamji S. X. Detection of protein palmitoylation in cultured hippocampal neurons by immunoprecipitation and acyl-biotin exchange (ABE). J Vis Exp. 2013; (72):50031.

Brigidi G. S., Santyr B., Shimell J., Jovellar B., Bamji S.X. Activity-regulated trafficking of the palmitoyl-acyl transferase DHHC5. Nat Commun. 2015; 6:8200

Brigidi G. S., Sun Y., Beccano-Kelly D., Pitman K., Mobasser M., Borgland S. L., Milnerwood A. J., Bamji S. X. Palmitoylation of δ-catenin by DHHC5 mediates activity-induced synapse plasticity. Nat Neurosci. 2014; 17(4):522-532.

Brooks-Kayal A. R. and Pritchett D. B. Developmental changes in human γ-aminobutyric acid A receptor subunit composition. Annals of Neurology. 1993; 34(5):687–693.

Buckmaster P. S., Zhang G. F., Yamawaki R. Axon sprouting in a model of temporal lobe epilepsy creates a predominantly excitatory feedback circuit. J. Neurosci. 2002; 22:6650–6658.

Buckmaster P. S. Mossy Fiber Sprouting in the Dentate Gyrus. In: Noebels JL, Avoli M, Rogawski MA, et al., editors. Jasper's Basic Mechanisms of the Epilepsies [Internet]. 4th edition. Bethesda (MD): National Center for Biotechnology Information (US); 2012. Available from: https://www.ncbi.nlm.nih.gov/books/NBK98174/

Bureau I., Bischoff S., Heinemann S. F., Mulle C. Kainate receptor-mediated responses in the CA1 field of wild-type and GluR6-deficient mice. J Neurosci. 1999; 19:653-663.

Burnashev N., Monyer H., Seeburg P. H., Sakmann B. Divalent ion permeability of AMPA receptor channels is dominated by the edited form of a single subunit. Neuron. 1992; 8:189–198.

Burnashev N., Rozov A. Genomic control of receptor function. Cell Mol Life Sci. 2000; 57(11):1499-1507.

Capili A. D. and Lima C. D. Taking it step by step: mechanistic insights from structural studies of ubiquitin/ubiquitin-like protein modification pathways. Curr Opin Struct Biol. 2007; 17:726–735.

Carta M., Fièvre S., Gorlewicz A., Mulle C. Kainate receptors in the hippocampus. Eur. J. Neurosci. 2014; 39:1835–1844.

Casillas-Espinosa P. M., Powell K. L., O'Brien T. J. Regulators of synaptic transmission: Roles in the pathogenesis and treatment of epilepsy. Epilepsia. 2012; 53:41-58.

Castillo P. E., Malenka R. C., Nicoll R. A. Kainate receptors mediate a slow postsynaptic current in hippocampal CA3 neurons. Nature. 1997; 388:182–186.

Cavalheiro E. A., Leite J. P., Bortolotto Z. A., Turski W. A., Ikonomidou C., Turski L. Long-term effects of pilocarpine in rats: structural damage of the brain triggers kindling and spontaneous recurrent seizures. Epilepsia. 1991; 32:778–782.

Cavalheiro E. A., Mello M. L., Leite J. P. The pilocarpine model of seizures. In: Pitkanen A., Schwartzkroin P. A., Moshe S. L., editors. Models of seizures and epilepsy. 2006, Elsevier; Burlington, MA: 2006. pp. 433–448.

Cavazos J. E. and Cross D. The role of synaptic reorganization in mesial temporal lobe epilepsy. Epilepsy & Behavior. 2006; 8:483-493.

Cavazos J. E., Sutula T. P. Progressive neuronal loss induced by kindling: a possible mechanism for mossy fiber synaptic reorganization and hippocampal sclerosis. Brain Res. 1990; 527:1-6.

Cavazos J. E., Zhang P., Qazi R., Sutula T.P. Ultrastructural features of sprouted mossy fiber synapses in kindled and kainic acid-treated rats. J. Comp. Neurol. 2003; 458:272–292.

Chamberlain S. E., González-González I. M., Wilkinson K. A., Konopacki F. A., Kantamneni S., Henley J. M., Mellor J. R. SUMOylation and phosphorylation of GluK2 regulate kainate receptor trafficking and synaptic plasticity. Nat Neurosci. 2012; 15(6):845–852.

Chamberlain S. E., Sadowski J. H., Teles-Grilo Ruivo L. M., Atherton L. A., Mellor J. R. Long-Term Depression of Synaptic Kainate Receptors Reduces Excitability by Relieving Inhibition of the Slow Afterhyperpolarization. J Neurosci. 2013; 33(22): 9536–9545.

Chamma I., Heubl M., Chevy Q., Renner M., Moutkine I., Eugene E., et al. Activity-dependent regulation of the K/Cl Transporter KCC2 membrane diffusion, clustering, and function in hippocampal neurons. J. Neurosci. 2013; 33:15488–15503.

Chamoun Z. Skinny hedgehog, an acyltransferase required for palmitoylation and activity of the hedgehog signal. Science. 2001; 293(5537):2080–2084.

Chapman A. G., Smith S. E., Meldrum B. S. The anticonvulsant effect of the non-NMDA antagonists, NBQX and GYKI 52466, in mice. Epilepsy Res. 1991; 9:92–96.

Chazot P. L. and Stephenson F. A. Molecular dissection of native mammalian forebrain NMDA receptors containing the NR1 C2 exon: direct demonstration of NMDA receptors comprising NR1, NR2A, and NR2B subunits within the same cortex. J. Neurochem. 1997; 69:2138–2144.

Chen G., Trombley P. Q., van den Pol A. N. Excitatory actions of GABA in developing rat hypothalamic neurones. J. Physiol. 1996; 494: 451-464.

Chen L., Chetkovich D. M., Petralia R. S., Sweeney N. T., Kawasaki Y., Wenthold R. J., Bredt D. S., Nicoll R. A. Stargazin regulates synaptic targeting of AMPA receptors by two distinct mechanisms. Nature. 2000; 408:936-943.

Cherubini E., Rovira C., Gaiarsa J. L., Corradetti R., Ben Ari Y. GABA mediated excitation in immature rat CA3 hippocampal neurons. Int. J. Dev. Neurosci. 1990; 8: 481-490.

Chetkovich D. M., Bunn R. C., Kuo S. H., Kawasaki Y., Kohwi M., Bredt D.S. Postsynaptic targeting of alternative postsynaptic density-95 isoforms by distinct mechanisms. The Journal of Neuroscience: The Official Journal of the Society for Neuroscience. 2002; 22(15):6415–6425.

Chittajallu R., Vignes M., Dev K. K., Barnes J. M., Collingridge G. L., Henley J. M. Regulation of glutamate release by presynaptic kainate receptors in the hippocampus. Nature. 1996; 379(6560):78–81.

Cho C. H., St-Gelais F., Zhang W., Tomita S., Howe J. R. Two families of TARP isoforms that have distinct effects on the kinetic properties of AMPA receptors and synaptic currents. Neuron. 2007; 55:890-904.

Cho E. and Park M. Palmitoylation in Alzheimer's disease and other neurodegenerative diseases. Pharmacological Research. 2016; 111:133–151.

Christensen J. K., Paternain A. V., Selak S., Ahring P. K., Lerma J. A mosaic of functional kainate receptors in hippocampal interneurons. J Neurosci. 2004; 24:8986–8993.

Clarke V. R., Collingridge G. L. Characterisation of the effects of ATPA, a GLU(K5) receptor selective agonist, on excitatory synaptic transmission in area CA1 of rat hippocampal slices. Neuropharmacology. 2002; 42(7):889-902.

Clifford D. B., Olney J. W., Maniotis A., Collins R. C., Zorumski C. F. The functional anatomy and pathology of lithium-pilocarpine and high-dose pilocarpine seizures. Neuroscience. 1987; 23:953–968.

Coelho-Silva L., Stephens G. J., Cimarosti H. Sumoylation and calcium signalling: potential roles in the brain and beyond. Neuronal Signaling. 2017; 1(3):20160010. doi:10.1042/NS20160010

Cohen I., Navarro V., Clemenceau S., Baulac M., Miles R. On the origin of interictal activity in human temporal lobe epilepsy in vitro. Science. 2002; 298(5597):1418-1421.

Coleman S. K., Cai C., Mottershead D. G., Haapalahti J. P., Keinänen K. Surface expression of GluR-D AMPA receptor is dependent on an interaction between its C-terminal domain and a 4.1 protein. J. Neurosci. 2003; 23: 798–806.

Collingridge G. L., Isaac J. T., Wang Y. T. Receptor trafficking and synaptic plasticity. Nat. Rev. Neurosci. 2004; 5:952–962.

Contractor A., Mulle C., Swanson G. T. Kainate receptors coming of age: milestones of two decades of research. Trends in Neurosciences. 2011; 34(3):154-63.

Contractor A., Swanson G., Heinemann S. F. Kainate receptors are involved in short- and long-term plasticity at mossy fiber synapses in the hippocampus. Neuron. 2001; 29(1):209–216.

Coombs I. D. and Cull-Candy S. G. Transmembrane AMPA receptor regulatory proteins and AMPA receptor function in the cerebellum. Neuroscience. 2009; 162:656-665.

Copits B. A. and Swanson G. T. Dancing partners at the synapse: auxiliary subunits that shape kainate receptor function. Nature Reviews Neuroscience. 2012; 13(10):675-86.

Copits B. A. and Swanson G. T. Kainate receptor post-translational modifications differentially regulate association with 4.1N to control activity-dependent receptor endocytosis. J. Biol. Chem. 2013; 288:8952–8965.

Copits B. A., Robbins J. S., Frausto S., Swanson G. T. Synaptic Targeting and Functional Modulation of GluK1 Kainate Receptors by the Auxiliary Neuropilin and Tolloid-Like (NETO) Proteins. Journal of Neuroscience. 2011; 31(20):7334-7340.

Cossart R., Esclapez M., Hirsch J. C., Bernard C., Ben-Ari Y. GluR5 kainate receptor activation in interneurons increases tonic inhibition of pyramidal cells. Nat Neurosci. 1998; 1:470–478.

Cossart R., Tyzio R., Dinocourt C., Esclapez M., Hirsch J. C., Ben-Ari Y., Bernard C. Presynaptic kainate receptors that enhance the release of GABA on CA1 hippocampal interneurons. Neuron. 2001; 29(2):497-508.

Coull J. A., Boudreau D., Bachand K., Prescott S. A., Nault F., Sík A., et al. Trans-synaptic shift in anion gradient in spinal lamina I neurons as a mechanism of neuropathic pain. Nature. 2003; 424:938–942.

Coulter D. A. , McIntyre D. C., Loscher W. Animal models of limbic epilepsies: What can they tell us? Brain Pathology. 2002; 12(2):240-256.

Coussen F., Perrais D., Jaskolski F., Sachidhanandam S., Normand E., Bockaert J., Marin P., Mulle C. Co-assembly of two glur6 kainate receptor splice variants within a functional protein complex. Neuron. 2005; 47(4):555–566.

Cowan R. W., Seidlitz E. P., Singh G. Glutamate signaling in healthy and diseased bone. Frontiers in endocrinology. 2012; 3:89.

Coyle J. T. Neurotoxic action of kainic acid. J Neurochem. 1983; 41:1-11.

Crepel V. Kainate receptors in epilepsy. WIREs Membr Transp Signal. 2013; 2:75–83. doi: 10.1002/wmts.80.

Crepel V. and Mulle C. Physiopathology of kainate receptors in epilepsy. Current Opinion in Pharmacology. 2015; 20:83-88.

Cross D. and Cavazos J. E. Synaptic reorganization in sabiculum and CA3 after early-life status epilepticus in the kainic acid rat model. Epilepsy Research. 2007; 73:156-165.

Cui C., Mayer M. L. Heteromeric kainate receptors formed by the coassembly of GluR5, GluR6, and GluR7. J Neurosci. 1999; 19(19):8281-8291.

Cull-Candy S., Brickley S., Farrat M. NMDA receptor subunits: diversity, development, and disease. Curr. Opin. Neurobiol. 2001; 11:327–335.

Cull-Candy S., Kelly L., Farrant M. Regulation of Ca2+-permeable AMPA receptors: synaptic plasticity and beyond. Curr Opin Neurobiol. 2006; 16:288-297.

Curia G., Longo D., Biagini G., Jones RSG. Avoli M. The pilocarpine model of temporal lobe epilepsy. Journal of neuroscience methods. 2008; 172(2):143-157. doi:10.1016/j.jneumeth.2008.04.019.

Dakoji S., Tomita S., Karimzadegan S., Nicoll R. A., Bredt D. S. Interaction of transmembrane AMPA receptor regulatory proteins with multiple membrane associated guanylate kinases. Neuropharmacology. 2003; 45:849–856.

Danscher G., Zimmer J. An improved Timm sulphide silver method for light and electron microscopic localization of heavy metals in biological tissues. Histochemistry. 1978; 55:27-40.

DeSouza S., Fu J., States B. A., Ziff E. B. Differential palmitoylation directs the AMPA receptor-binding protein ABP to spines or to intracellular clusters. J. Neurosci. 2002; 22:3493–3503.

Ding Y. X., Zhang Y., He B., Yue W. H., Zhang D., Zou L. P. A possible association of responsiveness to adrenocorticotropic hormone with specific GRIN1 haplotypes in infantile spasms. Dev Med Child Neurol. 2010; 52:1028–1032.

Dingledine R., Borges K., Bowie D., Traynelis S. F. The glutamate receptor ion channels. Pharmacol Rev. 1999; 51:7–61.

Dolci E. D. and Palade G. E. The biosynthesis and fatty acid acylation of the murine erythrocyte sialoglycoproteins. J. Biol. Chem. 1985; 260:10728–10735.

Dowd F. J. Cholinergic Agonists and Muscarinic Receptor Antagonists. In Dowd F., Johnson B., Mariotti A. Pharmacology and Therapeutics for Dentistry (Seventh Edition). 2017, Elsevier Health Sciences.

Dunning D. D., Hoover C. L., Soltesz I., Smith M. A., O'Dowd D. K. $GABA_{(A)}$ receptor mediated miniature postsynaptic currents and α-subunit expression in developing conical neurons. Journal of Neurophysiology. 1999; 82(6):3286–3297.

Dunphy J. T. and Linder M. E. Signalling functions of protein palmitoylation. Biochim. Biophys. Acta. 1998; 1436:245–261.

Durmuller N., Craggs M., Meldrum B. S. The effect of the non-NMDA receptor antagonist GYKI 52466 and NBQX and the competitive NMDA receptor antagonist D-CPPene on the development of amygdala kindling and on amygdala-kindled seizures. Epilepsy Res. 1994; 17(2):167–174.

Eftekhari S., Mehrabi S., Soleimani M., Hassanzadeh G., Shahrokhi A., Mostafavi H., Hayat P., Barati M., Mehdizadeh H., Rahmanzadeh R., Hadjighassem M. R., Joghataei M. T. BDNF modifies hippocampal KCC2 and NKCC1 expression in a temporal lobe epilepsy model. Acta Neurobiol Exp (Wars). 2014; 74(3):276-287.

Egebjerg J., Heinemann S. F. Ca^{2+} permeability of unedited and edited versions of the kainate selective glutamate receptor GluR6. Proc Natl Acad Sci U S A. 1993; 90(2):755–759.

El-Husseini A. E. and Bredt D. S. Protein palmitoylation: a regulator of neuronal development and function Nat. Rev. Neurosci. 2002; 3:791-802.

El-Husseini A. E., Craven S. E., Chetkovich D. M., Firestein B. L., Schnell E., Aoki C., Bredt D. S. Dual palmitoylation of PSD-95 mediates its vesiculotubular sorting, postsynaptic targeting, and ion channel clustering. J. Cell Biol. 2000; 148:159-172.

El-Husseini A. E., Schnell E., Dakoji S., Sweeney N., Zhou Q., Prange O., Gauthier-Campbell C., Aguilera-Moreno A., Nicoll R. A., Bredt D. S. Synaptic strength regulated by palmitate cycling on PSD-95. Cell. 2002; 108(6):849–863.

Endele S., Rosenberger G., Geider K., Popp B., Tamer C., Stefanova I., Milh M., Kortum F., Fritsch A., Pientka F. K., et al. Mutations in GRIN2A and GRIN2B encoding regulatory subunits of NMDA receptors cause variable neurodevelopmental phenotypes. Nat Genet. 2010; 42:1021– 1026.

Epsztein J., Represa A., Jorquera I., Ben-Ari Y., Crepel V. Recurrent mossy fibers establish aberrant kainate receptor-operated synapses on granule cells from epileptic rats. J Neurosci. 2005; 25:8229– 8239.

Epsztein J., Sola E., Represa A., Ben-Ari Y., Crepel V. A. selective interplay between aberrant EPSPKA and INaP reduces spike timing precision in dentate granule cells of epileptic rats. Cereb Cortex 2010; 20:898– 911.

Erreger K., Chen P. E., Wyllie D. J., Traynelis S. F. Glutamate receptor gating. Crit Rev Neurobiol. 2004; 16:187–224.

Esclapez M., Hirsch J. C., Ben-Ari Y., Bernard C. Newly formed excitatory pathways provide a substrate for hyperexcitability in experimental temporal lobe epilepsy. J Comp Neurol. 1999; 408:449–460.

Fabó D., Maglóczky Z., Wittner L., Pék A., Eross L., Czirják S., Vajda J., Sólyom A., Rásonyi G., Szucs A., Kelemen A., Juhos V., Grand L., Dombovári B., Halász P., Freund T. F., Halgren E., Karmos G., Ulbert I. Properties of in vivo interictal spike generation in the human subiculum. Brain. 2008; 131:485–499.

Fernandes H. B., Catches J. S., Petralia R. S., Copits B. A., Xu J., Russell T. A., Swanson G. T., Contractor A. High-affinity kainate receptor subunits are necessary for ionotropic but not metabotropic signaling. Neuron. 2009; 63:818–829.

Fernández I. S. and Loddenkemper T. Subunit composition of neurotransmitter receptors in the immature and in the epileptic brain. Biomed Research International. 2014; 2014. doi:10.1155/2014/301950

Fisahn A. Kainate receptors and rhythmic activity in neuronal networks: hippocampal gamma oscillations as a tool. J Physiol. 2005; 562:65-72.

Fisahn A., Contractor A., Traub R. D., Buhl E. H., Heinemann S. F., McBain C. J. Distinct roles for the kainate receptor subunits GluR5 and GluR6 in kainate-induced hippocampal gamma oscillations. J Neurosci. 2004; 24:9658–9668.

Fisher J. L. and Mott D. D. Distinct functional roles of subunits within the heteromeric kainate receptor. J Neurosci. 2011; 31:17113–17122.

Fisher J. L. and Mott D. D. The Auxiliary Subunits Neto1 and Neto2 Reduce Voltage-Dependent Inhibition of Recombinant Kainate Receptors. J Neurosci. 2012; 32(37):12928–12933.

Fisher J. L. The auxiliary subunits Neto1 and Neto2 have distinct, subunit-dependent effects at recombinant GluK1- and GluK2-containing kainate receptors. Neuropharmacology. 2015; 99:471-480.

Fisher M. T. and Fisher J. L. Contributions of different kainate receptor subunits to the properties of recombinant homomeric and heteromeric receptors. Neurosci. 2014; 278:70–80.

Franck J. E., Pokorny J., Kunkel D. D., Schwartzkroin P. A. Physiologic and morphologic characteristics of granule cell circuitry in human epileptic hippocampus. Epilepsia. 1995; 36:543-558.

French J. A., Krauss G. L., Biton V., et al. Adjunctive perampanel for refractory partial-onset seizures: Randomized phase III study 304. Neurology. 2012; 79:589–596.

French J. A., Krauss G. L., Steinhoff B. J., et al. Evaluation of adjunctive perampanel in patients with refractory partial-onset seizures: results of randomized global phase III study 305. Epilepsia. 2013; 54:117–125.

Frerking M. and Nicoll R. A. Synaptic kainate receptors. Curr Opin Neurobiol. 2000; 10:342–351.

Frerking M., Petersen C. C., Nicoll R. A. Mechanisms underlying kainate receptor-mediated disinhibition in the hippocampus. Proc Natl Acad Sci U S A. 1999; 96:12917–12922.

Friedman L. K. and Veliskova J. GluR2 hippocampal knockdown reveals developmental regulation of epileptogenicity and neurodegeneration. Mol Brain Res. 1998; 61:224–231.

Friedman L. K., Pellegrini-Giampietro D. E., Sperber E. F., Bennett M. V., Moshe S. L., Zukin R. S. Kainate-induced status epilepticus alters glutamate and GABAA receptor gene expression in adult rat hippocampus: an *in situ* hybridization study. J Neurosci. 1994; 14:2697–2707.

Fritsch B., Reis J., Gasior M., Kaminski R. M., Rogawski M. A. Role of gluk1 kainate receptors in seizures, epileptic discharges, and epileptogenesis. The Journal of Neuroscience: The Official Journal of the Society for Neuroscience. 2014; 34(17):5765–5775.

Fritsch B., Stott J. J., Joelle Donofrio J., Rogawski M. A. Treatment of early and late kainic acid-induced status epilepticus with the noncompetitive AMPA receptor antagonist GYKI 52446. Epilepsia. 2010; 51(1):108–117.

Fromer M., Pocklington A. J., Kavanagh D. H., Williams H. J., Dwyer S., Gormley P., Georgieva L., Rees E., Palta P., Ruderfer D. M., et al. De novo mutations in schizophrenia implicate synaptic networks. Nature. 2014; 506(7487):179–184.

Fujikawa D. G., Shinmei S. S., Cai B. Lithium-pilocarpine-induced status epilepticus produces necrotic neurons with internucleosomal DNA fragmentation in adult rats. Eur J Neurosci. 1999; 11:1605–1614.

Fujita S., Toyoda I., Thamattoor A. K., Buckmaster P. S. Preictal activity of subicular, CA1, and dentate gyrus principal neurons in the dorsal hippocampus before spontaneous seizures in a rat model of temporal lobe epilepsy. The Journal of Neuroscience: The Official Journal of the Society for Neuroscience. 2014; 34(50):16671–16687.

Fukata Y. and Fukata M. Epilepsy and synaptic proteins. Current Opinion in Neurobiology. 2017; 45:1–8.

Gabriel S., Njunting M., Pomper J. K., Merschhemke M., Sanabria E.R., Eilers A., Kivi A., Zeller M., Meencke H. J., Cavalheiro E.A., et al. Stimulus and potassium-induced epileptiform activity in the human dentate gyrus from patients with and without hippocampal sclerosis. J Neurosci. 2004; 24:10416– 10430.

Gagnon M., Bergeron M. J., Lavertu G., Castonguay A., Tripathy S., Bonin R. P., et al. Chloride extrusion enhancers as novel therapeutics for neurological diseases. Nat. Med. 2013; 19:1524–1528.

Gallyas F. Jr., Ball S. M., Molnar E. Assembly and cell surface expression of KA-2 subunit-containing kainate receptors. J Neurochem. 2003; 86:1414–1427.

Ganguly K., Schinder A. F., Wong S. T., Poo M. GABA itself promotes the developmental switch of neuronal GABAergic responses from excitation to inhibition. Cell. 2001; 105(4):521–532.

Garcia E. P., Mehta S., Blair L. A., Wells D. G., Shang J., Fukushima T., Fallon J. R., Garner C. C., Marshall J. SAP90 binds and clusters kainate receptors causing incomplete desensitization. Neuron 1998; 21:727–739.

Gashi E., Avallone J., Webster T., Friedman L. K. Altered excitability and distribution of NMDA receptor subunit proteins in cortical layers of rat pups following multiple perinatal seizures. Brain Res. 2007; 1145:56–65.

Gauthier-Campbell C., Bredt D. S., Murphy T. H., El-Husseini Ael-D. Regulation of dendritic branching and filopodia formation in hippocampal neurons by specific acylated protein motifs. Mol. Biol. Cell. 2004; 15:2205-2217.

Geiss-Friedlander R., Melchior F. Concepts in sumoylation: a decade on. Nature Rev Mol Cell Biol. 2007; 8:947–956.

Ghasemi M. and Schachter S. C. The NMDA receptor complex as a therapeutic target in epilepsy: a review. Epilepsy Behav. 2011; 22(4):617-640.

Glien M., Brandt C., Potschka H., Voigt H., Ebert U., Loscher W. Repeated low-dose treatment of rats with pilocarpine: low mortality but high proportion of rats developing epilepsy. Epilepsy Research. 2001; 46(2):111-119.

Globa A. K., Bamji S. X. Protein palmitoylation in the development and plasticity of neuronal connections. Current Opinion in Neurobiology. 2017; 45:210–220.

Graebenitz S., Kedo O., Speckmann E. J., et al. Interictal-like network activity and receptor expression in the epileptic human lateral amygdala. Brain. 2011; 134(10):2929–2947.

Gray P. C., Johnson B. D., Westenbroek R. E., Hays L. G., Yates III J. R., Scheuer T., Catterall W. A., Murphy B. J. Primary structure and function of an A kinase anchoring protein associated with calcium channels. Neuron. 1998; 20:1017-1026.

Greaves J., Gorleku O. A., Salaun C., Chamberlain L. H. Palmitoylation of the SNAP25 protein family specificity and regulation by DHHC palmitoyl transferases. J Biol Chem. 2010; 285:24629-24638.

Greger I. H., Khatri L., Kong X., Ziff E. B. AMPA receptor tetramerization is mediated by Q/R editing. Neuron. 2003; 40:763–774.

Greger I. H., Watson J. F., Cull-Candy S. G. Structural and functional architecture of AMPA-Type glutamate receptors and their auxiliary proteins. Neuron. 2017; 94:713-730.

Gregor P., O'Hara B. F., Yang X., Uhl G. R. Expression and novel subunit isoforms of glutamate receptor genes GluR5 and GluR6. Neuroreport. 1993; 4(12):1343–1346.

Grigorenko E. V., Bell W. L., Glazier S., Pons T., Deadwyler S. Editing status at the Q/R site of the GluR2 and GluR6 glutamate receptor subunits in the surgically excised hippocampus of patients with refractory epilepsy. Neuroreport. 1998; 9:2219-2224.

Gustavsson A., Svensson M., Jacobi F., Allgulander C., Alonso J., Beghi E., et al. Cost of disorders of the brain in Europe 2010. European Neuropsychopharmacology. 2011; 21(10):718-779.

Hampson D. R., Huie D., Wenthold R. J. Solubilization of kainic acid binding sites from rat brain. J Neurochem. 1987; 49:1209-l 215.

Hanada T. The AMPA receptor as a therapeutic target in epilepsy: Preclinical and clinical evidence. Journal of Receptor, Ligand and Channel Research. 2014; 7:39-50.

Hancock J. F., Magee A. I., Childs J. E., Marshall C. J. All ras proteins are polyisoprenylated but only some are palmitoylated. Cell. 1989; 57:1167–1177.

Hashimoto K., Fukaya M., Qiao X., Sakimura K., Watanabe M., Kano M. Impairment of AMPA receptor function in cerebellar granule cells of ataxic mutant mouse stargazer. J Neurosci. 1999; 19(14):6027-6036.

Hawkins L. M., Chazot P. L., Stephenson F. A. (1999) Biochemical evidence for the co-association of three N-methyl-D-aspartate (NMDA) R2 subunits in recombinant NMDA receptors. J. Biol. Chem. 1999; 274:27211–27218.

Hay R. T. SUMO: a history of modification. Mol. Cell. 2005; 18:1–12.

Hayashi T., Rumbaugh G., Huganir R. L. (2005). Differential regulation of AMPA receptor subunit trafficking by palmitoylation of two distinct sites. Neuron. 2005; 47(5):709–723.

Hayashi T., Thomas G. M., Huganir R. L. Neuron. Dual palmitoylation of NR2 subunits regulates NMDA receptor trafficking. 2009; 64:213–226.

Hayes D. M., Braud S., Hurtado D. E., McCallum J., Standley S., Isaac J. T., Roche K. W. Trafficking and surface expression of the glutamate receptor subunit, KA2. Biochem Biophys Res Commun. 2003; 310:8–13.

Heckmann M., Bufler J., Franke C., Dudel J. Kinetics of homomeric GluR6 glutamate receptor channels. Biophys J. 1996; 71:1743–1750.

Heine M., Groc L., Frischknecht R., Béïque J.-C., Lounis B., Rumbaugh G., Huganir R. L., Cognet L., Choquet D. Surface mobility of postsynaptic AMPARs tunes synaptic transmission. Science. 2008; 320:201–205.

Heinemann U., Beck H., Dreier J. P., Ficker E., Stabel J., Zhang C. L. The dentate gyrus as a regulated gate for the propagation of epileptiform activity. Epilepsy Res. Suppl. 1992; 7:273–280.

Henze D. A., Urban N. N., Barrionuevo G. The multifarious hippocampal mossy fiber pathway: a review. Neuroscience. 2000; 98:407-427.

Henze D. A., Wittner L., Buzsaki G. Single granule cells reliably discharge targets in the hippocampal CA3 network in vivo. Nat Neurosci. 2002; 5:790– 795.

Hepp R., Hay Y. A., Aguado C., Lujan R., Dauphinot L., Potier M. C., Nomura S., Poirel O., El Mestikawy S., Lambolez B., Tricoire L. Glutamate receptors of the delta family are widely expressed in the adult brain. Brain Struct Funct. 2015; 220(5):2797-2815. doi: 10.1007/s00429-014-0827-4.

Herb A., Bumashev N., Werner P., Sakmann B., Wisden W., Seeburg P. H. The KA-2 subunit of excitatory amino acid receptors shows widespread expression in brain and forms ion channels with distantly related subunits. Neuron. 1992; 8:775-785.

Hess D. T., Patterson S. I., Smith D. S., Skene J. H. Neuronal growth cone collapse and inhibition of protein fatty acylation by nitric oxide. Nature. 1993; 366:562–565.

Hess D. T., Slater T. M., Wilson M. C., Skene J. H. The 25 kDa synaptosomal-associated protein SNAP-25 is the major methionine-rich polypeptide in rapid axonal transport and a major substrate for palmitoylation in adult CNS. J. Neurosci. 1992; 12:4634–4641.

Hietakangas V., Anckar J., Blomster H. A., Fujimoto M., Palvimo J. J., Nakai A., Sistonen L. PDSM, a motif for phosphorylation-dependent sumo modification. Proceedings of the National Academy of Sciences of the United States of America. 2006; 103(1):45–50.

Hirbec H., Francis J. C., Lauri S. E., Braithwaite S. P., Coussen F., Mulle C., Dev K. K., Coutinho V., Meyer G., Isaac J.T.R., et al. Rapid and differential regulation of AMPA and kainate receptors at hippocampal mossy fibre synapses by PICK1 and GRIP. Neuron 2003; 37:625–638.

Hollmann M., Maron C., Heinemann S. N-glycosylation site tagging suggests a three transmembrane domain topology for the glutamate receptor GluR1. Neuron. 1994; 13(6):1331–1343.

Hornemann T. Palmitoylation and depalmitoylation defects. J Inherit Metab Dis. 2015; 38:179-186.

Hosford D. A., Crain B. J., Cao Z., et al. Increased AMPA-sensitive quisqualate receptor binding and reduced NMDA receptor binding in epileptic human hippocampus. J Neurosci. 1991; 11(2):428–434.

Houser C. R. Granule cell dispersion in the dentate gyrus of humans with temporal lobe epilepsy. Brain Res. 1990; 535:195–204.

Houser C. R. Neuronal loss and synaptic reorganization in temporal lobe epilepsy. Adv Neurol. 1999; 79:743-761.

Houser C. R., Miyashiro J. E., Swartz B. E., Walsh G. O., Rich J. R., Delgadoescueta A. V. Altered patterns of dynorphin immunoreactivity suggest mossy fiber reorganization in human hippocampal epilepsy. J Neurosci. 1990; 10:267– 282.

Huberfeld G., Wittner L., Clemenceau S., Baulac M., Kaila K., Miles R., et al. Perturbed chloride homeostasis and GABAergic signaling in human temporal lobe epilepsy. J. Neurosci. 2007; 27:9866–9873.

Huettner J. E. Kainate receptors and synaptic transmission. Prog Neurobiol. 2003; 70:387–407.

Huganir R. L. and Nicoll R. A. AMPARs and synaptic plasticity: the last 25 years. Neuron. 2013; 80:704-717.

Ibarretxe G., Perrais D., Jaskolski F., Vimeney A., Mulle C. Fast regulation of axonal growth cone motility by electrical activity. J Neurosci. 2007; 27:7684–7695.

Isaac J. T., Mellor J., Hurtado D., Roche K. W. Kainate receptor trafficking: physiological roles and molecular mechanisms. Pharmacol Ther. 2004; 104(3):163-172.

Isokawa M., Levesque M. F. Increased NMDA responses and dendritic degeneration in human epileptic hippocampal neurons in slices. Neurosci Lett. 1991; 132:212-216.

Itoh M., Yamashita M., Kaneko M., Okuno H., Abe M., Yamazaki M., Natsume R., Yamada D., Kaizuka T., Suwa R., et al. Deficiency of AMPAR-palmitoylation aggravates seizure susceptibility. The Journal of Neuroscience: The Official Journal of the Society for Neuroscience. 2018; 38(47):10220–10235.

Ivakine E. A., Acton B. A., Mahadevan V., Ormond J., Tang M., Pressey J. C., et al. Neto2 is a KCC2 interacting protein required for neuronal Cl- regulation in hippocampal neurons. Proc. Natl. Acad. Sci. U S A. 2013; 110:3561–3566.

Jaarsma D. and Korf J. A novel non-perfusion Timm method for human brain tissue. J Neurosci Methods. 1990; 35(2):125-131.

Jack A., Hamad M. I. K., Gonda S., Gralla S., Pahl S., Hollmann M., Wahle P. Development of cortical pyramidal cell and interneuronal dendrites: a role for kainate receptor subunits and NETO1. Molecular Neurobiology. 2018; 2018. doi:10.1007/s12035-018-1414-0.

Jackson A. C. and Nicoll R. A. The expanding social network of ionotropic glutamate receptors: TARPs and other transmembrane auxiliary subunits. Neuron. 2011; 70:178-199.

Jane D. E., Lodge D., Collingridge G. L. Kainate receptors: pharmacology, function and therapeutic potential. Neuropharmacology. 2009; 56:90–113.

Jarolimek W., Lewen A., Misgeld U. A furosemide-sensitive K^+-Cl^- cotransporter counteracts intracellular Cl^- accumulation and depletion in cultured rat midbrain neurons. J. Neurosci. 1999; 19: 4695-4704.

Jaskolski F., Coussen F., Nagarajan N., Normand E., Rosenmund C., Mulle C. Subunit composition and alternative splicing regulate membrane delivery of kainate receptors. J Neurosci. 2004; 24:2506–2515.

Jaskolski F., Normand E., Mulle C., Coussen F. Differential trafficking of GluR7 kainate receptor subunit splice variants. J Biol Chem. 2005; 280:22968–22976.

Jiang L., Xu J., Nedergaard M., Kang J. A kainate receptor increases the efficacy of GABAergic synapses. Neuron. 2001; 30:503–513.

Johansen T. H., Chaudhary A., Verdoorn T. A. Interactions among GYKI-52466, cyclothiazide, and aniracetam at recombinant AMPA and kainate receptors. Mol Pharmacol. 1995; 48:946-955.

Johnson E. S. Protein modification by SUMO. Annu Rev Biochem. 2004; 73:355–382.

Joseph D. J., Williams D. J., MacDermott A. B. Modulation of neurite outgrowth by activation of calcium-permeable kainate receptors expressed by rat nociceptive-like dorsal root ganglion neurons. Dev Neurobiol. 2011; 71:818–835.

Jung M. W., Mcnaughton B. L. Spatial selectivity of unit-activity in the hippocampal granular layer. Hippocampus. 1993; 3:165– 182.

Jürgen Dohmen R. Sumo protein modification. Bba - Molecular Cell Research. 2004; 1695(1):113–131.

Kakazu Y., Akaike N., Komiyama S., Nabekura J. Regulation of intracellular chloride by cotransporters in developing lateral superior olive neurons. J. Neurosci. 1999; 19: 2843-2851.

Kalashnikova E., Lorca Ramón A., Kaur I., Barisone G. A., Li B., Ishimaru T., Trimmer J. S., Mohapatra D. P., Díaz Elva. SynDIG1: an activity-regulated,

AMPA- receptor-interacting transmembrane protein that regulates excitatory synapse development. Neuron. 2010; 65(1):80–93.

Kaminski R. M., Banerjee M., Rogawski M. A. Topiramate selectively protects against seizures induced by ATPA, a GluR5 kainate receptor agonist. Neuropharmacology. 2004; 46:1097-1104.

Kang R., Swayze R., Lise M. F., Gerrow K., Mullard A., Honer W. G., El-Husseini A. Presynaptic trafficking of synaptotagmin I is regulated by protein palmitoylation. The Journal of Biological Chemistry. 2004; 279(48):50524–50536.

Kang R., Wan J., Arstikaitis P., Takahashi H., Huang K., Bailey A. O., Thompson J. X., Roth A. F., Drisdel R. C., Mastro R., Green W. N., Yates III J. R., Davis N. G., El-Husseini A. Neural palmitoyl-proteomics reveals dynamic synaptic palmitoylation. Nature. 2008; 456:904–909.

Kantamneni S., Wilkinson K. A., Jaafari N., Ashikaga E., Rocca D., Rubin P., et al. Activity-dependent SUMOylation of the brain-specific scaffolding protein GISP. Biochem. Biophys. Res. Commun. 2011; 409:657–662.

Károly N., Dobó E., Mihály A. Comparative immunohistochemical study of the effects of pilocarpine on the mossy cells, mossy fibres and inhibitory neurones in murine dentate gyrus. Acta neurobiologiae experimentalis. 2015; 75: 220-237.

Károly N., Mihály A., Dobó E. Comparative immunohistochemistry of synaptic markers in the rodent hippocampus in pilocarpine epilepsy. Acta Histochemica. 2011; 113(6):656–662.

Kato A. S., Burris K. D., Gardinier K. M., Gernert D. L., Porter W. J., Reel J., Ding C., Tu Y., Schober D. A., Lee M. R., et al. Forebrain-selective AMPA-receptor antagonism guided by TARP γ-8 as an antiepileptic mechanism. Nat Med. 2016; 22:1496-1501.

Kato A. S., Gill M. B., Yu H., Nisenbaum E. S., Bredt D. S. TARPs differentially decorate AMPA receptors to specify neuropharmacology. Trends in neurosciences. 2010; 33(5):241-248.

Kato A. S., Siuda E. R., Nisenbaum E. S., Bredt D. S. AMPA receptor subunit-specific regulation by a distinct family of type II TARPs. Neuron. 2008; 59:986-996.

Kato A. S., Zhou W., Milstein A. D., Knierman M. D., Siuda E. R., Dotzlaf J. E., Yu H., Hale J. E., Nisenbaum E. S., Nicoll R. A., Bredt D. S. New transmembrane AMPA receptor regulatory protein isoform, gamma-7, differentially regulates AMPA receptors. J Neurosci. 2007; 27(18):4969-4977.

Kaur I., Yarov-Yarovoy V., Kirk L. M., Plambeck K. E., Barragan E. V., Ontiveros E. S., Díaz E. Activity-dependent palmitoylation controls SynDIG1

stability, localization, and function. The Journal of Neuroscience: The Official Journal of the Society for Neuroscience. 2016; 36(29):7562–7568.

Kelsch W., Li Z., Eliava M., Goengrich C., Monyer H. GluN2B-containing NMDA receptors promote wiring of adult-born neurons into olfactory bulb circuits. The Journal of Neuroscience: The Official Journal of the Society for Neuroscience. 2012; 32(36):12603–12611.

Kelsch W., Li Z., Wieland S., Senkov O., Herb A., Göngrich C., Monyer H. GluN2B-containing NMDA receptors promote glutamate synapse development in hippocampal interneurons. The Journal of Neuroscience: The Official Journal of the Society for Neuroscience. 2014; 34(48):16022–16030.

Kerscher O., Felberbaum R., Hochstrasser M. Modification of proteins by ubiquitin and ubiquitin-like proteins. Annu Rev Cell Dev Biol. 2006; 22:159–180.

Kessels H. W., and Malinow R. Synaptic AMPA receptor plasticity and behavior. Neuron. 2009; 61:340-350.

Khalilov I., Hirsch J., Cossart R., Ben-Ari Y. Paradoxical anti-epileptic effects of a GluR5 agonist of kainate receptors. J Neurophysiol. 2002; 88:523–527.

Khalilov I., Holmes G. L., Ben-Ari Y. In vitro formation of a secondary epileptogenic mirror focus by interhippocampal propagation of seizures. Nat Neurosci. 2003; 6(10):1079-1085.

Khazipov R., Khalilov I., Tyzio R., Morozova E., Ben-Ari Y., Holmes G. L. Developmental changes in GABAergic actions and seizure susceptibility in the rat hippocampus. Eur J Neurosci. 2004; 19(3):590-600.

Khazipov R., Leinekugel X., Khalilov I., Gaiarsa J. L., Ben-Ari Y. Synchronization of GABAergic interneuronal network in CA3 subfield of neonatal rat hippocampal slices. J. Physiol. 1997; 498: 763-772.

Kidd F. L. and Isaac J. T. Developmental and activity-dependent regulation of kainate receptors at thalamocortical synapses. Nature. 1999; 400(6744):569-573.

Kiernan J. A. Anatomy of the Temporal Lobe. Epilepsy Research and Treatment. 2012, Article ID 176157, 12 pages. https://doi.org/10.1155/2012/176157.

Kim J., Dittgen T., Nimmerjahn A., Waters J., Pawlak V., Helmchen F., Schlesinger S., Seeburg P. H. et al. Sindbis vector SINrep(nsP2S726): a tool for rapid heterologous expression with attenuated cytotoxicity in neurons. J Neurosci Methods. 2004; 133:81–90.

Kim K. S., Yan D., Tomita S. Assembly and stoichiometry of the AMPA receptor and transmembrane AMPA receptor regulatory protein complex J. Neurosci. 2010; 30:1064-1072.

Konopacki F. A., Jaafari N., Rocca D. L., Wilkinson K. A., Chamberlain S., Rubin P., Kantamneni S., Mellor J. R., Henley J. M. Agonist-induced PKC phosphorylation regulates GluK2 SUMOylation and kainate receptor endocytosis. Proc Natl Acad Sci U S A. 2011; 108(49):19772–19777.

Kortenbruck G., Berger E., Speckmann E. J., Musshoff U. RNA editing at the Q/R site for the glutamate receptor subunits GLUR2, GLUR5, and GLUR6 in hippocampus and temporal cortex from epileptic patients. Neurobiol Dis. 2001; 8:459-468.

Korycka J., Lach A., Heger E., Bogusławska D., Wolny M., Toporkiewicz M., Augoff K., Korzeniewski J., Sikorski A. Human DHHC proteins: a spotlight on the hidden player of palmitoylation. Eur J Cell Biol. 2012; 91:107-117.

Koyama R. and Ikegaya Y. Mossy Fiber Sprouting as a Potential Therapeutic Target for Epilepsy. Current Neurovascular Research. 2004; 1:1-8.

Koyama R. Dentate Circuitry as a Model to Study Epileptogenesis. Biol. Pharm. Bull. 2016; 39(6):891-896.

Kraus J. E., Yeh G. C., Bonhaus D. W., Nadler J. V., McNamara J. O. Kindling induces the long-lasting expression of a novel population of NMDA receptors in hippocampal region CA3. J Neurosci. 1994; 14:4196-4205.

Krauss G. L., Serratosa J. M., Villanueva V., et al. Randomized phase III study 306: adjunctive perampanel for refractory partial-onset seizures. Neurology. 2012; 78:1408–1415.

Kumar S. S., Bacci A., Kharazia V., Huguenard J. R. A developmental switch of AMPA receptor subunits in neocortical pyramidal neurons. Journal of Neuroscience. 2002; 22(8):3005–3015.

Kutsuwada T., Sakimura K., Manabe T., Takayama C., Katakura N., Kushiya E., Natsume R., Watanabe M., Inoue Y., Yagi T., et al. Impairment of suckling response, trigeminal neuronal pattern formation, and hippocampal LTD in NMDA receptor epsilon 2 subunit mutant mice. Neuron. 1996; 16:333– 344.

Laezza F., Wilding T. J., Sequeira S., Coussen F., Zhang X. Z., Hill-Robinson R., Mulle C., Huettner J. E., Craig A. M. KRIP6: A novel BTB/kelch protein regulating function of kainate receptors. Mol. Cell. Neurosci. 2007; 34:539–550.

Langer M., Brandt C., Zellinger C., Löscher W. Therapeutic window of opportunity for the neuroprotective effect of valproate versus the competitive AMPA receptor antagonist NS1209 following status epilepticus in rats. Neuropharmacology. 2011; 61(5–6):1033–1047.

Langereis M. A., Rosas-Acosta G., Mulder K., Wilson V. G. Production of sumoylated proteins using a baculovirus expression system. J Virol Methods. 2007; 139(2):189–194.

Lanore F., Labrousse V. F., Szabo Z., Normand E., Blanchet C., Mulle C. Deficits in Morphofunctional Maturation of Hippocampal Mossy Fiber Synapses in a Mouse Model of Intellectual Disability. Journal of Neuroscience. 2012; 32(49):17882-17893.

Lason W., Turchan J., Przewlocka B., Labuz D., Mika J., Przewlocki R. Seizure-related changes in the glutamate R2 and R5 receptor genes expression in the rat hippocampal formation. J Neural Transm. 1997b; 104:125–133.

Lason W., Turchan J., Przewlocki R., Machelska H., Labuz D., Przewlocka B. Effects of pilocarpine and kainate-induced seizures on N-methyl-D-aspartate receptor gene expression in the rat hippocampus. Neuroscience. 1997a; 78:997-1004.

Lauri S. E., Bortolotto Z. A., Bleakman D., Ornstein P. L., Lodge D., Isaac J. T., Collingridge G. L. A critical role of a facilitatory presynaptic kainate receptor in mossy fiber LTP. Neuron. 2001; 32(4):697-709.

Lauri S. E., Segerstrale M., Vesikansa A., Maingret F., Mulle C., Collingridge G. L., Isaac J. T., Taira T. Endogenous activation of kainate receptors regulates glutamate release and network activity in the developing hippocampus. J Neurosci. 2005; 25(18):4473-4484.

Lauri S. E., Vesikansa A., Segerstrale M., Collingridge G. L., Isaac J. T., Taira T. Functional maturation of CA1 synapses involves activity-dependent loss of tonic kainate receptor-mediated inhibition of glutamate release. Neuron. 2006; 50(3):415-429.

Lavezzari G., McCallum J., Dewey C. M., Roche K. W. Subunit-specific regulation of NMDA receptor endocytosis. J Neurosci. 2004; 24:6383–6391.

Lavezzari G., McCallum J., Lee R., Roche K. W. Differential binding of the AP-2 adaptor complex and PSD-95 to the C-terminus of the NMDA receptor subunit NR2B regulates surface expression. Neuropharmacology. 2003; 45:729-737.

Leinekugel X., Tseeb V., Ben-Ari Y., Bregestovski P. Synaptic $GABA_A$ activation induces Ca^{2+} rise in pyramidal cells and interneurons from rat neonatal hippocampal slices. J. Physiol. 1995; 487:319-329.

Leite J. P., Bortolotto Z. A., Cavalheiro E. A. Spontaneous recurrent seizures in rats: an experimental model of partial epilepsy. Neurosci Biobehav Rev. 1990; 14:511–517.

Lemos T., Cavalheiro E. A. Suppression of pilocarpine-induced status epilepticus and the late development of epilepsy in rats. Experimental Brain Research. 1995; 102(3):423-428.

Lerma J. and Marques J. M. Kainate Receptors in Health and Disease. Neuron. 2013; 80(2):292-311.

Lerma J. Kainate receptor physiology. Curr Opin Pharmacol. 2006; 6:89–97.

Lerma J., Paternain A. V., Rodriguez-Moreno A., Lopez-Garcia J. C. Molecular physiology of kainate receptors. Physiological Reviews. 2001; 81(3):971-998.

Letts V. A., Felix R., Biddlecome G. H., Arikkath J., Mahaffey C. L., Valenzuela A., Bartlett II F., Mori Y., Campbell K. P., Frankel W. N. The mouse stargazer gene encodes a neuronal Ca2+-channel gamma subunit. Nat Genet. 1998; 19(4):340-347.

Lévesque M., Salami P., Gotman J., Avoli M. Two seizure-onset types reveal specific patterns of high-frequency oscillations in a model of temporal lobe epilepsy. J Neurosci. 2012; 32:13264–13272.

Li H., Khirug S., Cai C., Ludwig A., Blaesse P., Kolikova J., Afzalov R., Coleman S. K., Lauri S., Airaksinen M. S., Keinänen K., Khiroug L., Saarma M., Kaila K., Rivera C. KCC2 interacts with the dendritic cytoskeleton to promote spine development. Neuron. 2007; 56:1019–1033.

Li K. and Xu E. The role and the mechanism of gamma-aminobutyric acid during central nervous system development. Neurosci Bull. 2008; 24(3):195-200.

Li S. Y., Xu D. S., Jia H. T. AGS-induced expression of Narp is concomitant with expression of AMPA receptor subunits GluR1 and GluR2 in hippocampus but not inferior colliculus of P77PMC rats. Neurobiol Dis. 2003; 14(3):328–335.

Lieb J. P., Walsh GO, Babb T. L., Walter R. D., Crandall P. H. A comparison of EEG seizure patterns recorded with surface and depth electrodes in patients with temporal lobe epilepsy. Epilepsia. 1976; 17:137–160.

Lievens P. M., Kuznetsova T., Kochlamazashvili G., Cesca F., Gorinski N., Galil D. A., Cherkas V., Ronkina N., Lafera J., Gaestel M., Ponimaskin E., Dityatev A. ZDHHC3 Tyrosine Phosphorylation Regulates Neural Cell Adhesion Molecule Palmitoylation. Mol Cell Biol. 2016; 36(17):2208-2225.

Lin D.-T., Makino Y., Sharma K., Hayashi T., Neve R., Takamiya K., Huganir R. L. Regulation of AMPA receptor extrasynaptic insertion by 4.1N, phosphorylation and palmitoylation. Nat. Neurosci. 2009; 12:879–887.

Liu S. J. and Zukin R. S. Ca^{2+} permeable AMPA receptors in synaptic plasticity and neuronal death. Trends Neurosci. 2007; 30:126-134.

Liu Z., Nagao T., Desjardins G. C., Gloor P., Avoli M. Quantitative evaluation of neuronal loss in the dorsal hippocampus in rats with long-term pilocarpine seizures. Epilepsy Res. 1994; 17:237–247.

Lodge D. The history of the pharmacology and cloning of ionotropic glutamate receptors and the development of idiosyncratic nomenclature. Neuropharmacology. 2009; 56(1):6–21.

Longone P., Impagnatiello F., Mienville J. M., Costa E., Guidotti A. Changes in AMPA receptor-spliced variant expression and shift in AMPA receptor spontaneous desensitization pharmacology during cerebellar granule cell maturation *in vitro*. J. Mol. Neurosci. 1998; 11:23–41.

Löscher W. and Schmidt D. Epilepsy: perampanel-new promise for refractory epilepsy? Nat Rev Neurol. 2012; 8(12):661-662.

Löscher W. Animal models of epilepsy for the development of antiepileptogenic and disease-modifying drugs. A comparison of the pharmacology of kindling and post-status epilepticus models of temporal lobe epilepsy. Epilepsy Research. 2002; 50(1-2):105-123.

Lothman E. W., Stringer J. L., Bertram E. H. The dentate gyrus as a control point for seizures in the hippocampus and beyond. Epilepsy Res. Suppl. 1992; 7:301–313.

Lu J., Karadsheh M., Delpire E. Developmental regulation of the neuronal-specific isoform of K-Cl cotransporter KCC2 in postnatal rat brains. J. Neurobiol. 1999; 39:558-568.

Ludwig A., Li H., Saarma M., Kaila K., Rivera C. Developmental up-regulation of KCC2 in the absence of GABAergic and glutamatergic transmission. Eur J Neurosci. 2003; 18(12):3199-3206.

Luhmann H. J. and Prince D. A. Postnatal maturation of the GABAergic system in rat neocortex. J. Neurophysiol. 1991; 65:247-263.

Lurton D., El Bahh B., Sundstrom L., Rougier A. Granule cell dispersion is correlated with early epileptic events in human temporal lobe epilepsy. J. Neurol. Sci. 1998; 154:133–136.

Luscher C., and Malenka R. C. Drug-evoked synaptic plasticity in addiction: from molecular changes to circuit remodeling. Neuron. 2011; 69:650-663.

Mah S. J., Cornell E., Mitchell N. A., Fleck M. W. Glutamate receptor trafficking: endoplasmic reticulum quality control involves ligand binding and receptor function. J Neurosci. 2005; 25:2215–2225.

Mahadevan V., Dargaei Z., Ivakine E. A., Hartmann A.-M., Ng D., Chevrie J.R., Ormond J., Nothwang H. G., McInnes R. R., Woodin M. A. Neto2-null mice have impaired GABAergic inhibition and are susceptible to seizures. Front Cell Neurosci. 2015; 9:368.

Maher M. P., Wu N., Ravula S., Ameriks M. K., Savall B. M., Liu C. L., Lord B., Wyatt R. M., Matta J. A., Dugovic C., et al. Discovery and characterization of AMPA receptor modulators selective for TARP-gamma 8. J Pharmacol Exp Ther. 2016; 357:394-414.

Maingret F., Lauri S. E., Taira T., Isaac J. T. Profound regulation of neonatal CA1 rat hippocampal GABAergic transmission by functionally distinct kainate receptor populations. J Physiol. 2005; 567:131–142.

Malinow R., and Malenka R. C. AMPA receptor trafficking and synaptic plasticity. Annu. Rev. Neurosci. 2002; 25:103-126.

Marchi N., Oby E., Batra A., et al. In vivo and in vitro effects of pilocarpine: relevance to ictogenesis. Epilepsia. 2007; 48(10):1934–1946.

Marques J. M., Rodrigues R. J., Valbuena S., Rozas J. L., Selak S., Marin P., Aller M. I., Lerma J. CRMP2 tethers kainate receptor activity to cytoskeleton dynamics during neuronal maturation. J Neurosci. 2013; 33:18298–18310.

Martenson J. S., Tomita S. Synaptic localization of neurotransmitter receptors: comparing mechanisms for AMPA and GABAA receptors. Curr Opin Pharmacol. 2015; 20:102-108.

Martin S. and Henley J. M. Activity-dependent endocytic sorting of kainate receptors to recycling or degradation pathways. EMBO J. 2004; 23(24):4749–4759.

Martin S., Bouschet T., Jenkins E. L., Nishimune A., Henley J. M. Bidirectional Regulation of Kainate Receptor Surface Expression in Hippocampal Neurons. J Biol Chem. 2008; 283(52): 36435–36440.

Martin S., Nishimune A., Mellor J. R., Henley J. M. SUMOylation regulates kainate receptor-mediated synaptic transmission. Nature. 2007; 447:321–325.

Masukawa L. M., Higashima M., Hart G. J., Spencer D. D., O'Connor M. J. NMDA receptor activation during epileptiform responses in the dentate gyrus of epileptic patients. Brain Res. 1991; 562:176-180.

Mathern G. W., Adelson P. D., Cahan L. D., Leite J. P. Hippocampal neuron damage in human epilepsy: Meyer's hypothesis revisited. Prog Brain Res. 2002; 135:237–251.

Mathern G. W., Kuhlman P. A., Mendoza D., Pretorius J. K. Human fascia dentata anatomy and hippocampal neuron densities differ depending on the epileptic syndrome and age at first seizure. J Neuropathol Exp Neurol. 1997; 56:199–212.

Mathern G. W., Leite J. P., Babb T. L., et al. Aberrant hippocampal mossy fiber sprouting correlates with greater NMDAR2 receptor staining. Neuroreport. 1996; 7:1029-1035.

Mathern G. W., Pretorius J. K., Leite J. P., Kornblum H. I., Mendoza D., Lozada A., Bertram E. H. Hippocampal AMPA and NMDA mRNA levels and subunit immunoreactivity in human temporal lobe epilepsy patients and a rodent model of chronic mesial limbic epilepsy. Epilepsy Res. 1998; 32:154– 171.

Mathern G. W., Pretorius J. K., Mendoza D., Lozada A., Kornblum H. I. Hippocampal AMPA and NMDA mRNA levels correlate with aberrant fascia dentata mossy fiber sprouting in the pilocarpine model of spontaneous limbic epilepsy. J Neurosci Res. 1998; 54:734-753.

Matsuda K., Budisantoso T., Mitakidis N., Sugaya Y., Miura E., Kakegawa W., Yamasaki M., Konno K., Uchigashima M., Abe M., et al. Transsynaptic Modulation of Kainate Receptor Functions by C1q-like Proteins. Neuron. 2016; 90(4):752-767.

Mayer M. L., Westbrook G. L., Guthrie P. B. Voltage-dependent block by Mg^{2+} of NMDA responses in spinal cord neurones. Nature. 1984; 309:261-263.

McCawley L. J., Matrisian L. M. Matrix metalloproteinases: they're not just for matrix anymore! Curr Opin Cell Biol. 2001; 13(5):534-540.

Medina I., Friedel P., Rivera C., et al. Current view on the functional regulation of the neuronal K^+-Cl^- cotransporter KCC2. Front Cell Neurosci. 2014; 8:27. doi:10.3389/fncel.2014.00027.

Melyan Z., Wheal H. V., Lancaster B. Metabotropic-mediated kainate receptor regulation of IsAHP and excitability in pyramidal cells. Neuron. 2002; 34(1):107-114.

Mennesson M., Rydgren E., Lipina T., Sokolowska E., Kulesskaya N., Morello F., Ivakine E., Voikar V., Risbrough V., Partanen J., Hovatta I. Kainate receptor auxiliary subunit NETO2 is required for normal fear expression and extinction. Neuropsychopharmacology. 2019 Feb 15. doi: 10.1038/s41386-019-0344-5.

Menuz K. and Nicoll R. A. Loss of inhibitory neuron AMPA receptors contributes to ataxia and epilepsy in Stargazer mice. J Neurosci. 2008; 28:10599-10603.

Michaelis E. K. Molecular biology of glutamate receptors in the central nervous system and their role in excitotoxicity, oxidative stress and aging. Prog Neurobiol. 1998; 54:369–415

Michishita M., Ikeda T., Nakashiba T., Ogawa M., Tashiro K., Honjo T., Doi K., Itohara S., Endo S. Expression of Btcl2, a novel member of Btcl gene family, during development of the central nervous system. Developmental Brain Research. 2004; 153(1):135-142.

Michishita M., Ikeda T., Nakashiba T., Ogawa M., Tashiro K., Honjo T., Doi K., Itohara S., Endo S. A novel gene, Btcl1, encoding CUB and LDLa domains is expressed in restricted areas of mouse brain. Biochem Biophys Res Commun. 2003; 306:680–686.

Miller L. P., Johnson A. E., Gelhard R. E., Insel T. R. The ontogeny of excitatory amino acid receptors in the rat forebrain. II. Kainic acid receptors. Neuroscience. 1990; 35:45-51.

Milstein A. D. and Nicoll R. A. Regulation of AMPA receptor gating and pharmacology by TARP auxiliary subunits. Trends Pharmacol. Sci. 2008; 29:333-339.

Milstein A. D., Zhou W., Karimzadegan S., Bredt D. S., Nicoll R. A. TARP subtypes differentially and dose-dependently control synaptic AMPA receptor gating. Neuron. 2007; 55:905-918.

Mizumaru C., Saito Y., Ishikawa T., Yoshida T., Yamamoto T., Nakaya T., Suzuki T. Suppression of APP-containing vesicle trafficking and production of β-amyloid by AID/DHHC-12 protein. J Neurochem. 2009; 111:1213-1224.

Modebadze T., Morgan N. H., Pérès I. A., Hadid R. D., Amada N., Hill C., Williams C., Stanford I. M., Morris C. M., Jones R. S., Whalley B. J., Woodhall G. L. A Low Mortality, High Morbidity Reduced Intensity Status Epilepticus (RISE) Model of Epilepsy and Epileptogenesis in the Rat. PLoS One. 2016; 11(2):e0147265. doi: 10.1371/journal.pone.0147265.

Mohideen F., Capili A. D., Bilimoria P. M., Yamada T., Bonni A., Lima C. D. A molecular basis for phosphorylation-dependent SUMO conjugation by the E2 UBC9. Nat Struct Mol Biol. 2009; 16:945–952.

Molnár E. Analysis of the Expression Profile and Regional Distribution of Neurotransmitter Receptors and Ion Channels in the Central Nervous System Using Histoblots. In: Rafael Luján and Francisco Ciruela (eds.) Receptors and Ion Channel Detection in the Brain: Methods and Protocols. New York: Springer, 2016; 157-170. 978-1-4939-3063-0 (print), 978-1-4939-3064-7 (eBook).

Molnár E. and Isaac J. T. Developmental and activity dependent regulation of ionotropic glutamate receptors at synapses. Scientific World J. 2002; 2:27–47.

Molnár E. Molecular organization and regulation of glutamate receptors in developing and adult mammalian central nervous systems. In: Lajtha A, Vizi ES (eds). Handbook of neurochemistry and molecular neurobiology. Springer New York. 2008; 415–441. doi: 10-1007/978-0-387-30382-6_17.

Molnár E., Pickard L., Duckworth J. K. Developmental changes in ionotropic glutamate receptors: Lessons from hippocampal synapses. Neuroscientist. 2002; 8(2):143-153.

Monyer H., Burnashev N., Laurie D. J., Sakmann B., Seeburg P. H. Developmental and regional expression in the rat brain and functional properties of four NMDA receptors. Neuron. 1994; 12(3):529–540.

Morimoto-Tomita M., Zhang W., Straub C., Cho C. H., Kim K. S., Howe J. R., Tomita S. Autoinactivation of neuronal AMPA receptors via glutamate-regulated TARP interaction. Neuron. 2009; 61:101–112.

Mott D. D., Rojas A., Fisher J. L., Dingledine R. J., Benveniste M. Subunit-specific desensitization of heteromeric kainate receptors. J Physiol. 2010; 588:683–700.

Mueller A. L., Taube J. S., Schwartzkroin P. A. Development of hyperpolarizing inhibitory postsynaptic potentials and hyperpolarizing response to gamma-aminobutyric acid in rabbit hippocampus studied in vitro. J. Neurosci. 1984; 4:860-867.

Mulle C., Sailer A., Pérez-Otaño I., Dickinson-Anson H., Castillo P. E., Bureau I., Maron C., Gage F. H., Mann J. R., Bettler B., Heinemann S. F. Altered synaptic physiology and reduced susceptibility to kainate-induced seizures in GluR6-deficient mice. Nature. 1998; 392(6676):601-605.

Mulle C., Sailer A., Swanson G. T., Brana C., O'Gorman S., Bettler B., Heinemann S. F. Subunit composition of kainate receptors in hippocampal interneurons. Neuron. 2000; 28(2):475-484.

Nadler J. V. The recurrent mossy fiber pathway of the epileptic brain. Neurochem. Res. 2003; 28:1649–1658.

Nadler J. V., Perry B. W., Cotman C. W. Selective reinnervation of hippocampal area CA1 and the fascia dentata after destruction of CA3-CA4 afferents with kainic acid. Brain Res. 1980; 182:1–9.

Nagao T., Alonso A., Avoli M. Epileptiform activity induced by pilocarpine in the rat hippocampal-entorhinal slice preparation. Neuroscience. 1996; 72:399–408.

Namba T., Morimoto K., Sato K., Yamada N., Kuroda S. Antiepileptogenic and anticonvulsant effects of NBQX, a selective AMPA receptor antagonist, in the rat kindling model of epilepsy. Brain Res. 1994; 638(1–2):36–44.

Nasu-Nishimura Y., Jaffe H., Isaac J. T., Roche K. W. Differential regulation of kainate receptor trafficking by phosphorylation of distinct sites on GluR6. J Biol Chem. 2010; 285:2847–2856.

Naumenko V. S. and Ponimaskin E. Palmitoylation as a functional regulator of neurotransmitter receptors. Neural Plasticity. 2018; 2018:5701348–5701348. doi:10.1155/2018/5701348

Ng D., Pitcher G. M., Szilard R. K., Sertie A., Kanisek M., Clapcote S. J., et al. Neto1 is a novel CUB-domain NMDA receptor-interacting protein required for synaptic plasticity and learning. Plos Biology. 2009; 7(2): e1000041.

Ng G. Y., Mouillac B., George S. R., Caron M., Dennis M., Bouvier M., O'Dowd B. F. Desensitization, phosphorylation and palmitoylation of the human dopamine D1 receptor. Eur J Pharmacol. 1994; 267(1):7–19.

Nicoll R. A., Tomita S., Bredt D. Auxiliary subunits assist AMPA-type glutamate receptors. Science. 2006; 3:1253-1256.

Nissinen J., Lukasiuk K., Pitkanen A. Is mossy fiber sprouting present at the time of the first spontaneous seizures in rat experimental temporal lobe epilepsy? Hippocampus. 2001; 11:299–310.

Noebels J. L., Avoli M., Rogawski M., Olsen R., Delgado-Escueta A. V. "Jasper's Basic Mechanisms of the Epilepsies" Workshop. Epilepsia. 2010; 51:1-5.

Noritake J., Fukata Y., Iwanaga T., Hosomi N., Tsutsumi R., Matsuda N., Tani H., Iwanari H., Mochizuki Y., Kodama T., Matsuura Y., Bredt D. S., Hamakubo T., Fukata M. Mobile DHHC palmitoylating enzyme mediates activity-sensitive synaptic targeting of PSD-95. J. Cell Biol. 2009; 186:147–160.

Nowak L., Bregestovski P., Ascher P., Herbet A., and Prochiantz A. Magnesium gates glutamate-activated channels in mouse central neurones. Nature. 1984; 307:462-465.

Obrietan K. and van den Pol A. N. GABA neurotransmission in the hypothalamus. J. Neurosci. 1995; 15:5065-5077.

O'Dowd B. F, Hnatowich M., Caron M. G., Lefkowitz R. J., Bouvier M. Palmitoylation of the human beta 2-adrenergic receptor. Mutation of Cys341 in the carboxyl tail leads to an uncoupled nonpalmitoylated form of the receptor. J Biol Chem. 1989; 264(13):7564–7569.

Olson E. N. and Spizz G. Fatty acylation of cellular proteins. Temporal and subcellular differences between palmitate and myristate acylation. J. Biol. Chem. 1986; 261:2458–2466.

Orav E., Atanasova T., Shintyapina A., Kesaf S., Kokko M., Partanen J., Taira T., Lauri S. E. Neto1 guides development of glutamatergic connectivity in the hippocampus by regulating axonal kainate receptors. Eneuro. 2017; 4(3). doi:10.1523/ENEURO.0048-17.2017.

Osten P. and Stern-Bach Y. Learning from stargazin: the mouse, the phenotype and the unexpected. Curr. Opin. Neurobiol. 2006; 16:275-280.

Owens D. F., Boyce L. H., Davis M. B., Kriegstein A. R. Excitatory GABA responses in embryonic and neonatal cortical slices demonstrated by gramicidin perforated-patch recordings and calcium imaging. J. Neurosci. 1996; 16:6414-6423.

Pahl S., Tapken D., Haering S. C., Hollmann M. Trafficking of Kainate Receptors. Membranes (Basel). 2014; 4(3): 565–595.

Palacios-Filardo J., Aller MI., Lerma J. Synaptic Targeting of Kainate Receptors. Cereb Cortex. 2016; 26(4):1464-1472.

Palmer G. C., Stagnitto M. L., Ordy J. M., Griffith R. C., Napier J. J., Gentile R. J., Woodhead J. H., White H. S., Swinyard E. A. Preclinical profile of stereoisomers of the anticonvulsant remacemide in mice. Epilepsy Res. 1991; 8:36– 48.

Paoletti P., Vergnano A. M., Barbour B., Casado M. Zinc at glutamatergic synapses. Neuroscience. 2009; 158:126-136.

Parent J. M., Murphy G. G. Mechanisms and functional significance of aberrant seizure-induced hippocampal neurogenesis. Epilepsia 2008; 49(5):19–25.

Park P., Kang H., Sanderson T. M., Bortolotto Z. A., Georgiou J., Zhuo M., Kaang B. K., Collingridge G. L. The role of calcium-permeable AMPARs in long-term potentiation at principal neurons in the rodent hippocampus. Frontiers in Synaptic Neuroscience. 2018; 10. doi:10.3389/fnsyn.2018.00042

Paternain A. V., Morales M., Lerma J. Selective antagonism of AMPA receptors unmasks kainate receptor-mediated responses in hippocampal-neurons. Neuron. 1995; 14(1):185-189.

Paternain A. V., Rodriguez-Moreno A., Villarroel A., Lerma J. Activation and desensitization properties of native and recombinant kainate receptors. Neuropharmacol. 1998; 37:1249–1259.

Patten A. R., Yau S. Y., Fontaine C. J., Meconi A., Wortman R. C., Christie B. R. The Benefits of Exercise on Structural and Functional Plasticity in the Rodent Hippocampus of Different Disease Models. Brain Plast. 2015; 1(1):97–127.

Payne S. H. The utility of protein and mRNA correlation. Trends Biochem Sci. 2015; 40(1):1–3.

Pellegrini-Giampietro D. E., Gorter J. A., Bennett M. V., Zukin R. S. The GluR2 (GluR-B) hypothesis: $Ca^{(2+)}$-permeable AMPA receptors in neurological disorders. Trends Neurosci. 1997; 20:464–470.

Pepinsky R. B., Zeng C., Wen D., Rayhorn P., Baker D. P., Williams K. P., Bixler S. A., Ambrose C. M., Garber E. A., Miatkowski K., Taylor F. R., Wang E. A., Galdes A. Identification of a palmitic acid-modified form of human Sonic hedgehog. J. Biol. Chem. 1998; 273:14037–14045.

Peret A., Christie L. A., Ouedraogo D. W., Gorlewicz A., Epsztein J., Mulle C., et al. Contribution of Aberrant GluK2-Containing Kainate Receptors to Chronic Seizures in Temporal Lobe Epilepsy. Cell Reports. 2014; 8(2):346-353.

Perrais D., Pinheiro P. S., Jane D. E., Mulle C. Antagonism of recombinant and native GluK3-containing kainate receptors. Neuropharmacology. 2009; 56(1):131-140.

Petrini E. M., Lu J., Cognet L., Lounis B., Ehlers M. D., Choquet D. Endocytic trafficking and recycling maintain a pool of mobile surface AMPA receptors required for synaptic potentiation. Neuron. 2009; 63:92–105.

Pichler A., Gast A., Seeler J. S., Dejean A. and Melchior F. The nucleoporin RanBP2 has SUMO1 E3 ligase activity. Cell. 2002; 108:109-120.

Pickard L., Noel J., Henley J. M., Collingridge G. L., Molnár E. Developmental changes in synaptic AMPA and NMDA receptor distribution and AMPA receptor subunit composition in living hippocampal neurons. J Neurosci. 2000; 20(21):7922-7931.

Pickering D. S., Taverna F. A., Salter M. W., Hampson D. R. Palmitoylation of the GluR6 kainate receptor. Proceedings of the National Academy of Sciences of the United States of America. 1995; 92(26):12090–12094.

Pinheiro P. and Mulle C. Kainate receptors. Cell and Tissue Research. 2006; 326(2):457-482.

Pinheiro P. S. and Mulle C. Presynaptic glutamate receptors: physiological functions and mechanisms of action. Nat. Rev. Neurosci. 2008; 9:423-436.

Pinheiro P. S., Perrais D., Coussen F., Barhanin J., Bettler B., Mann J. R., Malva J. O., Heinemann S. F., Mulle C. GluR7 is an essential subunit of presynaptic kainate autoreceptors at hippocampal mossy fiber synapses. Proc Natl Acad Sci U S A. 2007; 104(29):12181-12186.

Pitkanen A., Mathiesen C., Ronn L. C., Moller A., Nissinen J. Effect of novel AMPA antagonist, NS1209, on status epilepticus. An experimental study in rat. Epilepsy Res. 2007; 74(1):45–54.

Poirier J. L., Capek R., De Koninck Y. Differential progression of Dark Neuron and Fluoro-Jade labelling in the rat hippocampus following pilocarpine-induced status epilepticus. Neuroscience. 2000; 97:59–68.

Ponimaskin E., Dityateva G., Ruonala M. O., Fukata M., Fukata Y., Kobe F., Wouters F. S., Delling M., Bredt D. S., Schachner M., Dityatev A. Fibroblast growth factor-regulated palmitoylation of the neural cell adhesion molecule determines neuronal morphogenesis. J Neurosci. 2008; 28(36):8897-8907.

Pratt G. D., Kokaia M., Bengzon J., et al. Differential regulation of N-methyl-D-aspartate receptor subunit messenger RNAs in kindling-induced epileptogenesis. Neuroscience. 1993; 57:307-318.

Pressey J. C., Mahadevan V., Khademullah C. S., Dargaei Z., Chevrier J., Ye W., Huang M., Chauhan A. K., Meas S. J., Uvarov P., Airaksinen M. S., Woodin M. A. A kainate receptor subunit promotes the recycling of the neuron-specific K^+-Cl^- co-transporter KCC2 in hippocampal neurons. J Biol Chem. 2017; 292(15):6190–6201.

Prince H. C., Tzingounis A. V., Levey A. I., Conn P. J. Functional downregulation of GluR2 in piriform cortex of kindled animals. Synapse. 2000; 38(4):489–498.

Puskarjov M., Ahmad F., Kaila K., Blaesse P. Activity-dependent cleavage of the K-Cl cotransporter KCC2 mediated by calcium-activated protease calpain. J. Neurosci. 2012; 32:11356–11364.

Racine R. J. Modification of seizure activity by electrical stimulation. II. Motor seizure. Electroencephalogr Clin Neurophysiol. 1972; 32(3):281-294.

Rajasekaran K., Todorovic M., Kapur J. Calcium-permeable AMPA receptors are expressed in a rodent model of status epilepticus. Ann Neurol. 2012; 72(1):91–102.

Rakhade S. N. and Jensen F. E. Epileptogenesis in the immature brain: emerging mechanisms. Nature Reviews Neurology. 2009; 5(7):380–391.

Rakhade S. N., Fitzgerald E. F., Klein P. M., et al. Glutamate receptor 1 phosphorylation at serine 831 and 845 modulates seizure susceptibility and hippocampal hyperexcitability after early life seizures. J Neurosci. 2012; 32(49):17800–17812.

Ray S. and Brecht M. Structural development and dorsoventral maturation of the medial entorhinal cortex. Elife. 2016; 5:e13343. doi: 10.7554/eLife.13343.

Reichling D. B., Kyrozis A., Wang J., MacDermott A. B. Mechanisms of GABA and glycine depolarization-induced calcium transients in rat dorsal horn neurons. J. Physiol. 1994; 476:411-421.

Ren Z., Riley N. J., Garcia E. P., Sanders J. M., Swanson G. T., Marshall J. Multiple trafficking signals regulate kainate receptor KA2 subunit surface expression. J Neurosci. 2003a; 23:6608–6616.

Ren Z., Riley N. J., Needleman L. A., Sanders J. M., Swanson G. T., Marshall J. Cell surface expression of GluR5 kainate receptors is regulated by an endoplasmic reticulum retention signal. J Biol Chem. 2003b; 278:52700–52709.

Represa A., Robain O., Tremblay E., Ben Ari Y. Hippocampal plasticity in childhood epilepsy. Neurosci Lett. 1989; 99:351– 355.

Riban V., Bouilleret V., Pham-LêBT L., Fritschy J. M., Marescaux C., Depaulis A. Evolution of hippocampal epileptic activity during the development of hippocampal sclerosis in a mouse model of temporal lobe epilepsy. Neuroscience. 2002; 112:101–111.

Ritter L. M., Unis A. S., Meador-Woodruff J. H. Ontogeny of ionotropic glutamate receptor expression in human fetal brain. Brain Res Dev Brain Res. 2001; 127(2):123-133.

Ritter L. M., Vazquez D. M., Meador-Woodruff J. H. Ontogeny of ionotropic glutamate receptor subunit expression in the rat hippocampus. Brain Res Dev Brain Res. 2002; 139(2):227-236.

Rivera C., Voipio J., Payne J. A., Ruusuvuori E., Lahtinen H., Lamsa K., Pirvola U., Saarma M., Kaila K. The K^+/Cl^- co-transporter KCC2 renders GABA hyperpolarizing during neuronal maturation. Nature. 1999; 397:251-256.

Rivera R., Rozas J. L., Lerma J. PKC-dependent autoregulation of membrane kainate receptors. EMBO J. 2007; 26(20):4359-4367.

Rodríguez-Moreno A. and Sihra T. S. (eds.). Role of kainate receptors in network activity during development. Kainate receptors: novel signaling insights. Springer, 2011. 81–91. doi: 10.1007/978-1-4419-9557-5_8.

Rogawski M. A. AMPA receptors as a molecular target in epilepsy therapy. Acta Neurologica Scandinavica. 2013; 127:9–18.

Rogawski M. A., Hanada T. Preclinical pharmacology of perampanel, a selective non-competitive AMPA receptor antagonist. Acta Neurol Scand Suppl. 2013; (197):19-24.

Rouach N., Byrd K., Petralia R. S., Elias G. M., Adesnik H., Tomita S., Karimzadegan S., Kealey C., Bredt D. S., Nicoll R. A. TARP gamma-8 controls hippocampal AMPA receptor number, distribution and synaptic plasticity. Nat Neurosci. 2005; 8(11):1525-1533.

Rozas J. L., Paternain A. V., Lerma J. Noncanonical signaling by ionotropic kainate receptors. Neuron. 2003; 39(3):543-553.

Ruiz A., Sachidhanandam S., Utvik J. K., Coussen F., Mulle C. Distinct subunits in heteromeric kainate receptors mediate ionotropic and metabotropic function at hippocampal mossy fiber synapses. J. Neurosci. 2005; 25:11710–11718.

Sachdeo R., Kramer L. D., Rosenberg A., Sachdeo S. Felbamate monotherapy: controlled trial in patients with partial onset seizures. Ann Neurol. 1992; 32:386–392.

Sager C., Tapken D., Kott S., Hollmann M. Functional modulation of AMPA receptors by transmembrane AMPA receptor regulatory proteins. Neuroscience. 2009; 158:45-54.

Sanchez R. M. and Jensen F. E. Maturational aspects of epilepsy mechanisms and consequences for the immature brain. Epilepsia. 2001; 42(5):577–585.

Sanchez R. M., Koh S., Rio C., et al. Decreased glutamate receptor 2 expression and enhanced epileptogenesis in immature rat hippocampus after perinatal hypoxia-induced seizures. J Neurosci. 2001; 21(20):8154–8163.

Sanders S. S. and Hayden M. R. Aberrant palmitoylation in Huntington disease. Biochemical Society Transactions. 2015; 43(2):205–210.

Sanders S. S., Martin D. D., Butland S. L., Lavallée-Adam M., Calzolari D., Kay C., Yates III J. R., Hayden M. R. Curation of the Mammalian Palmitoylome Indicates a Pivotal Role for Palmitoylation in Diseases and Disorders of the Nervous System and Cancers. PLoS Comput Biol. 2015; 11(8):e1004405.

Sarkisian M. R. Overview of the Current Animal Models for Human Seizure and Epileptic Disorders. Epilepsy Behav. 2001; 2(3):201-216.

Scharfman H., Goodman J., McCloskey D. Ectopic granule cells of the rat dentate gyrus. Dev. Neurosci. 2007; 29:14–27.

Scharfman H., Myers C. Hilar mossy cells of the dentate gyrus: a historical perspective. Frontiers in Neural Circuits. 2013; 6: 106. DOI:10.3389/fncir.2012.00106.

Schiffer H. H., Swanson G. T., Heinemann S. F. Rat GluR7 and a carboxy-terminal splice variant, GluR7b, are functional kainate receptor subunits with a low sensitivity to glutamate. Neuron. 1997; 19(5):1141–1146.

Schmidt-Hieber C., Jonas P., Bischofberger J. Subthreshold dendritic signal processing and coincidence detection in dentate gyrus granule cells. J Neurosci. 2007; 27:8430– 8441.

Schmitz D., Mellor J., Breustedt J., Nicoll R. A. Presynaptic kainate receptors impart an associative property to hippocampal mossy fiber long-term potentiation. Nat Neurosci. 2003; 6:1058–1063.

Schmitz D., Mellor J., Nicoll R. A. Presynaptic kainate receptor mediation of frequency facilitation at hippocampal mossy fiber synapses. Science. 2001; 291:1972–1976.

Schoen F. J., Mitchell R. N. Tissues, the Extracellular Matrix, and Cell–Biomaterial Interactions. In: Ratner B. D. Biomaterials Science: An Introduction to Materials in Medicine. 3rd ed. Hoffman AS, Lemons JE, Schoen FJ, editors. 2013, Kidlington, Oxford: Academic/Elsevier.

Seeburg P. H. and Hartner J. Regulation of ion channel/neurotransmitter receptor function by RNA editing. Current Opinion in Neurobiology. 2003; 13:279–283.

Seeburg P. H., Higuchi M., Sprengel R. RNA editing of brain glutamate receptor channels: mechanism and physiology. Brain Research Reviews. 1998; 26: 217–229.

Selak S., Paternain A. V., Aller M. I., Aller I. M., Picó E., Rivera R., Lerma J. A role for SNAP25 in internalization of kainite receptors and synaptic plasticity. Neuron. 2009; 63:357–371.

Semyanov A., Kullmann D. M. Kainate receptor-dependent axonal depolarization and action potential initiation in interneurons. Nat Neurosci. 2001; 4:718–723.

Seress L., Abraham H., Paleszter M., Gallyas F. Granule cells are the main source of excitatory input to a subpopulation of GABAergic hippocampal neurones as revealed by electron microscopic double staining for zinc histochemistry and parvalbumin immunocytochemistry. Exp Brain Res. 2001; 136:456-462.

Shaw G., Kamen R. A conserved AU sequence from the 3' untranslated region of GM-CSF mRNA mediates selective mRNA degradation. Cell. 1986; 46(5):659-667.

Shen L., Liang F., Walensky L. D., Huganir R. L. Regulation of AMPA receptor GluR1 subunit surface expression by a 4.1N-linked actin cytoskeletal association. J. Neurosci. 2000; 20:7932–7940.

Sheng N., Shi Y. S., Nicoll R. A. Amino-terminal domains of kainate receptors determine the differential dependence on Neto auxiliary subunits for trafficking. Proc Natl Acad Sci U S A. 2017; 114(5):1159-1164.

Shi Y., Lu W., Milstein A. D., Nicoll R. A. The stoichiometry of AMPA receptors and TARPs varies by neuronal cell type. Neuron. 2009; 62:633-640.

Shipston M. J. Ion channel regulation by protein palmitoylation. The Journal of Biological Chemistry. 2011; 286(11):8709–16. doi:10.1074/jbc.R110.210005.

Shorvon S. D. and Goodridge D. M. G. Longitudinal cohort studies of the prognosis of epilepsy: contribution of the National General Practice Study of Epilepsy and other studies. Brain. 2013; 136:3497-3510.

Sillanpaa M., Jalava M., Kaleva O., Shinnar S. Long-term prognosis of seizures with onset in childhood. N Engl J Med. 1998; 338:1715-1722.

Silva A. V., Regondi M. C., Cipelletti B., Frassoni C., Cavalheiro E. A., Spreafico R. Neocortical and hippocampal changes after multiple pilocarpine-induced status epilepticus in rats. Epilepsia. 2005; 46:636–642.

Sloviter R. S. Decreased hippocampal inhibition and a selective loss of interneurons in experimental epilepsy. Science. 1987; 235:73–76.

Sloviter R. S., Bumanglag A. V., Schwarcz R., Frotscher M. Abnormal dentate gyrus network circuitry in temporal lobe epilepsy. Jasper's Basic Mechanisms of the Epilepsies [Internet]. 4th ed. (Noebels JL, Avoli M, Rogawski MA, Olsen RW, Delgado-Escueta AV eds.), National Center for Biotechnology Information U.S.A. 2012.

Smolders I., Bortolotto Z. A., Clarke V. R., Warre R., Khan G. M., O'Neill M. J., Ornstein P. L., Bleakman D., Ogden A., Weiss B., Stables J. P., Ho K. H., Ebinger G., Collingridge G. L., Lodge D., Michotte Y. Antagonists of GLU(K5)-

containing kainate receptors prevent pilocarpine-induced limbic seizures. Nat Neurosci. 2002; 5:796-804.

Sobocińska J., Roszczenko-Jasinska P., Ciesielska A., Kwiatkowska K. Protein Palmitoylation and Its Role in Bacterial and Viral Infections. Front Immunol. 2018; 8:2003. doi:10.3389/fimmu.2017.02003.

Sohn H. and Park M. Palmitoylation-mediated synaptic regulation of AMPA receptor trafficking and function. Archives of Pharmacal Research. 2019; 2019 Mar 05. doi:10.1007/s12272-019-01134-z.

Sommer B., Burnashev N., Verdoorn T. A., Keinanen K., Sakmann B., Seeburg P. H. A glutamate receptor channel with high affinity for domoate and kainate. EMBO J. 1992; 11:1651–1656.

Sommer C., Roth S. U., Kiessling M. Kainate-induced epilepsy alters protein expression of AMPA receptor subunits GluR1, GluR2 and AMPA receptor binding protein in the rat hippocampus. Acta Neuropathol. 2001; 101(5):460–468.

Song I. and Huganir R. L. Regulation of AMPA receptors during synaptic plasticity. Trends in Neurosciences. 2002; 25(11):578–588.

Spencer S. S. and Spencer D. D. Entorhinal-hippocampal interactions in medial temporal lobe epilepsy. Epilepsia. 1994; 35:721–727.

Spencer S. S. Neural networks in human epilepsy: evidence of and implications for treatment. Epilepsia. 2002; 43:219–227.

Spencer S. S. Substrates of localization-related epilepsies: biologic implications of localizing findings in humans. Epilepsia. 1998; 39:114–123.

Spencer S. S., Spencer D. D., Williamson P. D., Mattson R. Combined depth and subdural electrode investigation in uncontrolled epilepsy. Neurology. 1990; 40:74–79.

Sprengel R., Brusa R., Feldmeyer D., Burnashev N., Hvalby O., et al. RNA editing in the brain. Naunyn-Schmiedebergs Archives of Pharmacology. 1998; 358: R370.

Stohr H., Berger C., Frohlich S., Weber B. H. F. A novel gene encoding a putative transmembrane protein with two extracellular CUB domains and a low-density lipoprotein class A module: isolation of alternatively spliced isoforms in retina and brain. Gene. 2002; 286(2):223-231.

Straub C, Zhang W, Howe JR. Neto2 Modulation of Kainate Receptors with Different Subunit Compositions. Journal of Neuroscience. 2011b; 31(22):8078-8082.

Straub C. and Tomita S. The regulation of glutamate receptor trafficking and function by TARPs and other transmembrane auxiliary subunits. Curr Opin Neurobiol. 2012; 22:488-495.

Straub C., Hunt D. L., Yamasaki M., Kim K. S., Watanabe M., Castillo P. E., Tomita S. Distinct functions of kainate receptors in the brain are determined by the auxiliary subunit Neto1. Nature Neuroscience. 2011a; 14(7):866-873.

Sumioka A., Yan D., Tomita S. TARP phosphorylation regulates synaptic AMPA receptors through lipid bilayers. Neuron. 2010; 66(5):755–767.

Sutula T., Cascino G., Cavazos J., Parada I., Ramirez L. Mossy fiber synaptic reorganization in the epileptic human temporal-lobe. Ann Neurol. 1989; 26:321–330.

Swanson G. T. Targeting AMPA and kainate receptors in neurological disease: therapies on the horizon? Neuropsychopharmacology. 2009; 34(1):249–250.

Swanson G. T., Kamboj S. K., Cull-Candy S. G. Single-channel properties of recombinant AMPA receptors depend on RNA editing, splice variation, and subunit composition. J Neurosci. 1997; 17(1):58–69.

Tabaczar S., Czogalla A., Podkalicka J., Biernatowska A., Sikorski A. F. Protein palmitoylation: Palmitoyl transferases and their specificity. Exp Biol Med (Maywood). 2017; 242(11):1150–1157.

Talos D. M., Fishman R. E., Park H., et al. Developmental regulation of α-amino-3-hydroxy-5-methyl-4-isoxazole- propionic acid receptor subunit expression in forebrain and relationship to regional susceptibility to hypoxic/ischemic injury. I. Rodent cerebral white matter and cortex. Journal of Comparative Neurology. 2006b; 497(1):42–60.

Talos D. M., Follett P. L., Folkerth R. D., et al. Developmental regulation of α-amino-3-hydroxy-5-methyl-4-isoxazole- propionic acid receptor subunit expression in forebrain and relationship to regional susceptibility to hypoxic/ischemic injury. II. Human cerebral white matter and cortex. Journal of Comparative Neurology. 2006a; 497(1):61–77.

Tang M., Ivakine E., Mahadevan V., Salter M.W., McInnes R.R. Neto2 Interacts with the Scaffolding Protein GRIP and Regulates Synaptic Abundance of Kainate Receptors. PLoS ONE. 2012; 7(12):e51433.

Tang M., Pelkey K. A., Ng D., Ivakine E., McBain C. J., Salter M. W., et al. Neto1 Is an Auxiliary Subunit of Native Synaptic Kainate Receptors. Journal of Neuroscience. 2011; 31(27):10009-18.

Tang Y. P., Shimizu E., Dube G. R., Rampon C., Kerchner G. A., Zhuo M., Liu G., Tsien J. Z. (1999) Genetic enhancement of learning and memory in mice. Nature. 1999; 401:63–69.

Tashiro A., Dunaevsky A., Blazeski R., Mason C. A., Yuste R. Bidirectional regulation of hippocampal mossy fiber filopodial motility by kainate receptors: a two-step model of synaptogenesis. Neuron. 2003; 38(5):773-784.

Tashiro K., Tada H., Heilker R., Shirozu M., Nakano T., Honjo T. Signal sequence trap: a cloning strategy for secreted proteins and type I membrane proteins. Science. 1993; 261(5121):600-603.

Taylor C. P., Vartanian M. G. Probenecid pretreatment enhances anticonvulsant action of NBQX in mice. Eur J Pharmacol. 1992; 213:151–153.

The UniProt Consortium. UniProt: a worldwide hub of protein knowledge. Nucleic Acids Res. 2019; 47: D506-515.

Thomas G. M., Hayashi T., Chiu S. L., Chen C. M., Huganir R. L. Palmitoylation by DHHC5/8 targets GRIP1 to dendritic endosomes to regulate AMPA-R trafficking Neuron. 2012; 73:482-496.

Tomita S. and Castillo P. E. Neto1 and Neto2: auxiliary subunits that determine key properties of native kainate receptors. Journal of Physiology-London. 2012; 590(10):2217-2223.

Tomita S., Byrd R. K., Rouach N., Bellone C., Venegas A., O'Brien J. L., Kim K. S., Olsen O., Nicoll R. A., Bredt D. S. AMPA receptors and stargazin-like transmembrane AMPA receptor-regulatory proteins mediate hippocampal kainate neurotoxicity. Proc Natl Acad Sci U S A. 2007; 104:18784-18788.

Tomita S., Chen L., Kawasaki Y., Petralia R. S., Wenthold R. J., Nicoll R. A., Bredt D. S. Functional studies and distribution define a family of transmembrane AMPA receptor regulatory proteins J. Cell Biol. 2003; 161:805-816.

Tomita S., Fukata M., Nicoll R. A., Bredt D. S. Dynamic interaction of stargazin-like TARPs with cycling AMPA receptors at synapses. Science. 2004; 303:1508-1511.

Tonnes J., Stierli B., Cerletti C., Behrmann J. T., Molnar E., Streit, P. Regional distribution and developmental changes of GluR1-flop protein revealed by monoclonal antibody in rat brain. J. Neurochem. 1999; 73:2195– 2205.

Topinka J. R. and Bredt D. S. N-terminal palmitoylation of PSD-95 regulates association with cell membranes and interaction with K^+ channel, Kv1.4. Neuron. 1998; 20:125–134.

Traynelis S. F., Wollmuth L. P., McBain C. J., Menniti F. S., Vance K. M., Ogden K. K., Hansen K. B., Yuan H., Myers S. J., Dingledine R., et al. Glutamate receptor ion channels: structure, regulation, and function. Pharmacol Rev. 2010; 62:405-496.

Turski L., Ikonomidou C., Turski W. A., Bortolotto Z. A., Cavalheiro E. A. Review: cholinergic mechanisms and epileptogenesis. The seizures induced by pilocarpine: A novel model of intractable epilepsy. Synapse. 1989; 3:154–171.

Turski L., Jacobsen P., Honoré T., Stephens D. N. Relief of experimental spasticity and anxiolytic/anticonvulsant actions of the alpha-amino-3- hydroxy-5-methyl-4-isoxazolepropionate antagonist 2,3-dihydroxy-6-nitro-7-sulfamoyl-benzo(F)quinoxaline. J Pharmacol Exp Ther. 1992; 260(2):742–747.

Turski W. A., Cavalheiro E. A., Schwarz M., Czuczwar S. L. J., Kleinrok Z., Turski L. Limbic seizures produced by pilocarpine I rats: behavioral, electroencephalographic and neuropathological study. Behav Brain Res. 1983; 9:315–335.

Valbuena S., Lerma J. Non-canonical signaling, the hidden life of ligand-gated ion channels. Neuron. 2016; 92:316–329.

Valluru L., Xu J., Zhu Y., Yan S., Contractor A., Swanson G.T. Ligand binding is a critical requirement for plasma membrane expression of heteromeric kainate receptors. J Biol Chem. 2005; 280:6085–6093.

Vandenberghe W., Nicoll R. A., Bredt D. S. Stargazin is an AMPA receptor auxiliary subunit. Proc. Natl. Acad. Sci. USA. 2005; 102:485-490.

Vernon C. G. and Swanson G. T. Neto2 assembles with kainate receptors in DRG neurons during development and modulates neurite outgrowth in adult sensory neurons. The Journal of Neuroscience: The Official Journal of the Society for Neuroscience. 2017; 37(12):3352–3363. doi:10.1523/JNEUROSCI.2978-16.2017.

Vezzani A. Pilocarpine-induced seizures revisited: what does the model mimic? Epilepsy Curr. 2009; 9(5):146-148.

Vignes M. and Collingridge G. L. The synaptic activation of kainate receptors. Nature. 1997; 388(6638):179-82.

Vignes M., Clarke V. R., Parry M. J., Bleakman D., Lodge D., Ornstein P. L., Collingridge G. L. The GluR5 subtype of kainate receptor regulates excitatory synaptic transmission in areas CA1 and CA3 of the rat hippocampus. Neuropharmacology. 1998; 37(10-11):1269-1277.

Világi I., Dobó E., Borbély S., Czégé D., Molnár E., Mihály A. Repeated 4-aminopyridine induced seizures diminish the efficacy of glutamatergic transmission in the neocortex. Experimental Neurology. 2009; 219(1):136–145.

Vincent P. and Mulle C. Kainate receptors in epilepsy and excitotoxicity. Neuroscience. 2009; 158(1):309-323.

Vismer M. S., Forcelli P. A., Skopin M. D., Gale K., Koubeissi M. Z. The piriform, perirhinal, and entorhinal cortex in seizure generation. Frontiers in Neural Circuits. 2015; 9:27. doi:10.3389/fncir.2015.00027.

Vissel B., Royle G. A., Christie B. R., Schiffer H. H., Ghetti A., Tritto T., Perez-Otano I., Radcliffe R. A., Seamans J., Sejnowski T., Wehner J. M., Collins A. C., O'Gorman S., Heinemann S. F. The role of RNA editing of kainate receptors in synaptic plasticity and seizures. Neuron. 2001; 29:217-227.

Vivithanaporn P., Yan S., Swanson G. T. Intracellular trafficking of KA2 kainate receptors mediated by interactions with coatomer protein complex I (COPI) and 14-3-3 chaperone systems. J Biol Chem. 2006; 281:15475–15484.

Vizuete A. F. K, Hansen F., Negri E., Leite M. C., de Oliveira D. L., Gonçalves C-A. Effects of dexamethasone on the Li-pilocarpine model of epilepsy: protection against hippocampal inflammation and astrogliosis. Journal of Neuroinflammation. 2018; 15(1):68. doi: 10.1186/s12974-018-1109-5.

Vu T. Q., Payne J. A., Copenhagen D. R. Localization and developmental expression patterns of the neuronal K-Cl cotransporter (KCC2) in the rat retina. J. Neurosci. 2000; 20:1414-1423.

Walensky L. D., Blackshaw S., Liao D. Z., Watkins C. C., Weier H. U.G., Parra M., Huganir R. L., Conboy J. G., Mohandas N., Snyder S. H. A novel neuron-enriched homolog of the erythrocyte membrane cytoskeletal protein 4.1. J. Neurosci. 1999; 15:6457-6467.

Wang J., Reichling D. B., Kyrozis A., MacDermott A. B. Developmental loss of GABA- and glycine-induced depolarization and Ca^{2+} transients in embryonic rat dorsal horn neurons in culture. Eur. J. Neurosci. 1994; 6:1275-1280.

Washbourne P., Cansino V., Mathews J. R., Graham M., Burgoyne R. D., Wilson M. C. Cysteine residues of SNAP-25 are required for SNARE disassembly and exocytosis, but not for membrane targeting. Biochem. J. 2001; 357:625–634.

Watanabe M. and Fukuda A. Development and regulation of chloride homeostasis in the central nervous system. Front Cell Neurosci. 2015; 9:371. doi: 10.3389/fncel.2015.00371.

Watanabe M. Developmental dynamics of gene expression for NMDA receptor channel. In The Ionotropic Glutamate Receptors. Monaghan, D.T. and Wenthold, R.J., Eds. Humana Press, Totowa, NJ. 1997.

Wenzel A., Fritschy J. M., Mohier H., Benke D. NMDA Receptor Heterogeneity During Postnatal Development of the Rat Brain: Differential Expression of the NR2A, NR2B, and NR2C Subunit Proteins. J. Neurochem. 1997; 68:469-478.

Wieser H. G. ILAE Commission on Neurosurgery of Epilepsy. ILAE Commission Report. Mesial temporal lobe epilepsy with hippocampal sclerosis. Epilepsia. 2004; 45:695–714.

Wilding T. J. and Huettner J. E. Antagonist pharmacology of kainate- and alpha-amino-3-hydroxy-5-methyl-4-isoxazolepropionic acid-preferring receptors. Molecular Pharmacology. 1996; 49(3):540-546.

Wilkinson K. A. and Henley J. M. Mechanisms, regulation and consequences of protein SUMOylation. Biochem J. 2010; 428:133–145.

Williams P. A., Wuarin J. P., Dou P., Ferraro D. J., Dudek F. E. Reassessment of the effects of cycloheximide on mossy fiber sprouting and epileptogenesis in the pilocarpine model of temporal lobe epilepsy. J Neurophysiol. 2002; 88:2075–2087.

Wisden W., Seeburg P. H. A complex mosaic of high-affinity kainate receptors in rat brain. J Neurosci. 1993; 13(8):3582-3598.

Witter M.P. Connectivity of the Hippocampus. In: Cutsuridis V., Graham B., Cobb S., Vida I. (eds) Hippocampal Microcircuits. Springer Series in Computational Neuroscience, 2010, vol 5. Springer, New York, NY

Wo Z. G. and Oswald R. E. Transmembrane topology of two kainate receptor subunits revealed by N-glycosylation. Proc Natl Acad Sci U S A. 1994; 91(15):7154–7158.

Wondolowski J., Frerking M. Subunit-dependent postsynaptic expression of kainate receptors on hippocampal interneurons in area CA1. J Neurosci. 2009; 29:563–574.

Wong H. K., Liu X.-B., Matos M. F., et al. Temporal and regional expression of NMDA receptor subunit NR3A in the mammalian brain. Journal of Comparative Neurology. 2002; 450(4):303–317.

Woolfrey K. M., Sanderson J. L., Dell'Acqua M. L. The palmitoyl acyltransferase DHHC2 regulates recycling endosome exocytosis and synaptic potentiation through palmitoylation of AKAP79/150. J Neurosci. 2015; 35:442-456.

Wu L-J., Xu H., Ren M., Zhuo M. Genetic and pharmacological studies of GluR5 modulation of inhibitory synaptic transmission in the anterior cingulate cortex of adult mice. Dev Neurobiol. 2007; 67:146–157.

Wyeth M. S., Pelkey K. A., Yuan X., Vargish G., Johnston A. D., Hunt S., Fang C., Abebe D., Mahadevan V., Fisahn A., et al. Neto auxiliary subunits regulate interneuron somatodendritic and presynaptic kainate receptors to control network inhibition. Cell Rep. 2017; 20(9): 2156–2168.

Wyeth M. S., Pelkey K. A., Petralia R. S., Salter M. W., McInnes R. R., McBain C. J. Neto Auxiliary Protein Interactions Regulate Kainate and NMDA Receptor Subunit Localization at Mossy Fiber-CA3 Pyramidal Cell Synapses. Journal of Neuroscience. 2014; 34(2):622-628.

Yamaguchi S., Donevan S. D., Rogawski M. A. Anticonvulsant activity of AMPA/kainate antagonists: comparison of GYKI 52466 and NBOX in maximal electroshock and chemoconvulsant seizure models. Epilepsy Res. 1993; 15:179–184.

Yan D. and Tomita S. Defined criteria for auxiliary subunits of glutamate receptors. Journal of Physiology-London. 2012; 590(1):21-31.

Yan S., Sanders J. M., Xu J., Zhu Y., Contractor A., Swanson G. T. A C-terminal determinant of GluR6 kainate receptor trafficking. J Neurosci. 2004; 24:679–691.

Yang Q., Zheng F., Hu Y., Yang Y., Li Y., Chen G., Wang W., He M., Zhou R., Ma Y., et al. zDHHC8 critically regulates seizure susceptibility in epilepsy. Cell Death & Disease. 2018; 9(8). doi:10.1038/s41419-018-0842-0.

Ying Z., Babb T. L., Comair Y. G., Bushey M., Touhalisky K. Increased densities of AMPA GluR1 subunit proteins and presynaptic mossy fiber sprouting in the fascia dentata of human hippocampal epilepsy. Brain Res. 1998; 798(1–2):239–246.

Yuste R. and Bonhoeffer T. Genesis of dendritic spines: Insights from ultrastructural and imaging studies. Nat Rev Neurosci. 2004; 5:24–34.

Yuste R. and Katz L. C. Control of postsynaptic Ca^{2+} influx in developing neocortex by excitatory and inhibitory neurotransmitters. Neuron. 1991; 6:334-344.

Zhang W., St-Gelais F., Grabner C. P., Trinidad J. C., Sumioka A., Morimoto-Tomita M., Kim K. S., Straub C., Burlingame A. L., Howe J. R., Tomita S. A Transmembrane Accessory Subunit that Modulates Kainate-Type Glutamate Receptors. Neuron. 2009; 61(3):385-96.

Zhang Y., Chen K., Sloan S. A., Bennett M. L., Scholze A. R., O'Keeffe S., Phatnani H. P., Guarnieri P., Caneda C., Ruderisch N., Deng S., Liddelow S. A., Zhang C., Daneman R., Maniatis T., Barres B. A., Wu J. Q. An RNA-sequencing transcriptome and splicing database of glia neurons, and vascular cells of the cerebral cortex. J Neurosci. 2014; 34(36):11929-11947.

Zhao Y., Kwon S. W., Anselmo A., Kaur K., White M. A. Broad Spectrum Identification of Cellular Small Ubiquitin-related Modifier (SUMO) Substrate Proteins. The Journal of biological chemistry. 2004; 279(20):20999-21002.

Ziff E. B. TARPs and the AMPA receptor trafficking paradox. Neuron. 2007; 53:627-633.

8 Appendix

8.1 Roles of Neto subunit proteins in agonist-induced internalisation and stability of GluK2/3-containing KARs

8.1.1 Background

To extend our research group's unpublished study (Dr Garry Whitehead findings), we investigated the effects of Neto proteins on the cell surface stability, internalisation and degradation rates of GluK2/3-containg KARs upon kainate stimulation. Dr Whitehead found that Neto2 regulates the endocytosis and surface degradation of recombinant GluK2 receptors in HEK293T cells following kainate stimulation. Co-expression of Neto2, but not Neto1, with GluK2 in HEK293T cells led to a significant reduction in GluK2 internalisation after 15 and 30 minutes of kainate treatment indicating that Neto2 stabilises cell surface GluK2 receptors. Parallel to this reduction in internalised GluK2, there was an increase in internalised Neto2 at the same time points. This may suggest that Neto2/GluK2 receptor association is altered in an activity-dependent manner favouring their dissociation and stabilising the receptor surface expression. In addition, Dr Whitehead also demonstrated that co-expression of Neto2 with GluK2 in HEK293T cells increased the half-life of surface GluK2 suggesting that Neto2 also stabilises surface GluK2 receptors under basal conditions.

Taking into consideration that the literature has controversial evidence for the role of Neto proteins on KARs' surface expression and that this effect has not been studied using endogenous receptors in active neurons, we hypothesized and aimed the following:

8.1.2 Aims

Hypothesis: Neto subunit proteins may stabilise neuronal KARs on the cell surface and alter their internalisation and degradation rate.

Aims

1) To establish the roles of Neto subunit proteins in agonist-mediated internalisation of neuronal GluK2/3-containing KARs.
2) To examine the impact of Neto2 auxiliary subunit protein on the degradation rate of GluK2/3-containing KARs in neurons.

8.1.3 Results

8.1.3.1 Role of Neto subunit proteins in agonist-mediated internalisation of neuronal GluK2/3-containing KARs.

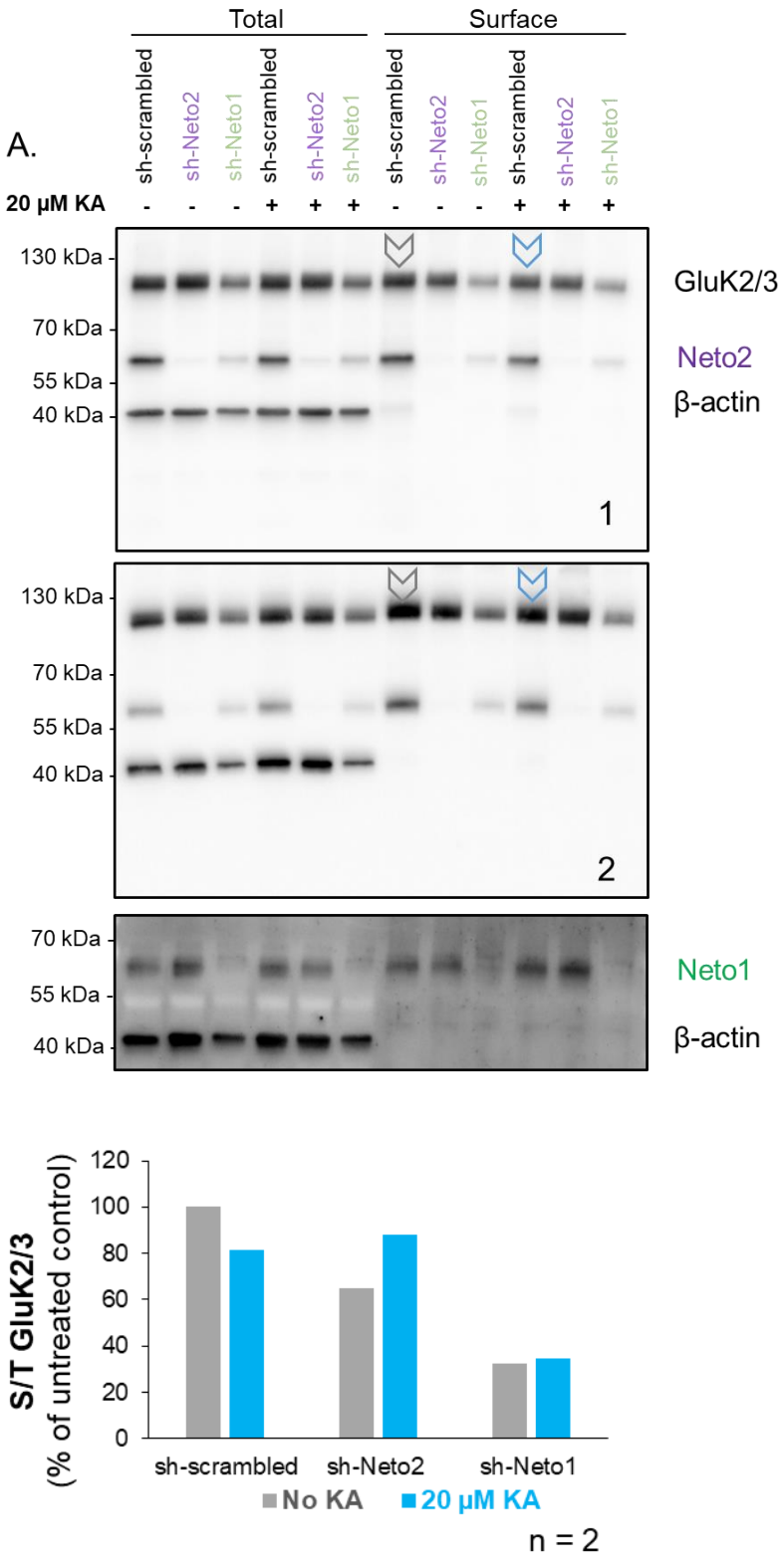

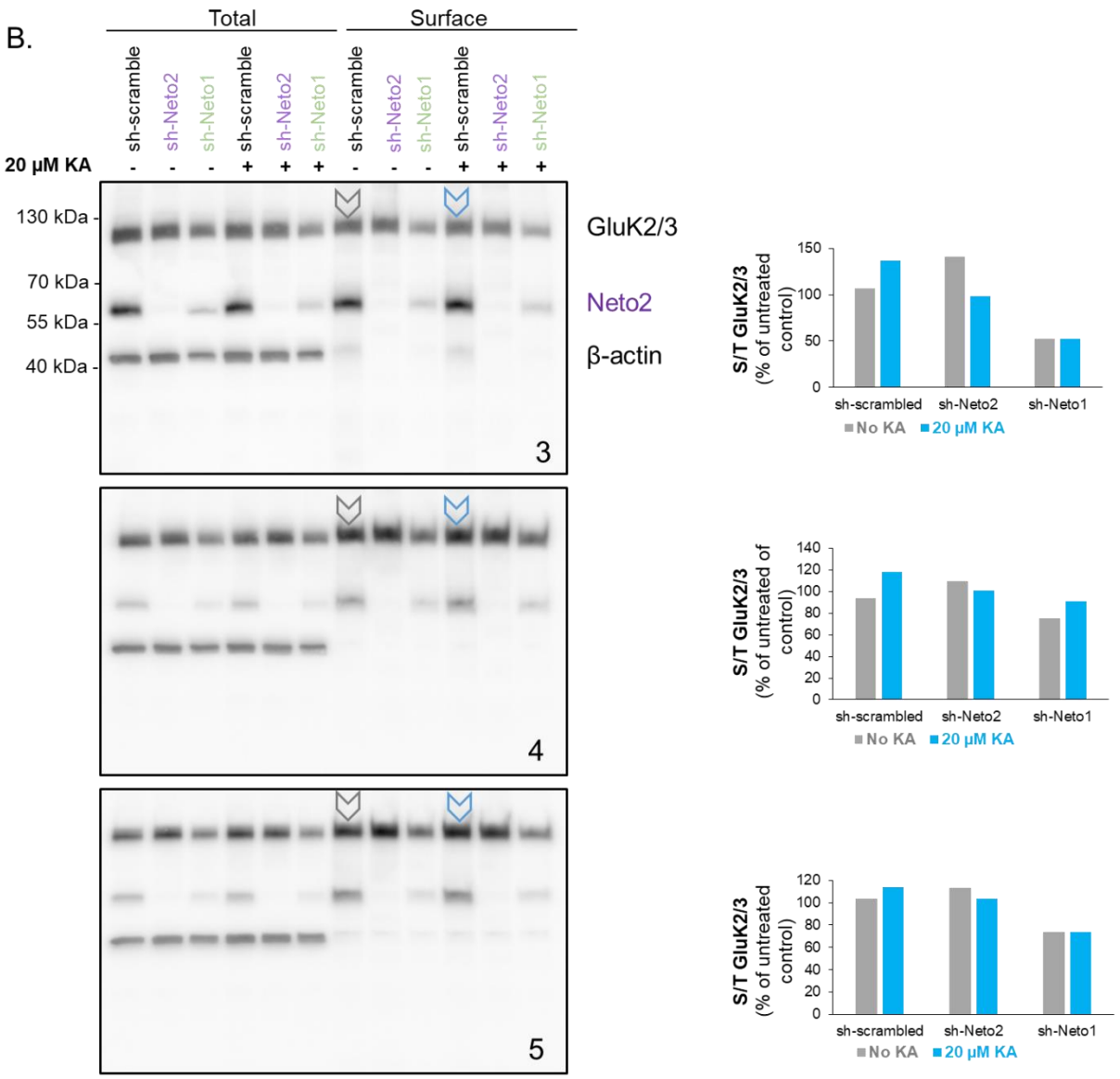
B.
Total
Surface
sh-scramble
sh-Neto2
sh-Neto1
20 μM KA
130 kDa
70 kDa
55 kDa
40 kDa
GluK2/3
Neto2
β-actin
3
4
5
S/T GluK2/3 (% of untreated control)
sh-scrambled
sh-Neto2
sh-Neto1
No KA
20 μM KA

Figure 1. The effect of Neto proteins on kainate-induced internalisation of GluK2/3-containing KARs. Cortical neurons at DIV 9-10 were treated with sh-scrambled, sh-Neto2 or sh-Neto1 lentiviruses. At DIV 14-15, neurons were pre-treated with 2 µM TTX (to block neuronal activity) then, with 20 µM kainate for 30 minutes as indicated. Cell surface biotinylation (n = 5) was performed to establish the effect of Neto proteins on agonist-mediated KAR internalisation. The first two blots and their quantification **(A, 1 and 2)** show the results of two independent experiments where the positive controls (internalisation of KARs upon kainate stimulation) worked (see grey and blue arrows for surface GluK2/3 expression without and with treatment, respectively). However, this positive control in the other next 3 independent experiments (**B, 3, 4, and 5** blots and next to them their quantification) failed to confirm the responsiveness of the neurons. Therefore, the GluK2/3 data could not be combined nor could statistical analysis be performed for an 'n' of two. Nonetheless, the knockdown of Neto subunit proteins was efficient as indicated by the intensity of the bands on the blots (**A**).

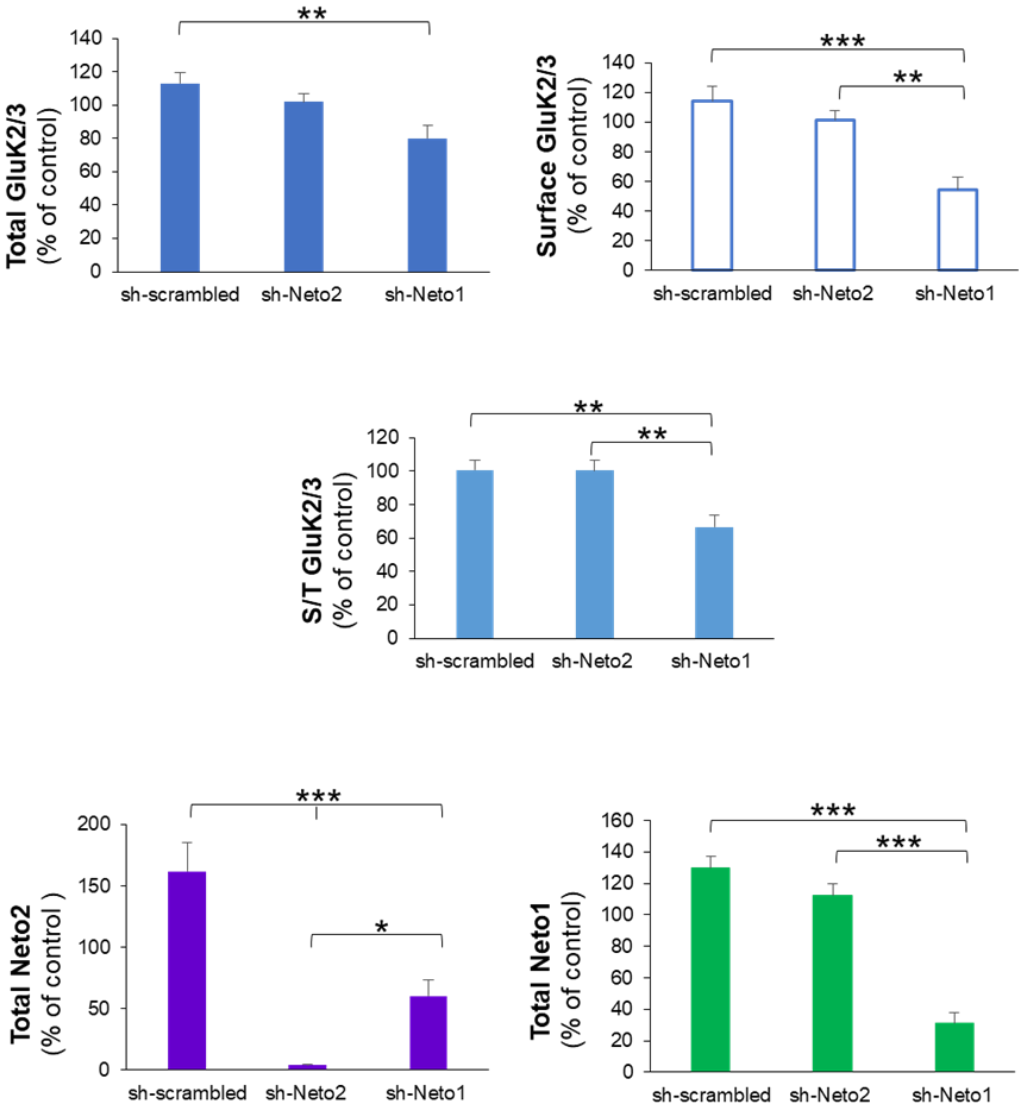

Figure 2. Effect of Neto proteins on the surface expression of GluK2/3-containing receptors. The bar graphs combine data from cell surface biotinylation experiments without kainate treatment. The ratio of GluK2/3 surface/total expression (n = 10) was found to be dependent on Neto1. It was significantly reduced when Neto1, but not Neto2, is knocked down compared to the scrambled [(66.5 ± 6.8, p = 0.002 and 100.4 ± 5.8, p = 0.99) vs sh-scrambled 100.8 ± 5.7, respectively]. Knocking down Neto2 (n = 10) significantly reduced its total expression compared to both the scrambled (~ 95% Neto2 KD efficiency) and sh-Neto1 [4.1 ± 0.7 vs (161.9 ± 23.5, p < 0.001 and 60.2 ± 13.3, p = 0.045), respectively]. There was significant reduction in the total Neto2 expression when Neto1 was reduced (60.2 ± 13.3 vs 161.9 ± 23.5, p < 0.001). In contrast, total Neto1 expression was not affected by knocking down Neto2 (129.7 ± 7.7 vs 112.4 ± 7.0, p = 0.25). The total Neto1 expression (n = 6) was significantly reduced when it was knocked down compared to the scrambled (70% Neto1 KD efficiency) and sh-Neto2 [31.0 ± 7.0 vs (129.7 ± 7.7 and 112.4 ± 7.0) respectively, both p < 0.001]. One-way ANOVA was used for the statistical analysis at a minimum confidence level of p < 0.05 with Tukey post hoc test. Data are represented as % of the control. Error bars indicate the standard error (SE).

8.1.3.2 The impact Neto2 auxiliary subunit protein on the degradation rate of GluK2/3-containing KARs in neurons.

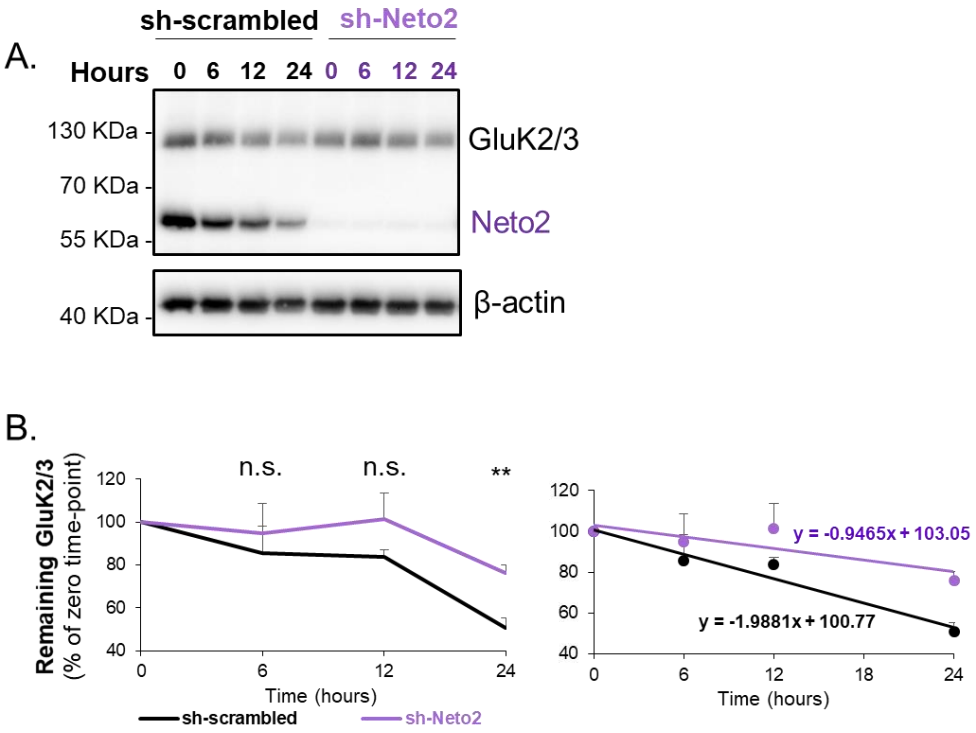

Figure 3. The impact of Neto2 subunit protein on the degradation rate of GluK2/3-containing KARs. Cortical neurons were treated with one of 2 different shRNA lentiviruses (sh-scrambled and sh-Neto2) at DIV 9-10. They were then (at DIV 14-15) treated with 25 µg/mL cycloheximide and the amount of two proteins (GluK2/3 and Neto2) was identified at 4 time-points (0, 6, 12 and 24 hours) **(A)**. Pixel intensity quantification (arbitrary unit) of the protein bands **(B)** is shown on the line chart (next to it is the chart of the line of best fit). GluK2/3 bands were normalised to their counterpart β-actin bands and then to the Zero time-point. Knocking down Neto2 did not change the remaining percent of GluK2/3 in any time point compared to the control except at 24 hours of cycloheximide treatment **(B)**.After 24 hours, the remaining amount of GluK2/3 was increased by ~ 33% when Neto2 subunit protein was knocked down (50.5 ± 4.6 vs 76.0 ± 4.0, p = 0.009). Student t-test was used for the statistical analysis (n = 4) at a minimum confidence level of $p < 0.05$. Error bars indicate the standard error.

GluK2/3		
Group	**% of zero time-point ±SE**	***p* - value**
6 hours of CHI		
sh-scrambled vs sh-Neto2	85.4 ± 12.7 vs 94.9 ± 13.8	0.63
12 hours of CHI		
sh-scrambled vs sh-Neto2	83.5 ± 3.4 vs 101.4 ± 12.1	0.21
24 hours of CHI		
sh-scrambled vs sh-Neto2	50.5 ± 4.6 vs 76.0 ± 4.0	0.009 *

Table 1. A summary of the remaining percent of GluK2/3 after cycloheximide treatment. The data represent the remaining percent of GluK2/3 from the zero time-point of cycloheximide when Neto2 protein was knocked down (sh-Neto2) compared to the knockdown control (sh-scrambled). The result of GluK2/3 reduction over time was not statistically significant between the knockdown control (sh-scrambled) and sh-Neto2 at each time point except at 24 hours after cycloheximide treatment. Removal of Neto2 increases GluK2/3 by ~ 33%.

Condition	GluK2/3 $t_{1/2}$ (hours)
sh-scrambled	25.5
sh-Neto2	56.0

Table 2. An estimation of GluK2/3 half-life. The data represent the calculated half-lifeof GluK2/3 under different conditions (sh-scrambled, sh-Neto2). GluK2/3 half-life (25.5 hr) was doubled (56.0 hrs) in the absence of Neto2 (sh-Neto2) indicating that GluK2/3 degradation rate slows down by 2x without Neto2 subunit protein.

8.1.4 Interpretation

Evidence from the literature (Martin and Henley, 2004; Martin et al., 2007; Martin et al., 2008; Konopacki et al., 2011; Copits and Swanson, 2013) demonstrated that GluK2-containg KARs are subjected to internalisation upon kainate stimulation. However, this positive control failed to confirm the responsiveness of the neurons in our experiments. Even the observed reduction (~20%) in the first two experiments (Figure 1A) did not reach the ~40% reduction reported in the literature (Martin and Henley, 2004; Martin et al., 2007; Martin et al., 2008; Konopacki et al., 2011; Copits and Swanson, 2013). This could be due to differences in the sensitivities and/or quality of primary dissociated neuronal cultures. While different batches of kainate were used, the pharmacological efficacy of this agonist has not been verified in other systems therefore its inactivity cannot be ruled out. In addition, the evidence from the literature was obtained from recombinant GluK2 expressed in neuronal cultures while in our experiments we investigated changes in the level of endogenous GluK2/3 KAR subunits.

It would be interesting to establish if agonist stimulation can alter the Neto-dependent modulatory effects of KARs trafficking in a similar way to TARPs/AMPARs. Following glutamate binding to AMPARs, TARPs dissociate from their interacting receptor providing a mechanism for the inhibition of excitotoxicity (Tomita et al., 2004; Morimoto-Tomita et al., 2009), which could have functional significance.

8.2 Mass spectrometry result of WT GluK2 and C858A, C71A

Description	Score	Coverage	# Proteins	MW [kDa]
GluK2 WT	2818.71	59.97	1	140.3
Clathrin heavy chain 1 OS=Homo sapiens GN=CLTC PE=1 SV=5 - [CLH1_HUMAN]	63.67	20.84	2	191.5
Albumin (Fragment) OS=Homo sapiens PE=2 SV=1 - [F6KPG5_HUMAN]	53.18	12.65	5	66.5
Keratin 1 OS=Homo sapiens GN=KRT1 PE=3 SV=1 - [H6VRF8_HUMAN]	50.75	30.28	5	66.0
Coatomer subunit alpha OS=Homo sapiens GN=COPA PE=1 SV=2 - [COPA_HUMAN]	36.09	14.46	1	138.3
Fatty acid synthase OS=Homo sapiens GN=FASN PE=1 SV=3 - [FAS_HUMAN]	30.81	6.93	1	273.3
Keratin, type I cytoskeletal 10 OS=Homo sapiens GN=KRT10 PE=1 SV=6 - [K1C10_HUMAN]	23.34	18.15	1	58.8
Keratin, type I cytoskeletal 9 OS=Homo sapiens GN=KRT9 PE=1 SV=3 - [K1C9_HUMAN]	19.91	16.05	1	62.0
Clustered mitochondria protein homolog (Fragment) OS=Homo sapiens GN=CLUH PE=1 SV=2 - [K7EIG1_HUMAN]	19.90	10.15	1	140.5
Bifunctional glutamate/proline--tRNA ligase OS=Homo sapiens GN=EPRS PE=1 SV=5 - [SYEP_HUMAN]	19.77	8.80	1	170.5
Keratin, type II cytoskeletal 2 epidermal OS=Homo sapiens GN=KRT2 PE=1 SV=2 - [K22E_HUMAN]	16.81	12.21	1	65.4
Polyubiquitin-C (Fragment) OS=Homo sapiens GN=UBC PE=1 SV=1 - [F5H265_HUMAN]	16.43	63.09	31	16.8
TBC1 domain family, member 4, isoform CRA_b OS=Homo sapiens GN=TBC1D4 PE=4 SV=1 - [A0A024R637_HUMAN]	12.74	5.62	2	146.5
Insulin receptor substrate 4 OS=Homo sapiens GN=IRS4 PE=1 SV=1 - [IRS4_HUMAN]	12.43	6.28	1	133.7
Probable 28S rRNA (cytosine(4447)-C(5))-methyltransferase OS=Homo sapiens GN=NOP2 PE=1 SV=2 - [NOP2_HUMAN]	11.17	7.27	1	89.2
ATP-dependent RNA helicase A OS=Homo sapiens GN=DHX9 PE=1 SV=4 - [DHX9_HUMAN]	11.10	5.91	1	140.9
High density lipoprotein binding protein (Vigilin), isoform CRA_a OS=Homo sapiens GN=HDLBP PE=1 SV=1 - [A0A024R4E5_HUMAN]	10.97	4.89	2	141.4
Keratin, type I cuticular Ha3-I OS=Homo sapiens GN=KRT33A PE=2 SV=2 - [KT33A_HUMAN]	8.62	9.90	2	45.9
cDNA FLJ14021 fis, clone HEMBA1002513, highly similar to Histone deacetylase 6 (Fragment) OS=Homo sapiens PE=2 SV=1 - [B3KNA1_HUMAN]	7.07	3.79	5	89.7
Nuclear autoantigenic sperm protein (Fragment) OS=Homo sapiens GN=NASP PE=1 SV=8 - [E9PPR5_HUMAN]	5.77	13.29	5	34.2
GEMIN5 protein OS=Homo sapiens GN=GEMIN5 PE=2 SV=1 - [B7ZLC9_HUMAN]	4.50	2.12	2	168.3
IARS protein OS=Homo sapiens GN=IARS PE=2 SV=1 - [Q6P0M4_HUMAN]	3.96	2.09	7	120.6
Enhancer of mRNA-decapping protein 4 OS=Homo sapiens GN=EDC4 PE=1 SV=1 - [EDC4_HUMAN]	3.89	1.71	1	151.6
Diaphanous homolog 1 (Drosophila) OS=Homo sapiens PE=2 SV=1 - [Q7KZJ7_HUMAN]	2.49	4.46	10	46.3

Description	Score	Coverage	# Proteins	MW [kDa]
GluK2 Mutant (C858A, C871A)	3103.39	65.94	1	140.3
Polyubiquitin-C (Fragment) OS=Homo sapiens GN=UBC PE=1 SV=8 - [F5H6Q2_HUMAN]	37.98	72.13	27	13.7
Clathrin heavy chain 1 OS=Homo sapiens GN=CLTC PE=1 SV=5 - [CLH1_HUMAN]	35.33	14.45	2	191.5
Serum albumin (Fragment) OS=Homo sapiens GN=ALB PE=1 SV=1 - [H0YA55_HUMAN]	32.65	11.01	8	51.5
Keratin 1 OS=Homo sapiens GN=KRT1 PE=3 SV=1 - [H6VRG2_HUMAN]	29.39	24.22	1	66.0
Keratin, type I cytoskeletal 10 OS=Homo sapiens GN=KRT10 PE=1 SV=6 - [K1C10_HUMAN]	26.97	21.58	1	58.8
Coatomer subunit alpha OS=Homo sapiens GN=COPA PE=1 SV=2 - [COPA_HUMAN]	25.38	11.19	1	138.3
Fatty acid synthase OS=Homo sapiens GN=FASN PE=1 SV=3 - [FAS_HUMAN]	23.76	4.62	1	273.3
Isoleucine--tRNA ligase, cytoplasmic OS=Homo sapiens GN=IARS PE=1 SV=1 - [J3KR24_HUMAN]	19.56	10.07	4	131.7
ATP-dependent RNA helicase A OS=Homo sapiens GN=DHX9 PE=1 SV=4 - [DHX9_HUMAN]	18.97	6.77	1	140.9
Keratin, type II cytoskeletal 2 epidermal OS=Homo sapiens GN=KRT2 PE=1 SV=2 - [K22E_HUMAN]	17.32	14.08	1	65.4
Bifunctional glutamate/proline--tRNA ligase OS=Homo sapiens GN=EPRS PE=1 SV=5 - [SYEP_HUMAN]	12.72	8.33	1	170.5
Clustered mitochondria protein homolog (Fragment) OS=Homo sapiens GN=CLUH PE=1 SV=2 - [I3L2B0_HUMAN]	9.72	4.61	3	138.1
TBC1 domain family, member 4, isoform CRA_b OS=Homo sapiens GN=TBC1D4 PE=4 SV=1 - [A0A024R637_HUMAN]	9.15	3.39	2	146.5
Insulin receptor substrate 4 OS=Homo sapiens GN=IRS4 PE=1 SV=1 - [IRS4_HUMAN]	7.63	4.93	1	133.7
Keratin, type I cytoskeletal 9 OS=Homo sapiens GN=KRT9 PE=1 SV=3 - [K1C9_HUMAN]	7.60	6.90	1	62.0
cDNA FLJ14021 fis, clone HEMBA1002513, highly similar to Histone deacetylase 6 (Fragment) OS=Homo sapiens PE=2 SV=1 - [B3KNA1_HUMAN]	5.65	2.69	5	89.7
cDNA FLJ53176, highly similar to Nuclear autoantigenic sperm protein OS=Homo sapiens PE=2 SV=1 - [B4DS57_HUMAN]	5.54	5.38	3	74.8
Vigilin (Fragment) OS=Homo sapiens GN=HDLBP PE=1 SV=2 - [C9JT62_HUMAN]	5.05	32.29	11	10.6
Desmoglein-2 OS=Homo sapiens GN=DSG2 PE=1 SV=2 - [DSG2_HUMAN]	5.02	2.68	1	122.2
Phosphoinositide phospholipase C (Fragment) OS=Homo sapiens GN=DKFZp434N101 PE=2 SV=1 - [Q9UFY1_HUMAN]	3.99	3.82	4	71.3
Enhancer of mRNA-decapping protein 4 OS=Homo sapiens GN=EDC4 PE=1 SV=1 - [EDC4_HUMAN]	3.41	1.71	1	151.6
Keratin, type I cytoskeletal 14 OS=Homo sapiens GN=KRT14 PE=1 SV=4 - [K1C14_HUMAN]	2.73	7.84	1	51.5